Radionucleidos naturales como trazadores de erosión, acumulación y transporte de sedimentos costeros: la playa de Las Canteras y la Bahía del Confital como caso de estudio

Natural radionuclides as tracers of coastal sediment erosion, accumulation and transport: the case study of Las Canteras Beach and El Confital Bay

Ana del Carmen Arriola Velásquez

Tesis Doctoral

Doctorado en Calidad Ambiental y Recursos Naturales (DOCARNA)

La Palmas de Gran Canaria

Diciembre, 2023

ULPGC
Universidad de Las Palmas de Gran Canaria

Universidad de Las Palmas de Gran Canaria

Doctorado en Calidad Ambiental y Recursos Naturales (DOCARNA)

Tesis Doctoral

Radionucleidos naturales como trazadores de erosión, acumulación y transporte de sedimentos costeros: la playa de Las Canteras y la Bahía del Confital como caso de estudio

Natural radionuclides as tracers of coastal sediment erosion, accumulation and transport: the case study of Las Canteras Beach and El Confital Bay

Ana del Carmen Arriola Velásquez

Directora: Dra. Alicia M. Tejera Cruz

Codirector: Dr. Pablo Martel Escobar

Firma doctoranda	Firma directora	Firma codirector
Dña. Ana del Carmen Arriola Velásquez	Dra. Alicia M. Tejera Cruz	Dr. Pablo Martel Escobar

Las Palmas de Gran Canaria

Diciembre 2023

D. Jesús García Rubiano COORDINADOR DEL PROGRAMA DE DOCTORADO DOCARNA DE LA UNIVERSIDAD DE LAS PALMAS DE GRAN CANARIA

INFORMA,

De que la Comisión Académica del Programa de Doctorado, en si sesión de fecha XX/XX/XXXX tomó el acuerdo de dar el consentimiento para su tramitación, a la tesis doctoral titulada "**Radionucleidos naturales como trazadores de erosión, acumulación y transporte de sedimentos costeros: la playa de Las Canteras y la Bahía del Confital como caso de estudio**" presentada por la doctoranda D/Dª Ana del Carmen Arriola Velásquez, dirigida por la Doctora Alicia Tejera Cruz y codirigida por el Doctor Pablo Martel Escobar.

Y para que conste, y a efectos de los previsto en el Artículo 25 del Reglamento de Estudios de Doctorado (BOULPGC 27/01/2023) de la Universidad de Las Palmas de Gran Canaria, firmo la presente en Las Palmas de Gran Canaria a, X de diciembre de dos mil veintitrés.

Agradecimientos / Acknowledgements

En primer lugar, quisiera agradecer a mis directores, los doctores Alicia Tejera Cruz y Pablo Martel Escobar, por la confianza depositada en mi para realizar esta tesis. Muchas gracias por todos los consejos y las discusiones científicas que sin duda me han ayudado a crecer tanto profesional como personalmente. Muchas gracias por enseñarme a desarrollar un pensamiento crítico y por siempre procurar que hubiera medios para realizar este trabajo. Además, agradezco mucho que me brindarais las oportunidades necesarias para poder explorar otros ámbitos científicos que van más allá de lo hecho en esta tesis. Muchas gracias por darme la oportunidad de conocer el fascinante mundo de la radiactividad ambiental y los radiotrazadores y, sobre todo, muchísimas gracias por la paciencia que habéis tenido conmigo siempre creyendo que esto saldría adelante incluso cuando yo no lo veía tan claro.

Por otro lado, también quiero agradecerle al grupo de investigación Interacción Radiación Materia (GIRMA) ya al resto de miembros del Departamento de Física de la Universidad de Las Palmas de Gran Canaria por proporcionarme la infraestructura y medios necesarios para llevar a cabo este trabajo. En especial quiero agradecer a mis compañeros del "Team Radón" que me han ayudado a diversificar y extender mis conocimientos sobre los distinta ámbitos de la radiactividad ambiental y me han acogido como una más del equipo a pesar de no ser titulada en física. Quiero agradeceros todo el esfuerzo que habéis hecho en este último tramo de la tesis para que pudiera estar más liberada de trabajo, sacar adelante los últimos artículos de la tesis y centrarme en llegar al final del camino, así como por los múltiples almuerzos en los que me habéis escuchado y aconsejado cuando lo he necesitado.

Muchas gracias al Dr. Ignacio Alonso y al Dr. Fernando Cámara por sus aportaciones a los diversos trabajos que conforman esta tesis. Gracias a ellos no solo se ha podido desarrollar una parte importante de este estudio, sino que también he podido darle otra perspectiva muy valiosa a la interpretación de los resultados obtenidos.

I want to thank Dr. Pieter Van Beek and the rest of his team for agreeing to host me in my first PhD stay at LEGOS without knowing me at all. He not only gave me the opportunity to learn new techniques and start creating an international network of collaborators but also helped me to bring back to my home lab other expertise in marine tracers that we did not have here. I want to also thank Dr. Walter Geibert and the rest of his team, with a special mention to Ingrid Stimac, for hosting me at AWI in the middle of a pandemic and, despite all the hurdles that came with it, helping me to obtain some results necessary for the development of this thesis and for helping me to extend my knowledge in the field of marine radioactivity.

Muchas gracias a mi familia que han sido un gran apoyo durante esta aventura. Muchas gracias a mis padres Joaquín y Ana Silvia por brindarme todas las oportunidades necesarias para poder llegar hasta aquí, por tener la paciencia de darme mi espacio cuando lo he necesitado y por aconsejarme sabiamente sobre cómo afrontar cualquier encrucijada. Muchas gracias a mis hermanos Silvia y Gerardo por escucharme cuando pensaba que me iba a volver loca y ayudarme a tomarme las cosas con más humor. También quiero agradecer al resto de mi familia que ha estado pendiente de mi tanto de este lado del Atlántico como del otro, y en especial a mi tía Ana y mi abuela Menchu. Siempre habéis estado ahí detrás, apoyándome sin hacer ruido, animándome a seguir adelante y recordándome que con humildad y perseverancia todo sale. Y antes de que se me olvide, Ángel muchas gracias por la foto de portada.

If there is someone who deserves all my gratitude and respect that is you, Sarah. You found me in the middle of this journey and you were brave (or crazy) enough to jump on board to finish it with me. I will never be able to thank you enough for all the support you gave me, not only at a personal level but also with your English corrections and suggestions to make my writing more fluid. You have been my compass and map to navigate this PhD ocean and in great part you are the reason I am now docking in port. A piece of this work and all my gratitude will be forever yours.

También quisiera agradecer a mis amigos por su gran apoyo. Ellos saben quiénes son y sin su ayuda esto no hubiera sido posible. Siempre han estado dispuestos a escucharme, aconsejarme, ayudarme en la medida de lo posible con cualquier cuestión de la tesis, llevarme al laboratorio a cambiar la muestra para que no me perdiera alguna quedada (porque aquí si engordamos, engordamos todos juntos) o incluso me han abierto las puertas de sus hogares y me han acogido cuando más lo he necesitado. In this group I want to also include all my international friends that I met during my scientific adventures around the world and who, despite me being terrible for long distance communication, have stayed there with me all these years. Sin todos vosotros nada de esto hubiera sido posible y siempre estaré agradecida. Somos la familia elegida y espero que sigamos celebrando todos nuestros logros juntos hasta que eso de que ya estamos ancianos sea cierto.

Finalmente, quiero acordarme de vosotros, María y Juan. Nuestros caminos se tuvieron que separar antes de lo deseado, pero espero que os alegréis de ver que he llegado hasta aquí.

ÍNDICE

RESUMEN

El transporte de sedimentos juega un papel clave en la evolución de las costas y puede tener consecuencias económicas, sociales y ambientales severas como el deterioro o destrucción de puertos y asentamientos costeros, así como la alteración de sus ecosistemas. Por ello, es necesario contar con herramientas que permitan estudiar los distintos procesos de erosión, transporte y acumulación de sedimentos y así poder realizar una planificación y gestión del litoral adecuadas. En esta tesis se realizó un estudio detallado de la viabilidad de los radionucleidos naturales presentes en sedimentos costeros como trazadores de sus procesos de erosión, acumulación y transporte. Como región de estudio se eligió la Bahía del Confital en el norte de la isla de Gran Canaria, España. Esta bahía presenta distintas dinámicas sedimentarias que incluyen la de la playa de Las Canteras, la cual destaca por combinar la dinámica de una playa expuesta a la acción del oleaje con la de una playa protegida frente a ella. Además, tanto la playa como el resto de la bahía presentan distintos tipos de sedimentos que en estudios previos a esta tesis habían mostrado un rango de concentraciones de actividad diverso. Por tanto, esta región es un laboratorio natural idóneo para estudiar la viabilidad de los radionucleidos naturales pertenecientes al propio sistema en estudio como trazadores de procesos asociados a la dinámica sedimentaria costera.

Para la primera parte de la tesis se llevó a cabo un análisis de la variabilidad espacio-temporal de las concentraciones de actividad de los radionucleidos naturales ^{226}Ra, ^{228}Ra y ^{40}K, del ^{210}Pb en exceso ($^{210}Pb_{ex}$) o no soportado por el ^{226}Ra del sedimento y de la ratio $^{226}Ra/^{228}Ra$ en las

arenas intermareales de la playa de Las Canteras durante un periodo de 3 años (2016 - 2019). Por un lado, los resultados del estudio de variabilidad espacial mostraron que las concentraciones de actividad del ^{226}Ra, ^{228}Ra y ^{40}K se distribuían siguiendo las distintas dinámicas sedimentarias marinas de la playa. De esta forma, las muestras recogidas en zonas de mayor acumulación de sedimentos presentaron concentraciones de actividad más altas que aquellas recogidas en zonas donde se produce una acumulación de sedimentos menor. Por otro lado, para el estudio de la variabilidad temporal de estas concentraciones de actividad se consideró la influencia de los cambios en los parámetros ambientales durante el muestreo y el contenido mineralógico de las muestras en dichas variaciones. Los resultados demostraron que los periodos de erosión y acumulación de sedimentos debidos a la acción del oleaje eran trazados por disminuciones y aumentos de la concentración de actividad de ^{226}Ra, ^{228}Ra y ^{40}K respectivamente. En el caso del $^{210}Pb_{ex}$ los resultados sugirieron que las variaciones espacio-temporales de sus concentraciones de actividad en la zona intermareal de la playa de Las Canteras estaban más influenciadas por la dinámica sedimentaria asociada al viento. En el caso de la ratio $^{226}Ra/^{228}Ra$, los resultados verificaron su uso como indicador de procesos de acumulación principalmente en zonas con contenido de minerales arcillosos.

Para la segunda parte de la tesis, se utilizaron las concentraciones de actividad del ^{226}Ra, ^{228}Ra, ^{40}K y $^{210}Pb_{ex}$ para estudiar los procesos de erosión, acumulación y transporte submarino que ocurren en la parte sumergida de la playa de Las Canteras y el resto de la Bahía del Confital. Con este fin, se analizaron las distribuciones espaciales de las actividades del ^{226}Ra, ^{228}Ra, ^{40}K y $^{210}Pb_{ex}$ en muestras recogidas en dos periodos de tiempo distintos (2005/2006 y 2022). Además, se examinó cómo

distintas características del sedimento y del transporte sedimentario afectaron a las variaciones de las concentraciones de actividad estudiadas. Los resultados mostraron que las variaciones de las actividades de los radionucleidos ^{226}Ra, ^{228}Ra y ^{40}K contenidos en los sedimentos costeros trazaban los distintos procesos de erosión y acumulación de sedimentos que habían ocurrido tanto en la zona sumergida de la playa como en las partes poco profundas de la bahía. En el caso del $^{210}Pb_{ex}$, se observó que sus altas concentraciones de actividad trazaban las zonas más profundas de la bahía. Por otro lado, en la parte sumergida de la playa, donde existe transporte de sedimentos, las altas concentraciones de actividad del $^{210}Pb_{ex}$ podrían trazar zonas de abrigo. En ambos casos, el $^{210}Pb_{ex}$ estaría identificando zonas donde la acumulación por sedimentación de partículas de la columna de agua se ve favorecida.

En resumen, los resultados obtenidos en los distintos estudios que conforman esta tesis sirven para proporcionar una serie de radiotrazadores viables para identificar distintos procesos de erosión, transporte y acumulación de sedimentos costeros. Además, se facilita una metodología que considera las distintas características del sedimento que hay que tener en cuenta en la utilización de dichos radiotrazadores. Finalmente, al ser un estudio desarrollado en un área con composición y dinámicas sedimentarias diversas, los resultados podrían aplicarse en otras partes del mundo y servir como base para el desarrollo de futuros estudios en la materia.

ABSTRACT

Sediment transport plays a key role in the evolution of the coastline and can have severe economic, social and environmental consequences including the damage or destruction of harbours and coastal settlements, as well as the alteration of the coastal ecosystems. Therefore, it is necessary to have tools to study sediment erosion, transport and accumulation to carry out proper coastal planning and management. This thesis presents a detailed study of the viability of natural radionuclides contained in coastal sediments as tracers of their erosion, transport and accumulation processes. The study region selected was El Confital Bay on the Island of Gran Canaria, Spain. This bay presents diverse dynamics including that of Las Canteras Beach, which combines the dynamic of a beach open to the wave action with that of a beach protected against it. Moreover, the beach and the bay have different types of sediments that in previous studies had shown a wide range of activity concentration values of natural radionuclides. Therefore, this region is an optimal natural laboratory for studying the viability of natural radionuclides belonging to the own system under study as tracers of coastal sediment dynamic processes.

For the first part of the thesis, a 3-year analysis (2016 – 2019) of the spatio-temporal variability of the activity concentrations of natural radionuclides ^{226}Ra, ^{228}Ra and ^{40}K, the excess or unsupported ^{210}Pb ($^{210}Pb_{ex}$) that is not in equilibrium with the ^{226}Ra of the sediment and the ratio $^{226}Ra/^{228}Ra$, was carried out in the intertidal zone of Las Canteras Beach. On one hand, the spatial variability study results showed that the activity concentrations of ^{226}Ra, ^{228}Ra and ^{40}K were distributed along the beach following the different marine dynamics present in it, dividing the

beach into three parts. This way, samples collected in areas with more accumulation of sediments displayed higher activity concentration values than those collected in areas where less accumulation of sediments occurs. On the other hand, for the temporal variability study, the influence of the changes on environmental conditions during the study period and the mineralogical content of the samples in their activity concentration values were considered. The results showed that the erosion and accumulation periods due to the wave action were traced by decreases and increases in the activity concentrations of ^{226}Ra, ^{228}Ra and ^{40}K, respectively. Regarding $^{210}Pb_{ex}$, all results in the intertidal zone of Las Canteras Beach suggested that the spatio-temporal variability of its activity concentration values was more influenced by wind transport. Concerning the ratio $^{226}Ra/^{228}Ra$, the results suggested its use as an indicator of accumulation processes, particularly in areas with clay mineral content.

For the second part of the thesis, the activity concentrations of ^{226}Ra, ^{228}Ra, ^{40}K and $^{210}Pb_{ex}$ were used to study the erosion, transport and accumulation processes occurring in the submerged part of Las Canteras Beach and the rest of El Confital Bay. For this purpose, the spatial distribution of the activity concentrations of ^{226}Ra, ^{228}Ra, ^{40}K and $^{210}Pb_{ex}$ were analysed in samples collected in two periods in time (2005/2006 and 2022). In addition, the influence different sediment and transport characteristics have on the activity concentration variations studied was examined. The results showed that the variability of the activities of the radionuclides ^{226}Ra, ^{228}Ra and ^{40}K contained in the coastal sediments traced the erosion and accumulation processes that had occurred in the submerged part of the beach, as well as in the shallower parts of the bay. Additionally, high activity concentrations of $^{210}Pb_{ex}$ seemed to trace

sheltered areas of the submerged beach and deep areas of the bay. In both cases $^{210}Pb_{ex}$ identified areas where accumulation by sedimentation of particles from the water column was favoured.

In summary, the results obtained in the different studies that constitute this thesis provide a series of radiotracers suitable for identifying coastal sediment erosion, transport and accumulation processes. In addition, a methodology is provided that considers different sediment characteristics to be taken into account in the use of these radiotracers. Finally, since the study was conducted in a region with diverse sedimentary composition and dynamics, the results could be applied to other parts of the world and be used as a basis for the development of future studies on the subject.

CAPÍTULO 1. Introducción

1.1. Origen y distribución de los radionucleidos presentes en el planeta

Vivimos rodeados de elementos radiactivos (radionucleidos) que tienen distintos orígenes y métodos de dispersión a lo largo de la superficie terrestre, teniendo la gran mayoría de estos radionucleidos un origen natural. Por un lado, se encuentran los radionucleidos primordiales o primigenios, cuya presencia en la corteza terrestre se remonta a la formación del planeta y se caracterizan por sus elevadas semividas ($t_{1/2}$). Por otro lado, existen radionucleidos cosmogénicos, con semividas notablemente más cortas, que se están produciendo continuamente en la atmósfera terrestre debido a las reacciones nucleares que tienen lugar por la interacción con la radiación cósmica. Además, otra parte de la radiactividad ambiental tiene un origen antropogénico, y es debida a la producción de radionucleidos artificiales en diferentes aplicaciones tecnológicas, médicas o de investigación.

Entre los radionucleidos naturales más abundantes que conforman la corteza terrestre se encuentran el ^{40}K ($t_{1/2}= 1.2\times10^{9}$ años) y aquellos que provienen de la cadena de desintegración radiactiva del ^{238}U ($t_{1/2}= 4.5\times10^{9}$ años) y del ^{232}Th ($t_{1/2}= 1.4\times10^{10}$ años). El contenido de estos radionucleidos en los distintos sedimentos varía en función del material, tipos de rocas y características geoquímicas que presenten los mismos (Froehlich, 2010; Livingston, 2004). En la tabla 1 se presentan algunos valores de actividad encontrados para ^{226}Ra (radionucleido descendiente del ^{238}U), ^{232}Th y ^{40}K en suelos y sedimentos de distintas zonas del mundo incluyendo la isla de Gran Canaria (Arnedo et al., 2017), lugar donde se desarrolla esta tesis. Además, también se incluye el valor medio dado para estos radionucleidos en suelos por el Comité de

las Naciones Unidas para el Estudio de los Efectos de las Radiaciones Atómicas (UNSCEAR – United Nations Scientific Committee of the Effects of Atomic Radiation). Los distintos resultados que se señalan en la tabla 1 son algunos ejemplos de cómo la concentración de los radionucleidos primordiales puede variar entre unas partes del mundo y otras.

País	^{226}Ra		^{232}Th		^{40}K		Referencia
	Rango	Media	Rango	Media	Rango	Media	
India	5.2 - 648.5	216.8	20.4 - 5137	1498	15.8 - 312.7	138.2	(Vineethkumar et al., 2020)
Irán	3.0 - 32.0	16.1	5.0 - 25.0	16.5	153 - 370	280.9	(Fallah et al., 2019)
Brasil	7050 - 8320	7810	17630 - 18450	17770	2220 - 3110	2660	(Vasconcelos et al., 2011)
Venezuela	2.6 - 28.9	11.4	4.2 - 41.8	14.5	15 - 421.2	153.4	(Alfonso et al., 2014)
Chipre	11.5 - 31.6	23	11.8 - 24.9	19	391.7 - 1014	628.1	(Abbasi et al., 2020)
Grecia	18 - 86	42	20 - 31	28	368 - 610	480	(Pappa et al., 2016)
España	4.9 - 89	34	5.6 - 147	44	24 - 1795	421	(Arnedo et al., 2017)
Nigeria	9 - 44*	23*	3 - 72	36	35 - 250	145	(Akpan et al., 2020)
Senegal	0 – 56.81*	17.04*	3.25 – 24.77	12.82	62.60 - 626	260.57	(Dione et al., 2018)
Media Mundial		32		45		420	(UNSCEAR, 2000)

*Actividad de ^{238}U

Tabla 1. Rangos y actividades medias de ^{226}Ra, ^{232}Th y ^{40}K en distintas partes del mundo. Los valores de actividad están dados en Bq kg^{-1}.

Por otro lado, tal y como se ha mencionado anteriormente, en el medioambiente también se pueden encontrar radionucleidos naturales que se forman en la atmósfera (los cosmogénicos). La radiación cósmica primaria que proviene del sol, las estrellas y del resto del espacio exterior está compuesta fundamentalmente por protones, partículas alfa y otros núcleos ligeros. Al llegar a la Tierra, estas partículas pueden interaccionar con los núcleos de los elementos de la atmósfera y generar

nuevos radionucleidos (como pueden ser ^{10}Be, ^{7}Be, ^{14}C, ^{3}H) que, posteriormente, llegan a la superficie del planeta por deposición seca o húmeda (Rodellas et al., 2023).

Por último, está el grupo de radionucleidos cuya concentración en el medio se debe a la intervención humana. Existen una serie de radionucleidos que son producidos de manera artificial por el bombardeo de un núcleo con partículas ligeras como protones, neutrones o partículas alfa (Pope, 1989). Algunos ejemplos de este tipo de radionucleidos podrían ser el ^{137}Cs, ^{90}Sr, ^{240}Pu, ^{239}Pu u otros de semivida más corta como el ^{131}I. Su presencia por todo el planeta se debe, entre otros, a los ensayos de las bombas nucleares a mediados del siglo XX, a algunos accidentes de la industria nuclear (fundamentalmente el de Chernóbil, y en mucha menor medida el de Fukushima Daiichi) y al uso de material radioactivo en distintos ámbitos como la medicina o la investigación (Yu, 2002). De la misma manera que existe una introducción de material radioactivo en el medio ambiente debido a actividad antropogénica, existen otras industrias no radiactivas que también pueden alterar la concentración de los radionucleidos naturales presentes en determinadas zonas del planeta. Algunos ejemplos de estas industrias, denominadas industrias de Material Radioactivo de Origen Natural (NORM - Naturally Occurring Radioactive Material) entre las que se encuentran la del fosfato, la del petróleo y gas, y algunas industrias metálicas o de la cerámica (Livingston, 2004).

Es importante destacar que las variaciones de la actividad que presentan los radionucleidos en el medio ambiente no siempre es la marcada por las leyes de desintegración radiactiva, sino que en diversas ocasiones estas variaciones pueden estar asociada a cambios químicos o

físicos del ecosistema que alteran la presencia de estos elementos radiactivos en el medio. Concretamente, en el caso de los océanos, los principales procesos de entrada de radionucleidos se muestran en la Fig. 1. Éstos pueden incluir, entre otros, la entrada atmosférica por deposición seca o húmeda, los vertidos industriales, las descargas fluviales que introducen radionucleidos disueltos en el agua y transportados por las partículas presentes en dichas descargas, las descargas de agua subterránea submarina (SGD – *Submarine groundwater discharges*) que introducen radionucleidos disueltos en ellas o las entradas sedimentarias que pueden incluir entradas de radionucleidos en el medio por difusión, bioturbación u otras formas de removilización desde los sedimentos al medio (Rodellas et al., 2023). La detección de estas variaciones de la actividad, diferentes a las marcadas por las leyes de desintegración radiactiva, asociadas con procesos como los anteriormente mencionados, constituye la base del uso de los radionucleidos naturales y antropogénicos como trazadores de distintos procesos continentales, costeros y oceánicos. Algunos ejemplos de sus características y usos como trazadores en el medio marino se describen en la siguiente sección.

Fig. 1. Diferentes vías de entrada de radionucleidos en el océano. Figura modificada de Rodellas et al., (2023).

1.2. Radionucleidos como trazadores de procesos marinos

En el océano se pueden encontrar desde fenómenos que ocurren en zonas muy localizadas y que tienen escalas temporales cortas a procesos que ocurren a mayores escalas espaciales y temporales. La mayoría de estos procesos están asociados a interacciones complejas en el océano o del océano con la atmósfera o la litosfera. A la hora de elegir un radiotrazador (un radionucleido como trazador) es importante que el elemento seleccionado tenga una serie de características que lo hagan adecuado para poder trazar dichos procesos. Algunas de ellas son: el tipo de vía de entrada del radionucleido al océano, el comportamiento fisicoquímico del radionucleido a utilizar o que tenga una semivida del orden de las escalas temporales del fenómeno a estudiar (Rodellas et al., 2023).

Las distintas vías de entrada de radionucleidos en el océano presentan componentes espacio temporales que limitarán el uso de ciertos radionucleidos para trazar determinados procesos (Rodellas et al., 2023). En el caso de la componente espacial, se pueden diferenciar dos tipos de vía de entrada de radionucleidos al océano. Por un lado, existen las vías de entrada que afectan a todo el planeta, como podría ser el fallout, la deposición seca o húmeda y la propia producción in situ de radionucleidos por el decaimiento de otros elementos radiactivos. El ^{7}Be es un ejemplo de radionucleido que es introducido en el océano por vías de entrada globales, ya que es depositado en la superficie del océano principalmente por la lluvia. Una vez entra en la columna de agua a través de la superficie se homogeniza en la capa de mezcla y esto permite trazar distintos fenómenos como las tasas de afloramiento (Kadko and Johns, 2011). Por otro lado, se encuentran las vías de entrada de radionucleidos que solo afectan a zonas localizada como podrían ser las

descargas de los ríos, que pueden introducir radionucleidos naturales o artificiales en océano (Léon et al., 2022; Yamashiki et al., 2014), o el aumento de la concentración de radionucleidos naturales en el medio marino debido al efecto de las industrias NORM (El Zrelli et al., 2019; González-Fernández et al., 2012).

En lo referido a la componente temporal de las vías de entrada de radionucleidos en medio marino, se diferencian las vías de entrada puntuales y las que se dan a largo plazo. Las vías de entradas puntuales hacen referencia a fenómenos que ocurren en un momento concreto como la entrada de radionucleidos al océano debido a accidentes nucleares como el ocurrido en Fukushima. Éstas son rutas que ocurren en un periodo de tiempo determinado y por tanto el suministro de radionucleidos en el medio está limitado en el tiempo. Las entradas a largo plazo son aquellas que son constantes en el tiempo como las descargas fluviales. Es importante recalcar que algunas vías de entrada a largo plazo pueden presentar fluctuaciones estacionales que provoquen que la cantidad de radionucleidos introducidos en el medio marino no sea constante, a pesar de producirse continuamente. Algunos ejemplos de esto se pueden encontrar en las descargas fluviales (Smith and Ellis, 1982) o en la entrada de radionucleidos por vía atmosférica (Baskaran and Swarzenski, 2007).

Por otro lado, desde el punto de vista fisicoquímico, los radionucleidos pueden presentar dos comportamientos que limitarían su uso como trazadores de distintos procesos en el océano; comportamiento conservativo o reactivo (Rodellas et al., 2023). El comportamiento conservativo indica que los radionucleidos presentan una interacción con las partículas marinas y la biota muy baja o incluso nula. Por tanto, la

única forma que tienen estos radionucleidos de movilizarse y/o desaparecer del medio marino es mediante el decaimiento radiactivo o por procesos físicos como puede ser el transporte de masas de agua. Algunos ejemplos de estos radionucleidos considerados conservativos son los radionucleidos naturales ^{40}K, ^{234}U y ^{238}U o algunos antropogénicos, como el ^{129}I o el ^{236}U que se han usado como trazadores del movimiento de masas de agua en el Océano Atlántico y en la zona del Ártico (Castrillejo et al., 2022; Wefing et al., 2021). Otro ejemplo de isótopos con carácter conservativo son los isótopos de Ra que se han utilizado para trazar la entrada de descargas de agua subterránea submarina al mar (Bejannin et al., 2017; Garcia-Orellana et al., 2021; Moore, 2006; Rodellas et al., 2017).

En caso de presentar comportamiento reactivo, al contrario que en el anterior, los radionucleidos en cuestión pueden ser retirados de la columna de agua por adsorción del elemento en las partículas del océano. Algunos de los ejemplos más comunes de este tipo de radionucleidos son el ^{234}Th, ^{210}Po y ^{210}Pb que se suele utilizar para trazar flujos material particulado en la columna de agua (Bam et al., 2021; Buesseler et al., 2020; Subha Anand et al., 2018). Otro ejemplo de la utilización de estos radionucleidos reactivos se encuentra en el uso del ^{210}Pb y ^{137}Cs para trazar tasas de sedimentación en zonas costeras (Shah et al., 2020). Además de esto, también hay radionucleidos como el ^{14}C o el ^{210}Po que pueden ser incorporado por organismos del medio marino (Faivre et al., 2015; Hemalatha et al., 2015; Tejera et al., 2019) y potencialmente podrían servir para trazar tanto procesos biológicos como posibles contaminantes que se encuentren en el medio y puedan ser bioacumulados.

Finalmente, el tercer aspecto que influye considerablemente en la elección de un determinado radiotrazador es la vida media del radionucleido seleccionado. Esta vida media establece el ritmo al que un elemento radiactivo se desintegra y por tanto tiene que ser coherente con la escala temporal del proceso a estudiar. Por ejemplo, los radionucleidos de vida corta (vidas medias de días) pueden ser útiles para estudiar procesos que ocurren en periodos de tiempo cortos. Un ejemplo de esto podría ser el uso de ^{224}Ra ($t_{1/2}$ = 3.7 días) y el ^{223}Ra ($t_{1/2}$=11.4 días) para trazar los tiempos de residencia y la edad aparente de masas de agua costeras (Dias et al., 2016; Hougham and Moran, 2007; Léon et al., 2022; Moore, 2000). Por otro lado, los radionucleidos con vidas medias más largas (vidas medias de años) se pueden usar para trazar fenómenos que ocurren en escalas temporales largas. Algunos ejemplos de esto son el uso de ^{230}Th ($t_{1/2}$= $7.5 \cdot 10^4$ años) y el ^{231}Pa ($t_{1/2}$= $3.3 \cdot 10^4$ años) para el estudio en paleoceanografía de los cambios históricos de circulación o el uso de ^{230}Th, ^{231}Pa y ^{14}C ($t_{1/2}$= 5730 años) para datación de sedimentos y cálculo de tasas de sedimentación ocurridas hace millones de años (Bradtmiller et al., 2014; Hajdas et al., 2021; Lippold et al., 2012; Not and Hillaire-Marcel, 2010).

Como se ha descrito, los radionucleidos presentan diferentes características a considerar para la elección de uno u otro como trazador de distintos procesos. Teniendo en cuenta lo indicado en este apartado, distintos radionucleidos se han aplicado de formas diversas en zonas costeras para trazar procesos sedimentarios. En la siguiente sección se describen más detalladamente este uso y la relevancia que los radionucleidos presentan como trazadores de dichos procesos.

1.3. Radionucleidos como trazadores de procesos sedimentarios costeros

Las líneas de costa y los fondos marinos costeros son áreas muy dinámicas que se encuentran siempre en constante cambio. Distintos agentes naturales como el oleaje, las corrientes costeras o el viento erosionan, transportan y acumulan sedimentos de forma natural en las distintas partes del litoral. Tendiendo esto en cuenta, intervenciones antropogénicas (como pueden ser la construcción de puertos, diques o paseos marítimos) pueden alterar esta dinámica natural de los sedimentos generando cambios, en ocasiones irreversibles, tanto en la geomorfología de la línea de costa como en los ecosistemas submarinos y terrestres costeros. Por ello, desde un punto de vista de protección y gestión de costas es importante tener herramientas para conocer la dinámica sedimentaria natural del litoral y entender cómo la intervención antropogénica pueda influir en esta. Además, conocer esta dinámica sedimentaria costera también puede ayudar a gestionar accidentes medioambientales que introduzcan algún tipo de contaminante que se acumule en los sedimentos y pueda alterar el ecosistema marino.

En este marco, los radionucleidos se han usado durante años como herramientas para trazar procesos asociados a la dinámica sedimentaria costera. El uso de estos elementos presenta grandes ventajas frente a otros trazadores ya que se pueden medir in situ o con cantidades de muestra relativamente pequeñas. Además, los radionucleidos presentes en la superficie del lecho marino siguen emitiendo cuando son movilizados hacia el interior de la columna sedimentaria permitiendo su medida incluso una vez son enterrados (International Atomic Energy Agency, 2014). Esto hace que los

radionucleidos no solo se usen para trazar transporte de sedimento, sino que también pueden usarse para calcular, entre otros, tasas de sedimentación.

Respecto al método de medida de estos radiotrazadores, partiendo de la base de que la mayor parte de radionucleidos usados son emisores gamma, existen distintos métodos de medida que se pueden aplicar. Por un lado, se pueden utilizar las medidas con espectrómetros gamma in situ (Androulakaki et al., 2015; Jones, 2001; Kilel et al., 2022; Tsabaris et al., 2023a, 2023b). Este tipo de medidas son útiles para mapear fondos marinos y en los últimos años también se han utilizado para medir transporte y acumulación de sedimentos en zonas de playas (Bezuidenhout, 2020; Mtshawu et al., 2023). La principal ventaja de estos detectores es que permiten producir mapas de distribución de radionucleidos en mucho menor tiempo del que sería necesario si se utilizasen datos obtenidos con muestras analizadas en el laboratorio.

Sin embargo, la medida in situ puede presentar algunas desventajas como su baja resolución espectral o que al espectrómetro le lleguen fotones que no procedan del sedimento. Esto podría ocurrir, por ejemplo, al medir en zonas sumergidas donde el espectrómetro podría recibir emisiones procedentes de otros materiales del fondo diferentes al sedimento, como las rocas presentes en el área de estudio. Otro ejemplo podría ocurrir al medir en zonas de playa con intervención antropogénica donde el detector podría recibir emisiones de los materiales de construcción presentes en la playa. Por ello, otra alternativa es la medida de muestras recogidas y analizadas en el laboratorio usando espectrómetros de alta resolución, como los espectrómetros gamma de germanio hiperpuro, o los alfa de PIPS (*Passivated Implanted Planar*

Silicon). La principal ventaja de las medidas en el laboratorio son que se evita las interferencias con otros materiales que no son objeto de estudio y se puede caracterizar el sedimento relacionando sus propiedades con las actividades de los radionucleidos presentes en el mismo.

En lo que respecta al uso de los radionucleidos de origen antropogénico como trazadores de dinámica sedimentaria, lo más común es el análisis de radionucleidos artificiales que son introducidos en el medio por el ser humano por distintos métodos. Uno de ellos consiste en la recogida de cierta cantidad de sedimentos del fondo marino y/o de ríos que son irradiados para activar distintos elementos radiactivos en ellos. Posteriormente estos sedimentos se reincorporan al medio y con distintos detectores se estudia su movimiento. Otra opción de uso de radionucleidos artificiales consiste en inyectar material radiactivo con características fisicoquímicas similares a las de los sedimentos del medio a estudiar y se rastrea la distribución de dicho trazador con detectores nucleares submarinos (International Atomic Energy Agency, 2014). Algunos ejemplos del uso de estos métodos se pueden encontrar en Corea (Kim et al., 2005) o en distintas partes de Latinoamérica como Brasil y Venezuela (Bandeira and Salim, 2017). La mayor ventaja del uso de estos radionucleidos de origen antropogénico es que tienen vidas medias cortas, lo cual facilita la repetibilidad del experimento en una misma zona. Una lista de los radionucleidos más comunes usados en este tipo de trabajos y su vida media se indican en la tabla 2.

Radionucleido	Vida media
Oro - 198 (^{198}Au)	2.7 días
Cromo - 51 (^{51}Cr)	27.8 días
Hafnio – 181+175 ($^{181+175}$Hf)	45 días
Iridio – 192 (^{192}Ir)	74 días
Escandio – 46 (^{46}Sc)	84 días
Tántalo – 182 (^{182}Ta)	115 días
Plata – 110 (^{110}Ag)	253 días
Tecnecio – 99m (^{99m}Tc)	6.02 horas
Indio – 113m (^{113m}In)	1.7 horas

Tabla 2. Radionucleidos comúnmente usados en investigaciones de transporte sedimentario y sus tiempos de vida media. Modificado de (International Atomic Energy Agency, 2014).

Por otro lado, los radionucleidos de origen antropogénico que llegan al medio marino a través del fallout también se pueden usar como trazadores de diversos procesos sedimentarios. Probablemente el radionucleido de origen antropogénico más ampliamente usado para monitorear estos procesos sea el ^{137}Cs. Debido a su vida media de 30 años, este radionucleido permite determinar tasas de sedimentación recientes en medios acuáticos. Un ejemplo de este uso se puede encontrar en la Bahía de Kastela (Croacia) donde el ^{137}Cs se usó para calcular tasas de sedimentación ocurridas en tres periodos de tiempo distintos; 1954 - 2005, 1963 – 2005/2006 y 1986-2005/2006 (Mikelić et al., 2017).

El problema de usar estos radionucleidos de origen antropogénico es que su presencia en el medio se debe a una introducción voluntaria o accidental por parte del ser humano, lo cual puede generar preocupación en el público general. Además, su uso se debe realizar siguiendo las normas establecidas por los organismos de regulación y protección nuclear de cada país. Por ello, una alternativa que se ha

estudiado en los últimos años es el uso de radionucleidos naturales como radiotrazadores de procesos sedimentarios. Al encontrarse de forma natural en el entorno, no requieren del trabajo previo de introducción en el medio de estudio. Además, con su uso no se corre el riesgo de infringir ninguna norma reguladora del país donde se desarrolla el estudio.

Además, estos radionucleidos se encuentran de forma natural en el medio ambiente y, por tanto, pueden participar de las distintas interacciones que se dan entre los sedimentos y las otras partes de los ecosistemas como podrían ser la biosfera o la hidrosfera. De esta manera, el estudio de estos radionucleidos naturales se puede aplicar no solo para trazar procesos de dinámica sedimentaria, sino que también se pueden utilizar para trazar fenómenos asociados a las interacciones entre el sedimento y el resto del ecosistema. Por ejemplo, existen casos en los que el análisis de la entrada al medio marino de isótopos de Ra disueltos desde el sedimento a través de las descargas de agua subterránea submarina (SGD) se han usado para establecer rutas de entrada de nutrientes desde la litosfera al océano (Sanial et al., 2015; Tamborski et al., 2018). Otro ejemplo del estudio de estas relaciones entre las diferentes partes del ecosistema se encuentra en el uso del ^{40}K para trazar sedimentación biogénica (Gulin et al., 2014). Es decir, usando la actividad de ^{40}K se puede conocer la cantidad de sedimento que proviene del material particulado de origen biológico que se encuentra en suspensión en la columna de agua.

Otra de las ventajas que presentan estos radionucleidos naturales en comparación con los artificiales que habitualmente se usan en trabajos de transporte de sedimentos, es que sus vidas medias varían desde días a miles de años, permitiendo así trazar distintos procesos asociados a la

dinámica sedimentaria con escalas de tiempo que varían desde meses a millones de años. Un ejemplo de esto lo podríamos encontrar en el uso de las actividades de radionucleidos como el ^{234}Th ($t_{1/2}$= 24.1 días), el ^{7}Be ($t_{1/2}$= 53.2 días), el ^{228}Th ($t_{1/2}$= 1.9 años), el ^{210}Pb ($t_{1/2}$= 22.3 años), ^{230}Th ($t_{1/2}$= $7.5 \cdot 10^4$ años) para calcular las tasas de acumulación, la datación de sedimentos o incluso la redistribución de sedimentos (Cooper and Grebmeier, 2018; Du et al., 2010; Feng et al., 2010; Li et al., 2021; Mahu et al., 2016; Not and Hillaire-Marcel, 2010; Renfro et al., 2016; Sun et al., 2020; Tamborski et al., 2022).

Por otro lado, se pueden encontrar algunos estudios donde radionucleidos con semividas más largas, y por tanto más estables en el tiempo, son usados para trazar el origen y el transporte que siguen los sedimentos costeros (Bezuidenhout, 2020; Lin et al., 2020; Thereska, 2009). Estos estudios parten del análisis de las variaciones espaciales de las actividades de radionucleidos naturales como el ^{232}Th, el ^{228}Ra, el ^{238}U, el ^{226}Ra o el ^{40}K , siendo estas variaciones un reflejo de zonas de erosión/acumulación o del transporte de los sedimentos estudiados. Teniendo en cuenta la variedad de estudios existentes, los radionucleidos naturales parecen ser una herramienta potente para trazar diversos procesos sedimentarios costeros.

No obstante, este uso de los radionucleidos naturales como radiotrazadores en zonas costeras no está exento de controversia o lagunas de conocimiento. Uno de los puntos de discusión entre los autores se centra en la relación existente entre el tamaño de grano y la cantidad de radionucleidos presentes en los sedimentos. En este marco, algunos autores han encontrado que los sedimentos con menor tamaño de grano, especialmente en tamaños de arcillas y limos (tamaños de

grano menores que 0.063 mm), presentan mayores actividades (Alfonso et al., 2014; Charkin et al., 2022; Huang et al., 2013; Ligero et al., 2001; Lin et al., 2020; Madruga et al., 2014). De acuerdo con estos autores, esto se debe a que los granos pequeños de sedimento presentan más superficie activa y por tanto la capacidad de adsorber radionucleidos del entorno es mayor. Esta relación se ha encontrado para distintos radionucleidos entre los que se incluyen, por ejemplo, el ^{40}K, el ^{228}Ra, el ^{226}Ra o el ^{238}U. Esto ha permitido el desarrollo y la aplicación de modelos que utilizan la actividad de los descendientes del ^{232}Th, el ^{238}U y el ^{40}K, al igual que el ^{137}Cs si lo hubiera, para describir y reproducir las diferentes facies sedimentarias que se pueden encontrar en el lecho marino (Ligero et al., 2009; Patiris et al., 2016).

Si bien esta relación de mayor actividad asociada a un menor tamaño de grano se encuentra en varias partes del mundo, algunos de estos mismos trabajos indican que esta relación solo puede ocurrir en presencia de tamaños de grano pequeños o en zonas con geologías similares a las estudiadas (Charkin et al., 2022; Ligero et al., 2001). De hecho, existen algunos estudios en los que esta hipótesis se contradice, por ejemplo, estudiando el origen geológico de los sedimentos usando las actividades de ^{232}Th, ^{238}U y ^{40}K como trazadores de este origen independientemente del tamaño de grano (Zebracki et al., 2015). Otros ejemplos los encontramos en estudios donde el incremento de la actividad de ^{40}K se asocia a un incremento de minerales portadores de potasio en las muestras (Roviello et al., 2020) o incluso hay trabajos donde se obtiene una desviación de la unidad para la ratio de las actividades de Th/U con actividades mayores de ^{232}Th que se asocian a la mineralogía de la zona (Ghosal et al., 2017). Por tanto, estos trabajos sugieren que la actividad de los radionucleidos en sedimentos costeros

podría estar más asociada a la naturaleza del sedimento que a su tamaño de grano.

Esta discrepancia tiene relevancia porque, tal y como se ha explicado previamente, conocer el comportamiento fisicoquímico de los radionucleidos es importante para entender su papel como trazadores de cualquier proceso en el medio marino. De hecho, si todos los radionucleidos cumplieran esa relación de mayor actividad cuanto menor tamaño de grano, el uso de los radionucleidos como trazadores de transporte sedimentario estaría limitado solo a zonas con sedimentos ligeros de tamaños de grano pequeños. Por ello, un estudio más detallado de las relaciones entre las variaciones de la actividad y distintas características del sedimento es necesario para determinar si el tamaño de grano es determinante en el papel de los radionucleidos naturales como trazadores del transporte de sedimentos o si, por el contrario, existen otras características que también deban ser consideradas. En consecuencia, en esta tesis se estudiará, entre otras cosas, estas relaciones para afianzar el conocimiento existente sobre la viabilidad de los radionucleidos naturales como trazadores de procesos asociados a la dinámica sedimentaria costera.

1.4. Geología y radiactividad natural en las playas de las Islas Canarias Orientales

Entre 2013 y 2015 (previamente al inicio de esta tesis) se llevó a cabo una campaña de recogida de 108 muestras de arena intermareal en 39 playas repartidas en las Islas Canarias Orientales (Gran Canaria, Fuerteventura, Lanzarote y La Graciosa). Para cada muestra se obtuvieron las concentraciones de actividad de los radionucleidos naturales ^{226}Ra, ^{232}Th y ^{40}K, así como los índices de riesgo radiológico

derivados de dichas concentraciones de actividad. Estos datos no se habían publicado con anterioridad y se aprovecharon para llevar a cabo un estudio comparativo de los niveles de radiactividad ambiental en las playas de las distintas islas mencionadas.

Las concentraciones de actividad de ^{226}Ra, ^{232}Th y ^{40}K obtenidas en las distintas playas mostraron que, en la isla de Gran Canaria, los valores de concentración de actividad eran generalmente más altos que en Fuerteventura, Lanzarote y La Graciosa. Además, al comparar las proporciones del ^{40}K vs ^{226}Ra, ^{40}K vs ^{232}Th y ^{232}Th vs ^{226}Ra, se pudo apreciar que un gran número de muestras de Gran Canaria presentaban proporciones similares a aquellas presentes en rocas volcánicas de alto contenido de ^{226}Ra, ^{232}Th y ^{40}K, como pueden ser las fonolitas o traquitas, las cuales solo se pueden encontrar en la isla de Gran Canaria. Por tanto, el análisis de estos datos mostró que en la componente terrígena de la arena de las playas de Gran Canaria puede incluir sedimentos que provengan de dichas rocas volcánicas de alta actividad.

Además de esto, el estudio de los índices de riesgo radiológico indicó que todos los valores se encontraban por debajo de los límites de seguridad establecidos internacionalmente. Por ello, desde un punto de vista radiológico, las playas de las Islas Canarias Orientales no suponen ningún riesgo para el ser humano. Sin embargo, a pesar de que todos índices de riesgo radiológico se encontraron por debajo de los límites de seguridad, se observó que en la isla de Gran Canaria también se encontraban valores más altos que en el resto de las islas. Un análisis estadístico confirmó que las diferencias observadas entre Gran Canaria y las otras islas eran significativas. Esto se podía deber a las diferencias en las litologías de las distintas islas ya que, tal y como se mencionó

anteriormente, solo en la isla de Gran Canaria se pueden encontrar rocas con alto contenido de ^{226}Ra, ^{232}Th y ^{40}K.

En el caso de Lanzarote y Fuerteventura también se encontraron diferencias significativas tanto en los índices de riesgo como en las actividades de ^{226}Ra y ^{232}Th. Sin embargo, las diferencias significativas presentes en estas dos islas no se pudieron explicar con el origen geológico de los sedimentos que componen la arena de las playas, ya que las dos islas comparten unidades geológicas similares. En cambio, teniendo en cuenta que las mayores concentraciones de actividad de ^{226}Ra y ^{232}Th se encontraron en la costa más urbanizada de la isla de Lanzarote, podría ser que la diferencia entre estas dos islas se debiese a la influencia de la intervención antropogénica en la costa de Lanzarote.

Por lo tanto, los resultados de este estudio indicaron que el contenido de radionucleidos naturales en la arena de las playas de la isla de Gran Canaria está fuertemente relacionado con el origen litológico del sedimento. Por ello, alguna de las playas de Gran Canaria se podría utilizar como laboratorio natural para evaluar la viabilidad de los radionucleidos naturales como el ^{226}Ra, el ^{232}Th y/o el ^{40}K como trazadores del transporte sedimentario marino que ocurre en playas. Finalmente, este análisis, que inicialmente no se había publicado y cuyos resultados ayudaron a la elección de la región de estudio de la tesis, se publicó posteriormente como un artículo científico en la revista *Environmental Pollution*. A continuación, se presenta una copia de dicho artículo.

Radiological risk assessment of beaches from volcanic oceanic islands: A case study of the Eastern Canary Islands (Spain)

Publicado en la revista *Environmental Pollution*

Año: 2024

Volumen: *340*

DOI: *https://doi.org/10.1016/j.envpol.2023.122809*

Journal Citation Report edición 2022: Categoría *Environmental Sciences*; Ranking *28/274*; Cuartil *Q1* (Decil *D1*)

Environmental Pollution 340 (2024) 122809

Contents lists available at ScienceDirect

Environmental Pollution

journal homepage: www.elsevier.com/locate/envpol

Radiological risk assessment of beaches from volcanic oceanic islands: A case study of the Eastern Canary Islands (Spain)☆

Ana del Carmen Arriola-Velásquez, Alicia Tejera *, Héctor Alonso, Neus Miquel-Armengol, Jesús G. Rubiano, Pablo Martel

Department of Physics, Instituto Universitario de Investigación en Estudios Ambientales y Recursos Naturales i-UNAT, Universidad de Las Palmas de Gran Canaria, Campus de Tafira, 35017, Las Palmas de Gran Canaria, Spain

ARTICLE INFO

Keywords:
Radionuclides
Volcanic islands
Coastal sediments
Radiological hazard index

ABSTRACT

This work constitutes the first survey that allows the establishment of baseline levels of environmental radioactivity in beach sands from the volcanic oceanic islands of La Graciosa, Lanzarote, Fuerteventura and Gran Canaria. Activity concentration values of ^{226}Ra, ^{232}Th and ^{40}K were measured by gamma spectroscopy in 108 samples, collected from 39 beaches across the whole study region. The radiological hazard risks associated with these sands were studied. The mean absorbed dose rate in the study region was 20 nGy h^{-1}, which is below the world average value. The mean outdoor annual effective dose for the beaches studied was 0.025 mSv y^{-1}, which is within the internationally accepted safe limit. Additionally, the assessment of the radium equivalent showed that all samples from the Eastern Canary Islands are below the safe limit of 370 Bq kg^{-1}. Despite not posing any radiological risk to the human population, the radiological hazard indices obtained in Gran Canaria were significantly higher than those of other islands. These significant differences seem to be related to the presence of sediments in the beaches of Gran Canaria that have their origin in lithologies with higher activity concentration values of ^{226}Ra, ^{232}Th and ^{40}K that are not present in the rest of the islands.

1. Introduction

Human exposure to ionizing radiation comes from different sources, including medical procedures, nuclear weapon testing, nuclear accidents, natural background radiation and exposure to artificial or natural sources of radiation due to different occupations (UNSCEAR, 2008). However, it is known that, for most individuals, the largest component of their total radiation exposure is due to natural background radiation (UNSCEAR, 2008, 2000). This natural background radiation mainly originates from the primordial radionuclides that constitute the Earth's crust. These primordial radionuclides include ^{40}K and those from the decay series ^{238}U, ^{232}Th and ^{235}U (Froehlich, 2010). The activity concentrations of these radionuclides across different parts of the world depend on the local geology and, thus, baseline studies of these natural background radiation levels are necessary, to be able to identify radiological hazards that can affect the human population.

Coastal and beach areas are very important to the general public, due to their economic and ecological value, and radiological hazard assessments have been carried out in different coastal areas around the world (Abbasi et al., 2020; Akpan et al., 2020; Al Shaaibi et al., 2023; Alfonso et al., 2014; Awad et al., 2022; Khandaker et al., 2019; Licínio et al., 2021; Rao et al., 2009; Shuaibu et al., 2017). In some of the studies, extremely high doses were reported in India (Vineethkumar et al., 2020), Brazil (Vasconcelos et al., 2011) and Malaysia (Shuaibu et al., 2017). These high doses were associated with the presence of monazite in sand grains, a mineral with high activity concentration values of ^{232}Th (Md. Jaffary et al., 2019). This represents an example of how geological variations in sediments around the globe can affect the population's radiation exposure. Thus, it is important to control the natural background radiation levels in high-value areas for humans, such as beaches.

In the case of the Eastern Canary Islands (La Graciosa, Lanzarote, Fuerteventura and Gran Canaria), studies of environmental radioactivity have focused on the soils of the islands (Arnedo et al., 2017) and groundwater (Alonso et al., 2015). Nevertheless, only a single study on beaches was found in the literature (Arnedo et al., 2013). This is striking,

☆ This paper has been recommended for acceptance by Jörg Rinklebe.

* Corresponding author.
E-mail address: alicia.tejera@ulpgc.es (A. Tejera).

https://doi.org/10.1016/j.envpol.2023.122809
Received 11 August 2023; Received in revised form 5 October 2023; Accepted 24 October 2023
Available online 31 October 2023

considering the fact that the Canary Islands represent one of the third most touristic areas in Spain, receiving more than 12 million tourists in 2022 (INE, 2022); the majority of those tourists were drawn to the islands by their beaches, which can be enjoyed all year long. Additionally, the Eastern Canary Islands are located within the main commercial routes between Europe, Africa and America; the port of La Luz in Gran Canaria is the fourth largest port in Spain. This means that many different types of ships (oil product tankers, crude oil tankers, bulk carriers, oil drilling platforms, container ships, ferries and cruise ships) arrive on the islands on a daily basis or pass by en-route to other destinations (MarineTraffic, 2023; Tichavska and Tovar, 2015). Therefore, not only the beaches of the Eastern Canary Islands are places of high occupancy throughout the year, but they also are under the constant threat of suffering some contamination originated in some of the many ships that arrive at its coasts every day. The presence of high concentrations of natural radionuclides in some of these ships, like in the scales that are generated in the pipes of oil drilling (Bou-Rabee et al., 2009), could lead to some radiological hazards that would affect not only the residents on the islands, but also the millions of tourists that visit their beaches every year.

Considering all of this, the main objective of this work is to establish reference levels of environmental background radioactivity on the beaches of the Eastern Canary Islands so any possible radiological contamination that could arrive on the beaches through seawater can be detected. For this purpose, intertidal sand samples from natural sandy beaches will be collected. The activity concentration values of natural radionuclides ^{226}Ra, ^{232}Th and ^{40}K and anthropogenic radionuclide ^{137}Cs, as well as the radiological hazard indices associated with these activities, will be evaluated. Additionally, the results obtained will be compared with the activity concentration values of natural radionuclides from the different lithologies of the volcanic oceanic islands. This will be useful to assess the impact that the diverse geology of these islands has on the natural radioactivity levels of their beaches, as well as to evaluate the effects that anthropogenic pressure from coastal zones might have already had on them.

2. Study region

The Canary Islands are located in the North East part of the Central Atlantic Ocean (between 27° 37′ 0″ and 29° 25′ 0″ north latitudes and from 13° 20′ 0″ to 18° 10′ 0″ west longitudes), in close proximity to the Western Sahara African coast (Fig. 1). The archipelago consists of eight islands and, from an administrative perspective, they are divided into two provinces: Santa Cruz de Tenerife, comprising the four western islands (Tenerife, La Palma, La Gomera and El Hierro) and the province of Las Palmas, which covers the four eastern islands (La Graciosa, Lanzarote, Fuerteventura and Gran Canaria) and some small islets. This study is focused on the province of Las Palmas and the study region will be referred to as the Eastern Canary Islands (ECI). This is because the ECI concentrate most of the main sandy beaches of the Canary Islands and they are the 11th most populated region of Spain, with more than 1 million residents (INE, 2021a). The main industrial activity of the islands is concentrated on the island of Gran Canaria and the most developed economic sector is tourism.

From a geological point of view, these islands have a volcanic oceanic island formation. They present three different units, as described in the work by Carracedo et al. (2002). The first unit is known as the Basal Complex (or pre-shield stage), composed of turbiditic sediments intruded by sheeted dike swarms and plutonic rocks, ranging from pyroxenites to carbonatites. The second unit corresponds to the shield edifices (from basic to acid rocks) and the third unit comprises post-shield cones (rejuvenation stage with ultrabasic to acid materials). The lithology found on the different islands varies from one island to another. In La Graciosa (LG), Lanzarote (LZ) and Fuerteventura (FV) the volcanic rocks found are mostly basalts while, in Gran Canaria (GC), in addition to basalts, a considerable amount of phonolites, trachytes and rhyolites (salic materials) can be found (I.G.M.E., 2021). Previous studies of the natural radiation levels of the soils of the ECI have proved that, due to the presence of phonolites, trachytes and rhyolites in soils of GC, the natural radioactivity levels that island are above those found for LZ and FV(Arnedo et al., 2017). This is because those salic materials present naturally higher natural gamma radiation than other volcanic rocks like basalts (Chiozzi et al., 2001; Fernández-Aldecoa et al., 1992). In addition, an initial local study carried out in GC (Arnedo et al., 2013)

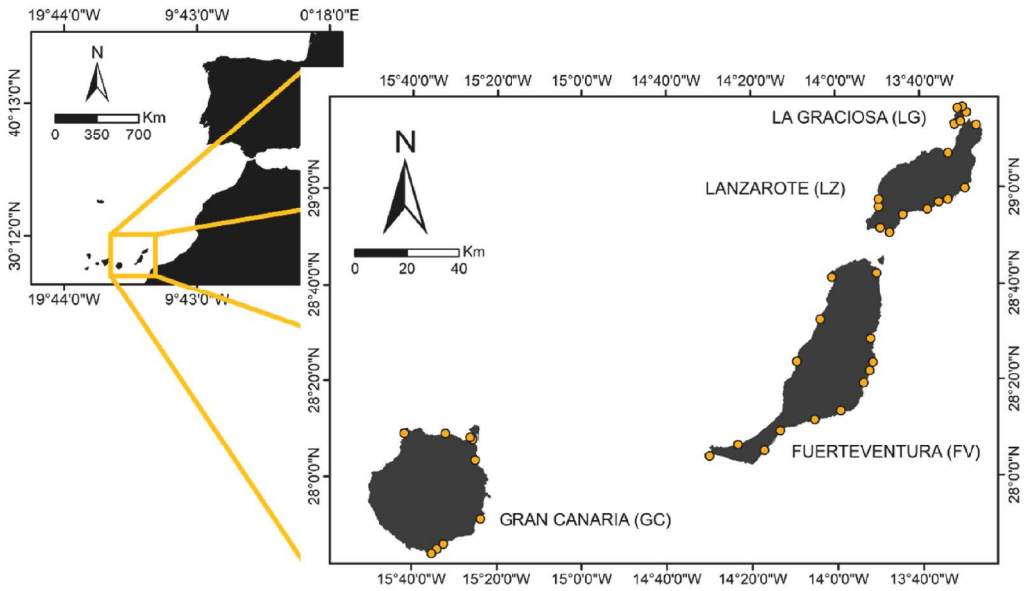

Fig. 1. Map of the location of the beach areas studied in the Eastern Canary Islands, Spain.

proved that sands from beaches that could contain salic volcanic materials (such as phonolites) presented higher activity concentration values of ^{226}Ra, ^{232}Th, and ^{40}K and higher absorbed dose rates than beaches without these materials in their sand.

3. Materials and methods

3.1. Collection and preparation of sand samples

In order to perform radiological risk assessments in beach areas, an extensive campaign was designed in the Eastern Canary Islands: i.e. La Graciosa (LG), Lanzarote (LZ), Fuerteventura (FV) and Gran Canaria (GC). A total of 108 sand samples were collected from 39 beaches spread across the four islands (Fig. 1). The coordinates of the exact sampling points on each beach are given in Table S1 (see Supplementary Appendix). Samples were collected from the intertidal zone during low tide. For each sample, a 1 m^2 square was drawn at each sampling point and the sand within it was mixed *in-situ*, to homogenize the sample. Then, the superficial sand sample was collected from the upper 5 cm.

After collection, all sand samples were taken to the laboratory and dried at 80 °C for 24 h. After, the samples were sieved through 1 mm mesh and stored in a PVC-trunk conical container, they were filled to 40 cm^3 and sealed with aluminum strips for one month before measurement. This storage period was designed to achieve secular equilibrium between ^{226}Ra, ^{222}Rn and its short-life progenies because the gamma peak of ^{214}Pb is used to determine ^{226}Ra (Bezuidenhout, 2013).

3.2. Gamma spectrometry analysis

Radionuclides in sand samples were determined by gamma spectrometry, using a Canberra Extended Range (XtRa) Germanium (model GX3518) spectrometer, with 38% relative efficiency, with respect to a 3″ x 3" active area NaI (Tl) detector, and nominal FWHM of 0.875 keV at 122 keV and 1.8 keV at 1.33 MeV. The spectrometer was coupled to a Canberra DSA-1000 multichannel analyzer with the software package Genie 2000. Efficiency calibration of the system was carried out using the Canberra LabSOCS package, based on the Monte Carlo method (Arnedo et al., 2017; Arriola-Velásquez et al., 2019, 2021; Guerra et al., 2017, 2015). For calibration, verification reference standards IAEA RGK-1 (potassium sulfate), RGU-1 (uranium ore) and RGTh-1 (thorium ore) were used. Energy calibration was performed using a^{155}Eu/^{22}Na (Canberra ISOXSRCE, 7F06-9/10138 series) and confirmed using the 1460.8 keV line of ^{40}K (IAEA RGK-1) (Arnedo et al., 2017).

The radionuclides of interest were analyzed using different photopeaks. Secular equilibrium between ^{214}Bi (609.3 keV) and ^{214}Pb (351.9 keV) was confirmed experimentally and thus, to avoid the coincidence summing effect affecting ^{214}Bi photopeak, the emission line of ^{214}Pb at 351.9 keV was chosen to determine ^{226}Ra activity concentration. Additionally, it is known that the 911.6 keV photopeak of ^{228}Ac shows high uncertainties in samples with low activity concentration values of ^{232}Th. In consequence, the emission line of ^{212}Pb at 238.6 keV was selected for determining the activity concentration of ^{232}Th after verifying its equilibrium with ^{228}Ac and ^{208}Tl (583.2 keV). This is because ^{212}Pb photopeak exhibits higher intensity than ^{208}Tl and it does not present coincidence summing effect. Activity concentrations of ^{40}K and ^{137}Cs were measured directly from their emission lines at 1460.8 keV and 661.8 keV, respectively. The counting time for each sample was approximately 24 h. The activity concentration values have been expressed according to the common standard of using only one significant figure for uncertainties; a coverage factor k = 1 was assumed.

3.3. Statistical analysis

Once the different radiological hazard indices were obtained, a Shapiro-Wilk normality test (Shapiro and Wilk, 1965) was used to evaluate the distribution of the results. Subsequently, a Kruskal-Wallis test (Theodorsson-Norheim, 1986) was used to evaluate the presence of significant differences in the radiological hazard indices obtained for the different islands. Moreover, a Wilcoxon rank sum test (Rosner and Glynn, 2009) was applied to identify which islands presented such differences among them. These tests were carried out with a significance level of 0.05.

4. Results and discussion

4.1. Activity concentration of ^{226}Ra, ^{232}Th and ^{40}K in the samples

The activity concentration of primordial radionuclides ^{226}Ra, ^{232}Th and ^{40}K was measured in 108 sand samples collected from 39 beaches spread across the Eastern Canary Islands: La Graciosa (LG), Lanzarote (LZ), Fuerteventura (FV) and Gran Canaria (GC). The mean activity concentration values obtained for ^{226}Ra, ^{232}Th and ^{40}K in LG were 10.9 ± 0.9, 3.5 ± 0.4 and 49 ± 5 Bq kg^{-1}, respectively. In the case of LZ, the mean activity concentration value for ^{226}Ra was 13.3 ± 1.0 Bq kg^{-1}, for ^{232}Th a mean activity of 9.2 ± 0.6 Bq kg^{-1} was found and for ^{40}K a mean activity concentration value of 76 ± 7 Bq kg^{-1} was reported. In the case of FV the mean activity concentration values found for these radionuclides were 7.5 ± 0.8 Bq kg^{-1} for ^{226}Ra, 5.6 ± 0.5 Bq kg^{-1} for ^{232}Th and 75 ± 7 Bq kg^{-1} for ^{40}K. Finally, for GC, the activity concentration values found for ^{226}Ra, ^{232}Th and ^{40}K were 19 ± 1 Bq kg^{-1}, 28 ± 1 Bq kg^{-1} and 530 ± 20 Bq kg^{-1}, respectively. The results showed that, in general, all islands have activity concentration values below the world average, set at 32 Bq kg^{-1} for ^{226}Ra, 45 Bq kg^{-1} for ^{232}Th and 420 Bq kg^{-1} for ^{40}K (UNSCEAR, 2000). An exception to this was found in GC, where the mean activity concentration value of ^{40}K was above the world average value. The whole list of activity concentration values obtained for each sampling point on each of the beaches studied is presented in Table S2 in the supplementary material. The relations between activity concentration of primordial radionuclides ^{226}Ra, ^{232}Th and ^{40}K in each sample are shown in Fig. 2. Additionally, the ratios of these primordial radionuclides which were found in phonolites, basalts, rhyolites and trachytes (the typical volcanic rocks that can be found in the Eastern Canary Islands), correspond to the slope of the represented color dash lines. The data from Alonso (2015) were used to calculate the ratios in the different volcanic rocks.

When observing the ratio value of ^{40}K/^{226}Ra (Figs. 2a) and ^{40}K/^{232}Th (Fig. 2b) for the volcanic rock in the Eastern Canary Islands, it would be appreciated that all of them presented higher values of ^{40}K than ^{226}Ra and ^{232}Th; this is particularly noticeable in the phonolites. Previous studies on the Island of Tenerife and in the Aeolian volcanic arc in Italy (both volcanic settlements) showed that phonolites, along with trachytes and rhyolites, are the rocks that present higher natural gamma radiation (Chiozzi et al., 2001; Fernández-Aldecoa et al., 1992). According to the Total Alkalinity Silica (TAS) diagram (Le Bas et al., 1986), phonolites are in the group of volcanic rocks that have the highest content of potassium (see Fig. S1). Therefore, these types of volcanic rocks would naturally have a higher ^{40}K content and this explains why they have higher activity concentration values of this gamma emitter). In the case of the ^{226}Ra/^{232}Th ratio (Fig. 2c), the phonolites and trachytes present a higher ^{232}Th content than ^{226}Ra. This contrasts with basalts, where these radionuclides seem to be in equilibrium, and rhyolites, that present slightly higher activity concentration values of ^{226}Ra.

Regarding the ^{40}K/^{226}Ra (Figs. 2a) and ^{40}K/^{232}Th (Fig. 2b) ratios in samples from La Graciosa, Lanzarote, Fuerteventura and Gran Canaria, it can be appreciated that the samples from the beaches of GC generally presented ratios (proportion of ^{40}K to ^{226}Ra and proportion of ^{40}K to ^{232}Th) higher than those found on the other islands, being even higher than the typical value found for phonolites in the ECI. In addition, the ^{226}Ra/^{232}Th ratio (Fig. 2c) showed that in general the samples from the beaches of GC presented lower ratios than the samples from the beaches of LG, LZ and FV. These results show that the samples from GC followed a similar pattern in their ratios to the phonolites and trachytes.

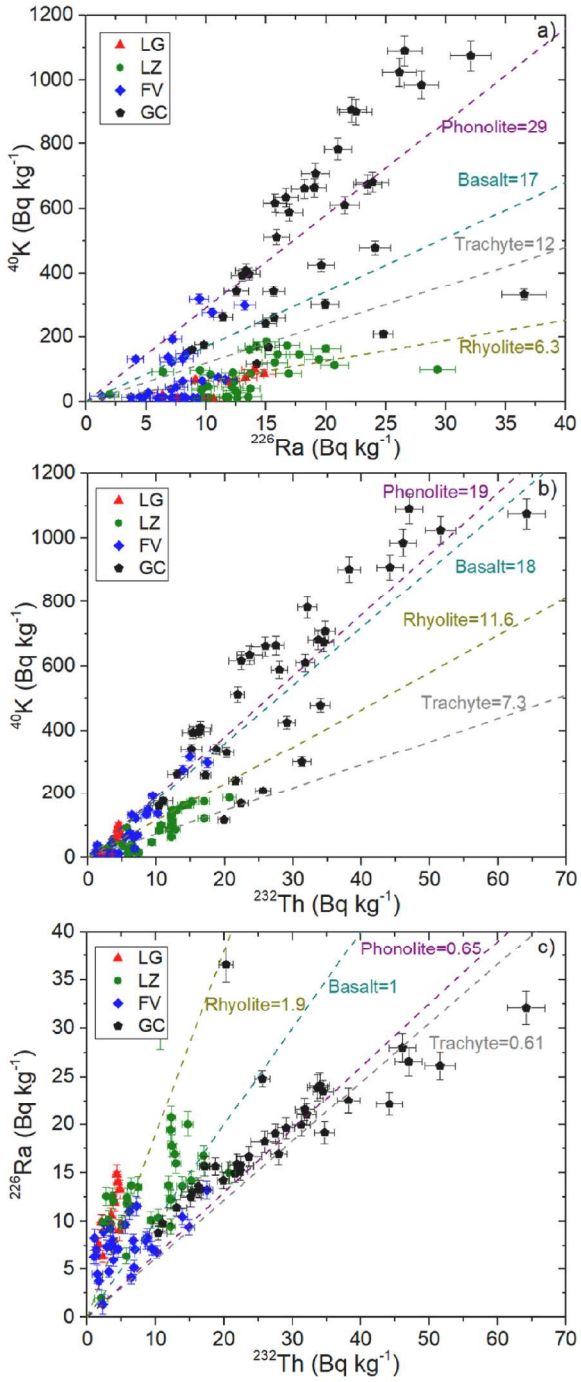

Fig. 2. Activity concentration values of a) ^{40}K vs^{226}Ra, b) ^{40}K vs ^{232}Th and c) ^{226}Ra vs ^{232}Th obtained for all sand samples in the different islands. Slopes of dash lines are the ratios calculated for different volcanic rocks from the data of Alonso (2015).

In the work of Arnedo et al. (2017), the activity concentration values of ^{226}Ra, ^{232}Th and ^{40}K were mapped in the soils of the Eastern Canary Islands. The results showed that, on GC, the maximum activity concentration values of ^{226}Ra (>50 Bq kg^{-1}), ^{232}Th (>90 Bq kg^{-1}) and ^{40}K (>1000 Bq kg^{-1}) were considerably higher than FV and LZ. This was related to the fact that in GC some volcanic rocks with high activity concentration values of ^{226}Ra, ^{232}Th and ^{40}K (such as phonolites and trachytes) could be found. In the other islands studied in that work, the geological composition of the soils was mostly basalts, which explained the lower activity concentration values found there in comparison to GC. In this study, the activity concentration values found in the beaches from GC are also higher than in the beaches from FV, LZ and LG. This is because the sediments that compose the beach sands of each island have its terrigenous source in the different rocks that can be found in them. Thus, differences in the activity concentration values found in sand samples from GC and the other islands seem to reflect the geological variations in the terrigenous source of sediments that can be found in the different islands.

4.2. Radiological risk assessment

4.2.1. The absorbed dose rate (nGy h^{-1}) and annual effective dose rate (mSv y^{-1})

The absorbed dose rate (D), in nGy h^{-1}, due to natural radio-isotopes at a height of 1 m above ground level, was calculated by using equation (1) (UNSCEAR, 2008, 2000):

$$D = 0.462A_{Ra} + 0.0417A_K + 0.604A_{Th} \quad (1)$$

where A_{Ra}, A_K and A_{Th} are the respective activity concentrations of ^{226}Ra, ^{40}K and ^{232}Th in Bq kg^{-1}. The mean dose rate obtained for each of the beaches studied is given in Table 1. For the ECI, the absorbed dose rate ranged from 3.1 to 72.6 nGy h^{-1}, with an average value of 20.8 nGy h^{-1}. The mean value obtained in this study was below the Spanish mean of 76 nGy h^{-1} and below the world average of 57 nGy h^{-1} (UNSCEAR, 2000). Nevertheless, at some locations on GC (e.g. El Inglés Beach and Maspalomas Beach), the values obtained were above the world average. Despite this, the mean absorbed dose rate obtained for the ECI was similar to others obtained from different parts of the Atlantic coast. A mean value of 20.6 nGy h^{-1} was found in Venezuala (Alfonso et al., 2014) and an average value of 26.8 nGy h^{-1} in the coast of Senegal (Dione et al., 2018). However, the mean value obtained for the absorbed dose rate in this study was relatively low, in comparison with other parts of the world, such as the coast of the Red Sea in Egypt, where a mean value of 38 nGy h^{-1} was found (Zakaly et al., 2021) or the east coast of Tamilnadu in India, where a value of 86.9 nGy h^{-1} was reported (Ravisankar et al., 2015). Additionally, much higher values have been found in other parts of the world, e.g. in Bahia (Brazil), where a value of 1792 nGy h^{-1} was reported (Vasconcelos et al., 2011), parts of Malaysia, where a value of 1748 nGy h^{-1} was found (Shuaibu et al., 2017) or in Mandaikadu in India where an absorbed dose rate of 4722 nGy h^{-1} was reported (Thangam et al., 2022). In all these cases, the high absorbed dose rate was related to the presence of monazite in the samples. This shows that the geological nature of the sediments found on beaches seems to influence the radiological risk caused by them.

Due to the warm weather that the ECI have all year long, the residents of the islands and the long-time visitors spend time on the beaches all year long as well as there are beach workers that everyday spend hours on them. Thus, the outdoor annual effective dose (AEDE), another type of absorbed dose in mSv y-1, was calculated according to (UNSCEAR, 2008, 2000):

$$AEDE = D \times F \times T \times O \times 10^{-6} \quad (2)$$

where D is the external dose rate (given in nGy h^{-1}), F is the absorbed dose to effective dose conversion factor (0.7 Sv Gy^{-1}), T is hours per year (8760 h y^{-1}), O is the occupancy factor (0.2) and 10^{-6} is the nano to

Table 1
Mean Absorbed dose rate (D) in nGy h^{-1}, Annual effective dose (AEDE) in mSv y^{-1}, Excess life cancer risk (ELCR) and Radium equivalent (Ra_{eq}) in Bq kg^{-1} obtained for each beach studied.

Island	Beach	D	AEDE	ELCR ($\times 10^{-3}$)	Ra_{eq}
LG	Pedro Barbas	7.5	0.009	0.04	16.46
LG	Playa del Ambar	6.3	0.008	0.03	13.68
LG	Las Conchas	5.1	0.006	0.03	11.02
LG	Francesa	10.8	0.013	0.06	23.07
LG	Caleta Sebo	13.2	0.016	0.07	27.89
Mean value in LG		**8.6**	**0.010**	**0.05**	**18.42**
LZ	Orzola	3.1	0.004	0.02	6.63
LZ	Teguise	12.4	0.015	0.07	27.24
LZ	Arrecife	9.7	0.012	0.05	21.08
LZ	Honda	22.6	0.028	0.12	48.63
LZ	Pto. Carmen	19.8	0.024	0.11	43.01
LZ	Quemada	27.2	0.033	0.15	58.96
LZ	Papagayo	7.2	0.009	0.04	15.84
LZ	P.BlancaLZ	9.6	0.012	0.05	20.53
LZ	Janubio	25.1	0.031	0.14	54.17
LZ	Hervideros	22.8	0.028	0.13	49.04
LZ	Famara	12.6	0.015	0.07	27.71
Mean value in LZ		**15.6**	**0.019**	**0.09**	**33.89**
FV	Corralejo	5.1	0.006	0.03	10.97
FV	P. BlancaFV	13.5	0.017	0.07	28.51
FV	Caleta de Fuste	10.5	0.013	0.06	22.54
FV	Salinas del Carmen	12.6	0.015	0.07	27.26
FV	Pozo Negro	15.4	0.019	0.09	32.45
FV	Las Playitas	11.3	0.014	0.06	23.52
FV	Gran Tarajal	23.6	0.029	0.13	49.46
FV	Costa Calma	8.7	0.011	0.05	18.97
FV	Jandia	7.1	0.009	0.04	15.51
FV	La Punta	7.7	0.009	0.04	17.09
FV	Cofete	7.5	0.009	0.04	16.08
FV	Ajuy	15	0.018	0.08	31.98
FV	Los Molinos	26.6	0.033	0.15	55.16
FV	El Cotillo	4.3	0.005	0.02	9.57
Mean value in FV		**12.1**	**0.015**	**0.07**	**25.65**
GC	El Puertito de Bañaderos	44.4	0.054	0.25	93.95
GC	Sardina del Norte	35.6	0.044	0.20	77.5
GC	La Laja	35.8	0.044	0.20	77.34
GC	Arinaga	33.8	0.041	0.19	71.92
GC	El Inglés	72.6	0.089	0.40	151.06
GC	Las Alcaravaneras	45.6	0.056	0.25	94.45
GC	Maspalomas	67.5	0.083	0.37	139.63
GC	San Agustín	57.9	0.071	0.32	120.6
GC	Las Canteras	33.3	0.041	0.18	68.78
Mean value in GC		**47.4**	**0.058**	**0.26**	**99.47**
Total mean value		**20.8**	**0.025**	**0.11**	**44.08**

milli conversion factor. The results obtained for the ECI show an average value of 0.025 mSv y^{-1}, which is below the world mean value of 0.07 mSv y^{-1} (UNSCEAR, 2000). However, in the case of El Inglés Beach, Maspalomas and San Agustin (all located in GC), the values obtained (Table 1) are higher than the world average. Nevertheless, all the values obtained in this study were below the maximum of 1 mSv y^{-1} recommended for the general public (ICRP, 2007). Considering the results obtained for the absorbed dose rate and the annual effective dose, the studied area does not pose a considerable radiological threat to the public. Moreover, it is noteworthy that in this radiological analysis, no ^{137}Cs was detected above the minimum detectable activity (MDA) that for our samples ranged between 2 and 3 Bq kg^{-1}.

4.2.2. Excess life cancer risk

The Excess life cancer risk (ELCR) gives information about the risk of developing cancer over a lifetime due to an exposure at a given radiation level. It is calculated using equation (3) (Al Shaaibi et al., 2023; Kolo et al., 2015):

$$ELCR = AEDE \times DL \times RF \quad (3)$$

where AEDE is the annual effective dose, in mSv y^{-1}, DL is the life expectancy (established as 82 for the Eastern Canary Islands, according to the Spanish National Statistics Institute (INE, 2021b)) and RF is the detriment-adjusted nominal risk coefficient for cancer, set at 0.055 Sv^{-1} (ICRP, 2007). The results for the ECI given in Table 1 ranged from 0.02–0.40 $\times 10^{-3}$ with a mean value of 0.11 $\times 10^{-3}$. The world average for the ELCR is set at 0.29 $\times 10^{-3}$ (Abdullahi et al., 2019; Al Shaaibi et al., 2023; Mohammed and Ahmed, 2017). This means that, even though the ELCR coefficient is higher than the world average (Table 1) on some beaches from GC (El Inglés Beach, Maspalomas and San Agustín), the ELCR is below the world average value on most of the beaches of the Eastern Canary Islands.

4.2.3. Radium equivalent

The Radium equivalent activity (Ra_{eq}) calculation assumes that the gamma dose rate produced by 370 Bq kg^{-1} of ^{226}Ra, 259 Bq kg^{-1} of ^{232}Th or 4810 Bq kg^{-1} of ^{40}K is the same (Beretka and Mathew, 1985). Therefore, it allows the comparation of the radiological risks of different samples combining the activity concentration values of ^{226}Ra, ^{232}Th and ^{40}K it is calculated from equation (4) (Beretka and Mathew, 1985; Elisha et al., 2013):

$$Ra_{eq} = A_{Ra} + 1.43A_{Th} + 0.077A_K \quad (4)$$

where A_{Ra}, A_K and A_{Th} are the respective activity concentrations of ^{226}Ra, ^{40}K and ^{232}Th in Bq kg^{-1}. In the case of the beaches on the Eastern Canary Islands, the values of the Ra_{eq} ranged between 6.63 and 151.06 Bq kg^{-1} with a mean value of 44.08 Bq kg^{-1}. These values are comparable with values found in other parts of the world, such as the Mediterranean coast from Egypt where Ra_{eq} ranged between 38.7 and 116.3 Bq kg^{-1} in beach sand samples with a mean value of 61.1 Bq kg^{-1} (Awad et al., 2022). Additionally, some of the results obtained in this work for Ra_{eq} are two or three times higher than other values that can be found around the world, like in the work of (Khandaker et al., 2019) where Ra_{eq} ranged between 37 and 50 Bq kg^{-1} and a mean value of 45.4 Bq kg^{-1} was reported. However, all values obtained in this world are below the safe limit of 370 Bq kg^{-1} (Beretka and Mathew, 1985).

4.3. Differences in the radiological hazard indices between the different Eastern Canary Islands

As mentioned in Subsection 4.2 (*Radiological risk assessment*), the radiological risk indices ranged widely between the beaches studied, with some of them having very low values and others having values higher than the world average. In fact, when comparing the mean hazard indices obtained for each island (Table 1), it can be seen that the mean values on the island of GC are considerably higher than the other islands, sometimes up to more than four times higher. In order to evaluate whether the differences found between the islands were significant, a Kruskal-Wallis test (Theodorsson-Norheim, 1986) and a Wilcoxon-rank sum test (Rosner and Glynn, 2009) were used. The results of these tests are represented in Table 2 and it can be seen that all of the radiological hazard index values obtained in GC were significantly different from the values obtained on the other islands. In addition, the values from LZ also showed significant differences from the values obtained from FV.

Fig. 3 shows the mean absorbed dose rate for each of the beaches studied, along with the geological map of the Eastern Canary Islands. The lithology on the geological map is represented following the same classification that Briones et al. (2023) obtained from the lithostratigraphic map of the Canary Islands, produced by the Spanish Geological and Mining Institute (I.G.M.E., 2021). According to this classification, the term 'Acidic' refers to intermediate and acid rocks such as phonolites, trachytes, trachybasalts, rhyolites, and syenites (and deposits formed from these rocks). The 'Basic' group includes basalts, basanites, tephrites, and phonolitic tephrites (and deposits formed from these rocks). 'Clays' include lake soils and sandy-clay soils. The term 'Deposits' refers to sand deposits and debris of generally variable

Table 2
Result of the Kruskal-Wallis test for identifying significant differences in the radiological hazard indices and the activity concentration values of ^{226}Ra, ^{232}Th and ^{40}K obtained for each sample and grouped by the island where they are located. The result of the p-value for the Wilcoxon rank sum test is also displayed in brackets to identify the groups that present significant differences between them.

Radiological hazard indices	Kruskal-Wallis p-value	Wilcoxon rank sum test
Absorbed dose rate (D)	5.1×10^{-15}	LZ-FV (5.0×10^{-3}) GC-LG (1.4×10^{-8}) GC-LZ (1.9×10^{-14}) GC-FV (2.4×10^{-15})
Annual effective dose (AEDE)	5.1×10^{-15}	LZ FV (5.0×10^{-3}) GC-LG (1.4×10^{-8}) GC-LZ (1.9×10^{-14}) GC-FV (2.4×10^{-15})
Excess life cancer risk (ELCR)	5.1×10^{-15}	LZ-FV (5.0×10^{-3}) GC-LG (1.4×10^{-8}) GC-LZ (1.9×10^{-14}) GC-FV (2.4×10^{-15})
Radium equivalent (Ra_{eq})	4.4×10^{-15}	LZ-FV (4.3×10^{-3}) GC-LG (1.4×10^{-8}) GC-LZ (2.3×10^{-14}) GC-FV (1.8×10^{-15})
^{226}Ra	7.7×10^{-14}	LZ-FV (4.1×10^{-9}) GC-LG (1.3×10^{-4}) GC-LZ (1.1×10^{-4}) GC-FV (3.2×10^{-15})
^{232}Th	7.1×10^{-15}	LZ-FV (1.1×10^{-2}) GC-LG (1.4×10^{-8}) GC-LZ (7.3×10^{-10}) GC-FV (1.8×10^{-15})
^{40}K	4.9×10^{-14}	GC-LG (2.1×10^{-5}) GC-LZ (2.8×10^{-11}) GC-FV (2.3×10^{-13})

Kruskal-Wallis p-value 0.05.
Wilcoxon rank sum test 0.05.

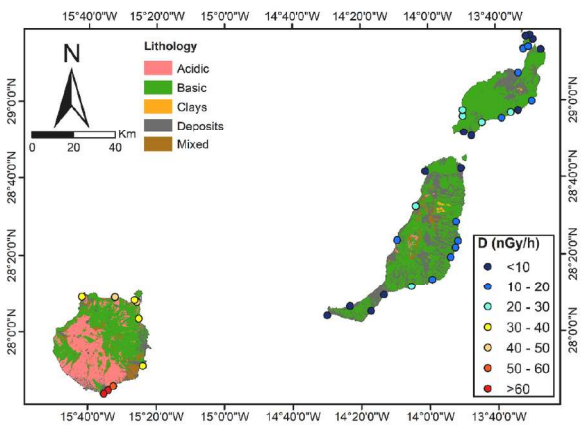

Fig. 3. Map of the mean absorbed dose rate (D) in nGy h^{-1} in each beach area studied combined with the geological map of the Eastern Canary Islands.

composition, depending on the surrounding lithology. Finally, the group labelled 'Mixed' includes lithology that combines volcanic rocks from the Acidic and Basic groups without the possibility of differentiating them.

When comparing the doses obtained for each island, by the different lithologies, it can be seen that the doses on GC are higher than for the rest of the islands. Regarding the lithology, GC also presents the highest content of acidic rocks, while LG, LZ and FV have a mostly basic lithology. As mentioned in Subsection 4.1 (*Activity concentration of ^{226}Ra, ^{232}Th and ^{40}K in the samples*), the acidic lithology was found to have higher contents of ^{226}Ra, ^{232}Th and ^{40}K. Hence, the external hazard indices, which are calculated from the activity concentration values of ^{226}Ra, ^{232}Th and ^{40}K, would be higher in these types of volcanic rocks. It can be seen that, in the southern parts of GC, where most of the acidic rocks are located, the highest absorbed dose rates can be found, these values being above the world mean value of 57 nGy h^{-1} (UNSCEAR, 2000). This suggests that, for the beaches of the Eastern Canary Islands, the radiological hazard indices highly depend on the lithology of the sediments that comprise the sand. This is similar to some of the beaches in Brazil and Malaysia (Shuaibu et al., 2017; Vasconcelos et al., 2011), where the presence of monazite caused high activity concentration values of ^{232}Th and, thus, the absorbed dose rates were higher than the world average.

In the case of LZ and FV, even though some significant differences were found for these islands when observing the map in Fig. 3, the absorbed dose rate differences were not as strong as those found for GC and the other islands. This is because the types of rocks that can be found in Lanzarote and Fuerteventura are similar and thus these significant differences could not be explained in relation to the changes in geology between the islands. To better understand why these differences appeared, a Kruskall-Wallis and a Wilcoxon-rank sum test were also performed to the activity concentration values of ^{40}K, ^{226}Ra and ^{232}Th found in each island (Table 2) to assess which radionuclide was responsible for the significant differences in the radiological hazard indices between FV and LZ. The results show that these two islands presented significant differences only in the activity concentration values of ^{226}Ra and ^{232}Th with a p-value from the Wilcoxon-rank sum test of 4.1×10^{-9} and 1.1×10^{-2} respectively. Considering that the highest activity concentration value of ^{226}Ra was found in Playa Honda (29 ± 1 Bq kg^{-1}) and the maximum activity concentration of ^{232}Th (20.7 ± 1.0 Bq kg^{-1}) was found in Playa Quemada (both beaches located in the most populated coast of LZ), it seems that the differences in absorbed dose rate between LZ and FV could be related to some anthropogenic influences. However, further studies are necessary to better understand the significant differences between these two islands.

5. Conclusions

A baseline of the environmental background radioactivity has been established for beaches of the Eastern Canary Island. The activity concentration values of natural radionuclides ^{226}Ra, ^{232}Th and ^{40}K in intertidal sand samples were analyzed and the radiological hazard indices associated to them were calculated. The mean absorbed dose rate had a value of 20.8 nGy h^{-1}, the mean annual effective dose was 0.025 mSv y^{-1}, the mean Excess life cancer risk value was of 0.11×10^{-3} and the mean radium equivalent obtained was 44.08 Bq kg^{-1}. All these values were below the international accepted limit for each radiological hazard index. Moreover, no ^{137}Cs was detected above the MDA. Thus, the beaches of the Eastern Canary Island do not pose a radiological risk for the public. Additionally, the activity concentration values of ^{226}Ra, ^{232}Th and ^{40}K, as well as the radiological hazard indices associated to them, were significantly higher in Gran Canaria than in the other islands. This seems to be due to the presence of lithologies with high activity concentrations of natural radionuclides, such as phonolites or trachytes, in Gran Canaria. In the case of Lanzarote and Fuerteventura, significant differences were also found between the islands, with Lanzarote presenting significantly higher radiological hazard indices and activity concentration values of ^{226}Ra and ^{232}Th. The lithologies in Lanzarote and Fuerteventura are similar and, considering that the highest activity concentration values of ^{226}Ra and ^{232}Th are present in the most urbanized coast of Lanzarote, it seems that these differences could be related to the anthropogenic pressure that the coast of Lanzarote has already suffered. Finally, this study establishes a methodology to determine the baseline levels of environmental background radioactivity in sandy beaches from volcanic oceanic islands. In addition, it provides a useful tool for authorities to detect future radiological

impacts on the coastal areas of the islands.

Author contributions statement

Ana del Carmen Arriola-Velásquez: methodology, formal analysis, investigation, writing - original draft, visualization. **Alicia Tejera**: methodology, investigation, supervision. **Héctor Alonso**: investigation. **Neus Miquel-Armengol**: data curation. **Jesús G. Rubiano**: conceptualization, supervision. **Pablo Martel**: conceptualization, methodology, investigation, writing - review & editing, supervision.

Declaration of competing interest

The authors declare that they have no known competing financial interests or personal relationships that could have appeared to influence the work reported in this paper.

Data availability

Data are available in the supplementary material file.

Acknowledgments

The lithostratigraphic maps were obtained from Cartografía Digital del Mapa Geológico y Continuo de España (GEODE) and were supplied by Instituto Geológico y Minero de España (I.G.M.E.).

Appendix A. Supplementary data

Supplementary data to this article can be found online at https://doi.org/10.1016/j.envpol.2023.122809.

References

Abbasi, A., Zakaly, H.M.H., Mirekhtiary, F., 2020. Baseline levels of natural radionuclides concentration in sediments East coastline of North Cyprus. Mar. Pollut. Bull. 161, 111793 https://doi.org/10.1016/j.marpolbul.2020.111793.

Abdullahi, S., Ismail, A.F., Samat, S., 2019. Determination of indoor doses and excess lifetime cancer risks caused by building materials containing natural radionuclides in Malaysia. Nucl. Eng. Technol. 51, 325–336. https://doi.org/10.1016/j.net.2018.09.017.

Akpan, A.E., Ebong, E.D., Ekwok, S.E., Eyo, J.O., 2020. Assessment of radionuclide distribution and associated radiological hazards for soils and beach sediments of Akwa Ibom Coastline, southern Nigeria. Arabian J. Geosci. 13, 753. https://doi.org/10.1007/s12517-020-05727-7/.

Al Shaaibi, M., Ali, J., Tsikouras, B., Masri, Z., 2023. Environmental radioactivity assessment of the Brunei Darussalam coastline of the South China Sea. Environ. Pollut. 323, 121288 https://doi.org/10.1016/j.envpol.2023.121288.

Alfonso, J.A., Pérez, K., Palacios, D., Handt, H., LaBrecque, J.J., Mora, A., Vásquez, Y., 2014. Distribution and environmental impact of radionuclides in marine sediments along the Venezuelan coast. J. Radioanal. Nucl. Chem. 300, 219–224. https://doi.org/10.1007/s10967-014-2999-z.

Alonso, H., 2015. El radón en suelos, rocas, materiales de construcción y aguas subterráneas de las Islas Canarias Orientales. Universidad de Las Palmas de Gran Canaria, Las Palmas de Gran Canaria.

Alonso, H., Cruz-Fuentes, T., Rubiano, J.G., González-Guerra, J., Cabrera, M., del, C., Arnedo, M.A., Tejera, A., Rodríguez-Gonzalez, A., Pérez-Torrado, F.J., Martel, P., 2015. Radon in groundwater of the northeastern gran Canaria aquifer. Water (Basel) 7, 2575–2590. https://doi.org/10.3390/w7062575.

Arnedo, M.A., Tejera, A., Rubiano, J.G., Alonso, H., Gil, J.M., Rodríguez, R., Martel, P., 2013. Natural radioactivity measurements of beach sands in gran Canaria, Canary Islands (Spain). Radiat. Protect. Dosim. 156, 75–86. https://doi.org/10.1093/rpd/nct044.

Arnedo, M.A., Rubiano, J.G., Alonso, H., Tejera, A., González, A., González, J., Gil, J.M., Rodríguez, R., Martel, P., Bolivar, J.P., 2017. Mapping natural radioactivity of soils in the eastern Canary Islands. J. Environ. Radioact. 166, 242–258. https://doi.org/10.1016/j.jenvrad.2016.07.010.

Arriola-Velásquez, A., Tejera, A., Guerra, J.G., Alonso, I., Alonso, H., Arnedo, M.A., Rubiano, J.G., Martel, P., 2019. Spatio-temporal variability of natural radioactivity as tracer of beach sedimentary dynamics. Estuar. Coast Shelf Sci. 231 https://doi.org/10.1016/j.ecss.2019.106476.

Arriola-Velásquez, A.C., Tejera, A., Guerra, J.G., Geibert, W., Stimac, I., Cámara, F., Alonso, H., Rubiano, J.G., Martel, P., 2021. ^{226}Ra, ^{228}Ra and ^{40}K as tracers of erosion and accumulation processes: a 3-year study on a beach with different sediment dynamics. Catena 207, 105705. https://doi.org/10.1016/j.catena.2021.105705.

I.G.M.E., 2021. Cartografía digital del Mapa Geológico y Continuo de España GEODE (Comunidad autónoma de Canarias). Instituto Geológico y Minero de España.

Awad, M., El Mezayen, A.M., El Azab, A., Alfi, S.M., Ali, H.H., Hanfi, M.Y., 2022. Radioactive risk assessment of beach sand along the coastline of Mediterranean Sea at El-Arish area, North Sinai, Egypt. Mar. Pollut. Bull. 177, 113494 https://doi.org/10.1016/j.marpolbul.2022.113494.

Beretka, J., Mathew, P.J., 1985. Natural radioactivity of Australian building materials, industrial wastes and by-products. Health Phys. 48, 87–95.

Bezuidenhout, J., 2013. Measuring naturally occurring uranium in soil and minerals by analysing the 352keV gamma-ray peak of ^{214}Pb using a NaI(Tl)-detector. Appl. Radiat. Isot. 80, 1–6. https://doi.org/10.1016/j.apradiso.2013.05.008.

Bou-Rabee, F., Al-Zamel, A., Al-Fares, R., Bem, H., 2009. Technologically enhanced naturally occurring radioactive materials in the oil industry (TENORM). A review. NUKLEONIKA 54, 3–9.

Briones, C., Jubera, J., Alonso, H., Olaiz, J., Santana, J.T., Rodríguez-Brito, N., Arriola-Velásquez, A.C., Miquel, N., Tejera, A., Martel, P., González-Díaz, E., Rubiano, J.G., 2023. Multiparametric analysis for the determination of radon potential areas in buildings on different soils of volcanic origin. Sci. Total Environ. 885, 163761 https://doi.org/10.1016/j.scitotenv.2023.163761.

Carracedo, J.C., Pérez-Torrado, F.J., Ancochea, E., Meco, J., Hernán, F., Cubas, C.R., Casillas, R., Rodríguez Badiola, E., Ahijado, A., 2002. Cenozoic Volcanism II: Canary Islands. Geological Society.

Chiozzi, P., Pasquale, V., Verdoya, M., Minato, S., 2001. Natural gamma-radiation in the Aeolian volcanic arc. Appl. Radiat. Isot. 55, 737–744.

Elisha, J.J., Yisa, J., Adeyemo, D.J., 2013. Radiological analysis of selected organic fertilizers in zaria local government area council, kaduna state, Nigeria: possible health implications. IOSR J. Appl. Phys. 5, 44–48.

Fernández-Aldecoa, J.C., Robayna, B., Allende, A., Poffijn, A., Hernández-Armas, J., 1992. Natural radiation in Tenerife (canary islands). Radiat. Protect. Dosim. 45, 545–548.

Froehlich, K., 2010. Environmental Radionuclides: Tracers and Timers of Terrestrial Processes, First. ed. Elsevier B.V., Amsterdam. https://doi.org/10.1016/S1569-4860(09)01613-1.

Guerra, J.G., Rubiano, J.G., Winter, G., Guerra, A.G., Alonso, H., Arnedo, M.A., Tejera, A., Gil, J.M., Rodríguez, R., Martel, P., Bolivar, J.P., 2015. A simple methodology for characterization of germanium coaxial detectors by using Monte Carlo simulation and evolutionary algorithms. J. Environ. Radioact. 149, 8–18. https://doi.org/10.1016/j.jenvrad.2015.06.017.

Guerra, J.G., Rubiano, J.G., Winter, G., Guerra, G., A, Alonso, H., Arnedo, M.A., Tejera, A., Martel, P., Bolivar, J.P., 2017. Computational characterization of HPGe detectors useable for a wide variety of source geometries by using Monte Carlo simulation and a multi-objective evolutionary algorithm. Nucl. Instrum. Methods Phys. Res. 858, 113–122. https://doi.org/10.1016/j.nima.2017.02.087.

ICRP, 2007. The 2007 Recommendations of the International Commission on Radiological Protection. ELSEVIER.

INE, 2021a. Instituto Nacional de Estadística [WWW Document]. Cifras oficiales de población resultantes de la revisión del Padrón municipal a 1 de enero. URL https://www.ine.es/jaxiT3/Datos.htm?t=2852#!tabs-tabla (accessed July.16.2023).

INE, 2021b. Instiuto Nacional de Estadística [WWW Document]. Indicadores de Mortalidad. URL https://www.ine.es/jaxiT3/Datos.htm?t=1485 (accessed July.14.2023).

INE, 2022. Instituto Nacional de Estadística [WWW Document]. Movimientos Turísticos en Fronteras. URL https://www.ine.es/jaxiT3/Datos.htm?t=23988 (accessed July.16.2023).

Jaffary, Md, N, A., Khoo, K.S., Mohamed, N.H., Yusof, M.A.W., Mohd Fadzil, S., 2019. Malaysian monazite and its processing residue: chemical composition and radioactivity. J. Radioanal. Nucl. Chem. 322, 1097–1105. https://doi.org/10.1007/s10967-019-06813-1.

Khandaker, M.U., Garba, N.N., Rohaizad, C.A.H.b.C., Bradley, D.A., 2019. Assessment of natural radioactivity levels in stony sand from black stone beach of kuantan, the peninsular Malaysia. Radioprotection 54, 211–218. https://doi.org/10.1051/radiopro/2019024.

Kolo, M.T., Aziz, S.A.B.A., Khandaker, M.U., Asaduzzaman, K., Amin, Y.M., 2015. Evaluation of radiological risks due to natural radioactivity around Lynas Advanced Material Plant environment, Kuantan, Pahang, Malaysia. Environ. Sci. Pollut. Control Ser. 22, 13127–13136. https://doi.org/10.1007/s11356-015-4577-5.

Le Bas, M.J., Le Maitre, R.W., Streckeisen, A., Zanettin, B., 1986. A chemical classification of volcanic rocks based on the total alkali-silica diagram. J. Petrol. 27, 745–750.

Licínio, M.V., Alencar, A.S. de, Lima, A.C., de Freitas, A.C., 2021. Natural radioactivity at beach sands in ilha grande, southeastern Brazil. J. Radioanal. Nucl. Chem. 327, 1277–1281. https://doi.org/10.1007/s10967-020-07587-7.

MarineTraffic, 2023. MarineTraffic: Global Ship Tracking Intelligence | AIS Marine Traffic [WWW Document]. URL https://www.marinetraffic.com/en/ais/home/centerx:-13.9/centery:28.2/zoom:8 (accessed July.16.2023).

Mohammed, R.S., Ahmed, R.S., 2017. Estimation of excess lifetime cancer risk and radiation hazard indices in southern Iraq. Environ. Earth Sci. 76 https://doi.org/10.1007/s12665-017-6616-7.

Rao, N.S., Sengupta, D., Guin, R., Saha, S.K., 2009. Natural radioactivity measurements in beach sand along southern coast of Orissa, Eastern India. Environ. Earth Sci. 59, 593–601. https://doi.org/10.1007/s12665-009-0057-x.

Ravisankar, R., Chandramohan, J., Chandrasekaran, A., Prince Prakash Jebakumar, J., Vijayalakshmi, I., Vijayagopal, P., Venkatraman, B., 2015. Assessments of radioactivity concentration of natural radionuclides and radiological hazard indices in sediment samples from the East coast of Tamilnadu, India with statistical

approach. Mar. Pollut. Bull. 97, 419–430. https://doi.org/10.1016/j.marpolbul.2015.05.058.

Rosner, B., Glynn, R.J., 2009. Power and sample size estimation for the wilcoxon rank sum test with application to comparisons of C statistics from alternative prediction models. Biometrics 65, 188–197. https://doi.org/10.1111/j.1541-0420.2008.01062.x.

Shapiro, S.S., Wilk, M.B., 1965. An analysis of variance test for normality (complete samples). Biometrika 52, 591–611. https://doi.org/10.2307/2333709.

Shuaibu, H.K., Khandaker, M.U., Alrefae, T., Bradley, D.A., 2017. Assessment of natural radioactivity and gamma-ray dose in monazite rich black Sand Beach of Penang Island, Malaysia. Mar. Pollut. Bull. 119, 423–428. https://doi.org/10.1016/j.marpolbul.2017.03.026.

Thangam, V., Rajalakshmi, A., Chandrasekaran, A., Arun, B., Viswanathan, S., Venkatraman, B., Bera, S., 2022. Determination of natural radioactivity in beach sands collected along the coastal area of Tamilnadu, India using gamma ray spectrometry. J. Radioanal. Nucl. Chem. 331, 1207–1223. https://doi.org/10.1007/s10967-022-08193-5.

Theodorsson-Norheim, E., 1986. Kruskal-Wallis test: BASIC computer program to perform nonparametric one-way analysis of variance and multiple comparisons on ranks of several independent samples. Comput. Methods Progr. Biomed. 23, 57–62. https://doi.org/10.1016/0169-2607(86)90081-7.

Tichavska, M., Tovar, B., 2015. Environmental cost and eco-efficiency from vessel emissions in Las Palmas Port. Transp Res E Logist Transp Rev 83, 126–140. https://doi.org/10.1016/j.tre.2015.09.002.

UNSCEAR, 2000. Sources and effects of ionizing radiation. Report of the United Nations Scientific Committee on the Effects of Atomic Radiation to the General Assembly, with Scientific Annexes. United Nations, New York.

UNSCEAR, 2008. Sources and effects of ionizing radiation. Report of the United Nations Scientific Committee on the Effects of Atomic Radiation to the General Assembly, with Scientific Annexes. United Nations, New York.

Vasconcelos, D.C., Pereira, C., Oliveira, A.H., Santos, T.O., Rocha, Z., de, B.C., Menezes, M.A., 2011. Determination of natural radioactivity in beach sand in the extreme south of Bahia , Brazil , using gamma spectrometry. Radiat. Protect. Environ. 34, 178–184.

Vineethkumar, V., Akhil, R., Shimod, K.P., Prakash, V., 2020. Geospatial analysis of the source of monazite deposits and the dynamics of natural radionuclides in the selected coastal environs of Kerala, south west coast of India. J. Radioanal. Nucl. Chem. 326, 983–996. https://doi.org/10.1007/s10967-020-07418-9.

Zakaly, H.M.H., Uosif, M.A.M., Issa, S.A.M., Tekin, H.O., Madkour, H., Tammam, M., El-Taher, A., Alharshan, G.A., Mostafa, M.Y.A., 2021. An extended assessment of natural radioactivity in the sediments of the mid-region of the Egyptian Red Sea coast. Mar. Pollut. Bull. 171, 112658 https://doi.org/10.1016/j.marpolbul.2021.112658.

Además del estudio llevado a cabo en las Islas Canarias Orientales, en 2013 se publicó un trabajo en el que únicamente se estudió el contenido de ^{226}Ra, ^{232}Th, ^{40}K y ^{137}Cs en arenas de playas de Gran Canaria, así como un análisis del impacto radiológico existente en dichas playas (Arnedo et al., 2013). En ese trabajo se analizaron siete playas; Las Canteras (LC), Las Alcaravaneras (LA) y La Laja (LL) en el norte de la isla, San Borondón (SB) y La Garita en el este y Maspalomas (M) y Playa del Inglés (EI) en el sur de la isla. En la tabla 3 se muestran los rangos y valores medios de concentraciones de actividad del ^{226}Ra, el ^{228}Ra y el ^{40}K obtenidos para cada playa, así como los valores de estos radionucleidos en los suelos de Gran Canaria (GC).

Playa	^{226}Ra		^{232}Th		^{40}K	
	Rango	Media	Rango	Media	Rango	Media
LC	7 - 19	14	7 - 25	15	83 - 629	390
LA	13 - 17	15	14 -26	19	393 - 726	550
LL	16 - 23	19	19 - 31	24	299 - 584	439
SB	22 - 30	26	25 - 35	30	417 - 640	529
LG	23 - 27	25	24 - 29	27	437 - 480	459
EI	14 - 29	23	12 - 42	31	206 - 1055	726
M	12 - 19	16	11 - 24	17	213 - 565	398
GC	7 - 88	35	6 - 139	48	27 - 1758	625

Tabla 3. Valores medios y rangos de las concentraciones de actividad de ^{226}Ra, ^{232}Th y ^{40}K en Bq kg^{-1} obtenidos para distintas playas de la isla de Gran Canaria. Modificado de Arnedo et al., (2013).

Los resultados mostraron que en la mayoría de las playas estudiadas las concentraciones de actividad del ^{226}Ra, el ^{232}Th y el ^{40}K variaban bastante, habiendo casos como en playa del Inglés donde los valores de concentración de actividad para el ^{40}K podía alcanzar los 1055 Bq kg^{-1}. En el caso de la playa de Las Canteras, los rangos obtenidos para la concentración de actividad del ^{226}Ra, el ^{232}Th y el ^{40}K también eran

bastante amplios, habiendo muestras que presentaban concentraciones de actividad de estos tres radionucleidos tres veces más altas que otras. Cabe destacar que en esta playa existe una parte totalmente expuesta a la acción del oleaje y otra parte protegida frente a ella. Por tanto, las diferencias obtenidas en las muestras de LC parecían estar vinculadas con una variabilidad espacial de las concentraciones de actividad del ^{226}Ra, el ^{232}Th y el ^{40}K que podría estar relacionada o no con las dinámicas sedimentarias de la playa.

Además de estos resultados, en el estudio de Arnedo et al., (2013) también se estudiaron y compararon las actividades del ^{226}Ra, el ^{232}Th y el ^{40}K en las arenas superficiales (0-5 cm) y profundas (20 – 30 cm) de la zona intermareal de cada playa. Los resultados mostraron que en general las arenas superficiales presentaban menores actividades que las arenas profundas. Los autores de dicho trabajo explicaron que esto se podía deber al transporte y la acumulación de sedimentos que contienen estos radionucleidos en la zona intermareal gracias a la acción de oleaje y de la marea. De acuerdo con esta explicación, una vez depositados los sedimentos en la zona intermareal, se produciría un enterramiento que transportase los radionucleidos contenidos en ellos hacia las zonas profundas de la columna de sedimento y por eso las arenas recogidas a mayor profundidad presentaban actividades más altas.

Por otro lado, en este estudio de 2013 también se analizaron las diferencias en las actividades encontrada de ^{226}Ra, ^{232}Th y ^{40}K en arenas de la zona seca y la zona intermareal (arena húmeda) de cada playa. Los resultados mostraron que en las playas más abiertas a la influencia de las corrientes como La Laja, Playa del Inglés y Maspalomas, las actividades eran mayores en la zona intermareal (Fig. 2).

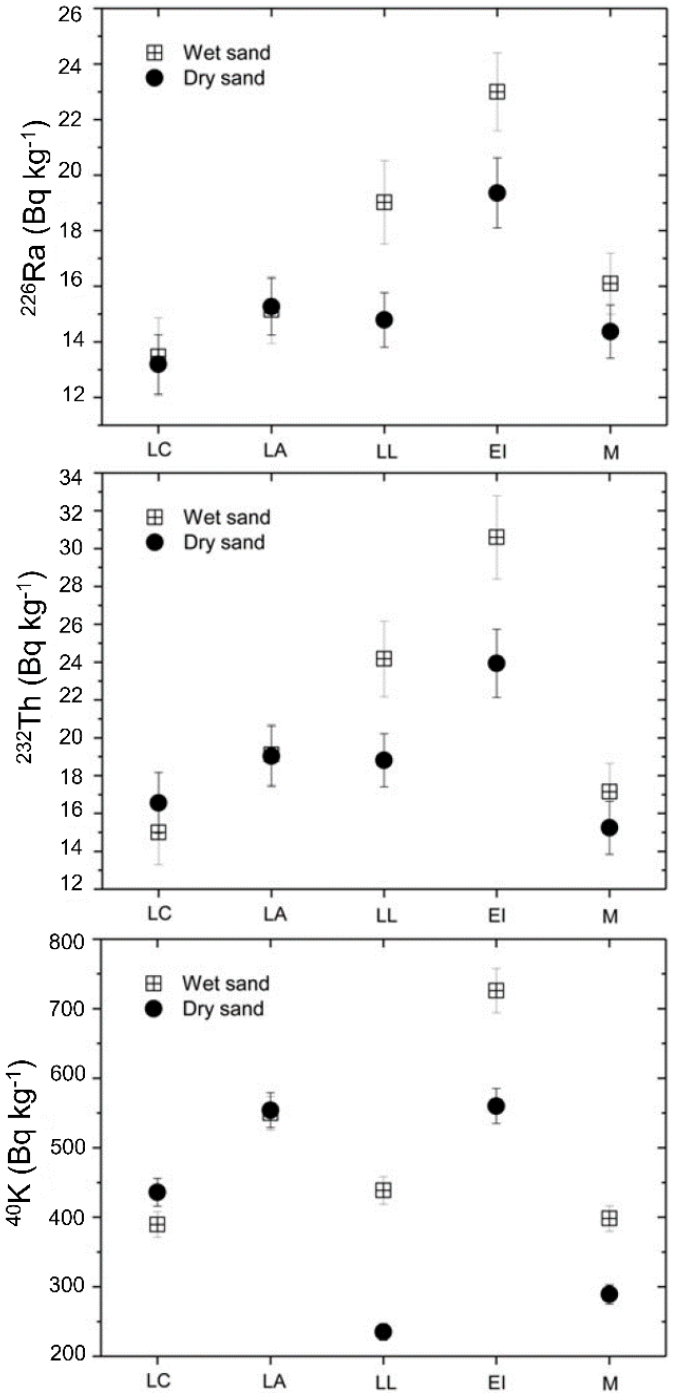

Fig. 2. Actividades de ^{226}Ra, ^{232}Th y ^{40}K en arena seca y húmeda de distintas playas de Gran Canaria. Modificado de (Arnedo et al., 2013).

Estos resultados junto a las diferencias encontradas entre la arena superficial y la arena profunda de la zona intermareal indicaron que las dinámicas marinas afectan a las concentraciones de actividad que se encuentra en los sedimentos de las playas de Gran Canaria. Por tanto, las playas de la isla podría ser objeto de estudio para evaluar el papel que tienen los radionucleidos naturales como trazadores de dinámica sedimentaria marina.

En resumen, los datos existentes previos a esta tesis de playas de las Islas Canarias Orientales sirvieron para establecer que las concentraciones de actividad de los radionucleidos naturales ^{226}Ra, ^{232}Th y ^{40}K en las arenas de Gran Canaria estaban relacionadas con el origen litológico de los sedimentos. Además, tanto en el estudio de Arnedo et al., (2013) como en el trabajo publicado para esta tesis se encontraron actividades menores en la parte de la playa de Las Canteras abierta a la acción del oleaje que en la parte protegida frente al mismo. Por tanto, los resultados obtenidos en estos trabajos sirvieron para seleccionar la playa de Las Canteras como región de estudio y plantaron la semilla que impulsó el desarrollo de esta tesis.

1.5. Dinámica y composición sedimentaria de La Bahía del Confital y la playa de Las Canteras

Como área de estudio de esta investigación se eligió la Bahía del Confital y la playa de Las Canteras, la cual forma parte de la bahía (Fig. 3).

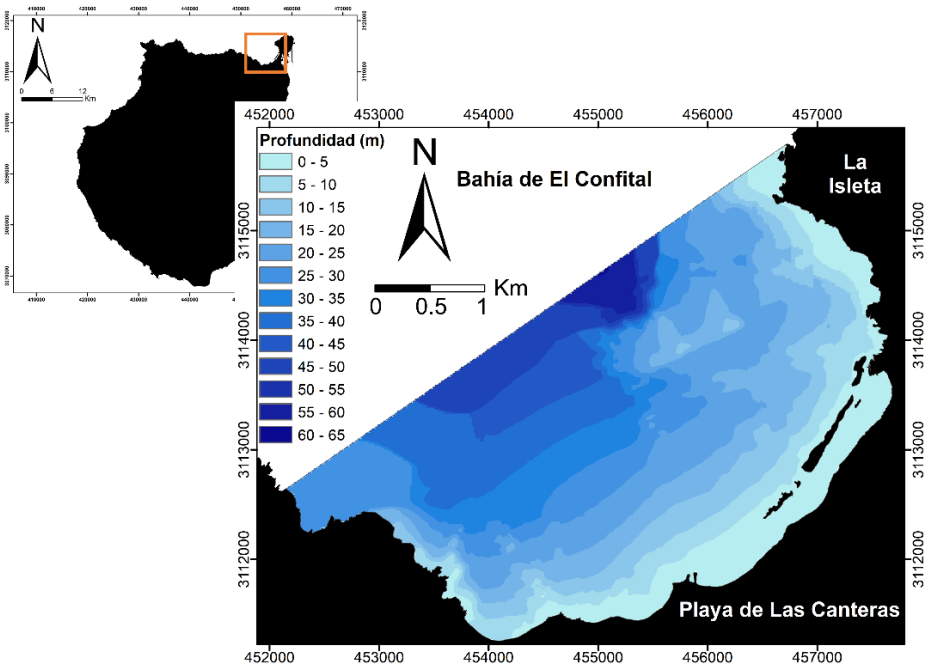

Fig. 3. Localización y batimetría de la Bahía del Confital. Las coordenadas están en el sistema UTM.

Por un lado, la Bahía del Confital tiene un tamaño de alrededor de 10 km^2 y se localiza en el norte de Gran Canaria en la ciudad de Las Palmas de Gran Canaria. Un estudio sedimentario previo realizado en la zona (Medina et al., 2006) describió que tanto el tamaño de grano como la naturaleza del sedimento es diferente en las distintas partes de la bahía (Fig. 4). De acuerdo con ese trabajo, el tamaño de grano varía de 0.13 a 3.66 mm, encontrándose los tamaños de grano medio mayores en las zonas noreste y suroeste de la bahía (Fig. 4A). En cuanto a la naturaleza

del sedimento, el contenido de carbonatos (Fig. 4B) es mayor en el noreste de la bahía, indicando que en esa zona se encuentran sedimentos que en su mayoría son de composición calcárea y orgánica. Otros estudios de la zona indicaron que, por el contrario, los sedimentos que predominan en la zona suroeste de la bahía tienen una naturaleza más terrígena e incluyen sedimentos provenientes de rocas fonolíticas y basálticas y tienen un bajo contenido en carbonatos (Balcells et al., 1990; Mangas and Julià-Miralles, 2015; Medina et al., 2006; Schmincke, 1993).

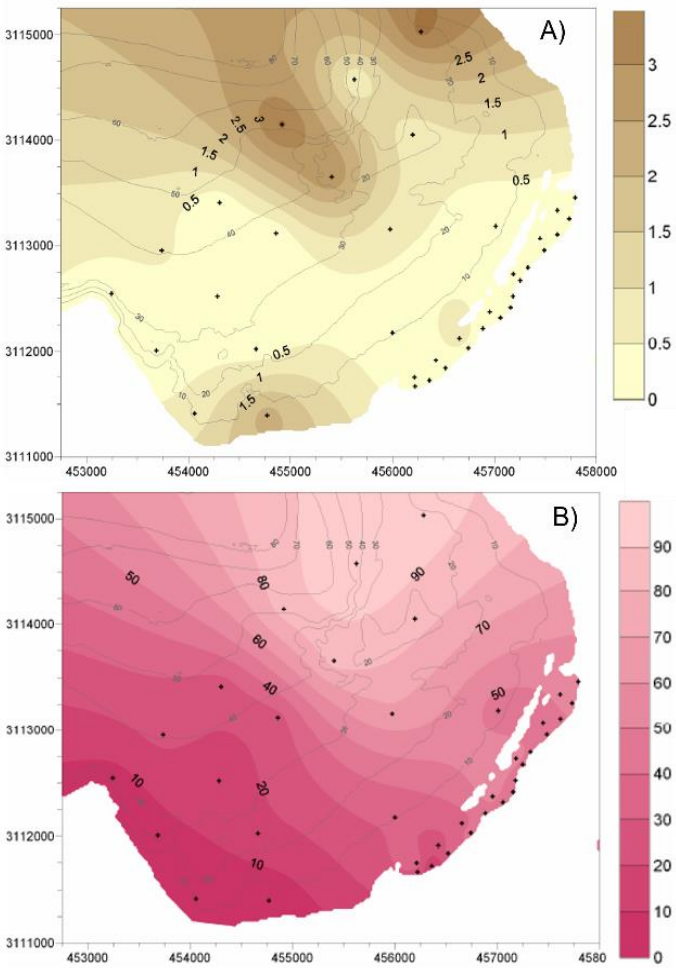

Fig.4. Distribución de A) tamaño de grano en mm y B) contenido de carbonatos en porcentaje en la Bahía del Confital. Modificado de Medina et al., (2006).

Por otro lado, la playa de Las Canteras es una playa de aproximadamente 3 km localizada en el sureste de la Bahía del Confital. Esta playa está dividida en tres arcos (norte, central y sur) y presenta una protección parcial proporcionada por una barra rocosa calcarenítica que se localiza enfrente del arco norte y arco central de la playa (Fig. 5). Esta barra no es un bloque completo, sino que presenta aberturas y fragmentaciones que son más notorias enfrente del arco central. La dirección del viento predominante en la playa es NNE, NE y ENE debido a los vientos alisios. La dirección de aproximación del oleaje predominante es del norte y durante eventos tormentosos del NW (Alonso, 2005, 1993). Esta playa ha sido ampliamente estudiada previamente y, por tanto, se puede encontrar en la bibliografía una descripción íntegra tanto de sus características sedimentarias, así como de las diferentes dinámicas sedimentarias que presenta en sus distintas partes.

De acuerdo con la literatura, los sedimentos que conforman la arena de la playa de Las Canteras tienen un tamaño entre 0.2 y 0.5mm, siendo los arcos norte y central los que presentan mayor tamaño (Alonso, 1993; Medina et al., 2006). El origen de estos sedimentos se localiza en el entorno geológico de la playa. Éste incluye rocas básicas de la isleta localizada en el noreste de la Bahía del Confital, la barra rocosa calcarenítica localizada enfrente de la playa, diferentes rocas volcánicas y magnetitas que llegan a través del Barranco de la Ballena en la parte sur de la playa y los bancos de arena sumergidos localizados en la Bahía del Confital (Balcells et al., 1990; Schmincke, 1993).

Fig. 5. Playa de Las Canteras y sus distintas partes. Coordenadas están dadas en el sistema UTM.

En cuanto a la naturaleza de estos sedimentos, varios estudios de calcimetría y petrología han permitido diferenciar los distintos materiales que componen la arena que se encuentra en la playa. En el arco norte, la arena presenta principalmente bioclastos y material calcáreo que podrían provenir de la zona noreste de la bahía llegando a la playa a través de las aberturas de la barra (Medina et al., 2006). Además, otros estudios indican que la arena del arco norte también presenta fragmentos de calcarenitas con un importante contenido de feldespatos en su componente terrígena (Alonso, 1993; Alonso and Pérez Torrado, 1992).

En el caso del arco sur, la acumulación de bioclastos y sedimentos carbonatados es menor y aumenta la presencia de sedimentos de origen terrígeno que provienen mayormente de la boca del barranco que desemboca allí. Entre estos materiales predominan los clinopiroxenos, anfíboles, óxidos de hierro y otros minerales pesados como, por ejemplo, los olivinos (Alonso, 1993; Alonso and Pérez Torrado, 1992; Medina et al., 2006). A esta zona de la playa también llegan líticos más ligeros como feldespatos, pero estos se redistribuyen a lo largo de la playa acorde a la dinámica sedimentaria de la zona (Alonso, 1993; Alonso and Pérez Torrado, 1992). En el caso de los feldespatos, además, se produce una particularidad y es que, con independencia de la época del año y la zona de la playa en la que aparezcan inicialmente, siempre tienden a transportarse y acumularse en la zona norte de la playa. La explicación a esto se puede encontrar en la forma del grano en la que se fragmentan. Estos minerales adquieren una forma laminar más hidrodinámica que, junto a su baja densidad, favorece su transporte y acumulación en zonas protegidas de la playa (Alonso, 1993). El arco central es una zona intermedia donde se puede encontrar una mezcla de materiales que se encuentran en el arco sur y en el arco norte.

En lo que a la dinámica sedimentaria se refiere, la playa de Las Canteras presenta variación estacional y dos tipos de dinámicas distintas influenciadas por la presencia o ausencia de la barra (Alonso, 2005, 1994, 1993; Alonso and Vilas, 1996). Por un lado, durante eventos de erosión se produce una pérdida de arena del arco sur (zona totalmente expuesta a la acción del oleaje) que es retirada de la playa por la acción del oleaje y posteriormente se transporta longitudinalmente dirección al arco norte. En los periodos de acreción, en cambio, el arco sur recibe un

incremento de arena proveniente del entorno de la playa (Alonso, 2005, 1994, 1993; Alonso and Vilas, 1996).

Por otro lado, el arco norte se encuentra bajo un periodo constante de acumulación de sedimentos. Esto se debe fundamentalmente a dos causas. Por un lado, antiguamente se producía un transporte eólico que trasladaba la arena que llegaba al arco norte hacia la zona del actual puerto en el este de la ciudad. Al edificarse la ciudad y construirse bloques de apartamentos en esa parte de la playa se interrumpió este transporte generando una acumulación de sedimentos en el arco norte de la playa. Por otro lado, la presencia de la barra localizada enfrente de la playa protege esta zona frente eventos erosivos. De esta manera, apenas se produce erosión del sedimento en esa zona en comparación con el arco sur y se favorece la acumulación de sedimentos en esta zona durante todo el año.

Considerando todo lo descrito en este apartado, se podría decir que la región de estudio seleccionada es un laboratorio natural idóneo para evaluar en profundidad el uso de radionucleidos naturales como trazadores de procesos de erosión, transporte y acumulación de sedimentos costeros. Esto se debe a que, al ser una zona con contenido sedimentario tan heterogéneo y dinámicas tan diversas, es de esperar que los resultados que se obtengan en este trabajo sean extrapolables a otras partes del mundo. De esta manera, los resultados de esta tesis podrían afianzar el conocimiento que se tiene de los radionucleidos naturales como trazadores de dinámicas sedimentarias.

CAPÍTULO 2. Objetivos de la tesis y trabajos publicados

2.1. Objetivos de la tesis

El objetivo principal de esta tesis consiste en realizar un análisis de la viabilidad de radionucleidos naturales presentes en el sedimento como trazadores de procesos de erosión, transporte y acumulación de sedimentos en zonas costeras. De esta manera, se pretende obtener un conjunto de radionucleidos naturales que puedan ser aplicados en distintas partes del mundo a la vez que se obtendrá una metodología de aplicación de dichos radiotrazadores. Para poder cumplir con este objetivo general, los objetivos específicos son:

1. **Realizar un análisis de la variabilidad espacio-temporal de la actividad de los radionucleidos naturales presentes en arenas de la playa de Las Canteras.** Se recogerán muestras de arena superficial en la zona intermareal de la playa una vez al mes durante un periodo de 3 años. Las muestras serán recogidas en 10 estaciones de muestreo repartidas a lo largo de la zona intermareal de la playa para asegurar que las muestras estudiadas están influenciadas por la dinámica marina que afectan a la playa. Cada muestra será analizada por espectrometría gamma para poder obtener la actividad de los radionucleidos primordiales presentes en ellas. Una vez obtenidas estas actividades se estudiará cómo varían a lo largo de la playa y del tiempo mediante el uso de diversos análisis estadísticos.
2. **Analizar la dependencia de las variaciones de los radionucleidos naturales con diferentes propiedades del sistema de estudio.** Para cada campaña se obtendrán los diversos datos meteorológicos, atmosféricos y oceanográficos en el momento de muestreo a través de medidas durante el muestreo y los datos históricos obtenidos de la web de Puertos del Estado y

de la Red de Control y Vigilancia de Calidad del Aire del Gobierno de Canarias. Se estudiarán las relaciones existentes entre los cambios en estos parámetros y los cambios encontrados en las actividades de los radionucleidos naturales presentes en las muestras. Esto permitirá entender mejor la influencia de distintos agentes erosivos que afectan a la región de estudio en los cambios de concentración de actividad encontrados.

3. **Estudiar las posibles relaciones existentes entre las características del sedimento y las actividades obtenidas en distintas muestras.** Se realizarán distintos análisis con el fin de obtener los datos granulométricos y de composición mineralógica de diversas muestras de arena tanto de la playa de Las Canteras como de la Bahía del Confital. Con los resultados obtenidos se estudiarán las correlaciones que puedan existir entre el tamaño de grano y la composición mineralógica con las distintas concentraciones de actividad que se encuentran en las muestras. Esto permitirá estudiar si las diferentes actividades presentes en cada tipo de sedimento dependen exclusivamente del tamaño de su grano o si existen otras características que influyen en dichas diferencias.
4. **Aplicar los radionucleidos naturales para trazar las diferentes dinámicas sedimentarias submarinas que ocurren en la Bahía del Confital.** Tras verificar el uso de los radionucleidos naturales como trazadores de los procesos de erosión, transporte y acumulación de sedimentos en la zona intermareal de la playa de Las Canteras, se aplicarán estos radionucleidos en la zona submarina de la playa y el resto de la bahía. Esto permitirá comprobar que los radionucleidos naturales

estudiados no solo se pueden utilizar en la zona intermareal de las playas sino que su uso se puede extender a otros entornos costeros como puede ser la parte sumergida de una bahía.

2.2. Presentación de los trabajos publicados y justificación de la unidad temática

Esta tesis está conformada por los siguientes artículos:

1) **Arriola-Velásquez, A. C.**, Tejera, A., Alonso, H., Miquel-Armengol, N., Rubiano, J.G., Martel, P. (2024). Radiological risk assessment of beaches from volcanic oceanic islands: A case study of the Eastern Canary Islands (Spain). Environmental Pollution, 340, 122809. https://doi.org/10.1016/j.envpol.2023.122809
2) **Arriola-Velásquez, A.**, Tejera, A., Guerra, J. G., Alonso, I., Alonso, H., Arnedo, M. A., Rubiano, J. G., Martel, P. (2019). Spatio-temporal variability of natural radioactivity as tracer of beach sedimentary dynamics. Estuarine, Coastal and Shelf Science, 231, 106476. https://doi.org/10.1016/j.ecss.2019.106476
3) **Arriola-Velásquez, A. C.**, Tejera, A., Guerra, J. G., Geibert, W., Stimac, I., Cámara, F., Alonso, H., Rubiano, J. G., Martel, P. (2021). ^{226}Ra, ^{228}Ra and ^{40}K as tracers of erosion and accumulation processes: A 3-year study on a beach with different sediment dynamics. CATENA, 207, 105705. https://doi.org/10.1016/j.catena.2021.105705
4) **Arriola-Velásquez, A. C.**, Tejera, A., Alonso, I., Cámara, F., Cantaluppi, M., Alonso, H., Miquel-Armengol, N., Rubiano, J.G., Martel, P. (2023). Natural radionuclides as tracers of coastal

sediment dynamics in El Confital Bay (Spain): spatial distribution and relationships with sediment characteristics. CATENA, 235, 107672. https://doi.org/10.1016/j.catena.2023.107672

El artículo 1, tal y como se ha indicado anteriormente, es una recopilación de datos anteriores al desarrollo de estas tesis correspondientes a muestras recogidas entre 2013 y 2015 en distintas playas de las Islas Canarias Orientales. Los resultados de este artículo, combinados con los de estudios anteriores sobre las actividades de ^{226}Ra, ^{232}Th y ^{40}K en las playas de Gran Canaria se utilizaron para seleccionar la región de estudio de esta tesis.

Los artículos 2, 3 y 4 son los artículos principales de la tesis y en ellos se abordan los distintos objetivos fijados para realizar el estudio de los radionucleidos naturales como trazadores de procesos de erosión, transporte y acumulación de sedimentos costeros. En el artículo 2 se utilizó una serie de datos de 1 año (2016 – 2017) para llevar a cabo un análisis de la variabilidad espacio-temporal de la actividad de los radionucleidos naturales de la zona intermareal de la playa de Las Canteras (Gran Canaria), así como un primer estudio de las relaciones existentes entre las distintas características del sedimento y las concentraciones de actividad encontradas. En el artículo 3 se llevó a cabo un estudio de la variabilidad temporal de los radionucleidos naturales encontrados en la arena intermareal de la misma playa utilizando una serie de datos de 3 años (2016 – 2019). Además, se estudió la influencia de los distintos agentes erosivos que afectan a la playa (como el oleaje y el viento), de los parámetros atmosféricos y del contenido mineralógico de las muestras en las variaciones de actividad de los radionucleidos

naturales. Estos dos artículos sirvieron para verificar la viabilidad de los radionucleidos naturales como trazadores de erosión, transporte y acumulación de sedimentos en la zona intermareal de la playa de Las Canteras.

Finalmente, el artículo 4 se centra en aplicar los radionucleidos naturales estudiados previamente para trazar las distintas dinámicas sedimentarias existentes en la zona sumergida de la playa de Las Canteras y el resto de la Bahía del Confital. Además, se realizó un análisis de la influencia de las distintas características del sedimento en las concentraciones de actividad encontradas. De esta forma, los artículos de esta tesis conforman una unidad temática que presentan una metodología para trazar erosión transporte y acumulación de sedimentos costeros usando los radionucleidos naturales como trazadores.

2.3. Thesis objectives

The main objective of this thesis is to analyse the viability of natural radionuclides contained in coastal sediments as tracers of their erosion, transport and accumulation. This way, the intention is to obtain a set of natural radionuclides that can be applied to other parts of the world while developing a methodology for their application. In order to achieve the main objective, the specific objectives are:

1. **Carry out an analysis of the spatio-temporal variability of the activity of the natural radionuclides present in the sands of Las Canteras Beach.** Superficial sand samples will be collected once a month for 3 years in the intertidal zone of the beach. Samples will be collected in 10 sampling stations located along the intertidal zone of the beach to ensure that the samples are influenced by the marine dynamics that affect the beach. Each sample will be analysed by gamma spectrometry to obtain the activity concentration values of their primordial radionuclides. Once these activities are obtained, different statistical analyses will be used to study their variations with time and along the beach.
2. **Analyse the correlations between the natural radionuclides variations and different properties of the system under study.** For each campaign, meteorological, atmospheric and oceanographic data at the time of sampling will be obtained through direct measurements and from historical data retrieved from the Puertos del Estado and the network of surveillance and control of air quality from the Canary Islands Government web pages. The relationships existing between changes in these parameters and the changes in the activity concentrations of

natural radionuclides will be studied. This way, the influence that the different erosion agents have in the changes of the activity concentrations found will be better comprehended.

3. **Study possible relationships between sediment characteristics and activities obtained in different samples.** Different analyses will be carried out to obtain granulometric and mineralogic data of the samples from Las Canteras Beach and the rest of El Confital Bay. With the results obtained, correlations between sediment grain size and mineralogical content with the activity concentrations found will be studied. This will enable verifying if the variability of activity concentration between samples depends only on their grain size or if other sediment characteristics influence those changes.
4. **Apply natural radionuclides to trace the different submarine sedimentary dynamics occurring in El Confital Bay.** After verifying the use of natural radionuclides as tracers of erosion, transport and accumulation of sediments in the intertidal zone of Las Canteras Beach, these radionuclides will be applied in the submerged part of the beach and the rest of the bay. This will prove that the natural radionuclides studied can not only be used in the intertidal zone of beaches, but their use can be extended to other coastal environments such as the submerged part of a bay.

2.4. Presentation of the published papers and thematic unit justification

The following papers constitute this thesis:

1) **Arriola-Velásquez, A. C.**, Tejera, A., Alonso, H., Miquel-Armengol, N., Rubiano, J.G., Martel, P. (2024). Radiological risk

assessment of beaches from volcanic oceanic islands: A case study of the Eastern Canary Islands (Spain). Environmental Pollution, 340, 122809. https://doi.org/10.1016/j.envpol.2023.122809

2) **Arriola-Velásquez, A.**, Tejera, A., Guerra, J. G., Alonso, I., Alonso, H., Arnedo, M. A., Rubiano, J. G., Martel, P. (2019). Spatio-temporal variability of natural radioactivity as tracer of beach sedimentary dynamics. Estuarine, Coastal and Shelf Science, 231, 106476. https://doi.org/10.1016/j.ecss.2019.106476

3) **Arriola-Velásquez, A. C.**, Tejera, A., Guerra, J. G., Geibert, W., Stimac, I., Cámara, F., Alonso, H., Rubiano, J. G., Martel, P. (2021). ^{226}Ra, ^{228}Ra and ^{40}K as tracers of erosion and accumulation processes: A 3-year study on a beach with different sediment dynamics. CATENA, 207, 105705. https://doi.org/10.1016/j.catena.2021.105705

4) **Arriola-Velásquez, A. C.**, Tejera, A., Alonso, I., Cámara, F., Cantaluppi, M., Alonso, H., Miquel-Armengol, N., Rubiano, J.G., Martel, P. (2023). Natural radionuclides as tracers of coastal sediment dynamics in El Confital Bay (Spain): spatial distribution and relationships with sediment characteristics. CATENA, 235, 107672. https://doi.org/10.1016/j.catena.2023.107672

Paper 1, as indicated above, is a compilation of data prior to the development of this thesis corresponding to samples collected between 2013 and 2015 from different beaches in the Eastern Canary Islands. The results of this article, combined with those of previous studies on the

activities of ^{226}Ra, ^{232}Th and ^{40}K on the beaches of Gran Canaria were used to select the study region of this thesis.

Papers 2, 3 and 4 are the main articles of the thesis and address the different objectives set for the study of natural radionuclides as tracers of coastal sediment erosion, transport and accumulation processes. In paper 2, a 1-year data series (2016 - 2017) was used to carry out an analysis of the spatio-temporal variability of the activity of natural radionuclides in the intertidal zone of Las Canteras Beach (Gran Canaria), as well as a first study of the relationships between the different characteristics of the sediment and the activity concentrations found. In paper 3, a 3-year data series (2016 - 2019) was used to perfom a study of the temporal variability of natural radionuclides found in the intertidal sand of the same beach. In addition, the influence of the different erosive agents affecting the beach (such as waves and wind), atmospheric parameters and the mineralogical content of the samples on the variations in the activity of the natural radionuclides was studied. These two articles verified the viability of natural radionuclides as tracers of erosion, transport and sediment accumulation in the intertidal zone of Las Canteras Beach.

Finally, paper 4 focuses on applying the natural radionuclides previously studied to trace the different sediment dynamics in the submerged area of Las Canteras Beach and the rest of El Confital Bay. In addition, a study of the influence of the different characteristics of the sediment on the activity concentrations found was carried out. Hence, the articles in this thesis constitute a thematic unit that presents a methodology for using natural radionuclides to trace erosion, transport and accumulation of coastal sediments.

CAPÍTULO 3. Publicaciones principales que conforman la tesis doctoral

3.1. Spatio-temporal variability of natural radioactivity as tracer of beach sedimentary dynamics

Publicado en la revista *Estuarine, Coastal and Shelf Science*

Año: *2019*

Volumen: *231*

DOI: *https://doi.org/10.1016/j.ecss.2019.106476*

Journal Citation Report edición 2019: Categoría *Marine & freshwater biology*; Ranking *26/67*; Cuartil *Q1*

Este artículo se centra en el estudio de la variabilidad espacial de la concentración de actividad del ^{226}Ra, el ^{232}Th, el ^{40}K y el ^{210}Pb no soportado ($^{210}Pb_{ex}$) en la zona intermareal de la playa de Las Canteras en la isla de Gran Canaria. Además, se realizó un primer estudio de las relaciones existentes entre las características del sedimento y las concentraciones de actividad encontradas. Adicionalmente, se llevó a cabo un primer estudio de la variabilidad temporal de la ratio $^{226}Ra/^{228}Ra$ sugerida en la literatura como trazador de periodos de erosión y acumulación en las zonas costeras (Dai et al., 2011).

Para la realización de este estudio se seleccionaron 10 puntos de muestreo repartidos por toda la zona intermareal de la playa y se recogieron muestras de arena superficial mensualmente desde septiembre de 2016 a agosto de 2017. Esto supuso un total de 120 muestras obtenidas a lo largo de un año. Al mismo tiempo se tomaron datos de pH, conductividad y temperatura en cada uno de los puntos de muestreo. Además del análisis de concentraciones de actividad de los distintos radionucleidos a estudiar, se realizó un análisis granulométrico usando el método de tamizado en seco (Alveirinho Dias, 2004) y el software GRADISTAT (Blott and Pye, 2001).

Una vez obtenidos todos los datos se utilizaron diversos análisis estadísticos para evaluar la distribución espacial del ^{226}Ra, el ^{232}Th, el ^{40}K y el $^{210}Pb_{ex}$. Primero, se aplicó un análisis de clúster (Ravisankar et al., 2014; Shaw, 2003) y un análisis de componentes principales (PCA) (Thomson and Emery, 2014) para obtener los diferentes grupos en los que agrupaban las muestras. Los resultados obtenidos mostraron tres zonas con concentraciones de actividad de ^{226}Ra, ^{232}Th y ^{40}K condicionadas por la dinámica que afectaba a cada parte de la playa. El

primer grupo (zona I) reunió las muestras que tenían menor actividad de concentración de ^{226}Ra, ^{232}Th y ^{40}K, siendo estas muestras las que procedían de estaciones de muestreo localizadas en la zona de la playa totalmente expuesta a la acción del oleaje. El segundo grupo (zona II) corresponde a las muestras recogidas enfrente de las distintas aberturas de la barra y sus actividades eran ligeramente más altas que las de la zona I. Finalmente, el tercer grupo (zona III) englobó las muestras de mayores concentraciones de actividad de ^{226}Ra, ^{232}Th y ^{40}K y que correspondían a las estaciones de muestreo de la parte de la playa que está completamente protegida frente a la acción del oleaje por la barra.

Además de este primer análisis estadístico, el PCA y un análisis de correlaciones permitieron evaluar las relaciones existentes entre las concentraciones de actividad del ^{226}Ra, ^{232}Th, ^{40}K y $^{210}Pb_{ex}$, el tamaño de grano medio, el sorting, pH, conductividad, temperatura y la densidad de las muestras. Por un lado, los resultados mostraron una fuerte correlación entre las concentraciones de actividad del ^{226}Ra, ^{232}Th y ^{40}K mientras que ninguno de estos radionucleidos presentó correlación alguna con el $^{210}Pb_{ex}$. Considerando que el $^{210}Pb_{ex}$ tiene un origen atmosférico (Hülse and Bentley, 2012; Szmytkiewicz and Zalewska, 2014) y dada la falta de correlación con los otros radionucleidos, los resultados obtenidos sugirieron que la distribución espacial de la actividad de $^{210}Pb_{ex}$ estaba principalmente controlada por la dinámica atmosférica. Por el contrario, la distribución espacial de las concentraciones de actividad del ^{226}Ra, ^{232}Th y ^{40}K podía estar principalmente influenciada por la dinámica marina.

Por otro lado, los análisis de correlaciones con el resto de las variables estudiadas mostraron una correlación directa entre las

concentraciones de actividad de ^{226}Ra, ^{232}Th y ^{40}K y el tamaño de grano medio de la muestra, al igual que una correlación inversa de estos radionucleidos con la densidad de la muestra. Esto quiere decir que las muestras con menor densidad y mayor tamaño de grano presentaron mayores concentraciones de actividad de ^{226}Ra, ^{232}Th y ^{40}K. Esto concuerda con lo encontrado en los grupos del análisis de clúster y PCA, ya que éstos agrupaban las muestras de menor actividad recogidas en la zona de la playa abierta al oleaje y que en su arena contienen un alto contenido en óxido de hierro, titanio y otros minerales pesados (teniendo por tanto mayor densidad). Por otro lado, estos análisis reunieron las muestras de la parte protegida de la playa que también son las que tenían mayor tamaño de grano, menor densidad y concentraciones de actividad más altas. Por ende, el análisis de correlaciones parece reforzar la idea de que las concentraciones de actividad del ^{226}Ra, ^{232}Th y ^{40}K trazan la distribución de los distintos sedimentos de la playa. En el caso del $^{210}Pb_{ex}$ no se encontraron correlaciones significativas con ninguna de las características del sedimento.

Además de este análisis de la variabilidad espacial, se llevó a cabo un análisis de la variabilidad temporal de la ratio $^{226}Ra/^{228}Ra$ en las distintas zonas establecidas por el análisis espacial (zonas I, II y III). Esta ratio fue propuesta en el trabajo de Dai et al., (2011) debido a la mayor movilidad del ^{228}Ra (radionucleido hijo del ^{232}Th) frente al ^{226}Ra en los minerales arcillosos. Debido a esto, en épocas de acumulación habría un mayor aporte de ^{228}Ra y por tanto la ratio sería menor que 1 mientras que, en épocas de erosión, al darse una mayor pérdida de ^{228}Ra, el valor de la ratio se situaría por encima de 1. Los resultados mostraron que en la parte de la playa que se encuentra protegida frente a la acción del oleaje la ratio siempre tuvo un valor por debajo de 1. Estos resultados

son acordes a lo que se podría esperar ya que esta zona es la que se encuentra bajo un periodo de acumulación constante. En cambio, en la parte de la playa que se encuentra abierta a la acción del oleaje, y por tanto donde se pueden encontrar periodos diferenciados de erosión y acumulación, la ratio presentaba valores por encima y por debajo de 1. Por tanto, los resultados de este primer análisis temporal indicaron que la ratio $^{226}Ra/^{228}Ra$ podría ser un indicador adecuado para trazar los periodos de erosión y de acumulación en las playas. Sin embargo, con los resultados de este artículo también se puso de manifiesto que un estudio más largo de la variabilidad temporal de la ratio y los radionucleidos estudiados era necesario para poder verificar adecuadamente su uso como trazadores de la erosión, transporte y acumulación de sedimentos en la zona intermareal de la playa.

Estuarine, Coastal and Shelf Science 231 (2019) 106476

Contents lists available at ScienceDirect

Estuarine, Coastal and Shelf Science

journal homepage: http://www.elsevier.com/locate/ecss

Spatio-temporal variability of natural radioactivity as tracer of beach sedimentary dynamics

A. Arriola-Velásquez, A. Tejera *, J.G. Guerra, I. Alonso, H. Alonso, M.A. Arnedo, J.G. Rubiano, P. Martel

Department of Physics, Instituto Universitario de Investigación en Estudios Ambientales y Recursos Naturales i-UNAT. Universidad de Las Palmas de Gran Canaria, Campus de Tafira, Las Palmas de Gran Canaria, 35017, Spain

ARTICLE INFO

Keywords:
Natural radionuclides
Tracer
Sedimentary processes
Erosion/accretion

ABSTRACT

Knowledge of coastal sedimentary dynamics is an essential tool in the sustainable management of high-value natural places, such as beaches, which play an important role in human life. With this aim, spatio-temporal variations of activity concentrations of the main natural radionuclides in intertidal sand samples were measured in order to analyse their role as tracers of different sedimentary processes on a beach with wide and diversified sedimentary dynamics (Las Canteras beach at Gran Canaria Island). The radionuclides studied were ^{226}Ra, ^{232}Th, ^{40}K and ^{210}Pb$_{ex}$. A cluster analysis and a principal component analysis performed by using stationary averages of the studied radionuclides activity concentrations and other quantities, such as grain size and or bulk density, were developed. These analyses divided the beach into three zones of sediment distribution related to one of the main geomorphological characteristics of the beach. Finally, annual variations in ^{226}Ra/^{228}Ra ratios were used to study erosion and accretion periods on the beach.

1. Introduction

As is known, natural radionuclides include primordial radioactive elements in the earth's crust, their radioactive progeny and cosmogenic radionuclides, which originate in the earth's atmosphere by interaction with cosmic radiation and detected on the earth's surface due to fallout. Naturally occurring radionuclides most commonly found on the earth's crust are primordial nuclides, mainly ^{40}K and the elements from the ^{238}U and ^{232}Th day series. Concentrations of these elements on the earth's surface vary widely from one zone to another depending on their geology as well as other factors such as geochemical and geophysical conditions. The natural radioactivity of a beach is mainly conditioned by the composition of its sands and sediments, which originate from different rocks (with different radionuclide composition) that suffer weathering, erosion and subsequent transport by the action of different agents.

In recent years, numerous assessments of environmental radioactivity (not only of natural origin, but also of anthropogenic ones) have been developed in beach sands and marine sediments from different parts of the world (Abdi et al., 2008; Casas-Ruiz et al., 2012; Fares, 2017; Huang et al., 2015; Korkulu and Özkan, 2013; Malain et al., 2012; Pappa et al., 2016; Shuaibu et al., 2017). In most of these studies, the activity concentrations found for ^{226}Ra (from ^{238}U series decay), ^{232}Th and ^{40}K are on a comparable range among them. However, in some places like Miami Bay in Malaysia (Shuaibu et al., 2017), the northeast coast of Tamilnadu in India (Suresh Gandhi et al., 2014) and Cumuruxatiba Beach in Brazil (Vasconcelos et al., 2011), the activity concentration values are two orders of magnitude higher than in other parts of the world. In fact, in the radiological protection framework, the aim of the aforementioned papers, is radioactive background monitoring of beaches through estimation of radiological exposure to humans due to radionuclides in beach sediments. In this regard, external gamma dose rates and several different radiation hazard indices were estimated in Gran Canaria beaches, and any radiological risks were assessed (Arnedo et al., 2013).

Furthermore, radionuclides in sediments have been used as tracers of different coastal processes including those related to dynamic processes on beaches. For example, ^{238}U, ^{232}Th and ^{40}K have been used as proxy of coastal heavy mineral resources or to estimate biogenic sedimentation (Ghosal et al., 2017; Gulin et al., 2014). Also, particle-reactive radionuclides such as ^{234}Th, ^{210}Pb, ^{7}Be and ^{137}Cs have been used as tracers of sedimentary processes in order to determine sediment transport, sediment accretion/erosion or accumulation and mixing rates (Al-Mur et al.,

* Corresponding author.
E-mail address: alicia.tejera@ulpgc.es (A. Tejera).

https://doi.org/10.1016/j.ecss.2019.106476
Received 30 April 2019; Received in revised form 23 October 2019; Accepted 5 November 2019
Available online 8 November 2019

2017; Carvalho et al., 2016; Du et al., 2010; Mahu et al., 2016; Oguri et al., 2012; Renfro et al., 2016; Woszczyk et al., 2017). It is precisely within this field of application of radionuclides that the aim of the present work is framed.

The main objective of this paper is to analyse the spatial and temporal variability of gamma emitter radionuclides present in the intertidal beach sand in order to study its role as tracers of common sedimentary processes. For this purpose, we have selected a beach (Las Canteras beach in Gran Canaria island) with a diverse sedimentary dynamic, combining the characteristic dynamic of a closed beach with that associated with a beach open to wave action.

2. Study region

Las Canteras beach is one of the most important urban beaches in Spain. It is located in El Confital bay (Medina et al., 2006), an important protected area north of the island of Gran Canaria, in the city of Las Palmas de Gran Canaria (Fig. 1). Las Canteras beach is approximately 3 km long, delimited by La Isleta Isthmus in the north and a breakwater ("Baja de Núñez") in the south. This beach can be divided into three different sectors: the northern arch, the central arch and the southern arch (Fig. 1). Between the central arch and northern arch, there is a smaller sector, "Playa Chica", with physical limitations to the exchange of sediments with the rest of the beach. At high tide periods, tide currents are to the NE, while during low tide periods, they are SW. The wind direction is mainly NE, NNE and ENE due to the trade winds. During spring tides, the tidal range is greater than 2.5 m; during neap tides, it is approximately 1 m. The mean wave approaching direction is north and, during big storms, comes from the northwest. The average significant wave height is 1.42 ± 0.6 m, reaching up to 4 m in winter (Alonso, 1993, 2005).

As described in Alonso (1993), the sediments that compose the beach sand are thought to be provided by the Isleta Isthmus, La Ballena Ravine and the beach rock that can be found in different parts of the beach. Also, they could come from submerged sandbars that are located between the bathymetric curve of 50 m and the beachfront. This work explains that the sand across the beach can be considered medium and fine sands, with a size around 0.25 mm in diameter. The calcimetry and petrographic analysis of Alonso (1993), Alonso and Pérez Torrado (1992) and Medina et al. (2006), show that the lowest amount of organic matter appears on the southern arch of the beach. A geochemical analysis performed on two sand samples from the southern and northern arch,

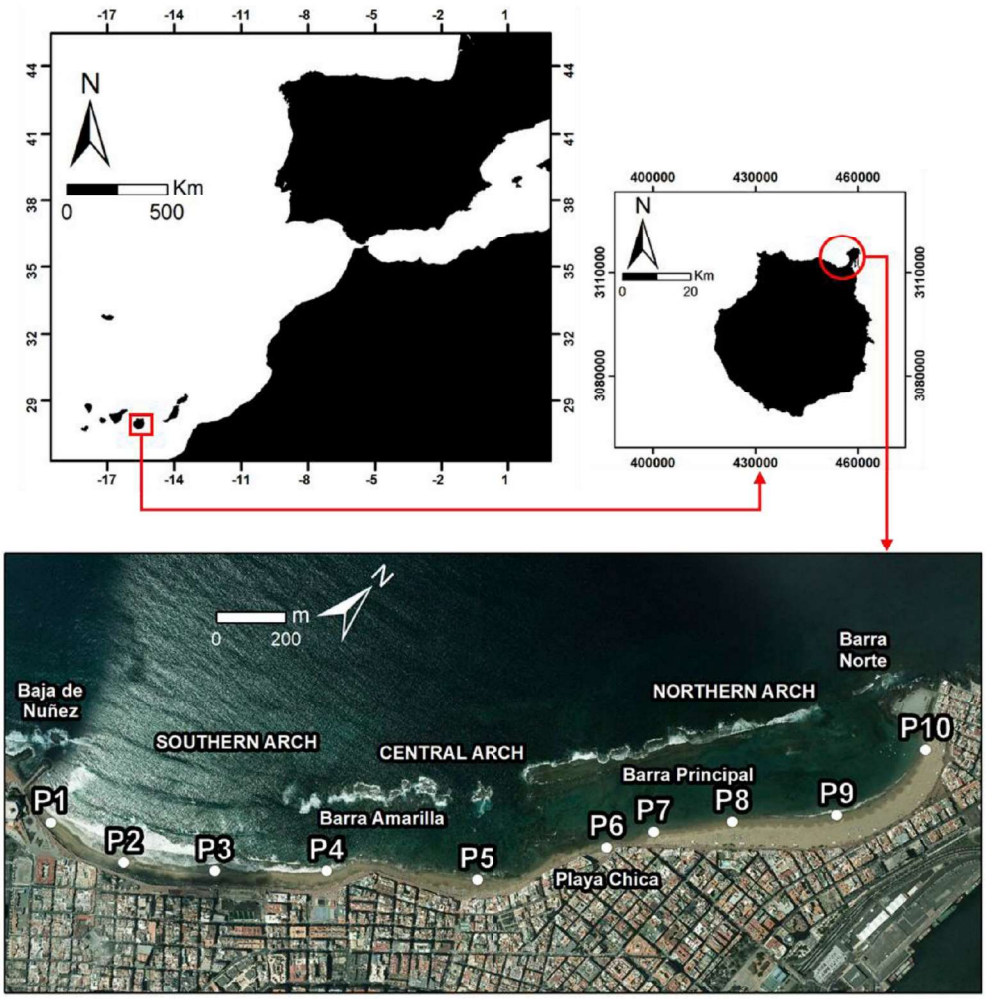

Fig. 1. Location, division and sampling points on Las Canteras beach. Coordinates are in the UTM system.

respectively, showed an enrichment in metal components (TiO_2, Fe_2O_3, MgO, V, Sc, Co and Cr) in the first one, while the organic sand (from north arch) presented higher amounts of K_2O, Na_2O, CaO, U, Sr, Ba, As and Th (Arnedo et al., 2013).

In front of the beach, there is a natural rocky bar offshore that emerges during low tide. This bar neither closes the whole beach nor is a complete block as shown in Fig. 1. Instead, it is fragmented in different sections with openings between them. The first part, located in the northern arch, presents an opening between the "Barra Norte" and the "Barra Principal." This part of the beach is completely protected against wave action. On the south part of the "Barra Principal," there is another opening, and the "Barra Amarilla" establishes the end of the protected part of the beach. The southern arch of the beach is completely exposed to the open ocean (Medina et al., 2006).

The sedimentary balance and dynamic of this beach has been studied, especially since building and development near the beach. Different studies (Alonso, 1993, 1994; 2005; Alonso and Vilas, 1996) indicate that the beach presents a seasonal variability with two different periods: erosion and accretion. According to these studies, erosional periods normally occur during intense storm events, so it is logical to expect them to occur during winter, while periods of accretion occur in summer. Furthermore, the beach has a different behaviour in its distinct parts due to the influence of many factors such as the presence of the natural offshore rocky bar and the type of sediments found on the different parts. During erosional periods, the southern arch loses a high amount of sediment that is transported longitudinally to the northern arch. During periods of accretion, sand from submerged sandbars is cross-transported to the beach so that the amount of sediment on the beach increases forming berms. Moreover, there are beach cusps formed on the northern arch during this period that can favor the presence of edge waves that generate longitudinal transport to the southern arch. Even though the sedimentary dynamic has long been studied in Las Canteras beach, there is still missing information about the origin and exchange of the sediment between the beach and the bay.

3. Material and methods

3.1. Samples collection and preparation

Ten points were selected in each campaign for sand sampling (Fig. 1). Four were located on the southern arch, one in the central arch, another one at Playa Chica, and the last four in the northern arch. In order to study any spatial and temporal variabilities on the radionuclides distribution along the beach, sand samples were taken monthly from September 2016 to August 2017 (120 samples in total). Moreover, pH, temperature and electroconductivity were measured at each sampling point. For this, a hole was made in the area of the square of each sampling point, digging until the water inside the soil emerged into the surface of the hole. Then pH, temperature and electroconductivity were measured from a sample of this water with a portable pH metre.

In order to consider the marine dynamic influence, samples were collected in the intertidal zone during low tide. For each one of them a square of 1 m^2 was drawn on the sand at each sampling point and, after mixing them *in situ*, samples were taken from the superficial sand from about 0 to 5 cm depth. Once in the laboratory, they were oven dried at 80 °C for 24 h. After this period, they were taken out of the oven and sieved through a 1 mm mesh size sieve to homogenise them. Finally, samples were kept inside PVC-trunk conical containers filled to 40 cm^3, then sealed with aluminium strips due to their impermeability to radon gas, and stored for approximately one month. This period was necessary to allow secular equilibrium between ^{226}Ra and ^{222}Rn and its short-lived progeny (as ^{214}Pb, used for determining ^{226}Ra).

3.2. Gamma emission analysis

The determination of radionuclides in sand samples by gamma spectrometry analysis was carried out using a Canberra Extended Range (XtRa) Germanium spectrometer, model GX3518, with 38% relative efficiency with respect to a 3″ x 3″ active area NaI (Tl) detector and nominal FWHM of 0.875 keV at 122 keV and 1.8 keV at 1.33 MeV. It works coupled to a Canberra DSA-1000 multichannel analyser with the software package Genie 2000. Efficiency calibration of the system was performed using the Canberra LabSOCS package based on the Monte Carlo method (Arnedo et al., 2017; G. Guerra et al., 2015, 2017). Calibration was verified using reference standards for IAEA RGK-1 (potassium sulfate), RGU-1 (uranium ore) and RGTh-1 (thorium ore). Energy calibration was carried out using a$^{155}Eu/^{22}Na$ (Canberra ISOXSRCE, 7F06-9/10138 series) and confirmed using the 1460.8 keV line of ^{40}K (IAEA RGK-1) (Arnedo et al., 2017).

The radionuclides of interest were determined from different photopeaks. ^{226}Ra was determined from the ^{214}Pb using the 351.9 keV emission line. The ^{210}Pb was directly measured using the emission line of 46.5 keV. The activity concentration of ^{232}Th was calculated from ^{228}Ac by the emission line of 911.2 keV. This emission line was also used to determine ^{228}Ra. Activity concentrations of ^{40}K and ^{137}Cs were directly measured using emission lines 1460.8 keV and 661.8 keV, respectively. The counting time for each sample was around 24 h. Finally, ^{210}Pb originates after the decay of ^{226}Ra, that produces ^{222}Rn, a 3.8 days half-life gas that partially diffuses into the atmosphere where it rapidly decays into ^{210}Pb. This fraction of ^{210}Pb is adsorbed to atmospheric aerosols and deposited as fallout over the earth's surface leading to unsupported or excess $^{210}Pb_{ex}$ (Al-Mur et al., 2017; Hülse and Bentley, 2012; Szmytkiewicz and Zalewska, 2014). The activity $^{210}Pb_{ex}$ was determined by the difference between the activity concentrations of ^{210}Pb and ^{226}Ra.

3.3. Granulometric analysis

Some aliquots were taken at each sampling point during the October 2016 campaign and a grain size analysis was carried out by dry sieving (Alveirinho Dias, 2004). Around 100 g of each sample were used. The aliquots were weighed and passed through five different sieves from 1 to 0.0625 mm at 1 ϕ intervals. Then, the portion retained on each sieve was weighed separately. The results were analysed by the GRADISTAT software (Blott and Pye, 2001).

3.4. Statistical analysis

A correlation analysis and two types of multivariate statistical analyses were performed to evaluate the spatial distribution of the activity concentration of ^{226}Ra, ^{232}Th, ^{40}K and $^{210}Pb_{ex}$, and its relations with other characteristics of the samples. The first multivariate analysis used was a cluster analysis (CA). This analysis identifies and classifies observations with similar characteristics within groups known as clusters. Observations in the same cluster are considered similar to each other and different to the observations in another cluster. Similarity is a measure of distance between any two individual variables (Ravisankar et al., 2014, 2015; Shaw, 2003) and, for this analysis, the Euclidian distance between the observations was used. Also, there are multiple types of CA and, in this work, the hierarchical CA was selected.

The second multivariate analysis was a principal component analysis (PCA) or empirical orthogonal functions (EOF) analysis (Thomson and Emery, 2014). This analysis takes a number of variables and converts them so that they can be more easily analysed, giving information about how variables relate with each other and identifying different groups of variables (Abramson et al., 2010; Guerrero et al., 2016; Thomson and Emery, 2014). According to literature, if the variance explained by the principal components is equal to or higher than 70%, the fitted principal component to the data is good (Ravisankar et al., 2014, 2015; Zhang et al., 2005).

4. Results and discussion

4.1. Activity concentrations

A Shapiro-Wilk normality test (Shapiro and Wilk, 1965) was performed on the activity concentration values of ^{226}Ra, ^{232}Th, ^{40}K and ^{210}Pb$_{ex}$ in each sampling point. The normality null hypothesis cannot be rejected at significance level of 0.05 for all activity concentrations samples except but the activity concentration of ^{210}Pb$_{ex}$ in sampling point P9 where normality behaviour cannot be rejected at level of significance 0.03 (p-value 0.033). The activity concentrations of ^{226}Ra, ^{232}Th, ^{40}K and ^{210}Pb$_{ex}$ for each sampling point are shown in the boxplots in Fig. 2. For ^{226}Ra, the activity concentration ranged between 5.4 ± 0.6 and 24.4 ± 1.4 Bq kg^{-1} with a mean value of 13.9 ± 0.9 Bq kg^{-1}; for ^{232}Th, it fluctuated between 6.4 ± 1.2 and 32.1 ± 2.0 Bq kg^{-1} with a mean value of 18.0 ± 1.6 Bq kg^{-1}; from 52 ± 6 to 810 ± 40 Bq kg^{-1} with a mean value of 429 ± 20 Bq kg^{-1} for ^{40}K; and between 12.4 ± 5.2 and 62.9 ± 6.4 Bq kg^{-1} with a mean value of 34.8 ± 5.5 Bq kg^{-1} for ^{210}Pb$_{ex}$.

A comparison of mean activity concentrations of ^{226}Ra, ^{232}Th and ^{40}K obtained in this work at Las Canteras beach, and those values referenced for other coastal sediments, is shown in Table 1. When comparing the results obtained in both studies at Las Canteras beach, it can be appreciated that although the activity concentration values given in this work are slightly higher, the results obtained in both works are similar. The values found for Las Canteras beach are also similar to others found for Xiamen Island in China (Huang et al., 2015), in sediments from the Cadiz Bay in Spain (Casas-Ruiz et al., 2012) and for values obtained in Tema Harbour in Ghana (Botwe et al., 2017), being slightly higher for ^{232}Th. In other places, like Iran (Abdi et al., 2008), the Oman Sea (Darabi-Golestan et al., 2017) and the Yangtze Estuary (Wang et al., 2017), the values found for the different radionuclides are all slightly higher, except for the case of the ^{40}K in Iran, which has a similar value to Las Canteras beach. In other places like Tamil Nadu in India (Punniyakotti and Ponnusamy, 2018) or in Henties Bay in Namibia (Onjefu et al., 2017), the variability is higher, with values for ^{226}Ra being one order of magnitude higher than the value obtained for Las Canteras beach. In Brazil, it is possible to find places like Bahia Coast (Veiga et al., 2006) where the values for ^{226}Ra and ^{232}Th are one order higher than the values found in this study, but the mean activity concentration for ^{40}K is one order of magnitude lower than the values obtained in Las Canteras beach. The activity concentration values obtained in Cumuruxatiba beach, on the south of Bahia in Brazil, (Vasconcelos et al., 2011), correspond to dark sand and show much higher values in comparison to everywhere else. These variations are probably due to the different minerals that can be found in the different places aforementioned, manifesting the variability in activity concentration in different places, which is related to the variation in the components of the sediments. Finally, when comparing with the worldwide values, ^{226}Ra and ^{232}Th are below the world mean, while ^{40}K is slightly higher than the mean value given by the United Nations Scientific Committee on the Effects of Atomic Radiation (UNSCEAR, 2000) for soil content.

4.2. Spatial analysis

When analysing the changes along the beach of the mean activity concentration for each radionuclide, an increase in ^{226}Ra, ^{232}Th and ^{40}K

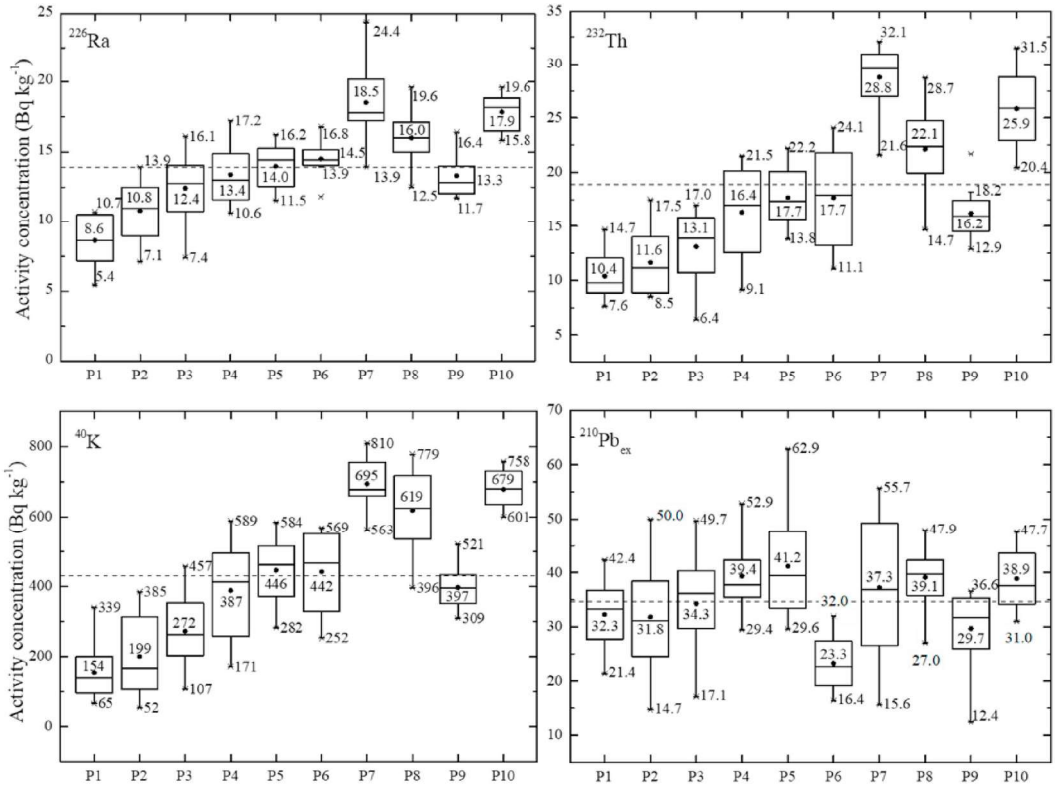

Fig. 2. Boxplots of the activity concentrations found for each sampling point for ^{226}Ra, ^{232}Th, ^{40}K and ^{210}Pb$_{ex}$. The dash line indicates the mean activity concentration value. The numbers that appear in each whisker correspond to the maximum and minimum activity concentration values. The number in the middle indicates the mean activity concentration value for each sampling point.

Table 1
Comparison of activity concentrations (Bq kg^{-1}) of ^{226}Ra, ^{232}Th and ^{40}K of Las Canteras beach sand and beach sand and marine sediments from coastal zones of other countries around the world.

Location	^{226}Ra		^{232}Th		^{40}K		Reference
	Range	Mean	Range	Mean	Range	Mean	
Las Canteras (Spain)	5.4–24.4	13.9	6.4–32	18.0	52–810	429	This work
Las Canteras (Spain)	7–19	14	7–25	15	83–629	390	Arnedo et al. (2013)
Xiamen Island (China)	7.9–25.7	14.6	6.7–41.4	10.9	197.4–421.3	396.4	Huang et al. (2015)
Cumuruxatiba (Brazil)	7050–8320	7810	17630–18450	17770	2220–3110	2660	Vasconcelos et al. (2011)
Persian Gulf (Iran)	17–48	35	15–45	26	146–500	395	Abdi et al. (2008)
Sediments of Cadiz Bay (Spain)	3–41	13	3–73	19	105–1342	451	Casas-Ruiz et al. (2012)
Oman sea (Arabic Gulf)	8–55	28	5–42	22	250–980	640	Darabi-Golestan et al. (2017)
Tema Harbour (Ghana)	–	14	–	30	–	325	Botwe et al. (2017)
Henties Bay (Namibia)	25.32–235.55	175.59	[1]BDL–77.99	40.17	222.39–482.16	349.66	Onjefu et al. (2017)
Bahia Coast (Brazil)	10–572	184	14–173	533	25–62	42	Veiga et al. (2006)
Tamil Nadu Coast (India)	[2]BDL–370.77	12.3	[2]BDL –3773.6	59.03	[2]BDL –525.9	197.03	Punniyakotti and Ponnusamy (2018)
Yangtze Estuary (China)	13.7–52.3	24.3	26.1–71.9	40.9	392–898	628	Wang et al. (2017)
Worldwide		32		45		420	UNSCEAR (2000)

BDL-Below detection limit: (1) not provided by authors, and (2) 2.22, 2.15, and 8.83 Bq kg^{-1} for ^{238}U,^{232}Th, and ^{40}K, respectively.

is found from the southern to the northern arch of the beach. However, for ^{210}Pb$_{ex}$ this variation is not present, being the value of activity concentration similar all along the beach except for P6 (Playa Chica). This seems to indicate that the spatial distribution of ^{210}Pb$_{ex}$ is controlled by a different agent than the spatial distribution of ^{226}Ra, ^{232}Th and ^{40}K. Hence, the main dynamic agents contributing to the spatial distribution of these radionuclides could be related to wind for ^{210}Pb$_{ex}$ (see section 3.2), and to waves and nearshore currents that transport the sediments for ^{226}Ra, ^{232}Th and ^{40}K. However, the distribution of the surface activity concentration of ^{210}Pb$_{ex}$ is also influenced by the mixing or sediment accumulation rates (de Carvalho Gomes et al., 2009; Palanques et al., 2017; Szmytkiewicz and Zalewska, 2014). Thus, an analysis of ^{210}Pb activity concentration in sediment cores should be performed to better understand the agents that affect the spatial distribution of this element.

In addition to activity concentration values, other quantities were also measured. These include average grain size (ϕ), sorting, pH, conductivity (mS cm^{-1}), *in situ* temperature (°C) and bulk density (g cm^{-3}) for each sampling point (Table 2). Temperature (T), pH and conductivity (EC) show small variation along the beach, so a loss of radionuclides in a specific beach zone by chemical mobility between marine water and intertidal sand seems to be dismissed, even though a further analysis should be done.

A Shapiro-Wilk normality test (Shapiro and Wilk, 1965) was performed with a significance level of 0.05 to quantities aforementioned and mean activity concentration values of ^{226}Ra, ^{232}Th, ^{40}K and ^{210}Pb$_{ex}$ (averaging for each point and for all the campaigns). The results indicate that almost all of them follow a normal distribution, since all of them have a p-value > 0.05, except for the grain size, which had a p-value of 0.02. Additionally, a performed correlation analysis is shown in Table 3. All coefficients correspond to the Pearson correlation coefficient (Ahlgren et al., 2003) except those relative to average grain size where Spearman correlation coefficients (Siegel and Castellan, 1988) were used. The p-value obtained for each correlation coefficient is also represented, being that correlation coefficients are statistically significant when p-values < 0.05. Moreover, a strong correlation was considered when p-value < 0.005.

Strong positive correlations appear between activity concentrations of ^{226}Ra, ^{232}Th and ^{40}K, and negative correlations between these activities and bulk densities of the samples. The temperature of the sample and the grain size also presented a moderate negative correlation with activity concentrations. Nevertheless, it is important to mention that temperature correlation could be related to the sampling hour, as samples with higher activity concentrations were systematically picked up earlier in the morning than samples from the part of the beach with less activity. Conductivity and pH did not present a significant correlation with the activity concentrations, which again suggest that the chemical mobility does not influence the variations of activity concentration of ^{226}Ra, ^{232}Th and ^{40}K. Thus, temperature, pH and conductivity were no longer considered for the rest of this study. In the case of ^{210}Pb$_{ex}$, there is no significant correlation between this variable and the others. This seems to reinforce the idea that the main agents controlling the distribution of ^{210}Pb$_{ex}$ are different than those controlling the distribution of the other radionuclides.

Once the descriptive statistic was established, the CA was performed by using activity concentrations of ^{226}Ra, ^{232}Th and ^{40}K. The dendrogram obtained from the cluster analysis is shown in Fig. 3. At a distance of 100, three different clusters appear; the first one with sampling points P1, P2 and P3; the second one with sampling points P4, P9, P5 and P6 and the third one with sampling points P7, P10 and P8 (Fig. 1). The classification obtained almost agrees with the geographical distribution of the sampling points except for the second group, where sampling

Table 2
Non-radioactive data and results obtained from granulometric analysis of the samples from Las Canteras beach. Mean values for pH, conductivity (EC), temperature (T), bulk density (ρ) of the sample, grain size in ϕ units, sorting, skewness and the classification of the samples depending on granulometric parameters are included.

Sampling point	pH	EC	T	ρ	Grain size	Sorting	Skewness	Classification		
		mS cm^{-1}	°C	g cm^{-3}	ϕ	ϕ	ϕ	Grain size	Sorting	Skewness
P1	8.09	54.03	21.25	2.030	2.532	0.414	0.141	Fine Sand	Well Sorted	Fine Skewed
P2	8.05	57.26	21.04	2.025	2.521	0.401	0.125	Fine Sand	Well Sorted	Fine Skewed
P3	8.17	57.72	20.82	1.945	2.449	0.450	−0.168	Fine Sand	Well Sorted	Coarse Skewed
P4	7.99	55.07	20.53	1.830	2.186	0.601	−0.230	Fine Sand	Moderately Well Sorted	Coarse Skewed
P5	8.13	56.92	20.42	1.812	2.304	0.623	−0.260	Fine Sand	Moderately Well Sorted	Coarse Skewed
P6	8.14	56.58	20.45	1.826	1.437	0.900	0.039	Medium Sand	Moderately Sorted	Symmetrical
P7	8.12	57.20	20.47	1.671	2.049	0.671	−0.211	Fine Sand	Moderately Well Sorted	Coarse Skewed
P8	8.24	56.80	20.30	1.712	2.409	0.470	−0.192	Fine Sand	Well Sorted	Coarse Skewed
P9	8.27	56.83	20.32	1.812	2.202	0.591	−0.268	Fine Sand	Moderately Well Sorted	Coarse Skewed
P10	8.13	55.95	20.60	1.668	2.194	0.586	−0.246	Fine Sand	Moderately Well Sorted	Coarse Skewed

Table 3
Correlation coefficients matrix of activity concentrations of ^{226}Ra, ^{232}Th, ^{40}K, $^{210}Pb_{ex}$, pH, electroconductivity (EC), temperature (T), grain size in the ϕ scale, sorting and, bulk density (ρ) of samples. Correlation coefficients are shown in the bottom left diagonal and p-value at the top right diagonal in cursive.

	^{226}Ra	^{232}Th	^{40}K	$^{210}Pb_{ex}$	pH	EC	T	Size	Sorting	ρ
^{226}Ra	1	*0.000*	*0.000*	*0.312*	*0.489*	*0.294*	*0.017*	*0.016*	*0.143*	*0.000*
^{232}Th	0.972	1	*0.000*	*0.251*	*0.577*	*0.518*	*0.051*	*0.033*	*0.219*	*0.000*
^{40}K	0.979	0.980	1	*0.242*	*0.418*	*0.490*	*0.015*	*0.043*	*0.189*	*0.000*
$^{210}Pb_{ex}$	0.357	0.401	0.408	1	*0.615*	*0.903*	*0.603*	*0.960*	*0.326*	*0.245*
pH	0.249	0.201	0.289	−0.182	1	*0.200*	*0.161*	*0.855*	*0.935*	*0.366*
EC	0.369	0.233	0.248	−0.045	0.443	1	*0.258*	*0.651*	*0.776*	*0.567*
T	−0.730	−0.629	−0.736	−0.188	−0.479	−0.395	1	*0.187*	*0.071*	*0.005*
Size	−0.733	−0.673	−0.648	−0.018	−0.067	0.164	0.455	1	*0.000*	*0.077*
Sorting	0.498	0.427	0.452	−0.347	0.030	0.103	−0.592	−0.903	1	*0.149*
ρ	−0.960	−0.948	−0.985	−0.406	−0.321	−0.207	0.810	0.584	−0.492	1

*p = 0.000 corresponds to p < 0.005 (strong correlation).

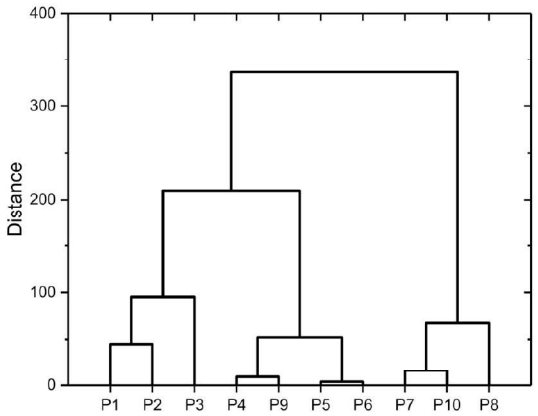

Fig. 3. Dendrogram showing clustering for the different sampling points based on their activity concentrations of ^{226}Ra, ^{232}Th and ^{40}K.

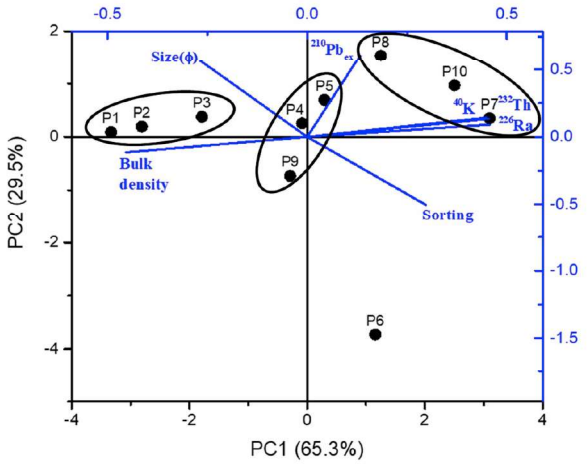

Fig. 4. Biplot of loading plot with the eigenvectors obtained for the grain size in the phi scale (Size ϕ), sorting, mass of the sample and activity concentrations of ^{226}Ra, ^{232}Th, ^{40}K and $^{210}Pb_{ex}$ (blue axes) and scores of observations (black axes). (For interpretation of the references to colour in this figure legend, the reader is referred to the Web version of this article.)

points of the southern and northern arch are gathered together. The explanation for this, however, can be found, if the location of the sampling points is analysed. The first group of points, which will be referred to as Zone I, is located on the part of the beach without a natural offshore rocky bar, therefore, the beach is completely exposed to wave action. The second group, which will be referred to as Zone II, is the one where sampling points are located near the different openings in the bar described earlier. The last group, which will be referred to as Zone III, includes the sampling points that are located in the parts of the beach that are fully protected by the "Barra Norte" and the "Barra Principal" on the northern arch. Therefore, the presence of the distinct parts of the offshore rocky bar seems to be one of the main influences in the distribution of sediment transport and accumulation of radionuclides along the beach. This behaviour, referenced at least for Zone I and III by Alonso (1993), could be interpreted as a validation of the role of ^{226}Ra, ^{232}Th and ^{40}K as tracers of beach sedimentary dynamics.

PCA results are shown in the biplot in Fig. 4. In this biplot, the first two principal components (PC1 and PC2) are represented with an explanation of the total variance of 65.3 and 29.5%, respectively. On the one hand, activity concentrations of ^{226}Ra, ^{232}Th and ^{40}K present very small values of PC2, which means that the variance of these radionuclides is mostly explained by PC1 (Fig. 4 and Table 4). On the other hand, variance of $^{210}Pb_{ex}$ is mainly explained by PC2 with factor loadings of 0.13 and 0.61, respectively (Table 4). This indicates that there is a higher correlation between the first three radionuclides, while $^{210}Pb_{ex}$ follows a different pattern. This agrees with the results obtained from the correlation analysis and, again, reinforces the idea that radionuclide distribution along the beach is controlled by different agents and origins. Hence, the marine sedimentary dynamic could control ^{226}Ra, ^{232}Th and ^{40}K distribution while other causes, such as the aeolian sedimentary dynamic, would be the one controlling the distribution of $^{210}Pb_{ex}$. In addition, the inverse correlation that exists between the grain size and the bulk density of the sample with the activity concentration of ^{226}Ra, ^{232}Th and ^{40}K is also represented. However, grain size values are given in the ϕ scale and this scale is opposite to metrics (Krumbein, 1934). Therefore, higher values in ϕ units indicate sediments are finer, thus, grain sizes and activity concentrations are directly correlated.

Moreover, Fig. 4 also exhibits the scores that the sampling locations

Table 4
Factor loadings of radiological variables on three significant principal components. Percentage of variance explained by each principal component and their cumulative percentage of total variance are also given.

Variables	PC1	PC2	PC3
^{226}Ra	0.46	0.09	−0.19
^{232}Th	0.45	0.14	−0.26
^{40}K	0.46	0.13	−0.18
$^{210}Pb_{ex}$	0.13	0.61	0.75
Size	−0.27	0.56	−0.21
Sorting	0.30	−0.50	0.51
Bulk density	−0.45	−0.11	0.05
% of Variance	65.3	29.5	3.9
Cumulative %	65.3	94.8	98.7

obtained on the PCA. These scores give an idea of how the observations are grouped and how they relate with the different variables. Results for ^{226}Ra, ^{232}Th and ^{40}K are mostly influenced by PC1, and three groups can be defined along this axis. The first group shows negative values of PC1 and includes sampling points P1, P2 and P3, all of them with the lowest activity concentration values of these radionuclides (Fig. 2). The second group includes all sampling points located around zero in the PC1 axis. These sampling points are P4, P5 and P9, all of them with intermediate activity concentrations. The third group refers to sampling points P7, P8 and P10. All of them present positive values in PC1 and their activity concentration values are the highest. The distribution of the sampling locations is slightly different from the one shown in Fig. 3, but it follows the same general pattern. Sampling points P1, P2 and P3 (Zone I) corresponds to negative values of PC1, sampling points P4, P5 and P9 (Zone II) are located close to zero values of PC1 and sampling stations P7, P8 and P10 (Zone III) show the higher values in PC1. The only exception is sampling point P6, located in a very particular place (mentioned in Section 2), so it could be under the influence of other variables.

Focusing on the second eigenvector (PC2), it mostly explains the variance associated with ^{210}Pb$_{ex}$, as was pointed out, perhaps mainly driven by aerosol dynamics. This component splits Zone II into two groups. On the one hand, the lowest values of PC2 correspond to sampling points P6 and P9, which present lower activity concentrations of this radionuclide (Fig. 2). Specifically, sampling P6 is in an area of the beach that is well protected against wind action, which could explain the lowest values of ^{210}Pb$_{ex}$ for that location (not only of Zone II, but for the entire beach). Opposite behaviour is followed by sampling stations P4 and P5, which show higher values of PC2 as a result of their ^{210}Pb$_{ex}$ activity concentrations higher than P6 and P9. However, the obtained values for P4 and P5 are of the same order as the ones obtained for ^{210}Pb$_{ex}$ in the rest of the beach. In other words, sampling points from Zone II scored mainly on PC2, while the rest scored mostly on PC1 (except P8 with similar scores in both PC1 and PC2). In view of the above, as well as PC1 and PC2 percentages of total variance, it could be said that the influence of ^{226}Ra, ^{232}Th and ^{40}K on sedimentary dynamics of Zones I and III is more of a determining factor than in Zone II where other dynamical agents could be considered.

Moreover, Zone I shows the lowest values in activity concentration of ^{226}Ra, ^{232}Th and ^{40}K, as well as in grain size (highest in ϕ units) and the highest in bulk density. Sediments in this area are fine sands (0.177 mm average size) with a high proportion of metal components. Bulk density values respond to the sediment density, and therefore, to their composition. In this area, most common sediments are heavy-metal oxides (mostly magnetite and ilmenite) and pyroxenes (Alonso, 1993; Alonso and Pérez Torrado, 1992), whose densities are 5.18, 4.75 and 3.3 g cm^{-3} for magnetite, ilmenite and pyroxenes, respectively. On the other hand, the most common material at the northern sector of the beach (sampling points P7, P8 and P10, Zone III) are bioclastic sands (0.215 mm average size) rich in calcite and aragonite with a density of 2.75 and 2.93 g cm^{-3}, respectively, and, according to what was stated in Section 2, with higher proportions of K_2O, as well as of Th and U, than Zone I. This agrees with the fact that samples collected from Zone I, where the mineral composition is dominant, shows lower activities of ^{232}Th, ^{226}Ra and ^{40}K and higher bulk density. The scores obtained by samples from Zone III, samples of more calcareous and organic origin, are opposite to those from Zone I, pointing out that these samples have lower mass and higher activity concentration.

4.3. Temporal analysis

Dai et al. (2011) suggested the use of the ratio ^{226}Ra/^{228}Ra as a tracer for erosion and accretion periods in a marine environment. According to them, ^{228}Ra and ^{226}Ra are more present in the crystal framework of clay minerals, but the carbonate and exchangeable phases contain more ^{228}Ra. Thus, accretion or erosion periods could be measured by a change in the ratio between ^{226}Ra and ^{228}Ra. Hence, during accretion periods, the input of ^{228}Ra would be higher and the value of the ratio would be less than 1 (i.e., the natural ratio of ^{232}Th/^{238}U was assumed); a value higher than 1 would indicate an erosional period. Some crystals from clay minerals and zeolites have been found in the north of Las Canteras beach, (Mangas and Julià-Miralles, 2015). Therefore, this ratio could be used to perform the temporal analysis. Moreover, as the spatial analysis presented three different sectors along the beach, that could be related to different dynamic behaviour, the analysis was performed in each one of these zones.

Fig. 5 shows the results after applying the ^{226}Ra/^{228}Ra ratio to the three zones of the beach. Zone III is the area that is fully protected by the natural offshore rocky bar, and all values are lower than 1. This would indicate that Zone III presented a constant accretion during the whole study period. Moreover, from March 2017 to August 2017, there seems to be a decrease in the ratio values, compared to the values obtained in October and December 2016, suggesting a more intense accretion of sediments during the first mentioned period.

Zone II is the part of the beach located opposite to the openings of the calcarenitic bar, so it is likely to have a more complex dynamic. Two periods could be differentiated. The first one occurs from September 2016 through February 2017, when values of ^{226}Ra/^{228}Ra ratio were around 1, indicating small changes in sediment volume. The second period occurs from March through August 2017, and the ratio is clearly less than 1, suggesting accretion, which should be stronger in July and August.

In Zone I, September 2016 and February 2017 present ^{226}Ra/^{228}Ra ratios around 1.25, indicating strong erosion, while October 2016 and July 2017 show ^{226}Ra/^{228}Ra ratios around 0.75, indicating strong deposition. The rest of the months have values around 1. The strong variability suggests that the processes of erosion and accretion in this area are stronger than in the others, involving large amount of sediments that are moved away in the case of erosion and accumulated in the case of accretion.

Unfortunately, we do not have data of volume changes along the beach for the same study period, which could be used to confirm or discard what has been inferred from ^{226}Ra/^{228}Ra ratios. Nevertheless, previous studies in this beach point out that Zone III presents a clear accumulative trend in the long term, Zone II shows much lower volume changes because of the presence of a rocky substratum that is present all along this area, and Zone I presents a very strong seasonal variability, consisting of erosive periods during winter followed by strong accretion during summer (Alonso, 1993; Alonso and Vilas, 1996). Obtained ratios of ^{226}Ra/^{228}Ra seem to confirm the accretion at Zone III, certain seasonal changes at Zone II and strong changes at Zone I. However, further studies with longer time series are necessary to better understand the temporal variability of the environmental radioactivity of the beach, and to get a better correlation with the sedimentary dynamics at this beach. In addition to testing whether the decision value for the ^{226}Ra/^{228}Ra ratio is 1 or somewhat lower, depends on more adequate average natural ^{232}Th/^{238}U ratio in Las Canteras.

5. Conclusions

The analysis of spatial and temporal variations of activity concentrations of ^{226}Ra, ^{232}Th and ^{40}K of intertidal sand samples seems to indicate its feasibility to trace different characteristic processes of the sedimentary dynamics at Las Canteras beach (which involves typical dynamics of both a wave action protected beach and one open to this action).

A CA and a PCA were carried out to evaluate the spatial variability of activity concentrations, showing that sampling points are grouped in three zones with activity concentration values conditioned by the morphology of the natural offshore rocky bar. Thus, the sampling points that are not influenced by the rocky bar correspond to Zone I and present the lowest activity concentrations of ^{226}Ra, ^{232}Th and ^{40}K. Zone II includes sampling points that are located near the different openings in the

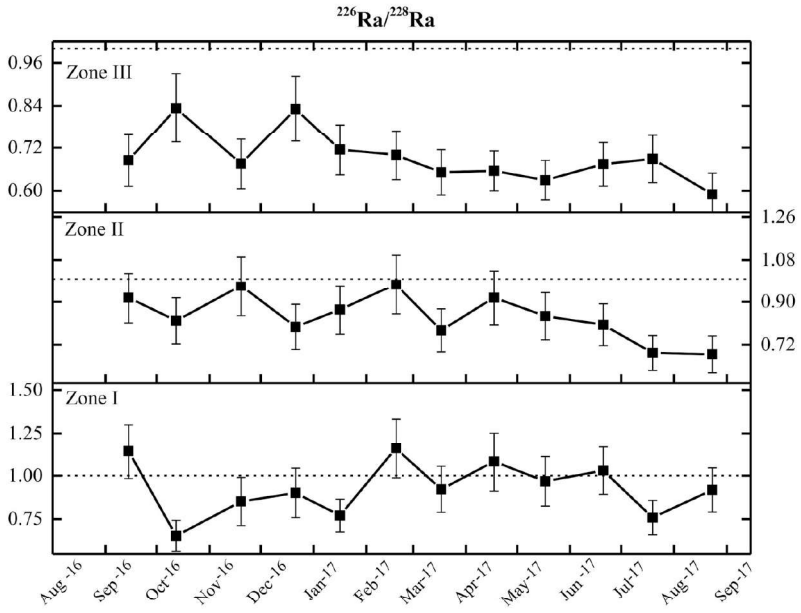

Fig. 5. Mean $^{226}Ra/^{228}Ra$ ratios for each campaign in each zone of Las Canteras beach. Dash lines correspond to value 1 for the ratio.

bar. Being that this zone is partially protected from wave action, it presents intermediate values of activity concentrations. Finally, Zone III refers to sampling points that are in parts of the beach that are fully protected by the "Barra Norte" and "Barra Principal" on the northern arch. Sampling points in this area present the highest values in activity concentration. Therefore, it seems viable that ^{226}Ra, ^{232}Th and ^{40}K can be used as tracers of the distribution of sediments along the beach based on the different marine dynamics related to the morphology of the offshore rocky bar at Las Canteras beach.

The temporal analysis was performed by mean of the ratio $^{226}Ra/^{228}Ra$ in order to evaluate erosion and accretion of sediment periods along the beach. The results suggest that Zones I and II could be affected by either erosion or accretion, while Zone III shows a steady accretionary process, which agrees with previous studies at Las Canteras beach. However, a longer-term study would be necessary to better understand the relation between temporal variability of the environmental radioactivity and beach erosion/accretion periods.

Finally, the use of these natural radionuclides as tracers of the different sedimentary dynamics of Las Canteras beach could provide useful information for beach anthropogenic management, as well as to control and manage any spills that may occur near the beach. Moreover, this study could easily be extended to the management of other beaches of similar sedimentary dynamics.

Declaration of competing interest

The authors declare that they have no known competing financial interests or personal relationships that could have appeared to influence the work reported in this paper.

References

Abdi, M.R., Kamali, M., Vaezifar, S., 2008. Distribution of radioactive pollution of ^{238}U, ^{232}Th, ^{40}K and ^{137}Cs in northwestern coasts of Persian Gulf, Iran. Mar. Pollut. Bull. 56, 751–757. https://doi.org/10.1016/j.marpolbul.2007.12.010.

Abramson, L., Lee, C., Liu, Z., Wakeham, S., Szlosek, J., 2010. Exchange between suspended and sinking particles in the northwest Mediterranean as inferred from the organic composition of *in situ* pump and sediment trap samples. Limnol. Oceanogr. 55, 725–739. https://doi.org/10.4319/lo.2009.55.2.0725.

Ahlgren, P., Jarneving, B., Rousseau, R., 2003. Requirements for a cocitation similarity measure, with special reference to Pearson's correlation coefficient. J. Assoc. Inf. Sci. Technol. 54, 550–560. https://doi.org/10.1002/asi.10242.

Al-Mur, B.A., Quicksall, A.N., Kaste, J.M., 2017. Determination of sedimentation, diffusion, and mixing rates in coastal sediments of the eastern Red Sea via natural and anthropogenic fallout radionuclides. Mar. Pollut. Bull. 122, 456–463. https://doi.org/10.1016/j.marpolbul.2017.05.054.

Alonso, I., 1993. Procesos sedimentarios en la playa de Las Canteras (Gran Canaria). Universidad de Las Palmas de Gran Canaria.

Alonso, I., 1994. Spatial beach morphodynamics. An example from Canary Islands, Spain. Litoral, 94, 169–183.

Alonso, I., 2005. Costa Norte: playa de las Canteras. In: Hernández, L., Alonso, I., Mangas, J., Yanes, A. (Eds.), Tendencias Actuales En Geomorfología Litoral. Universidad de Las Palmas de Gran Canaria, La Palmas de Gran Canaria, pp. 219–238.

Alonso, I., Pérez Torrado, F.J., 1992. Estudio sedimentológico de la playa de Las Canteras (Gran Canaria). Datos preliminares. III Congreso Geológico España tomo 2, 131–135.

Alonso, I., Vilas, F., 1996. Variabilidad sedimentaria en la playa de Las Canteras (Gran Canaria). Geogaceta 20, 428–430.

Alveirinho Dias, J., 2004. A análise sedimentar e o conhecimento dos sistemas marinhos: uma introdução à oceanografia geológica, first ed. Universidade do Algarve, Faro, p. 84.

Arnedo, M.A., Rubiano, J.G., Alonso, H., Tejera, A., González, A., González, J., Gil, J.M., Rodríguez, R., Martel, P., Bolivar, J.P., 2017. Mapping natural radioactivity of soils in the eastern Canary Islands. J. Environ. Radioact. 166, 242–258. https://doi.org/10.1016/j.jenvrad.2016.07.010.

Arnedo, M.A., Tejera, A., Rubiano, J.G., Alonso, H., Gil, J.M., Rodríguez, R., Martel, P., 2013. Natural radioactivity measurements of beach sands in gran Canaria, Canary Islands (Spain). Radiat. Prot. Dosim. 156, 75–86. https://doi.org/10.1093/rpd/nct044.

Blott, S.J., Pye, K., 2001. Technical communication Gradistat : a grain size distribution and statistics package for the analysis of unconsolidated sediments. Earth Surf. Process. Landforms 26, 1237–1248. https://doi.org/10.1002/esp.261.

Botwe, B.O., Schirone, A., Delbono, I., Barsanti, M., Delfanti, R., Kelderman, P., Nyarko, E., Lens, P.N.L., 2017. Radioactivity concentrations and their radiological significance in sediments of the Tema Harbour (Greater Accra, Ghana). J. Radiat. Res. Appl. Sci. 10, 63–71. https://doi.org/10.1016/j.jrras.2016.12.002.

Carvalho, F.M., da Costa Lauria, D., Araújo Ribeiro, F.C., Tonelli Fonseca, R., da Silva Peres, S., Falcão Martins, N.S., 2016. Natural and man-made radionuclides in sediments of an inlet in Rio de Janeiro State, Brazil. Mar. Pollut. Bull. 107, 269–276. https://doi.org/10.1016/j.marpolbul.2016.03.059.

Casas-Ruiz, M., Ligero, R.A., Barbero, L., 2012. Estimation of annual effective dose due to natural and man-made radionuclides in the metropolitan area of the Bay of Cadiz (SW of Spain). Radiat. Prot. Dosim. 150, 60–70. https://doi.org/10.1093/rpd/ncr360.

Dai, Z.J., Du, J.Z., Chu, A., Zhang, X.L., 2011. Sediment characteristics in the north branch of the Yangtze estuary based on radioisotope tracers. Environ. Earth Sci. 62, 1629–1634. https://doi.org/10.1007/s12665-010-0647-7.

Darabi-Golestan, F., Hezarkhani, A., Zare, M.R., 2017. Assessment of ^{226}Ra, ^{238}U, ^{232}Th, ^{137}Cs and ^{40}K activities from the northern coastline of Oman Sea (water and sediments). Mar. Pollut. Bull. 118, 197–205. https://doi.org/10.1016/j.marpolbul.2017.02.064.

de Carvalho Gomes, F., Godoy, J.M., Godoy, M.L.D.P., Lara de Carvalho, Z., Tadeu Lopes, R., Sanchez-Cabeza, J.A., Drude de Lacerda, L., Cesar Wasserman, J., 2009. Metal concentrations, fluxes, inventories and chronologies in sediments from Sepetiba and Ribeira Bays: a comparative study. Mar. Pollut. Bull. 59, 123–133. https://doi.org/10.1016/j.marpolbul.2009.03.015.

Du, J., Wu, Y., Huang, D., Zhang, J., 2010. Use of ^{7}Be, ^{210}Pb and ^{137}Cs tracers to the transport of surface sediments of the Changjiang Estuary, China. J. Mar. Syst. 82, 286–294. https://doi.org/10.1016/j.jmarsys.2010.06.003.

Fares, S., 2017. Measurements of natural radioactivity level in black sand and sediment samples of the Temsah Lake beach in Suez Canal region in Egypt. J. Radiat. Res. Appl. Sci. 10, 194–203. https://doi.org/10.1016/j.jrras.2017.04.007.

Ghosal, S., Agrahari, S., Guin, R., Sengupta, D., 2017. Implications of modelled radioactivity measurements along coastal. Estuar. Coast Shelf Sci. 184, 83–89.

Guerra, J.G., Rubiano, J.G., Winter, G., Guerra, A.G., Alonso, H., Arnedo, M.A., Tejera, A., Gil, J.M., Rodríguez, R., Martel, P., Bolivar, J.P., 2015. A simple methodology for characterization of germanium coaxial detectors by using Monte Carlo simulation and evolutionary algorithms. J. Environ. Radioact. 149, 8–18. https://doi.org/10.1016/j.jenvrad.2015.06.017.

Guerra, J.G., Rubiano, J.G., Winter, G., Guerra, A.G., Alonso, H., Arnedo, M.A., Tejera, A., Martel, P., Bolivar, J.P., 2017. Computational characterization of HPGe detectors usable for a wide variety of source geometries by using Monte Carlo simulation and a multi-objective evolutionary algorithm. Nucl. Instrum. Methods Phys. Res., Sect. A: Accel. Spectrom. Detect. Assoc. Equip. 858, 113–122. https://doi.org/10.1016/j.nima.2017.02.087.

Guerrero, J.L., Vallejos, Á., Cerón, J.C., Sánchez-Martos, F., Pulido-Bosch, A., Bolívar, J. P., 2016. U-isotopes and ^{226}Ra as tracers of hydrogeochemical processes in carbonated karst aquifers from arid areas. J. Environ. Radioact. 158–159, 9–20. https://doi.org/10.1016/j.jenvrad.2016.03.015.

Gulin, S.B., Gulina, L.V., Sidorov, I.G., Proskurnin, V.Y., Duka, M.S., Moseichenko, I.N., Rodina, E.A., 2014. ^{40}K in the Black Sea: a proxy to estimate biogenic sedimentation. J. Environ. Radioact. 54, 231–242. https://doi.org/10.1016/j.jenvrad.2014.02.011.

Huang, Y., Lu, X., Ding, X., Feng, T., 2015. Natural radioactivity level in beach sand along the coast of Xiamen Island, China. Mar. Pollut. Bull. 91, 357–361. https://doi.org/10.1016/j.marpolbul.2014.11.046.

Hülse, P., Bentley, S.J., 2012. A ^{210}Pb sediment budget and granulometric record of sediment fluxes in a subarctic deltaic system: the Great Whale River, Canada. Estuar. Coast Shelf Sci. 109, 41–52. https://doi.org/10.1016/j.ecss.2012.05.019.

Korkulu, Z., Özkan, N., 2013. Determination of natural radioactivity levels of beach sand samples in the black sea coast of Kocaeli (Turkey). Radiat. Phys. Chem. 88, 27–31. https://doi.org/10.1016/j.radphyschem.2013.03.022.

Krumbein, W.C., 1934. Size frequency distributions of sediments. J. Sediment. Res. 4, 65–77. https://doi.org/10.1306/D4268EB9-2B26-11D7-8648000102C1865D.

Mahu, E., Nyarko, E., Hulme, S., Swarzenski, P., Asiedu, D.K., Coale, K.H., 2016. Geochronology and historical deposition of trace metals in three tropical estuaries in the Gulf of Guinea. Estuar. Coast Shelf Sci. 177, 31–40. https://doi.org/10.1016/j.ecss.2016.05.007.

Malain, D., Regan, P.H., Bradley, D.A., Matthews, M., Al-Sulaiti, H.A., Santawamaitre, T., 2012. An evaluation of the natural radioactivity in Andaman beach sand samples of Thailand after the 2004 tsunami. Appl. Radat. Isot. 70, 1467–1474. https://doi.org/10.1016/j.apradiso.2012.04.017.

Mangas, J., Julià-Miralles, M., 2015. Geomorfología y naturaleza de las bajas submareales de Bajo Fernando, Los Roquerillos y La Zabala (NE de Gran Canaria). Geotemas 15, 37–40.

Medina, R., Bastón, S., Cánovas, V., Torres, A., Luque, Á., Alonso, I., Sánchez, I., Ortega, A., Rodríguez, S., Martín, J.A., 2006. Estudio integral de la playa de Las Canteras. Technical Report Dirección General de Costas.

Oguri, K., Harada, N., Tadai, O., 2012. Excess ^{210}Pb and ^{137}Cs concentrations, mass accumulation rates, and sedimentary processes on the Bering Sea continental shelf. Deep-Sea Res 193–204. https://doi.org/10.1016/j.dsr2.2011.03.007 part II 61–64.

Onjefu, S.A., Taole, S.H., Kgabi, N.A., Grant, C., Antoine, J., 2017. Assessment of natural radionuclide distribution in shore sediment samples collected from the North Dune beach, Henties Bay, Namibia. J. Radiat. Res. Appl. Sci. 10, 301–306. https://doi.org/10.1016/j.jrras.2017.07.003.

Palanques, A., Lopez, L., Guillén, J., Puig, P., Masqué, P., 2017. Decline of trace metal pollution in the bottom sediments of the Barcelona City continental shelf (NW Mediterranean). Sci. Total Environ. 579, 755–767. https://doi.org/10.1016/j.scitotenv.2016.11.031.

Pappa, F.K., Tsabaris, C., Ioannidou, A., Patiris, D.L., Kaberi, H., Pashalidis, I., Eleftheriou, G., Androulakaki, E.G., Vlastou, R., 2016. Radioactivity and metal concentrations in marine sediments associated with mining activities in Ierissos Gulf, North Aegean Sea, Greece. Appl. Radiat. Isot. 116, 22–33. https://doi.org/10.1016/j.apradiso.2016.07.006.

Punniyakotti, J., Ponnusamy, V., 2018. Environmental radiation and potential ecological risk levels in the intertidal zone of southern region of Tamil Nadu coast (HBRAs), India. Mar. Pollut. Bull. 127, 377–386. https://doi.org/10.1016/j.marpolbul.2017.11.026.

Ravisankar, R., Chandramohan, J., Chandrasekaran, A., Prince Prakash Jebakumar, J., Vijayalakshmi, I., Vijayagopal, P., Venkatraman, B., 2015. Assessments of radioactivity concentration of natural radionuclides and radiological hazard indices in sediment samples from the East coast of Tamilnadu, India with statistical approach. Mar. Pollut. Bull. 97, 419–430. https://doi.org/10.1016/j.marpolbul.2015.05.058.

Ravisankar, R., Sivakumar, S., Chandrasekaran, A., Prince Prakash Jebakumar, J., Vijayalakshmi, I., Vijayagopal, P., Venkatraman, B., 2014. Spatial distribution of gamma radioactivity levels and radiological hazard indices in the East Coastal sediments of Tamilnadu, India with statistical approach. Radiat. Phys. Chem. 103, 89–98. https://doi.org/10.1016/j.radphyschem.2014.05.037.

Renfro, A.A., Cochran, J.K., Hirschberg, D.J., Bokuniewicz, H.J., Goodbred Jr., S.L., 2016. The sediment budget of an urban coastal lagoon (Jamaica Bay, NY) determined using ^{234}Th and ^{210}Pb. Estuar. Coast Shelf Sci. 180, 136–149.

Shapiro, S.S., Wilk, M.B., 1965. An analysis of variance test for normality (complete samples). Biometrika 52, 591–611. https://doi.org/10.2307/2333709.

Shaw, P.J., 2003. Multivariate Statistics for the Environmental Science, First. ed. Hodder Headline Group, London, p. 244.

Shuaibu, H.K., Khandaker, M.U., Alrefae, T., Bradley, D.A., 2017. Assessment of natural radioactivity and gamma-ray dose in monazite rich black Sand Beach of Penang Island, Malaysia. Mar. Pollut. Bull. 119, 423–428. https://doi.org/10.1016/j.marpolbul.2017.03.026.

Siegel, S., Castellan, J.N., 1988. Nonparametric Statistics for the Behavioural Science, Second. McGraw-Hill, New York, p. 399.

Suresh Gandhi, M., Ravisankar, R., Rajalakshmi, A., Sivakumar, S., Chandrasekaran, A., Pream Anand, D., 2014. Measurements of natural gamma radiation in beach sediments of north east coast of Tamilnadu, India by gamma ray spectrometry with multivariate statistical approach. J. Radiat. Res. Appl. Sci. 7, 7–17. https://doi.org/10.1016/j.jrras.2013.11.001.

Szmytkiewicz, A., Zalewska, T., 2014. Sediment deposition and accumulation rates determined by sediment trap and ^{210}Pb isotope methods in the outer puck bay (Baltic Sea). Oceanologia 56, 85–106. https://doi.org/10.5697/oc.56-1.085.

Thomson, R.E., Emery, W.J., 2014. The spatial analyses of data fields. In: Thomson, R.E., Emery, W.J. (Eds.), Data Analysis Methods in Physical Oceanography. Elsevier Science, Amsterdam, pp. 335–340. https://doi.org/10.1017/CBO9781107415324.004.

UNSCEAR, 2000. Sources and Effects of Ionizing Radiation. Report of the United Nations Scientific Committee on the Effects of Atomic Radiation to the General Assembly, with Scientific Annexes. United Nations, New York.

Vasconcelos, D.C., Pereira, C., Oliveira, A.H., Santos, T.O., Rocha, Z., Menezes, M.Â.de B. C., 2011. Determination of natural radioactivity in beach sand in the extreme south of Bahia, Brazil, using gamma spectrometry. Radiat. Prot. Environ. 34, 178–184. https://doi.org/10.4103/0972-0464.101714.

Veiga, R., Sanches, N., Anjos, R.M., Macario, K., Bastos, J., Iguatemy, M., Aguiar, J.G., Santos, A.M.A., Mosquera, B., Carvalho, C., Filho, M.B., Umisedo, N.K., 2006. Measurement of natural radioactivity in Brazilian beach sands. Radiat. Meas. 41, 189–196. https://doi.org/10.1016/j.radmeas.2005.05.001.

Wang, J., Du, J., Bi, Q., 2017. Natural radioactivity assessment of surface sediments in the Yangtze Estuary. Mar. Pollut. Bull. 114, 602–608. https://doi.org/10.1016/j.marpolbul.2016.09.040.

Woszczyk, M., Poreba, G., Malinowski, Ł., 2017. ^{210}Pb, ^{137}Cs and ^{7}Be in the sediments of coastal lakes on the Polish coast: implications for sedimentary processes. J. Environ. Radioact. 169 (170), 174–185. https://doi.org/10.1016/j.jenvrad.2017.01.015.

Zhang, H., Lu, Y., Dawson, R.W., Shi, Y., Wang, T., 2005. Classification and ordination of DDT and HCH in soil samples from the Guanting Reservoir, China. Chemosphere 60, 762–769. https://doi.org/10.1016/j.chemosphere.2005.04.023.

3.2. ^{226}Ra, ^{228}Ra and ^{40}K as tracers of erosion and accumulation processes: A 3-year study on a beach with different sediment dynamics

Publicado en la revista *CATENA*

Año: *2021*

Volumen: *207*

DOI: *https://doi.org/10.1016/j.catena.2021.105705*

Journal Citation Report edición 2021: Categoría *Geoscience, Multidisciplinary*; Ranking *17/202*; Cuartil *Q1* (Decil *D1*)

Tras la conclusión del trabajo anterior en este trabajo se realizó un estudio en profundidad de la variabilidad temporal de las actividades de ^{226}Ra, ^{228}Ra (radionucleido hijo del ^{232}Th), ^{40}K y plomo en exceso ($^{210}Pb_{ex}$) durante un periodo de tres años, así como de la ratio $^{226}Ra/^{228}Ra$ en las distintas zonas de la playa de Las Canteras establecidas por el análisis espacial del trabajo anterior que conforma esta tesis (Arriola-Velásquez et al., 2019). Esto incluye la zona I correspondiente a la parte de la playa totalmente expuesta a la acción de oleaje, la zona II que incluye las partes de la playa localizadas enfrente de las aberturas de la barra y la zona III, la zona totalmente protegida por la barra frente a la acción del oleaje. Para ello se tomaron muestras mensuales de arena intermareal en 10 puntos de la playa desde septiembre de 2016 a agosto de 2019, siendo un total de 360 muestras recogidas y analizadas en un periodo de 3 años.

Además, para cada campaña se tomaron datos horarios de la presión atmosférica, la temperatura del aire, la humedad relativa, y los niveles de PM_{10} de una estación cercana al lugar de muestreo de la red de vigilancia y control de la calidad del aire del Gobierno de Canarias. Así mismo, se seleccionó una boya cercana a la zona de estudio de la red de Puertos del Estado del Gobierno de España de donde se extrajeron los datos de la dirección de aproximación del oleaje, la altura de ola significativa (H_s), la dirección del viento y la velocidad del viento. Estos datos se obtuvieron con el fin de analizar la influencia de los cambios de las condiciones ambientales y los distintos agentes erosivos que actúan en la playa en la variación de las concentraciones de actividad de los radionucleidos estudiados.

Una vez obtenidos todos los datos primero se llevó a cabo un análisis de las correlaciones existentes entre las concentraciones de actividad media encontradas para ^{226}Ra, ^{228}Ra, ^{40}K, $^{210}Pb_{ex}$ y la ratio $^{226}Ra/^{228}Ra$ en cada zona y los distintos parámetros medioambientales. En cada una de las tres zonas se encontró una fuerte correlación entre las concentraciones de actividad del ^{226}Ra, ^{228}Ra y ^{40}K. Esto reforzó la hipótesis del artículo anterior que indicaba que la dinámica responsable de la variación de ^{226}Ra, ^{228}Ra y ^{40}K era la misma para toda la playa.

Además, los resultados también mostraron una correlación inversa entre la H_s y las concentraciones de actividad de ^{226}Ra, ^{228}Ra y ^{40}K para la zona I (zona expuesta frente a la acción del oleaje). Esto indicó que en los periodos en los que la H_s fue más alta (normalmente asociados a tormentas y temporales) la concentración de actividad de estos radionucleidos fue menor. Por el contrario, en las épocas con alturas de ola significativa menores (periodos con más calma en los que se favoreció la acumulación de sedimentos en la playa) las concentraciones de actividad de ^{226}Ra, ^{228}Ra y ^{40}K fueron mayores. Esta correlación sugirió que en la zona I los agentes de erosión marinos fueron los que más afectaron a la variación en las concentraciones de actividad de ^{226}Ra, ^{228}Ra y ^{40}K durante los periodos de erosión y acumulación de sedimentos.

Por otro lado, en las zonas II y III no se encontró ninguna correlación entre los parámetros ambientales y las actividades de ^{226}Ra, ^{228}Ra y ^{40}K. Teniendo en cuenta que estos tres radionucleidos parecen estar fundamentalmente dominados por la dinámica marina de la playa, que la zona II y la zona III están localizadas en la parte de la playa protegida por la barra y que el oleaje sufre una difracción al chocar con

la barra, esta falta de correlación era lógica ya que los datos de dirección de aproximación del oleaje y H_s fueron tomados de una boya localizada en el exterior de la bahía. Por tanto, estudios más exhaustivos de la dinámica del oleaje existente entre la barra y la línea de costa serían necesarios para entender exactamente cómo la variación del oleaje afecta a estas dos zonas.

En el caso del $^{210}Pb_{ex}$ no se encontró ninguna correlación con el resto de los radionucleidos en ninguna de las zonas, sugiriendo de nuevo que la dinámica que controla la distribución de $^{210}Pb_{ex}$ es distinta a la que controla la distribución de los otros radionucleidos estudiados. Así mismo, tampoco se encontró ninguna correlación con el resto de los parámetros ambientales. Por ello, el $^{210}Pb_{ex}$ no se consideró más en este trabajo.

En lo que a la ratio $^{226}Ra/^{228}Ra$ se refiere, en las tres zonas se encontraron correlaciones inversas entre la ratio y la actividad de ^{228}Ra, siendo estas correlaciones más fuertes en las zonas II y III. De esta manera se puso de manifiesto que en la playa de Las Canteras el ^{228}Ra presentaba más movilidad que el ^{226}Ra. Esta mayor movilidad del ^{228}Ra frente al ^{226}Ra fue descrita en el trabajo de Dai et al., (2011) para los minerales arcillosos, sugiriendo así dicha ratio como indicador de periodos de erosión y acumulación en presencia de estos minerales. En la literatura sobre la composición mineralógica del entorno geológico de la playa de Las Canteras, se encontraron referencias a la presencia de minerales arcillosos en las zonas próximas al arco norte (Mangas and Julià-Miralles, 2015). Además, los estudios de dinámica sedimentaria de Las Canteras también indican un transporte longitudinal de sedimentos entre unas zonas y otras de la playa, pudiendo ser éste una vía de

transporte de granos de minerales arcillosos desde el norte de la playa hacia la zona abierta a la acción del oleaje. Esto explicaría por qué las correlaciones más fuertes se encontraron en las zonas II y III, las zonas más cercanas a la localización de minerales arcillosos.

Por otro lado, para las zonas II y III también se encontró una correlación inversa entre la ratio y la concentración de actividad de ^{40}K. Algunos estudios de la literatura indican que en minerales arcillosos las concentraciones de actividad del ^{40}K son de un orden de magnitud mayores que las del ^{232}Th (radionucleido padre de ^{228}Ra) y del ^{226}Ra (Hewamanna et al., 2001; Raghu et al., 2020). Esta diferencia en las concentraciones de actividad de ^{40}K en minerales arcillosos es igual a la encontrada en la playa de Las Canteras para las zonas II y III. Por tanto, los resultados obtenidos en el análisis de correlaciones sugirieron que la ratio ^{226}Ra/^{228}Ra podría estar trazando la presencia de estos minerales arcillosos en las zonas II y III y su transporte longitudinal en la playa.

Para estudiar más a fondo el papel del ^{226}Ra, ^{228}Ra, ^{40}K y la ratio ^{228}Ra/^{226}Ra como trazadores de las dinámicas sedimentarias marinas, se analizó si las concentraciones de actividad de los distintos radionucleidos y el valor de la ratio en cada zona presentaban diferencias significativas en base a la dirección de aproximación del oleaje y la H_s de cada campaña. Para ello se llevaron a cabo un análisis ANOVA de un factor y un Test HSD (Honestly-significant-difference) de Tukey (Williams and Abdi, 2010) . Los resultados mostraron que en la parte totalmente expuesta a la acción del oleaje las concentraciones de actividad de ^{228}Ra, ^{226}Ra y ^{40}K presentaban diferencias significativas, siendo las concentraciones de actividad más altas en las campañas donde la altura de ola significativa era baja y con oleaje del NE. Esto quiere decir que

en periodos en los que la acumulación de sedimentos se vio favorecida, las actividades de dichos radionucleidos fueron mayores. En cuanto a las zonas II y III, no se encontraron diferencias significativas para ninguno de los grupos. Esto podría deberse a la protección que la barra brinda a estas zonas de la playa. Por tanto, los resultados de este análisis nuevamente sugirieron que el ^{226}Ra, ^{228}Ra y ^{40}K son candidatos viables para trazar dinámicas sedimentarias marinas.

En el caso de la ratio $^{228}Ra/^{226}Ra$, no se encontraron diferencias significativas para ninguna de las zonas. En el artículo donde se sugería esta ratio como indicador de procesos de erosión y acumulación (Dai et al., 2011) se especificaba que, en circunstancias de acumulación, el valor de la ratio estaría por debajo de 1. La zona III de la playa está descrita como una zona de acumulación constante y durante todo el estudio presentó valores por debajo de 1. Por tanto, la falta de diferencias significativas en esta zona pareció estar relacionada con este periodo de acumulación continuo. Considerando esto y la información obtenida del estudio de correlaciones, los resultados de este trabajo sugirieron que la ratio $^{228}Ra/^{226}Ra$ podría ser útil para identificar periodos de erosión y acumulación de sedimentos siempre que éstos presentasen minerales arcillosos.

Finalmente, el análisis de la variación de la composición mineralógica demostró que en periodos de acumulación, cuando se encontraron las actividades más altas de ^{226}Ra, ^{228}Ra y ^{40}K, se daba un importante incremento en la cantidad de feldespatos potásicos encontrados en las muestras de la zona totalmente expuesta al oleaje (zona I). En la zona III, la variación de la composición de este mineral portador de potasio no era tan marcada como en la zona I.

Adicionalmente, el análisis de composición química de elementos con características químicas similares al Ra mostró que estos elementos presentaron un incremento en periodos de acumulación y una disminución en periodos de erosión para la zona I. Esto concuerda con el comportamiento presentado por el ^{40}K y por tanto sugieren que las variaciones de ^{226}Ra y ^{228}Ra están también asociadas a las variaciones de la cantidad de feldespatos potásicos transportados transversal y longitudinalmente en la playa en las distintas épocas. Por ello, el resultado de este estudio confirmó la viabilidad del uso del ^{226}Ra, ^{228}Ra y particularmente ^{40}K como trazadores de procesos de dinámica sedimentaria marina en zonas intermareales de la playa de Las Canteras.

Catena 207 (2021) 105705

Contents lists available at ScienceDirect

Catena

journal homepage: www.elsevier.com/locate/catena

^{226}Ra, ^{228}Ra and ^{40}K as tracers of erosion and accumulation processes: A 3-year study on a beach with different sediment dynamics

A.C. Arriola-Velásquez [a], A. Tejera [a,*], J.G. Guerra [a], W. Geibert [b], I. Stimac [b], F. Cámara [c], H. Alonso [a], J.G. Rubiano [a], P. Martel [a]

[a] Department of Physics, Instituto Universitario de Investigación en Estudios Ambientales y Recursos Naturales i-UNAT, Universidad de Las Palmas de Gran Canaria, Campus de Tafira, 35017 Las Palmas de Gran Canaria, Spain
[b] Alfred Wegener Institute, Helmholtz Centre for Polar and Marine Research, Bremerhaven, Germany
[c] Dipartimento di Scienze della Terra, Università degli Studi di Milano, via Sandro Botticelli 23, 20133 Milano, Italy

ARTICLE INFO

Keywords:
Radionuclides
Tracers
Coastal sediments
Beach
Erosion/accumulation

ABSTRACT

The aim of this study is to analyse the role of natural radionuclides ^{226}Ra, ^{228}Ra, ^{40}K and unsupported ^{210}Pb (^{210}Pb$_{ex}$), as erosion and accumulation process tracers. For this purpose, a complex system, including both the characteristic dynamics of a closed beach and those associated with a beach open to wave action, was studied. A 3-year study of monthly variation of ^{226}Ra, ^{228}Ra, ^{40}K and ^{210}Pb$_{ex}$ was carried out at Las Canteras beach, on the Island of Gran Canaria (Spain), covering several erosion and accumulation periods. A correlation analysis, ANOVA test and Tukey's Honestly Significant Difference (HSD) Test proved that the marine erosion and accumulation agents influenced the activity concentration values found for the different radionuclides. Moreover, the geochemical analysis of samples from maximum and minimum activity concentration values showed that the natural radionuclides studied could be suitable tracers for studying beach sediment dynamics in erosion and accumulation periods.

1. Introduction

Natural radioactivity on the Earth's surface has different origins; principally it is generated by the primordial elements in the Earth's crust. The rest is generated by the interaction of cosmogenic radiation with the atmosphere and its deposition onto the planet surface by different processes. The most common radionuclides on the Earth's crust are ^{40}K and those that come from the radioactive decay chains of ^{238}U and ^{232}Th. The geochemical composition of the Earth's crust influences the different types of sediments and rocks that crop out at the surface around the world, varying its radioactivity levels from one place to another. In coastal areas, the geochemical and geophysical conditions also influence in the levels of radioactivity that can be found in its sediments. For example, in areas where permeable sediments can be found, processes such as tidal pump affect the coastal aquifers and create a flow of water known as submarine groundwater discharges (SGD) (Burnett et al., 2003; Moore, 2007). In these cases, when salty water gets in contact with the surface sediments of the aquifer Ra isotopes are transferred to the water from the sediments. Therefore, these sediments will present a lower activity concentration or Ra radionuclides than they normally would. Within this framework, some studies have been focused on the use of natural radionuclides in coastal waters as tracers of possible sediment derived inputs of nutrients or contaminants in the ocean (Kipp et al., 2020; Sanial et al., 2015; Tamborski et al., 2018). Other studies have focus on the measurement of natural radionuclides contained in sediments to assess the sediment transfer time in river systems as well as river flood reconstructions (Chabaux et al., 2012, 2006; Yang et al., 2013). Moreover, there are studies that focused on the use of natural radionuclides in sediments as tracers of sediment sources and transport pathways in coastal areas (Bezuidenhout, 2020; Huang et al., 2013; Lin et al., 2020; Thereska, 2009; Wang et al., 2018). In addition, some studies have also used the natural radionuclides content in core sediments to measure sedimentation rates, sediment redistribution or sediment dating (Giffin and Corbett, 2003; Li et al., 2021; Sun et al., 2020). All of these studies are examples that show the relevance of using natural radionuclides as tracers of sediment dynamics and processes related to it.

In the case of Las Canteras beach, located in El Confital Bay in the

* Corresponding author.
E-mail address: alicia.tejera@ulpgc.es (A. Tejera).

https://doi.org/10.1016/j.catena.2021.105705
Received 31 May 2021; Received in revised form 26 August 2021; Accepted 29 August 2021
Available online 7 September 2021

north of the Island of Gran Canaria (Spain), previous studies have established a baseline of environmental radioactivity in sand samples and algae arrivals (Arnedo et al., 2013; Arriola-Velásquez et al., 2019; Tejera et al., 2019). Las Canteras beach is divided into three arches and has a rocky bar offshore that protects the northern and central arches (Fig. 1). This bar is not a whole block and presents openings that create different sections, predominantly in the central arch. Therefore, the part of the beach that is most protected against wave action by the natural offshore rocky bar is the northern arch, whereas the southern arch is totally exposed to the wave action (Alonso, 1994, 1993; Alonso and Vilas, 1996). In this framework, the 1 year study by Arriola-Velásquez et al. (2019) provided information about the spatial distribution of natural radionuclides ^{226}Ra, ^{232}Th and ^{40}K, along the beach. The sampling points with lower activity concentrations of these radionuclides were in the parts of the beach with no protection from the bar, while the sampling points that were fully protected by the rocky bar presented higher activity concentration values. The sampling points that were in front of the openings of the bar displayed intermediate activity concentration values. This seemed to indicate that the spatial distribution of these natural radionuclides was related to the different sediment dynamics that can be found on Las Canteras beach, depending on the presence or absence of the natural offshore rocky bar and its openings. Moreover, in that work, a temporal variability study was performed for the first time. The ^{226}Ra/^{228}Ra ratio proposed by Dai et al. (2011) was used for that purpose. According to their study, ^{228}Ra and ^{226}Ra are more present in the crystal framework of clay minerals, but the carbonate and exchangeable phases contain more ^{228}Ra. Thus, accretion or erosion periods could be measured by a change in the ratio between ^{226}Ra and ^{228}Ra, assuming the natural ratio ^{232}Th/^{238}U. Therefore, during accumulation periods the input of ^{228}Ra would be higher and the ratio would have a value below 1. During erosion periods, on the contrary, the ratio would have a value above 1. In the case of Las Canteras beach some crystals from clay minerals and zeolites had been found in the north part of it (Mangas and Julià-Miralles, 2015). Hence, the use of this ratio as a tracer of erosion and accumulation period seemed suitable for the study of Arriola-Velásquez et al. (2019). The results showed a constant accumulation period when a full protection of the bar was present. However, for the open part of the beach and the parts located in front of the opening, the results exhibited the need for a further temporal analysis to better understand the temporal variability of radionuclides in these parts of the beach.

The results obtained for the spatial and temporal variability of the natural radionuclides at Las Canteras beach in 2019 seemed to indicate that the radionuclides studied were tracing the sediment dynamics that had been studied for this region. According to these previous studies, the beach presents seasonal variability in its sedimentary budget (Alonso, 1994, 1993; Alonso and Vilas, 1996). In erosion periods, the southern arch, being totally exposed to the wave action, loses a large amount of sediments that suffer a lengthwise transport to the northern and central arch. On the other hand, in accumulation periods, the whole beach receives an inflow of sediments. Under these circumstances, some berms appear in the northern arch and a lengthwise transport can occur to the southern arch. The sediments that arrive on the beach come from the geological environment, basic volcanic rocks from La Isleta, in the northeast of El Confital bay, phonolitic lava flow from the southwestern side of the bay, basic rocks and magnetite from the mouth of La Ballena ravine in the south part of the beach, submerged sandbars located between the bathymetric curve of 50 m and the beachfront and the natural offshore calcarenite rocky bar (Balcells et al., 1990; Schmincke, 1993). Some calcimetry and petrological analyses of the beach sand, as well as the geological composition of El Confital Bay define the different geological materials that can be found along Las Canteras beach. The northern arch presents a higher bioclast and calcareous content than the southern arch. Nevertheless, the northern part of the beach has a higher content of calcarenite that contains mainly feldspar crystals in its terrigenous part. Therefore, feldspars are also accumulated in the northern part of the beach. On the other hand, the outlet of the ravine that ends in Las Canteras beach is located in the southern part. Hence, this part tends to accumulate clinopyroxenes and other heavy minerals, such as olivine, amphiboles and Fe-Ti oxides that come from this ravine while the lighter lithics are redistributed along the beach (Alonso, 1993; Alonso and Pérez Torrado, 1992; Mangas and Julià-Miralles, 2015; Medina et al., 2006). All of these differences between one part of Las Canteras beach and another make it an ideal natural laboratory to monitor the changes in natural radionuclides associated with distinct sediment dynamics. The beach presents two parts with different sediment dynamic and composition. The south part is opened to the wave action and tends to accumulate heavy minerals. The northern part is

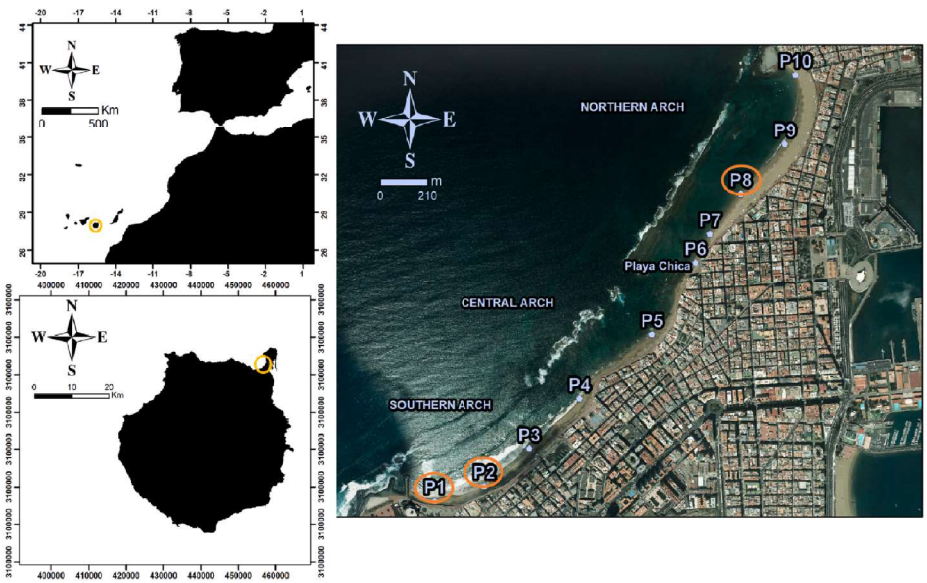

Fig 1. Location of the study region and the sampling points in Las Canteras beach. Coordinates are in the UTM system.

protected against the wave action by the natural offshore rocky bar and presents more calcarenite and organic material. Therefore, the results obtained in this beach could resemble to the evaluation of radiotracers of sediment dynamics in two different beaches with different marine dynamics and mineralogical composition. Hence, radiotracers that trace sediment dynamics in both parts of the beach would have a wider use and could be suggested as tracers that can be used in other parts of the world. In addition, radiotracers that only seemed to work in one part of the beach could be suggested as tracers of sediment dynamics of beaches with similar characteristics to one the different parts of Las Canteras beach.

In essence, previous studies at Las Canteras beach have provided information on the spatial variability of environmental radionuclides which seems to follow the dynamics under which the different parts of the beach are subjected. However, a further temporal analysis is necessary, to prove the viability of natural radionuclides as tracers of beach sediment dynamics. Therefore, the aim of this work is to provide a deeper analysis of the temporal variability of natural radionuclides at Las Canteras beach. For this purpose, the changes in activity concentrations of natural radionuclides will be analysed over a period of 3 years. Moreover, the relations between these variations in activity concentration and different erosion and accumulation agents, such as significant wave height or wind speed, will be evaluated. Finally, the geochemical differences in samples from erosion and accumulation periods will be studied. Las Canteras beach was selected for this study due to the combination of the characteristic dynamics of a closed beach and those associated with a beach open to wave action. This would allow the results of this work to be applied to other places around the world.

2. Material and methods

2.1. Sample collection and preparation

A total of 360 samples were taken during the study period. Sand collection was undertaken monthly for three years, from September 2016 to August 2019. Ten samples were selected for each campaign (Fig. 1): four in the southern arch, one in the central arch, one in Playa Chica and the last four in the northern arch.

In order to study the marine interactions with the distribution of radionuclides, superficial samples were taken during low tide in the intertidal zone of Las Canteras beach. At each sampling point, a square of 1 m^2 was drawn and, after mixing in situ, samples were taken from the superficial sand (between 0 and 5 cm depth). After the samples were taken to the laboratory, they were dried at 80 °C for 24 h. They were then sieved through a 1 mm mesh size to homogenise them and kept inside PVC-trunk conical containers, filled to 40 cm^3. They were sealed with aluminium strips, because they are impermeable to radon gas. Finally, the samples were stored for a duration of approximately one month before measurement to allow secular equilibrium between ^{226}Ra and ^{222}Rn and its short-lived progenies (as ^{214}Pb is used for determining ^{226}Ra) (Bezuidenhout, 2013).

2.2. Meteorological, oceanographic and PM_{10} data

To establish if variations in environmental conditions during the different campaigns affected the variations in activity concentration of radionuclides, the effect of environmental conditions were studied. For this, hourly atmospheric conditions (atmospheric pressure, air temperature, relative humidity and PM_{10} levels) were taken from a station belonging to the network of surveillance and control of air quality, run by the Canary Islands Government, during campaign hours. In addition, data of wave approach direction and significant wave height at low tide in the distinct campaigns were taken from a buoy of the Puertos del Estado surveillance network, belonging to the government of Spain. Wind approach direction and wind speed data were also obtained from the same station at Puertos del Estado.

2.3. Gamma emission analysis

The determination of radionuclides in sand samples by gamma spectrometry analysis was carried out using a Canberra Extended Range (XtRa) Germanium spectrometer (model GX3518), with 38% relative efficiency with respect to a 3″ x 3″ active area NaI (Tl) detector and nominal FWHM of 0.875 keV at 122 keV and 1.8 keV at 1.33 MeV. It is coupled to a Canberra DSA-1000 multichannel analyser with the Genie 2000 software package. Efficiency calibration of the system was performed using the Canberra LabSOCS package, based on the Monte Carlo method (Arnedo et al., 2017; Arriola-Velásquez et al., 2019; Guerra et al., 2017, 2015). Calibration was verified using reference standards for IAEA RGK-1 (potassium sulfate), RGU-1 (uranium ore) and RGTh-1 (thorium ore). Energy calibration was carried out using a 155Eu/22Na (Canberra ISOXSRCE, 7F06-9/10138 series) and confirmed using the 1460.8 keV line of ^{40}K (IAEA RGK-1) (Arnedo et al., 2017).

The radionuclides of interest were determined from different photopeaks. ^{226}Ra was determined from ^{214}Pb, using the 351.9 keV emission line. ^{210}Pb was directly measured using the 46.5 keV emission line. The activity concentration of ^{228}Ra was calculated from ^{228}Ac by the 911.2 keV emission line. Activity concentrations of ^{40}K and ^{137}Cs were directly measured using emission lines 1460.8 keV and 661.8 keV, respectively. The counting time for each sample was around 24 h.

In addition, ^{210}Pb is derived from the decay of ^{222}Rn (half-life of 3.8 days). This ^{222}Rn is a gas progeny of ^{226}Ra that partially diffuses into the atmosphere where it rapidly decays into ^{210}Pb. Then, this ^{210}Pb falls back to the earth's surface by wet and dry deposition. This deposited ^{210}Pb is not in equilibrium with its progenies ^{226}Ra and it is known as unsupported or excess $^{210}Pb_{ex}$ (Gaspar et al., 2017; Hülse and Bentley, 2012; Wakiyama et al., 2010). Thus, the activity of $^{210}Pb_{ex}$ was determined by the difference between the activity concentrations of ^{210}Pb and ^{226}Ra.

2.4. ICP-OES, ICP-MS and X-ray diffraction analysis

Inductively-coupled, plasma, optical emission spectrometry (ICP-OES) was used to carry out a multi-element analysis (Pozebon, 2002) of the samples and an inductively-coupled plasma mass spectrometry (ICP-MS) analysis was used to report the activity concentrations of uranium and thorium radioisotopes (Halliday et al., 1998; Walder and Freedman, 1992; Zheng et al., 2003) for each sample. The accuracy and repeatability of the results for both analyses were confirmed by using two reference materials (UREM-11 bulk sample of low-grade uranium ore and MESS-4 Beaufort Sea sediment) alongside the samples. Moreover, in the case of the ICP-MS analysis, a third reference material (IAEA-385 Irish sea sediment) was also used for method validation.

The ICP-MS instrument, as described in Pittauer et al. (2018), has a jet interface and uses an APEX-IR desolvation to maximize ion transmission of the samples. The effects of instrumental mass bias and uranium hybrid formation were controlled to make sure the results were clear of these effects. Furthermore, the results obtained for ^{238}U were not directly measured by the detector but calculated from the activity obtained for ^{235}U and the natural ratio $^{238}U/^{235}U$.

Finally, Powder X-ray diffraction (XRPD) data acquisition was carried out by an X'Pert PRO (PANalytical) Diffractometer, in θ-2θ Bragg-Brentano geometry, equipped with an X'Celerator LPS detector. The 5° to 80° 2θ range was investigated using CuKα radiation, working at 40 kV current tension, 40 mA current intensity and collecting at 0.02° steps, with a fixed divergence slit angle of 0.25°. Samples were ground on an agate mortar and then pressed in a back-load sample holder. The sample holder was spun during data acquisition. Diffraction patterns were analysed using X'Pert HighScore v. 2.1 (PANalytical©) software and mineral phases were matched using PDF2 (ICDD).

Selected grains of sample PLC18_8.2 were also checked by single crystal X-ray diffraction (SCXRD) using a Rigaku Oxford Diffraction XtaLAB Synergy diffractometer equipped with a PhotonJet (Mo) X-ray

Source, operating at 50 kV and 1 mA, and a Hybrid Pixel Array detector at 62 mm from the sample position. Intensity data was extracted from the images using CrysAlisPro 1.171.40.71a (Rigaku Oxford Diffraction, 2020). Crystal structures were refined using SHELX-2018 (Sheldrick, 2015) starting for atom coordinates collected from literature. Crystallographic information files including the results of these structure refinements are included in this paper as electronic supplementary material.

2.5. Proficiency test

In order to establish whether the measurements of radionuclides were optimal, the Analytical Laboratories for the Measurement of Environmental Radioactivity (ALMERA) proficiency test was performed (IAEA, 2011; Osvath et al., 2016; Shakhashiro et al., 2012). For this test, two parameters were calculated and, depending on the results of both parameters, the activity value given for one sample would be acceptable and/or different from the ones of another sample. First, the u-test was calculated following Eq. (1):

$$u_{test} = \frac{|A_A - A_B|}{\sqrt{u_A^2 + u_B^2}} \quad (1)$$

where A_A corresponds to the activity concentration value of one sample from the minimum activity concentration campaign, u_A is the uncertainty associated with that activity, A_B is the activity concentration value obtained for one sample from the same sampling point in the maximum activity concentration campaign and u_B is the uncertainty of that measurement. This u-test was performed with a limiting value to determine if a result passes the test of 2.58 for a 99% level of probability ($u_{test} < 2.58$). Therefore, when $u > 2.58$ the pair of values reported was significantly different.

On the other hand, to assess the uncertainty of the reported measurements, the P_{score} was calculated with the following equation:

$$P_{score} = \sqrt{\left(\frac{u_A}{A_A}\right)^2 + \left(\frac{u_B}{A_B}\right)^2} \quad (2)$$

where A_A corresponds to the activity concentration value of one sample from the minimum activity concentration campaign, u_A is the uncertainty associated with that activity, A_B is the activity concentration value obtained for the samples corresponding to the same sampling point in the maximum activity concentration campaign and u_B is the uncertainty of that measurement. According to this test, when the P_{score} < Limit of Acceptable Precision (LAP), the results give scores that are acceptable for the claimed uncertainty. The LAP values used in the evaluation of P_{score} correspond to the values given in IAEA (2011) of 20% for all of the radionuclides analysed in this study.

2.6. Statistical analysis

First, a correlation analysis between the meteorological, oceanographic and radioactivity data was performed. Then, different statistical tests were performed with the activity concentration of the different radionuclides of interest divided into groups established by the environmental conditions. Levene's test (Schultz, 1985) was carried out to evaluate the homogeneity of the variance. After that, a one-way ANOVA test was performed to evaluate the presence of significant differences among the different groups. Finally a Tukey's Honestly Significant Difference (HSD) Test (Williams and Abdi, 2010) was used to establish the exact groups within which significant differences were found.

3. Results and discussion

3.1. Activity concentrations

A Shapiro-Wilk test (Shapiro and Wilk, 1965) was carried out for each time series of the values of activity concentration (for ^{226}Ra, ^{228}Ra, ^{40}K and $^{210}Pb_{ex}$) corresponding to each sampling point (360 data for each radionuclide). For all of the results, the data showed a normal distribution at a significance level of 0.05, except for the values in the series of ^{40}K for sampling points P1 and P2. For these sampling points, normality was found at a significance level of 0.01. The boxplot in Fig. 2 shows the activity concentration of ^{226}Ra, ^{228}Ra, ^{40}K and $^{210}Pb_{ex}$ for each sampling point during the whole study period. The activity concentration of ^{226}Ra ranged from 4.6 ± 0.7 to 24.9 ± 1.5 Bq kg^{-1} with a mean value of 13.3 ± 0.9 Bq kg^{-1}. In the case of ^{228}Ra, the activity concentration values were reported between 4.7 ± 1.3 and 33.3 ± 2.9 Bq kg^{-1} with a mean value of 17.0 ± 1.6 Bq kg^{-1}. Regarding ^{40}K, activity concentration values fluctuated from below the detection limit of 4 Bq kg^{-1} (BDL) to 842 ± 37 Bq kg^{-1} with a mean value of 405 ± 19 Bq kg^{-1}. Finally, $^{210}Pb_{ex}$ varied from 11.3 ± 3.8 to 65.9 ± 6.8 Bq kg^{-1} with a mean value of 32.7 ± 5.7 Bq kg^{-1}.

The data shows similar behaviour to that in the work of Arriola-Velásquez et al. (2019). There were, generally, lower activities in sampling points in the southern arch, the area being fully open to wave action, and a progressive increase of the activity concentration of ^{226}Ra, ^{228}Ra and ^{40}K in the northern arch, the area protected by the offshore rocky bar. The $^{210}Pb_{ex}$ reports the same behaviour as in the previous study, with similar activity concentration values found along the beach. This reinforces the conclusions found in that work and enhances the proposed idea of the use of the distribution of ^{226}Ra, ^{228}Ra and ^{40}K as tracers of marine sediment dynamics due to its distribution along the beach, conditioned by the morphology of the natural offshore rocky bar. Furthermore, the results of this study were analysed from the perspective of the three zones of activity distribution along the beach that appeared in the study of 2019, i.e. an area totally exposed to the wave interactions (zone I), an area located in front of the openings of the offshore rocky bar (zone II) and an area fully protected against wave action (zone III).

Additionally, the temporal series for the mean values of ^{226}Ra, ^{228}Ra, ^{40}K and the ratio ^{226}Ra/^{228}Ra for each of the zones of the beach are shown in Fig. 3. In zone I, ^{226}Ra, ^{228}Ra and ^{40}K follow a similar pattern with maxima activity concentration values mostly seen in the summer months, with some exceptions, and lower activity concentration values in winter months. For zone II, some alternations of maxima and minima activity concentration values appear. In the case of zone III, the three radionuclides show similar behaviour with rather constant activity concentrations for the whole study region. This seems to be tracing what is described in the literature about the sedimentary transport and budget in Las Canteras beach (Alonso, 1994, 1993; Alonso and Vilas, 1996). According to this, during erosion periods, the open part of the beach (zone I in this study) loses a large amount of sand that is transported lengthwise to the closed part of the beach (zone III in this study), while, during accumulation periods, there is an input of sediments to the open part of the beach. The erosion periods would occur when a storm event hits the beach, which would be more likely to occur in winter. Therefore, the maximum and minimum activity concentration values found for ^{226}Ra, ^{228}Ra an ^{40}K in zone I seem to be tracing the input and output of sand in this part of the beach during the different periods. In the case of zone III, the literature explains that this part is in a constant accumulation period, so that could explain the constant activity concentration values found for this part. In comparison to these radionuclides, $^{210}Pb_{ex}$ does not show much of a difference for the whole study period, except for the activity concentration of September 2017 in zone I that is slightly higher to the rest. This reinforces the idea that the agents controlling the changes in $^{210}Pb_{ex}$ are different from the ones controlling the distribution of the other radionuclides studied (Arriola-Velásquez et al., 2019).

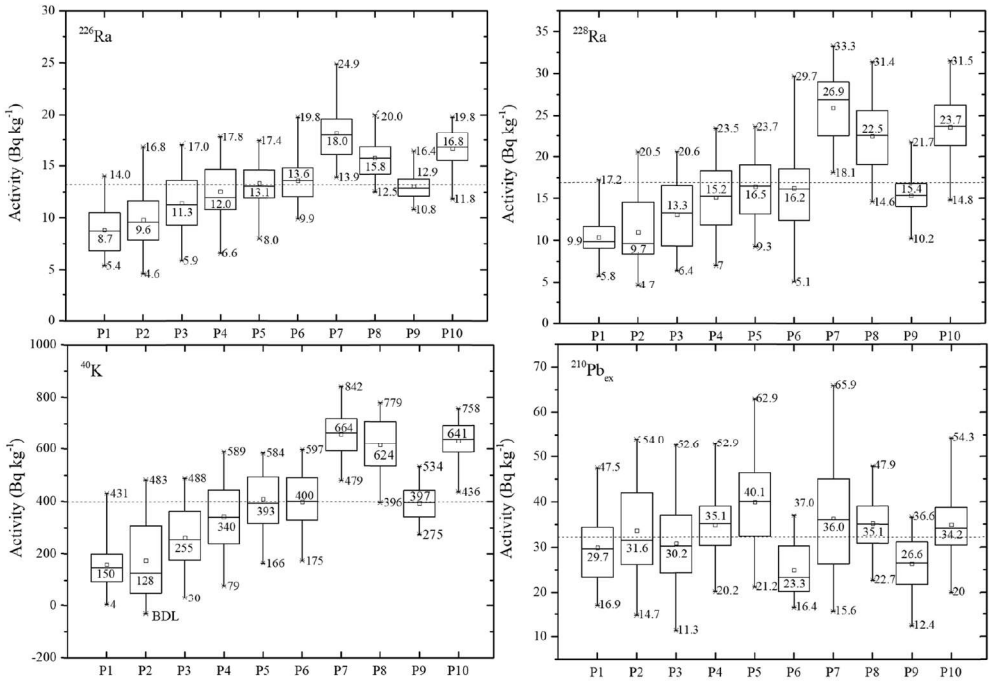

Fig. 2. Boxplots of the activity concentrations found for each sampling point for ^{226}Ra, ^{228}Ra, ^{40}K and $^{210}Pb_{ex}$. The dash line indicates the mean activity concentration value. The numbers that appear in each whisker correspond to the maximum and minimum activity concentration values. The number in the middle indicates the mean activity concentration value for each sampling point.

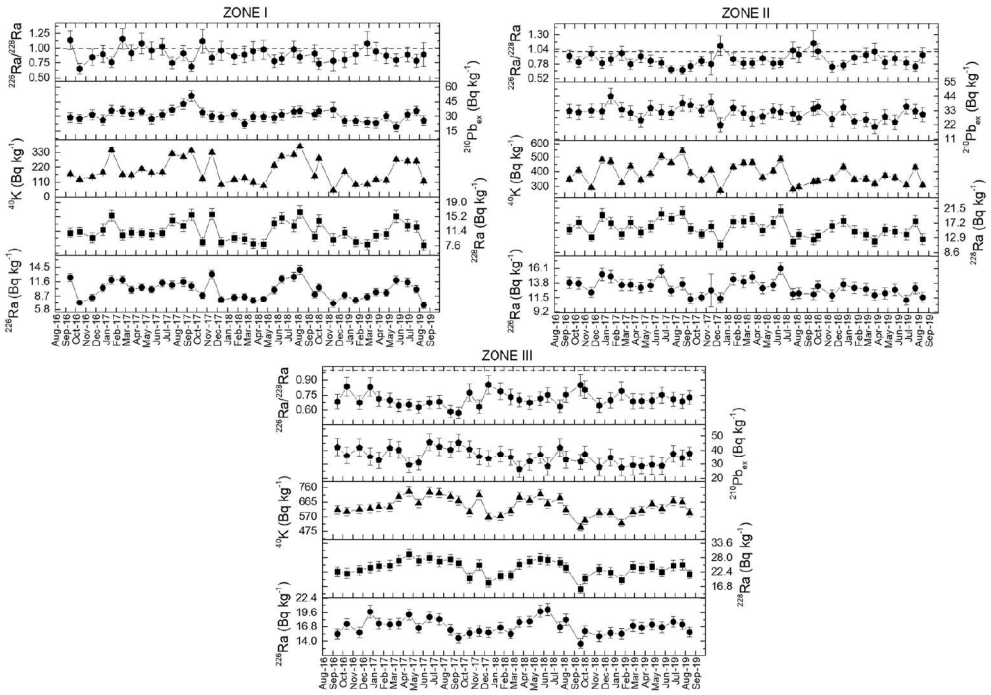

Fig. 3. Temporal series of the activity concentration of ^{226}Ra, ^{228}Ra, ^{40}K, $^{210}Pb_{ex}$ and the ratio $^{226}Ra/^{228}Ra$ during the study period for the different zones established in (Arriola-Velásquez et al., 2019) for Las Canteras beach.

Thus, $^{210}Pb_{ex}$ does not seem to be a good tracer of marine sediment dynamics, while ^{226}Ra, ^{228}Ra and ^{40}K seem to be good candidates for tracing erosion and accumulation periods.

Finally, the results for $^{226}Ra/^{228}Ra$ show different things in the different zones. According to what was suggested for this ratio in the literature (Dai et al., 2011), when this ratio was below 1, it would indicate an accumulation period. On the other hand, values above 1 would indicate an erosion period. In Fig. 3, the limit is marked with a dashed line and it can be appreciated that for zone III, all of the values are below 1. This would indicate a constant accumulation period, which agrees with what is described in the literature for the closed part of the beach. However, in zones I and II the results are not so conclusive and clear differences do not appear between summer and winter months. In the work of Dai et al. (2011) the use of this ratio was based on the presence of clay minerals in the study region. The northeastern part of El Confital bay, where the northern arch of the beach (zone III) is located, is

Table 1
Correlation coefficients matrix of activity concentration of ^{226}Ra, ^{228}Ra, ^{40}K, $^{210}Pb_{xc}$, the ratio $^{226}Ra/^{228}Ra$, wave approach direction, significant wave height (H_S), wind approach direction, wind speed, PM_{10}, temperature (T), relative humidity (RH) and atmospheric pressure (PRB) for A) Zone I, B) Zone II and C) Zone III. The p-value is set at 0.05.

(A) ZONE I	Wave approach direction	H_S (m)	Wind approach direction	Wind speed (m s^{-1})	PM_{10}	T (°C)	RH (%)	PRB (mb)	^{226}Ra	^{228}Ra	^{40}K	$^{210}Pb_{ex}$	$^{226}Ra/^{228}Ra$
Wave aproach direction	1	*0.516*	*0.230*	*0.386*	*0.996*	*0.545*	*0.515*	*0.869*	*0.020*	*0.016*	*0.005*	*0.326*	*0.683*
H_S (m)	0.112	1	*0.087*	*0.000*	*0.579*	*0.009*	*0.280*	*0.059*	*0.000*	*0.000*	*0.000*	*0.035*	*0.294*
Wind aproach direction	0.205	−0.290	1	*0.074*	*0.611*	*0.038*	*0.950*	*0.016*	*0.744*	*0.625*	*0.479*	*0.245*	*0.381*
Wind speed	−0.149	0.584	−0.301	1	*0.451*	*0.059*	*0.277*	*0.078*	*0.318*	*0.108*	*0.038*	*0.017*	*0.162*
PM_{10}	0.001	0.096	−0.088	0.130	1	*0.090*	*0.000*	*0.341*	*0.803*	*0.965*	*0.657*	*0.953*	*0.624*
T (°C)	−0.104	−0.429	0.347	−0.318	0.287	1	*0.175*	*0.016*	*0.149*	*0.103*	*0.025*	*0.029*	*0.764*
RH (%)	−0.112	−0.185	−0.011	−0.186	−0.626	−0.231	1	*0.450*	*0.757*	*0.580*	*0.493*	*0.635*	*0.510*
PRB (mb)	0.028	0.318	−0.398	0.297	0.163	−0.398	−0.130	1	*0.206*	*0.124*	*0.181*	*0.249*	*0.508*
^{226}Ra	−0.385	−0.603	−0.056	−0.171	0.043	0.245	0.053	−0.216	1	*0.000*	*0.000*	*0.068*	*0.662*
^{228}Ra	−0.399	−0.633	0.084	−0.272	0.008	0.276	0.095	−0.261	**0.797**	1	*0.000*	*0.019*	*0.001*
^{40}K	−0.457	−0.688	0.122	−0.347	0.077	0.373	0.118	−0.228	**0.824**	**0.940**	1	*0.003*	*0.023*
$^{210}Pb_{ex}$	−0.168	−0.352	0.199	−0.394	−0.010	0.363	0.082	−0.197	0.308	0.390	0.477	1	*0.318*
$^{226}Ra/^{228}Ra$	0.071	0.180	−0.150	0.238	0.085	−0.052	−0.113	0.114	0.075	**−0.517**	−0.378	−0.171	1
p-value 0.05													

(B) ZONE II	Wave approach direction	H_S (m)	Wind approach direction	Wind speed (m s^{-1})	PM_{10}	T (°C)	RH (%)	PRB (mb)	^{226}Ra	^{228}Ra	^{40}K	$^{210}Pb_{ex}$	$^{226}Ra/^{228}Ra$
Wave aproach direction	1	*0.516*	*0.230*	*0.386*	*0.996*	*0.545*	*0.515*	*0.869*	*0.864*	*0.867*	*0.488*	*0.918*	*0.753*
H_S (m)	0.112	1	*0.087*	*0.000*	*0.579*	*0.009*	*0.280*	*0.059*	*0.338*	*0.087*	*0.117*	*0.010*	*0.143*
Wind aproach direction	0.205	−0.290	1	*0.074*	*0.611*	*0.038*	*0.950*	*0.016*	*0.648*	*0.117*	*0.138*	*0.374*	*0.051*
Wind speed	−0.149	0.584	−0.301	1	*0.451*	*0.059*	*0.277*	*0.078*	*0.572*	*0.436*	*0.556*	*0.070*	*0.114*
PM_{10}	0.001	0.096	−0.088	0.130	1	*0.090*	*0.000*	*0.341*	*0.837*	*0.500*	*0.808*	*0.864*	*0.310*
T (°C)	−0.104	−0.429	0.347	−0.318	0.287	1	*0.175*	*0.016*	*0.076*	*0.840*	*0.615*	*0.413*	*0.515*
RH (%)	−0.112	−0.185	−0.011	−0.186	−0.626	−0.231	1	*0.450*	*0.280*	*0.476*	*0.521*	*0.860*	*0.876*
PRB (mb)	0.028	0.318	−0.398	0.297	0.163	−0.398	−0.130	1	*0.215*	*0.968*	*0.981*	*0.466*	*0.357*
^{226}Ra	0.030	−0.165	0.079	0.097	−0.036	−0.299	−0.185	0.212	1	*0.000*	*0.000*	*0.143*	*0.085*
^{228}Ra	−0.029	−0.289	0.266	−0.134	−0.116	−0.035	−0.123	−0.007	**0.764**	1	*0.000*	*0.024*	*0.000*
^{40}K	−0.119	−0.266	0.252	−0.102	−0.042	−0.087	−0.111	0.004	**0.744**	**0.950**	1	*0.011*	*0.000*
$^{210}Pb_{ex}$	−0.018	−0.424	0.153	−0.305	−0.030	0.141	−0.030	0.126	0.249	0.375	0.420	1	*0.056*
$^{226}Ra/^{228}Ra$	0.054	0.249	−0.328	0.268	0.174	−0.112	0.027	0.158	−0.291	**−0.804**	**−0.731**	−0.322	1
p-value 0.05													

(C) ZONE III	Wave approach direction	H_S (m)	Wind approach direction	Wind speed (m s^{-1})	PM_{10}	T (°C)	RH (%)	PRB (mb)	^{226}Ra	^{228}Ra	^{40}K	$^{210}Pb_{ex}$	$^{226}Ra/^{228}Ra$
Wave aproach direction	1	*0.516*	*0.230*	*0.386*	*0.996*	*0.545*	*0.515*	*0.869*	*0.538*	*0.188*	*0.112*	*0.608*	*0.264*
H_S (m)	0.112	1	*0.087*	*0.000*	*0.579*	*0.009*	*0.280*	*0.059*	*0.194*	*0.042*	*0.025*	*0.461*	*0.165*
Wind aproach direction	0.205	−0.290	1	*0.074*	*0.611*	*0.038*	*0.950*	*0.016*	*0.138*	*0.157*	*0.181*	*0.233*	*0.685*
Wind speed	−0.149	0.584	−0.301	1	*0.451*	*0.059*	*0.277*	*0.078*	*0.875*	*0.114*	*0.118*	*0.160*	*0.013*
PM_{10}	0.001	0.096	−0.088	0.130	1	*0.090*	*0.000*	*0.341*	*0.906*	*0.964*	*0.343*	*0.343*	*0.991*
T (°C)	−0.104	−0.429	0.347	−0.318	0.287	1	*0.175*	*0.016*	*0.853*	*0.218*	*0.232*	*0.043*	*0.191*
RH (%)	−0.112	−0.185	−0.011	−0.186	−0.626	−0.231	1	*0.450*	*0.297*	*0.286*	*0.698*	*0.406*	*0.610*
PRB (mb)	0.028	0.318	−0.398	0.297	0.163	−0.398	−0.130	1	*0.512*	*0.020*	*0.006*	*0.424*	*0.022*
^{226}Ra	−0.106	−0.221	0.252	0.027	0.020	0.032	−0.179	−0.113	1	*0.000*	*0.000*	*0.584*	*0.995*
^{228}Ra	−0.225	−0.341	0.241	−0.268	−0.008	0.211	−0.183	−0.387	**0.675**	1	*0.000*	*0.455*	*0.000*
^{40}K	−0.270	−0.374	0.228	−0.265	−0.163	0.204	−0.067	−0.453	**0.587**	**0.915**	1	*0.107*	*0.000*
$^{210}Pb_{ex}$	−0.088	−0.127	0.204	−0.239	−0.163	0.340	−0.143	−0.137	−0.094	0.128	0.273	1	*0.143*
$^{226}Ra/^{228}Ra$	0.191	0.236	−0.070	0.410	−0.002	−0.223	0.088	0.380	0.001	**−0.726**	**−0.687**	−0.249	1
p-value 0.05													

the only part where clay minerals have been found in previous studies of the region (Mangas and Julià-Miralles, 2015). Therefore, This could explain why the ratio seems to work in the protected part of Las Canteras beach (i.e. the northern part) but does not seem to work so well for the other two parts to the south. Thus, further analysis of this ratio is necessary to evaluate its precision in tracing erosion and accumulation periods for the whole beach.

3.2. Analysis of the relationships between environmental variables and activity concentration changes

Aerosols and atmospheric parameters are known to be correlated with the transport of natural radionuclides such as ^{40}K and $^{210}Pb_{ex}$ (Dueñas et al., 2017; Karlsson et al., 2008; López-Pérez et al., 2013). Moreover, studies in the Canary Islands have found correlations between the deposition of materials floating in the sea, such as plastic debris, wave approach direction and the significant wave height (Herrera et al., 2018). Therefore, correlation analysis was carried out between the mean activity concentration values found during the whole study period for ^{226}Ra, ^{228}Ra, ^{40}K and $^{210}Pb_{ex}$ and the ratio $^{226}Ra/^{228}Ra$ in the different zones of the beach, as well as the atmospheric and marine parameters described in section 2 of this work. The results are shown in Table 1. The p-value obtained for each correlation coefficient is also represented, and is statistically significant when p-values < 0.05. However, when a p-value was < 0.05, but the correlation coefficient was below 0.5, no correlation was considered. Moreover, a strong correlation was considered when p-value < 0.005 and the correlation coefficient was >0.6.

All three zones presented a strong correlation in the activity concentration of ^{226}Ra, ^{228}Ra and ^{40}K between each other, while no correlation was found with the activity concentration of $^{210}Pb_{ex}$. This supports the hypothesis that the agents controlling the distribution of the first three radionuclides are different from the ones controlling the distribution of unsupported ^{210}Pb. Furthermore, zone I only presented an inverse correlation between the activity concentration of ^{226}Ra, ^{228}Ra and ^{40}K and the significant wave height. This indicates that, when there is a higher significant wave height, higher waves hit the beach and the activity concentration of those radionuclides is lower. According to the literature (Alonso, 2005, 1994, 1993; Alonso and Vilas, 1996), when a big storm event hits the southern arch of the beach, where all sampling points from zone I are located, there is a loss of sediment from the beach, that is transported lengthwise to the northern arch. On the contrary, when there is an accumulation period, the amount of sediments in the southern arch increases, as well as in the northern arch. The northern part is protected by the natural offshore rocky bar and is in a constant accumulation period. This sedimentary behaviour seems to agree with what occurs with natural radionuclide concentrations in zone I, when facing large significant wave heights, normally related to storm events. In zones II and III, the activity concentration of the different radionuclides did not show any correlation with any of the atmospheric or marine parameters either but still presented correlations among ^{226}Ra, ^{228}Ra and ^{40}K. The results for zones II and III (the areas that are in front of the natural offshore rocky bar and its openings) are what would be expected. According to the literature (Medina et al., 2006), the wave approach direction suffers diffraction when waves hit the bar and its openings, creating internal currents between the bar and the beach line. Therefore, it would be expected that the data obtained from a buoy outside El Confital Bay would not present any correlation with the activity concentration values in these two areas. Thus, these internal currents should be further studied to better understand the behaviour of natural radionuclide distributions associated with the sediments in the closed and semi-closed parts of the beach. In the case of $^{210}Pb_{ex}$, no correlation was found with any of the atmospheric or marine parameters in any of the three zones. Therefore, this element was no longer considered in the rest of this study.

Regarding the $^{226}Ra/^{228}Ra$ ratio, all three zones presented an inverse correlation with the activity concentration of ^{228}Ra, showing a higher correlation in zones II and III. This means that when the activity concentration of ^{228}Ra was higher the ratio would be lower. The use of this ratio as an indicator of erosion and accumulation periods in the work of Dai et al. (2011) was based on the higher mobility of ^{228}Ra against ^{226}Ra in the crystal framework of clay minerals. According to their study, during erosion periods the ratio would be higher due to the loss of ^{228}Ra and during accumulation periods the ratio would be lower due to the higher input of ^{228}Ra contained in the clay minerals of the sediments. For Las Canteras beach, clay minerals have been found in the north-northeast part of El Confital Bay where the protected area of Las Canteras beach is located (Mangas and Julià-Miralles, 2015). This could explain why the correlation is stronger for zones II and III since those are the areas closest to where clay minerals were found. In addition, for zones II and III the correlation analysis also points out an inverse correlation between the ratio and ^{40}K. In previous studies it has been found that clay materials have activity concentration values of ^{40}K one order of magnitude higher than the activity concentration values of ^{232}Th (the parent radionuclide of ^{228}Ra) and ^{226}Ra (Hewamanna et al., 2001; Raghu et al., 2020). This differences in activity concentration values seems to agree to with the results obtained for ^{226}Ra, ^{228}Ra and ^{40}K in Las Canteras beach for the area where clay minerals are present (northern part of the beach). Moreover, the sediment dynamics described in literature for Las Canteras beach explains that during erosion periods there is a lengthwise transport of sediment from the southern arch to the northern arch. On the contrary, during accumulation periods a sediment transport from the northern arch to the south part of the beach occurs (Alonso, 2005, 1993; Alonso and Vilas, 1996). Therefore, the presence of the clay minerals that were reported in the work of Mangas and Julià-Miralles, (2015) and its movement along the beach during erosion and accumulation periods could explain the inverse correlation between the ratio $^{226}Ra/^{228}Ra$ and the activity concentration values of ^{228}Ra and ^{40}K, since these clay minerals could be transporting both radionuclides. This seems to point out the role these radionuclides have as tracers of the transport of sand along the beach during erosion and accumulation periods. However, it is important to mention that some petrographic studies also show that feldspars tend to accumulate in the northern part of the beach (Alonso and Pérez Torrado, 1992). Thus, these minerals could also be contributing to the changes in ^{40}K. In addition, the ratio did not have any correlation with the activity concentration of ^{226}Ra, and thus only the presence of clay minerals in the northern part of the beach could not justify the changes observed for ^{226}Ra, ^{228}Ra and ^{40}K during erosion and accumulation periods in the whole beach. Hence, the ratio does not seem to be a suitable tracer for the sediment dynamics of the whole beach.

The results of the correlation analysis are shown as azimuth plots in Fig. 4. These plots represent the variation of activity concentration of ^{226}Ra, ^{228}Ra and ^{40}K according to the wave approach direction and the significant wave height in each campaign. It can be appreciated how, for zone I, the activity concentration values seemed to be higher when the significant wave height was smaller. In the cases of zones II and III, this pattern does not appear, which could again be related to the fact that these two areas are protected by the natural offshore rocky bar. The azimuth plots for the ratio $^{226}Ra/^{228}Ra$ are also presented in Fig. 5 but no pattern seems to appear. The results of the ANOVA and the Tukey's test that appear in Table 2 confirm what was observed in the azimuth plots. The ANOVA test for a prob-F level of 0.05 pointed out that for zone I there were significant differences in the different groups established for each radionuclide based on the significant wave height. The Tukey's test with a p-value of 0.05 showed that these differences were indeed between the groups of lower wave height and higher and medium wave height. As explained previously, the literature indicates that big storm events erode the sediments in the southern arch of Las Canteras beach since it is totally exposed to the wave action. Therefore, if the radionuclides used in this study show a similar pattern, when high, significant wave heights hit that part of the beach, it seems that these radionuclides are, indeed, tracing the sediment dynamics of the beach. Thus, its role as

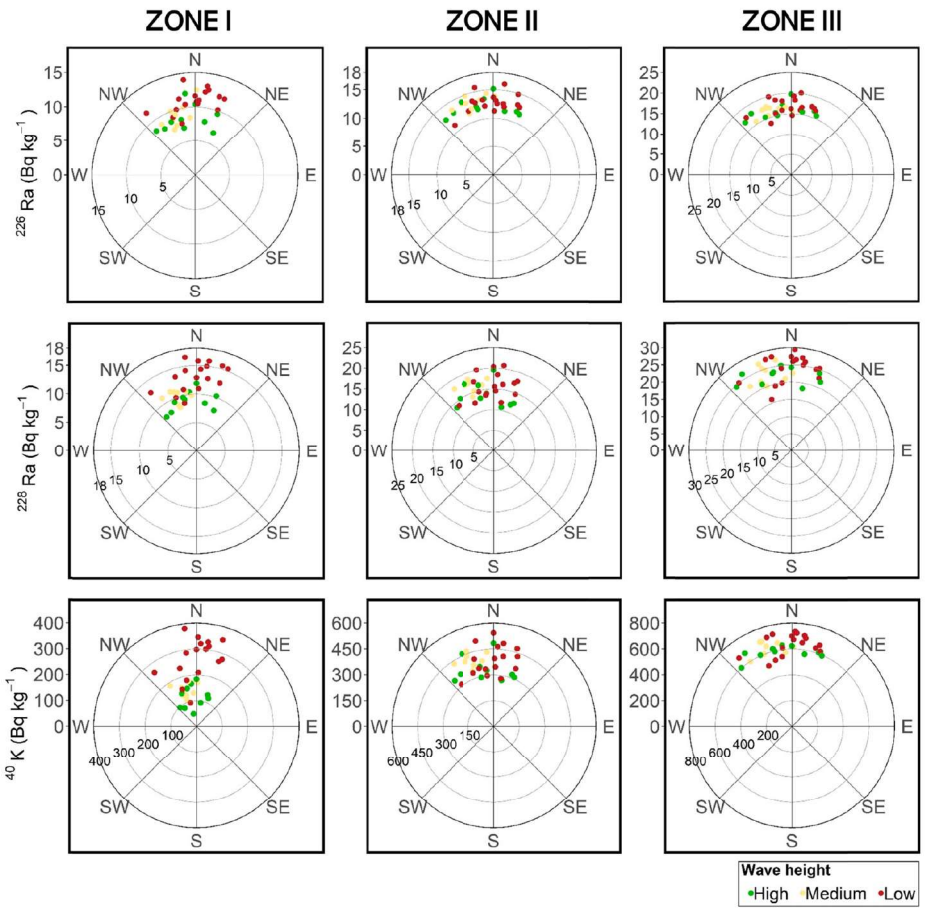

Fig. 4. Azimuth plot of wave height and direction and activity concentration of ^{226}Ra, ^{228}Ra and 40 K for the different zones in Las Canteras beach.

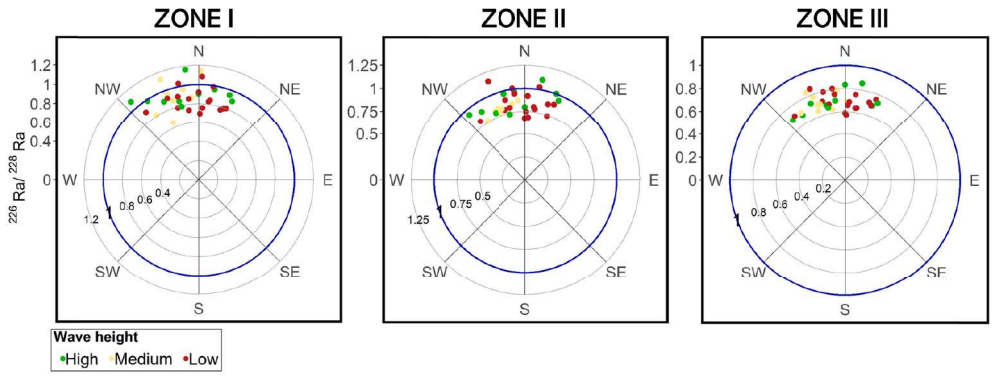

Fig. 5. Azimuth plot of wave height and direction and activity concentration of the ratio ^{226}Ra/ ^{228}Ra. In blue is marked the limit of 1. (For interpretation of the references to colour in this figure legend, the reader is referred to the web version of this article.)

a tracer of these dynamics can be confirmed. In zones II and III, no significant differences were found. This could be related to the protection against wave action that the offshore rocky bar offers to the sampling points in these two zones.

The results relating to wave approach direction also reported significant differences between the campaigns where the wave approach direction was NE and those when it was NW, in zone I. Since this behaviour was not clear in the azimuth plots, the boxplots of Fig. 6 were made. It represents the activity concentration values of ^{226}Ra (Fig. 6a), ^{228}Ra (Fig. 6b) and ^{40}K (Fig. 6c) for the campaigns with NE and NW wave approach directions. It shows that, in campaigns with a NE wave approach direction, the activity concentration values of these elements

Table 2
One-way ANOVA test for the identification of the presence of significant differences in the temporal series of ^{226}Ra, ^{228}Ra. ^{40}K and the ratio ^{226}Ra/^{228}Ra for the different campaigns in the different zones of Las Canteras beach. The result of the p-value for the Tukey's test is also displayed to identify the groups that present significant differences between them.

Area	Field	F	Prob-F	Tuckey's test
ZONE I				
^{226}Ra	Significant wave height	9.61900	0.0005110	Low-high (0.0009) Low-medium (0.0114)
	Wave direction	6.02300	0.0194000	NW-NE (0.0194)
^{228}Ra	Significant wave height	19.14000	0.0000030	Low-High (0.0000065) Low- Medium (0.0004618)
	Wave direction	6.67200	0.0143000	NW-NE (0.0142665)
^{40}K	Significant wave height	25.34000	0.0000002	Low-High (0.0000008) Low- Medium (0.0000358)
	Wave direction	9.12100	0.0047700	NW-NE (0.0047708)
^{226}Ra/^{228}Ra	Significant wave height	1.98000	0.1540000	–
	Wave direction	0.21400	0.6470000	–
ZONE II				
^{226}Ra	Significant wave height	0.73900	0.4850000	–
	Wave direction	0.02600	0.8720000	–
^{228}Ra	Significant wave height	1.97400	0.1550000	–
	Wave direction	0.01300	0.9100000	–
^{40}K	Significant wave height	1.58700	0.2200000	–
	Wave direction	0.41700	0.5230000	–
^{226}Ra/^{228}Ra	Significant wave height	1.66000	0.2060000	–
	Wave direction	0.05400	0.8180000	–
ZONE III				
^{226}Ra	Significant wave height	0.63300	0.5370000	–
	Wave direction	0.35700	0.5540000	–
^{228}Ra	Significant wave height	0.98400	0.3850000	–
	Wave direction	1.64500	0.2080000	–
^{40}K	Significant wave height	1.72000	0.1950000	–
	Wave direction	2.41200	0.1300000	–
^{226}Ra/^{228}Ra	Significant wave height	0.22000	0.8040000	–
	Wave direction	1.16300	0.2890000	–

ANOVA prob-F 0.05.
Tuckey's test p-value 0.05.

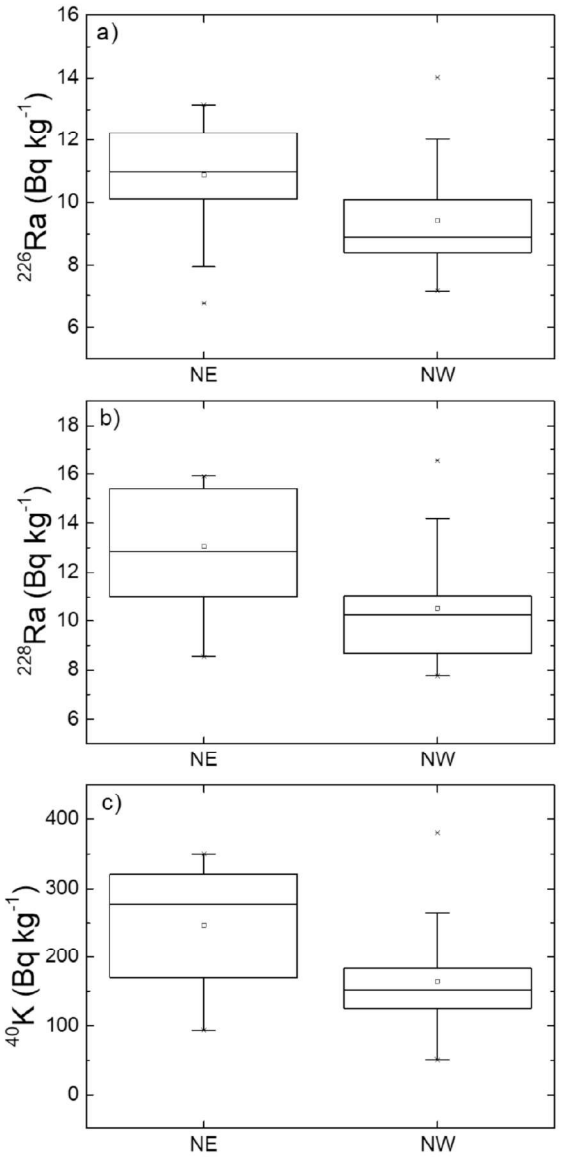

Fig. 6. Boxplot of the activity concentrations obtained for zone I in each campaign for each of the wave approach directions. (a) ^{226}Ra, (b) ^{228}Ra and (c) ^{40}K.

were higher. The NE part of the bay and the north part of the beach is where the clay minerals and feldspars were found (Alonso and Pérez Torrado, 1992; Mangas and Julià-Miralles, 2015). Therefore, the results point to the possible influence of the minerals located in the northern part of the beach, in the changes of activity concentration values found in zone I during the whole study period. In this case, zones II and III did not show any significant differences either.

Regarding the ratio ^{226}Ra/^{228}Ra, no significant differences were found for any of the three zones. According to the literature (Alonso, 2005, 1993; Alonso and Vilas, 1996) the area fully protected by the natural offshore rocky bar (zone III) is in a constant accumulation period. Moreover, zone II is also protected by the bar, so the lack of significant differences can be expected in these two parts of the beach. However, although the absence of significant differences in zones II and III could be explained due to the presence of the bar, this would not justify what happens in zone I. Clay minerals are not the only minerals that could contain ^{228}Ra and ^{40}K. Therefore, despite the fact that it seemed to work well in previous studies as a tracer of erosion and accumulation periods (Arriola-Velásquez et al., 2019; Dai et al., 2011), these ratios might not be completely suitable as a tracer for marine sediment dynamics in Las Canteras beach. Instead, the results suggest that ^{226}Ra, ^{228}Ra and ^{40}K are more suitable tracers of the sediment dynamics of the beach.

3.3. ICP-MS, multi-element and mineralogical analysis

The maximum gamma activity campaign (August 2018) was considered an accumulation campaign and the minimum gamma activity campaign (November 2018) an erosion one. Thus, 3 samples were selected from the accretion campaign and 3 samples were selected from

the erosion campaign. These 6 samples were studied to further comprehend the variations in the radioactivity, chemical and mineralogy composition of the beach sand during erosion and accumulation periods. Moreover, out of the 3 samples from each campaign 2 belonged to sampling stations P1 and P2 and the third one to sampling station P8 (Fig. 1.). Sampling stations P1 and P2 belong to the open part of the beach so the results of these stations would give clearer information about erosion and accumulation periods since that part is the one more affected by the different seasons. In contrast, sampling station P8 belongs to the protected part of the beach. This sampling station is in a constant accumulation period and, therefore, not many changes should be expected in its composition during erosion and accumulation seasons. By choosing these 6 samples it was expected to better understand the role of natural radionuclides as a tracers of sedimentary dynamics in Las Canteras beach.

In Table 3, the results for the activity concentration values found in each sample for ^{235}U, ^{238}U, ^{234}U, ^{230}Th and ^{232}Th by ICP-MS are shown, as well as the activity concentration values of ^{226}Ra, ^{228}Ra and ^{40}K found by gamma spectrometry. The results seem to present higher values of activity concentration in sampling points P1 and P2 in August 2018, than in November 2018, while sampling point P8 seems to stay quite stable for all activity concentration values in both campaigns. The results of the proficiency test (IAEA, 2011; Osvath et al., 2016; Shakhashiro et al., 2012) are also given in Table 3. In the case of sample PLC18_11.2 (corresponding to sampling point 2), the activity of ^{40}K was below the detection limit (BDL). Thus, the u_{test} and the P_{score} values were calculated using half of the minimum activity detectable, as an activity concentration value of that sample.

These results show that samples from sampling points P1 and P2, corresponding to zone I, present significant differences for the activity concentrations of all radionuclides. On the contrary, the samples from sampling point P8 in zone III did not present significant differences for almost any radionuclide, except for ^{235}U and ^{238}U. However, ^{238}U is calculated from the ^{235}U value and the natural ratio ^{238}U/^{235}U, so this explains why both present the same values in the proficiency test. Therefore, this means that the primordial uranium isotopes ^{235}U and ^{238}U are the only radionuclides that actually differ between one sample and the other. According to the literature (Alonso, 2005, 1994, 1993; Alonso and Vilas, 1996), the northern arch of Las Canteras beach is in a constant accumulation period, while the southern arch is the one that suffers variability in the loss and accumulation of sediments. Sampling points 1 and 2 are located in zone I, which is the area totally exposed to the wave action, while sampling point 8 is located in zone III in the northern arch, in the area protected by the offshore rocky bar. Therefore, it makes sense that samples from zone I present significant differences between the maximum and minimun activity concentration campaigns, whereas the sample from zone III does not have such differences. These results mean that, over time, there is a variation between maximum and minimum activity concentration in the area totally exposed to the wave action and, thus, these radionuclides could be good tracers for marine sediment dynamics in the open beach. Considering the activity concentration values of ^{232}Th, ^{228}Ra, ^{230}Th and ^{226}Ra obtained for all samples, if the ratios ^{232}Th/^{228}Ra and ^{230}Th/^{226}Ra were calculated, all of them would be approximately 1. This means that both Ra radioisotopes would be in equilibrium with their parents and, thus, their activity is also controlled by their parent radionuclides. Therefore, the parent radionuclides could also be following the same marine sediment dynamics and be used as tracers of the beach sediment dynamics.

In order to better understand the geochemical composition of the sediments transported along Las Canteras beach, a multi-element analysis and mineralogical analysis were carried out on the same six samples that were chosen for the ICP-MS analysis. The results of the multielement analysis for total rock composition of Ba, Ca, Mg and K are shown in Table 4. Total potassium was analysed to evaluate if similar

Table 4
Multielement analysis of the total rock composition of each sand sample. Concentrations given in g kg-1 of Ba, Ca, Mg and K were analyzed.

Sample	Ba	Ca	Mg	K
LOD of detector	0.0002	0.0552	0.0034	0.0203
LOB	0.0113	3.1764	0.384	0.109
LOD of the method	0.0226	6.3529	0.7681	0.2181
LOQ	0.0435	11.9209	1.4904	0.4227
PLC18_8.1	0.3176 ± 0.0005	192 ± 1	23.29 ± 0.30	13.13 ± 0.06
PLC18_8.2	0.3611 ± 0.0047	172 ± 2	22.21 ± 0.24	16.03 ± 0.10
PLC18_8.8	0.3805 ± 0.0023	167 ± 1	15.48 ± 0.09	21.69 ± 0.06
PLC18_11.1	0.1579 ± 0.0013	141 ± 1	66.80 ± 0.63	2.30 ± 0.02
PLC18_11.2	0.0519 ± 0.0005	25 ± 0	36.18 ± 0.18	0.65 ± 0.01
PLC18_11.8	0.3484 ± 0.0021	163 ± 1	14.58 ± 0.12	22.27 ± 0.08

Table 3
Activity concentrations in Bq kg^{-1} found for radionuclides ^{235}U, ^{238}U, ^{234}U, ^{230}Th and ^{232}Th measured by ICP-MS measurement and for ^{226}Ra, ^{228}Ra and ^{40}K measured by gamma spectrometry. In addition, the results of the proficiency test parameter u_{test} and P_{score} described in IAEA (2011), Osvath et al. (2016), Shakhashiro et al. (2012).

Sample	Sampling point	Date	^{235}U	^{238}U*	^{234}U	^{230}Th	^{232}Th	^{226}Ra	^{228}Ra	^{40}K
PLC18_8.1	P1	August 2018	0.717 ± 0.003	15.58 ± 0.06	16.92 ± 0.23	14.50 ± 0.87	14.81 ± 1.91	14.01 ± 0.95	17.23 ± 1.80	431 ± 20
PLC18_8.2	P2	August 2018	0.841 ± 0.004	18.27 ± 0.10	19.27 ± 0.19	17.88 ± 1.06	21.41 ± 1.94	16.81 ± 1.00	20.45 ± 1.79	483 ± 22
PLC18_8.8	P8	August 2018	0.906 ± 0.006	19.68 ± 0.12	20.64 ± 0.20	17.94 ± 0.47	22.99 ± 1.89	16.35 ± 1.05	24.45 ± 1.89	606 ± 27
PLC18_11.1	P1	November 2018	0.348 ± 0.003	7.56 ± 0.06	8.25 ± 0.13	8.60 ± 0.89	8.16 ± 0.91	6.30 ± 0.53	7.37 ± 0.95	81 ± 6
PLC18_11.2	P2	November 2018	0.388 ± 0.004	8.43 ± 0.08	9.44 ± 0.17	9.08 ± 0.62	8.43 ± 0.11	9.19 ± 1.36	9.38 ± 2.45	BDL
PLC18_11.8	P8	November 2018	0.975 ± 0.006	21.17 ± 0.14	21.60 ± 0.33	19.97 ± 0.82	27.79 ± 0.56	15.78 ± 1.02	28.92 ± 2.09	655 ± 29

Sampling points	Dates of comparation	u_{test}	P_{score}	u_{test}	P_{score}	u_{test}	P_{score}	u_{test}	P_{score}	u_{test}	P_{score}	u_{test}	P_{score}	u_{test}	P_{score}	u_{test}	P_{score}
P1	August -	99.40	0.82	99.40	0.82	32.43	2.11	4.74	11.96	3.15	17.01	7.08	10.83	4.85	16.56	16.76	8.74
P2	November	78.53	1.07	78.53	1.07	39.33	2.02	7.16	9.06	6.68	9.15	4.51	15.98	3.65	27.54	19.03	55.45
P8	2018	8.11	0.90	8.11	0.90	2.50	1.80	2.13	4.90	2.43	8.48	0.39	9.10	1.59	10.58	1.24	6.28

* ^{238}U is calculated from the value of ^{235}U and the natural ratio ^{235}U/^{238}U.

behaviour to that of ^{40}K during erosion and accumulation periods could be found. The results showed that total K had lower values in the samples from the erosion period from zone I (PLC18_11.1 and PLC18_11.2); they also show an increase in samples from the same stations during accumulation periods (PLC18_11.8 and PLC18_8.1). In the samples from zone III the results obtained for both samples (PLC18_11.8 and PLC18_8.8) do not present such a strong difference. Moreover, Ca and Ba also displayed a similar change to K, whereas Mg had the opposite behaviour, with higher concentrations during erosion periods and lower concentrations during accumulation periods. Therefore, it could be said that Ca and Ba followed a similar pattern to K. Since it was not possible to analysed Ra through this method and considering that the alkaline earth elements Ra and Ba have similar chemical properties, it was assumed that Ra also followed the pattern of K. Thus, this could also explain why ^{226}Ra and ^{228}Ra have followed a similar distribution to ^{40}K. Thus, these three radionuclides would be transported along with Ca and Ba in the lighter fraction of the sand that moves into and along the beach during erosion and accumulation periods. Therefore, ^{226}Ra and ^{228}Ra could also be used as tracers of the sediment dynamics of the beach.

The results of the SCXRD (Single Crystal X-ray Difraction) allowed the determination that feldspar is anorthoclase ($Ab_{0.73}Or_{0.27}$), clinopyroxene is diopside ($CaMgSi_2O_6$) and olivine is forsterite ($Fo_{0.82}$, Fo = Mg_2SiO_4). The observed cell parameters are reported in Table 5. Both feldspar and clinopyroxene show extended solid solution (i.e. change in composition) that change lattice parameters and thus the angles at which crystal planes diffract. Having an estimation of the chemical composition through SCXRD allowed us to select more appropriate PDF files for matching more precisely the observed d-spacing in the powder X-ray pattern among the large number of available ones. XRPD (Powder X-ray diffraction) results on the studied sand samples were characterised by the presence of abundant feldspar (anorthoclase, $(Na,K)AlSi_3O_8$), calcite (trigonal $CaCO_3$) and aragonite (orthorhombic $CaCO_3$), plus variable amounts of (diopsidic) clinopyroxene and minor amounts of (forsteritic) olivine and amphibole (probably a ferro-hornblende or a ferro-pargasite; cell parameters are $a = 9.872(13)$, $b = 18.100(10)$, $c = 5.304(5)$ Å, $\alpha = 90°$, $\beta = 105.42(11)°$, $\gamma = 90°$, and $V = 914(2)$ Å^3). However, there are modal differences between high energy seasons (erosion periods) and low energy seasons (accumulation periods) in some of the samples as shown on the three diffraction diagrams that appear in Fig. 7.

Fig. 7a shows the comparison of the diffraction diagrams of the samples belonging to station P1 during erosion (PLC18_11.1) and accumulation (PLC8_8.1) periods. There are evidently differences because anorthoclase, calcite and aragonite are reduced in high-energy season, where higher density Mg-rich mineral phases (diopside, amphibole, and minor olivine) have been preferentially concentrated. In low energy seasons, sand predominantly comprises anorthoclase, calcite and aragonite instead. Trace amounts of illite ($K_{1-x}Al_2[Al_{1-x}Si_{3+x}]O_{10}(OH)_2$) were found in both seasons.

In Fig. 7b, the diffraction diagrams of the samples for station P2 are shown. These diagrams display more clearly the difference in mineral content for both seasons in zone I. The feldspar (mainly anorthoclase), calcite and aragonite are absent in high-energy seasons, whereas higher density mineral Fe/Ti oxides (ilmenite, hematite and magnetite) have been concentrated, along with Mg-rich phases (diopside and some olivine). The total rock composition is therefore higher in Mg, whereas Ca remains because of diopside, but its concentration decreases. Potassium, mainly concentrated in feldspar, is highly reduced in high-energy season sediments. In low energy season sediments, anorthoclase (as well as some sanidine $KAlSi_3O_8$ to a lesser degree) and carbonates are

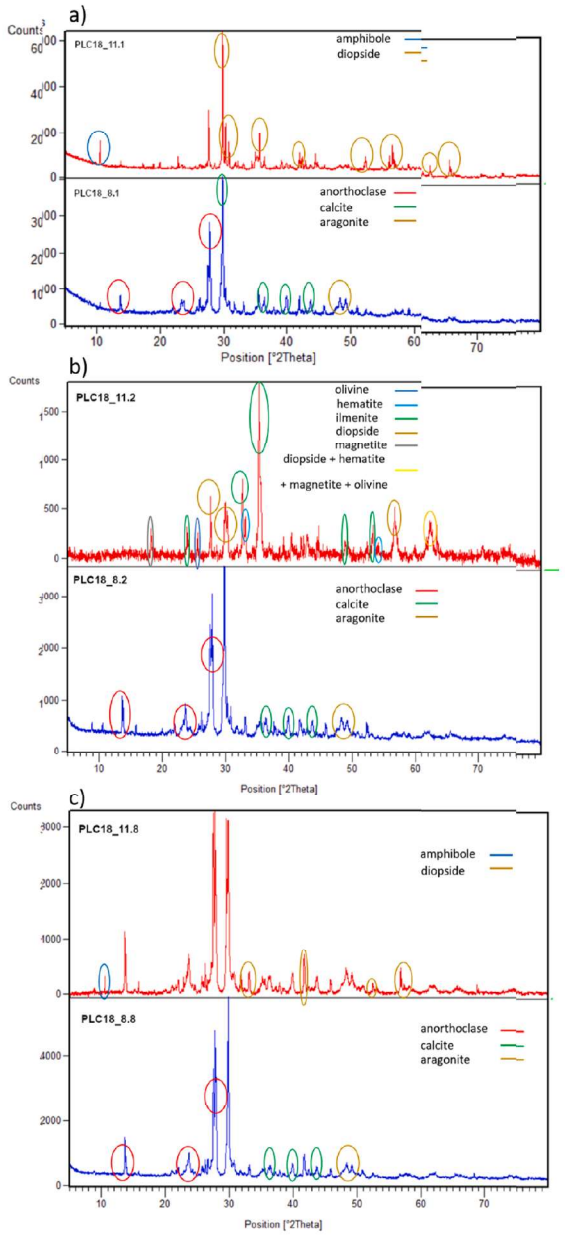

Fig. 7. Comparation of diffraction diagrams in erosion (PLC18_11) and accumulation (PLC18_8) periods for. (a) Samples PLC18_11.1 and PLC18_8.1 (zone I), (b) Samples PLC18_11.2 and PLC18_8.2 (zone I) and (c) Samples PLC18_11.8 and PLC18_8.8 (zone III).

Table 5
Cell parameters and approximate chemical composition of the crystal studied by SCXRD.

	Forsterite $Mg_{0.82}Fe_{0.18}SiO_4$	Diopside $CaMgSi_2O_6$	Anorthoclase $Na_{0.73}K_{0.27}AlSi_3O_8$
s.g.	*Pbnm*	*C2/c*	*C2/m*
a (Å)	4.7689(7)	9.725(3)	8.3036(14)
b (Å)	10.2480(14)	8.8791(11)	12.9749(10)
c (Å)	6.0071(8)	5.2674(7)	7.1522(7)
α (°)	90	90	90
β (°)	90	105.96(2)	116.167(9)
γ (°)	90	90	90
V (Å^3)	293.58(7)	437.31(16)	691.59(15)

s.g. = space group.

predominant, while diopside and amphibole (as well as some phyllosilicate, probably illite) are minor. Olivine has not been observed here but some cristobalite (SiO_2) is present instead.

Finally, Fig. 7c presents the diffraction diagrams of the samples from station P8, belonging to zone III. In this case, feldspar (mainly anorthoclase) calcite and aragonite are the dominant mineral phases in both high and low energy seasons. Sand is only slightly richer in diopside in high energy seasons and some amphibole (and very minor hematite and olivine) also becomes concentrated. This location is protected by an offshore rocky bar and is, therefore, less exposed to tidal changes and to mineral variation because energy in the water is much reduced. Therefore, the selection of minerals as a function of density is not allowed.

The results of the XRPD showed that accumulation periods in zone I, and especially sampling point P2, show that potassium is mainly concentrated in feldspar, probably anorthoclase. These feldspars appear during accumulation periods in zone I and disappear in erosion periods, while being present in zone III all the time. This means that this feldspar, which contains potassium, is present whenever and wherever the activity concentration of ^{40}K is higher. Therefore, it could be said that ^{40}K is tracing the movement of this feldspar contained in the light fraction of the sand along and into the beach, making it a good tracer for beach sediment dynamics. Moreover, the multi-element analysis shows that other elements, like Ba (which is also fractionated in feldspar, usually in trace amounts), follow the same pattern as K. These elements have a similar chemical behaviour to Ra and so it is suggested that ^{226}Ra and ^{228}Ra could also be used as tracers of the beach sediment dynamics.

4. Conclusions

The analysis of the temporal variability of natural radionuclides during this 3 year-long study suggests that the radionuclides ^{226}Ra, ^{228}Ra and ^{40}K in the sand of Las Canteras beach are closely following marine sediment dynamics, together with their parent isotopes. The statistical analysis showed that these three radionuclides present higher activity concentration values in periods with low significant wave height and a NE wave approach direction. These periods are expected in a low energy season when the accumulation of sediments occur on the beach. During high wave height periods the activity concentration of these radionuclides decreased. The ratio $^{226}Ra/^{228}Ra$, previously suggested as a tracer of beach sediment dynamics with a data series of 1 year, did not show any significant differences in erosion or accumulation periods for all of the beach. This indicates that the ratio might not be appropriate to trace sediment dynamics in zones I and II. However, zone III (which is fully protected by the natural offshore rocky bar) showed a ratio value constantly below 1, indicating a constant accumulation period as has been described for this part of the beach. Thus, the lack of significant differences in this area could be pointing out the absence of differences between accumulation and erosion periods. In addition, as already pointed out in the preliminary study, $^{210}Pb_{xc}$ (driven by atmospheric and wind transport) does not seem to be relevant as a tracer of the accumulation/erosion processes of the beach, due to marine sediment transport. Therefore, ^{226}Ra, ^{228}Ra and ^{40}K seem to be more suitable tracers of the beach sediment dynamics during erosion and accumulation periods at Las Canteras beach.

Moreover, the multi-element analysis of total rock composition of the sand that can be found in the different parts of the beach, indicates that Ca and Ba follow a similar dynamic to K. Ba has similar chemical behaviour to Ra and, thus, this could explain the similar pattern to ^{40}K that ^{226}Ra, ^{228}Ra have. This makes them good candidates as tracers of sediment dynamics in coastal areas. In addition, the mineralogical analysis suggests that the activity concentration values found for ^{40}K correspond to the displacement of feldspar grains with high K content, abundant in the light fraction of the sand that moves into and along the beach during accumulation and erosion periods. Thus, ^{40}K seems to be the most fitting tracer of the sediment dynamics at Las Canteras beach.

Declaration of Competing Interest

The authors declare that they have no known competing financial interests or personal relationships that could have appeared to influence the work reported in this paper.

Acknowledgements

The authors of this study acknowledge the help of the Marine Geochemistry division of the Alfred Wegener Institute, Helmholtz Centre for Polar and Marine Research (AWI) in Bremerhaven, Germany for letting them use their facilities for the development of part of this study in the framework of the ERASMUS + traineeship programme.

F.C. acknowledges financial support from the grant "Ricerca Locale 2014", Università di Milano, and by the grant from the Italian Ministry of Education (MIUR) through the 'Dipartimenti di Eccellenza 2018–2022' project.

The authors of this study also acknowledge the financial support by the grant of the Agencia Canaria de Investigación Innovación y Sociedad de la Información Gobierno De Canarias (ACIISI) through the projects CEI2019-10 and CEI2019-13.

Appendix A. Supplementary material

Supplementary data to this article can be found online at https://doi.org/10.1016/j.catena.2021.105705.

References

Alonso, I., 2005. Costa Norte : Playa De Las Canteras, in: Hernández, L., Alonso, I., Mangas, J., Yanes, A. (Eds.), Tendencias Actuales En Geomorfología Litoral. Universidad de Las Palmas de Gran Canaria, La Palmas de Gran Canaria, pp. 219–238.

Alonso, I., 1994. Spatial beach morphodynamics. An example from Canary Islands, Spain. Litoral 94, 169–183.

Alonso, I., 1993. Procesos sedimentarios en la playa de Las Canteras (Gran Canaria). Universidad de Las Palmas de Gran Canaria.

Alonso, I., Pérez Torrado, F.J., 1992. Estudio sedimentológico de la playa de Las Canteras (Gran Canaria). Datos preliminaries. III Congr. geológico España y tomo 2, 131–135.

Alonso, I., Vilas, F., 1996. Variabilidad sedimentaria en la playa de Las Canteras (Gran Canaria). Geogaceta 20, 428–430.

Arnedo, M.A., Rubiano, J.G., Alonso, H., Tejera, A., González, A., González, J., Gil, J.M., Rodríguez, R., Martel, P., Bolivar, J.P., 2017. Mapping natural radioactivity of soils in the eastern Canary Islands. J. Environ. Radioact. 166, 242–258. https://doi.org/10.1016/j.jenvrad.2016.07.010.

Arnedo, M.A., Tejera, A., Rubiano, J.G., Alonso, H., Gil, J.M., Rodriguez, R., Martel, P., 2013. Natural radioactivity measurements of beach sands in gran Canaria, Canary Islands (Spain). Radiat. Prot. Dosim. 156 (1), 75–86. https://doi.org/10.1093/rpd/nct044.

Arriola-Velásquez, A., Tejera, A., Guerra, J.G., Alonso, I., Alonso, H., Arnedo, M.A., Rubiano, J.G., Martel, P., 2019. Spatio-temporal variability of natural radioactivity as tracer of beach sedimentary dynamics. Estuar. Coast. Shelf Sci. 231, 106476. https://doi.org/10.1016/j.ecss.2019.106476.

Balcells, R., Barrera, J.L., Ruiz García, M.T., (Cartographers), 1990. Geological Map 1101-I-II Las Palmas de Gran Canaria, 1:25000 IGME.

Bezuidenhout, Jacques, 2020. The investigation of natural radionuclides as tracers for monitoring sediment processes. J. Appl. Geophys. 181, 104135. https://doi.org/10.1016/j.jappgeo.2020.104135.

Bezuidenhout, J., 2013. Measuring naturally occurring uranium in soil and minerals by analysing the 352keV gamma-ray peak of ^{214}Pb using a NaI(Tl)-detector. Appl. Radiat. Isot. 80, 1–6. https://doi.org/10.1016/j.apradiso.2013.05.008.

Burnett, William C., Bokuniewicz, Henry, Huettel, Markus, Moore, Willard S., Taniguchi, Makoto, 2003. Groundwater and pore water inputs to the coastal zone. Biogeochemistry 66 (1/2), 3–33.

Chabaux, F., Blaes, E., Granet, M., Roupert, R. di C., Stille, P., 2012. Determination of transfer time for sediments in alluvial plains using 238U–234U-230Th disequilibria: the case of the Ganges river system. Comptes Rendus – Geosci. 344, 688–703. https://doi.org/10.1016/j.crte.2012.10.013.

Chabaux, François, Granet, Mathieu, Pelt, Eric, France-Lanord, Christian, Galy, Valier, 2006. ^{238}U–^{234}U-^{230}Th disequilibria and timescale of sedimentary transfers in rivers: clues from the Gangetic plain rivers. J. Geochem. Explor. 88 (1-3), 373–375. https://doi.org/10.1016/j.gexplo.2005.08.078.

Dai, Zhi-Jun, Du, Jin-Zhou, Chu, Ao, Zhang, Xiao-Ling, 2011. Sediment characteristics in the North Branch of the Yangtze Estuary based on radioisotope tracers. Environ. Earth Sci. 62 (8), 1629–1634. https://doi.org/10.1007/s12665-010-0647-7.

Dueñas, C., Gordo, E., Liger, E., Cabello, M., Cañete, S., Pérez, M., de la Torre-Luque, P., 2017. ^{7}Be, ^{210}Pb and ^{40}K depositions over 11 years in Málaga. J. Environ. Radioact. 178–179, 325–334. https://doi.org/10.1016/j.jenvrad.2017.09.010.

Gaspar, L., Webster, R., Navas, A., 2017. Fate of $^{210}Pb_{ex}$ fallout in soil under forest and scrub of the central Spanish Pre-Pyrenees. Eur. J. Soil Sci. 68 (3), 259–269. https://doi.org/10.1111/ejss.2017.68.issue-310.1111/ejss.12427.

Giffin, D., Corbett, D.R., 2003. Evaluation of sediment dynamics in coastal systems via short-lived radioisotopes. J. Mar. Syst. 42 (3-4), 83–96. https://doi.org/10.1016/S0924-7963(03)00068-X.

Guerra, J.G., Rubiano, J.G., Winter, G., Guerra, A.G., Alonso, H., Arnedo, M.A., Tejera, A., Martel, P., Bolivar, J.P., 2017. Computational characterization of HPGe detectors usable for a wide variety of source geometries by using Monte Carlo simulation and a multi-objective evolutionary algorithm. Nucl. Instrum. Methods Phys. Res. Sect. A Accel. Spectrom. Detect. Assoc. Equip. 858, 113–122. https://doi.org/10.1016/j.nima.2017.02.087.

Guerra, J.G., Rubiano, J.G., Winter, G., Guerra, A.G., Alonso, H., Arnedo, M.A., Tejera, A., Gil, J.M., Rodríguez, R., Martel, P., Bolivar, J.P., 2015. A simple methodology for characterization of germanium coaxial detectors by using Monte Carlo simulation and evolutionary algorithms. J. Environ. Radioact. 149, 8–18. https://doi.org/10.1016/j.jenvrad.2015.06.017.

Halliday, Alex N., Lee, Der-Chuen, Christensen, John N., Rehkämper, Mark, Yi, Wen, Luo, Xiaozhong, Hall, Chris M., Ballentine, Chris J., Pettke, Thomas, Stirling, Claudine, 1998. Applications of multiple collector-ICPMS to cosmochemistry, geochemistry, and paleoceanography. Geochemica Cosmochim. Acta 62 (6), 919–940.

Herrera, A., Asensio, M., Martínez, I., Santana, A., Packard, T., Gómez, M., 2018. Microplastic and tar pollution on three Canary Islands beaches: an annual study. Mar. Pollut. Bull. 129, 494–502. https://doi.org/10.1016/j.marpolbul.2017.10.020.

Huang, D., Du, J., Deng, B., Zhang, J., 2013. Distribution patterns of particle-reactive radionuclides in sediments off eastern hainan island, china: Implications for source and transport pathways. Cont. Shelf Res. 57, 10–17. https://doi.org/10.1016/j.csr.2012.04.019.

Hülse, Peter, Bentley, Samuel J., 2012. A ^{210}Pb sediment budget and granulometric record of sediment fluxes in a subarctic deltaic system: the Great Whale River, Canada. Estuar. Coast. Shelf Sci. 109, 41–52. https://doi.org/10.1016/j.ecss.2012.05.019.

IAEA, 2011. ALMERA Proficiency Test : Determination of Natural and Artificial Radionuclides in Soil and Water, Analytical Quality in Nuclear Applications. Vienna.

Karlsson, L., Hernandez, F., Rodríguez, S., López-Pérez, M., Hernandez-Armas, J., Alonso-Pérez, S., Cuevas, E., 2008. Using ^{137}Cs and ^{40}K to identify natural Saharan dust contributions to PM10 concentrations and air quality impairment in the Canary Islands. Atmos. Environ. 42 (30), 7034–7042. https://doi.org/10.1016/j.atmosenv.2008.06.016.

Kipp, L.E., Spall, M.A., Pickart, R.S., Kadko, D.C., Moore, W.S., Dabrowski, J.S., Charette, M.A., 2020. Observational and modeling evidence of seasonal trends in sediment-derived material inputs to the Chukchi Sea. J. Geophys. Res. Ocean. 125, 1–13. https://doi.org/10.1029/2019JC016007.

Li, Wenpeng, Li, Xinxin, Mei, Xi, Zhang, Fan, Xu, Jingping, Liu, Chunru, Wei, Chuanyi, Liu, Qingsong, 2021. A review of current and emerging approaches for Quaternary marine sediment dating. Sci. Total Environ. 780, 146522. https://doi.org/10.1016/j.scitotenv.2021.146522.

Lin, Wuhui, Feng, Yu, Yu, Kefu, Lan, Wenlu, Wang, Yinghui, Mo, Zhenni, Ning, Qiuyun, Feng, Liangliang, He, Xianwen, Huang, Yinlin, 2020. Long-lived radionuclides in marine sediments from the Beibu Gulf, South China Sea: Spatial distribution, controlling factors, and proxy for transport pathway. Mar. Geol. 424, 106157. https://doi.org/10.1016/j.margeo.2020.106157.

López-Pérez, M., Ramos-López, R., Perestelo, N.R., Duarte-Rodriguez, X., Bustos, J.J., Alonso-Pérez, S., Cuevas, E., Hernández-Armas, J., 2013. Arrival of radionuclides released by the Fukushima accident to Tenerife (Canary Islands). J. Environ. Radioact. 116, 180–186. https://doi.org/10.1016/j.jenvrad.2012.09.011.

Mangas, J., Julià-Miralles, M., 2015. Geomorfología y naturaleza de las bajas submareales de Bajo Fernando, Los Roquerillos y La Zabala (NE de Gran Canaria). Geo-Temas 15, 37–40.

Medina, R., Bastón, S., Cánovas, V., Torres, A., Luque, Á., Alonso, I., Sánchez, I., Ortega, A., Rodríguez, S., Martín, J.A., 2006. Estudio integral de la playa de Las Canteras, Technical Report Dirección General de Costas.

Moore, W.S., 2007. Radon and radium isotopes as tracers of coastal mixing and submarine groundwater discharge. Water Environ. News 23, 14–23.

Osvath, I., Tarjan, S., Pitois, A., Groening, M., Osborn, D., 2016. IAEA ' s ALMERA network: supporting the quality of environmental radioactivity measurements. Appl. Radiat. Isot. 109, 90–95. https://doi.org/10.1016/j.apradiso.2015.12.062.

Pittauer, D., Roos, P., Qiao, J., Geibert, W., Elvert, M., Fischer, H.W., 2018. Pacific Proving Grounds radioisotope imprint in the Philippine Sea sediments. J. Environ. Radioact. 186, 131–141. https://doi.org/10.1016/j.jenvrad.2017.06.021.

Pozebon, D., 2002. Marine sediment analysis using inductively coupled plasma optical emission spectrometry. At. Spectrosc. 23, 111–118.

Rigaku Oxford Diffraction, 2020. *CrysAlisPro*, version 1.171.40.71a. Rigaku Corporation, Oxford, UK.

Sanial, V., van Beek, P., Lansard, B., Souhaut, M., Kestenare, E., D'Ovidio, F., Zhou, M., Blain, S., Blain, S., 2015. Use of Ra isotopes to deduce rapid transfer of sediment-derived inputs off Kerguelen. Biogeosciences 12, 1415–1430. https://doi.org/10.5194/bg-12-1415-2015.

Schmincke, H.U., 1993. Geological field guide of Gran Canaria, sixth ed. Pluto-Press, Kiel (Germany).

Schultz, B.B., 1985. Levene' s test for relative variation. Syst. Zool. 34 (4), 449–456.

Shakhashiro, A., Tarjan, S., Ceccatelli, A., Kis-benedek, G., Betti, M., 2012. IAEA-447: a new certified reference material for environmental radioactivity measurements. Appl. Radiat. Isot. 70, 1632–1643. https://doi.org/10.1016/j.apradiso.2012.03.024.

Shapiro, S.S., Wilk, M.B., 1965. An analysis of variance test for normality (complete samples). Biometrika 52, 591–611. https://doi.org/10.2307/2333709.

Sheldrick, G.M., 2015. Crystal structure refinement with SHELXL. Acta Crystallogr. Sect. C Struct. Chem. 71, 3–8. https://doi.org/10.1107/S2053229614024218.

Sun, X., Fan, D., Liao, H., Liu, M., Tian, Y., Zhang, X., Yang, Z., 2020. Variation in sedimentary ^{210}Pb over the last 60 years in the Yangtze River Estuary: new insight to the sedimentary processes. Mar. Geol. 427, 106240. https://doi.org/10.1016/j.margeo.2020.106240.

Tamborski, J., Bejannin, S., Garcia-Orellana, J., Souhaut, M., Charbonnier, C., Anschutz, P., Pujo-pay, M., Conan, P., Crispi, O., Monnin, C., Stieglitz, T., Rodellas, V., Andrisoa, A., Claude, C., van Beek, P., 2018. A comparison between water circulation and terrestrially-driven dissolved silica fluxes to the Mediterranean Sea traced using radium isotopes. Geochim. Cosmochim. Acta 238, 496–515. https://doi.org/10.1016/j.gca.2018.07.022.

Tejera, A., Pérez-Sánchez, L., Guerra, G., Arriola-Velásquez, A.C., Alonso, H., Arnedo, M. A., Rubiano, G., Martel, P., 2019. Natural radioactivity in algae arrivals on the Canary coast and dosimetry assessment. Sci. Total Environ. 658, 122–131. https://doi.org/10.1016/j.scitotenv.2018.12.140.

Thereska, J., 2009. Natural radioactivity of coastal sediments as tracer in dynamic sedimentology. Nukleonika 54, 45–50.

Wakiyama, Y., Onda, Y., Mizugaki, S., Asai, H., Hiramatsu, S., 2010. Soil erosion rates on forested mountain hillslopes estimated using ^{137}Cs and $^{210}Pb_{ex}$. Geoderma 159 (1-2), 39–52. https://doi.org/10.1016/j.geoderma.2010.06.012.

Walder, A.J., Freedman, P.A., 1992. Isotopic ratio measurement using a double focusing magnetic sector mass analyser with an inductively coupled plasma as an ion source. J. Anal. Atomic Spectrom. 7, 571–575.

Wang, Jinlong, Zhang, Weiguo, Baskaran, Mark, Du, Jinzhou, Zhou, Feng, Wu, Hui, 2018. Fingerprinting sediment transport in river-dominated margins using combined mineral magnetic and radionuclide methods. J. Geophys. Res. Ocean. 123 (8), 5360–5374. https://doi.org/10.1029/2018JC014174.

Williams, L.J., Abdi, H., 2010. Tukey 's honestly significant difference test (HSD). Encycl. Res. Des. 2–7.

Yang, Wei-feng, Chen, Min, Zhang, Xin-xing, Guo, Zhi-gang, Li, Guang-xue, Ma, Qiang, Yang, Jun-hong, Huang, Yi-pu, 2013. Thorium isotopes (^{228}Th, ^{230}Th, ^{232}Th) and applications in reconstructing the Yangtze and Yellow River floods. Int. J. Sedim. Res. 28 (4), 588–595. https://doi.org/10.1016/S1001-6279(14)60015-9.

Zheng, Y., Weinman, B., Cronin, T., Fleisher, M.Q., Anderson, R.F., 2003. A rapid procedure for the determination of thorium, uranium, cadmium and molybdenum in small sediment samples by inductively coupled plasma-mass spectrometry: application in Chesapeake Bay. Appl. Geochem. 18, 539–549.

3.3. Natural radionuclides as tracers of coastal sediment dynamics in El Confital Bay (Spain): spatial distribution and relationships with sediment characteristics

Publicado en la revista *CATENA*

Año: *2024*

Volumen: 235

DOI: *https://doi.org/10.1016/j.catena.2023.107672*

Journal Citation Report edición 2022: Categoría *Geoscience, Multidisciplinary*; Ranking *17/201*; Cuartil *Q1* (Decil *D1*)

En este último trabajo se usaron las actividades de ^{226}Ra, ^{228}Ra, ^{40}K y ^{210}Pb en exceso ($^{210}Pb_{ex}$) para trazar las dinámicas sedimentarias submarinas de la Bahía del Confital. Adicionalmente, y teniendo en cuenta que los sedimentos en las distintas partes de la bahía presentan variabilidad tanto en su naturaleza como su tamaño de grano, se realizó un análisis más extenso de las relaciones existentes entre las características del sedimento y las actividades de ^{226}Ra, ^{228}Ra, ^{40}K y $^{210}Pb_{ex}$. De esta manera los resultados del estudio mostraron un caso de aplicación de los radionucleidos naturales para trazar dinámicas sedimentarias costeras. Además, se realizó un análisis exhaustivo de las relaciones entre las características del sedimento y los cambios de actividad encontrados en ellos.

Para llevar a cabo este estudio se analizó la distribución espacial de las concentraciones de actividad de los emisores gamma ^{226}Ra, ^{228}Ra, ^{40}K y $^{210}Pb_{ex}$ de 39 muestras de sedimento submarino recogidas a lo largo de la Bahía del Confital y las zonas intermareal y submarina de la playa de Las Canteras durante la primera mitad de 2022. Además, se analizó la distribución espacial de las concentraciones de actividad de ^{226}Ra, ^{228}Ra y ^{40}K de 37 muestras pertenecientes a una campaña anterior que se tomaron para la realización de un estudio sedimentario de la Bahía del Confital entre los años 2005 y 2006 (Medina et al., 2006).

Por otro lado, también se realizó un análisis de granulometría usando el método de tamizado en seco (Alveirinho Dias, 2004) y el software GRADISTAT (Blott and Pye, 2001). Las fracciones obtenidas para cada tamaño de grano se guardaron por separado y se obtuvieron los valores de concentración de actividad de ^{226}Ra, ^{228}Ra, ^{40}K y $^{210}Pb_{ex}$ para aquellas que presentaban suficiente material para analizarlas por

espectrometría gamma. Así mismo, 6 muestras pertenecientes a las zonas de alta y baja actividad de la bahía fueron seleccionadas para analizar su contenido mineralógico.

Los resultados del análisis de distribución espacial de la actividad de ^{226}Ra, ^{228}Ra y ^{40}K mostraron que en ambos periodos de tiempo la Bahía del Confital se dividió en las mismas dos zonas; una de alta actividad al oeste de la bahía y otra de baja actividad en el este. En media las dos campañas no presentaron diferencias significativas y, por tanto, se dedujo que las concentraciones de actividad de estos radionucleidos en ambas campañas pertenecían a los mismos sedimentos, estando los cambios en la distribución espacial de estas actividades más asociados al transporte y redistribución de sedimentos dentro de la propia bahía.

Al analizar las diferencias en la distribución espacial de las actividades de ^{226}Ra, ^{228}Ra y ^{40}K en las distintas épocas (2005/2006 y 2022) se pudo apreciar cómo en la costa oeste los máximos de actividad de los tres radionucleidos se habían desplazado desde la línea de costa hacia el interior de la Bahía del Confital. Este cambio sugirió un transporte de sedimentos desde la costa a la parte profunda de la bahía. Para poder encontrar posibles agentes responsables de este transporte de sedimentos se calculó la profundidad de cierre (Hallermeier, 1981) en cada año transcurrido desde 2005 a 2021. Esta profundidad de cierre establece la profundidad a la cual deja de producirse un transporte transversal del sedimento debido a la acción del oleaje. Para la Bahía del Confital se estableció una profundidad de cierre alrededor de los 9 m, aunque hubo años en los que esta profundidad llegó a alcanzar 12 m debido a una intensidad del oleaje mayor que en otros años. Esto quiere

decir que eventos tormentosos severos podrían haber generado el transporte observado en la zona oeste de la bahía.

Como la profundidad de cierre se estableció en 9 m, también se hizo un análisis y comparación de la variabilidad espacial de las actividades de ^{226}Ra, ^{228}Ra y ^{40}K solo en la parte sumergida de la playa de Las Canteras para las dos campañas estudiadas. Los resultados mostraron que la parte sumergida de la playa presentaba la misma distribución espacial que se encontró en los dos artículos previos de esta tesis realizados en la zona intermareal (Arriola-Velásquez et al., 2019, 2021). De esta manera, las concentraciones de actividad más altas se localizaron en la zona sumergida protegida por la barra, indicando así que esta zona está bajo un periodo constante de acumulación. En la parte sur de la playa sumergida, la parte totalmente expuesta a la acción del oleaje, las concentraciones de actividad de ^{226}Ra, ^{228}Ra y ^{40}K fueron más bajas mostrando que, al igual que ocurría en la zona intermareal, esta parte de la playa sumergida es la más afectada por los periodos de erosión y acumulación de sedimentos. Así mismo, en ambas épocas se observó un aumento progresivo de la actividad desde el arco sur al arco norte, lo cual indicaba el transporte longitudinal de sedimentos que se da entre una parte de la playa y la otra. Por tanto, los radionucleidos ^{226}Ra, ^{228}Ra y ^{40}K también trazan la dinámica sedimentaria marina existente en la zona sumergida de la playa de Las Canteras.

Por otro lado, también se analizó la distribución espacial de la actividad de $^{210}Pb_{ex}$ tanto en la Bahía del Confital como en la playa de Las Canteras. El $^{210}Pb_{ex}$ se introduce en la columna de agua adsorbido a las partículas de polvo atmosférico y si se da poca erosión del fondo se transportan y acumulan en el lecho marino por un proceso de

sedimentación. Los resultados de este estudio mostraron que, para la Bahía del Confital, las concentraciones de actividad de $^{210}Pb_{ex}$ más altas se localizaron en las profundidades mayores y en las zonas sumergidas de la playa de Las Canteras protegidas frente a la acción del oleaje. Por tanto, los resultados de este estudio sugieren que el $^{210}Pb_{ex}$ puede ser utilizado para trazar zonas de abrigo y poca erosión del fondo marino donde se produce acumulación de partículas de la columna de agua por sedimentación.

Para el estudio de las relaciones existentes entre el tamaño de grano y las actividades de ^{226}Ra, ^{228}Ra, ^{40}K y $^{210}Pb_{ex}$ se aplicaron distintos análisis estadísticos. Primero se hizo un análisis de correlaciones entre las actividades de ^{226}Ra, ^{228}Ra, ^{40}K y $^{210}Pb_{ex}$, el tamaño de grano medio de las muestras, el sorting de la muestra, el porcentaje de arena gruesa, arena media, arena fina, arena muy fina y lodo (limos y arcillas), la profundidad de recogida y la densidad de las muestras. Además de esto, se realizó un análisis de diferencias significativas en las actividades de ^{226}Ra, ^{228}Ra, ^{40}K y $^{210}Pb_{ex}$ encontradas en las distintas fracciones de tamaño de grano.

Los resultados obtenidos mostraron que las mayores concentraciones de actividad de ^{226}Ra, ^{228}Ra y ^{40}K no estaban asociadas a los tamaños de grano pequeños, lo cual difiere de lo sugerido por otros autores (Alfonso et al., 2014; Ligero et al., 2001; Lin et al., 2020). Además, el análisis mineralógico mostró que el incremento de la actividad de estos radionucleidos en muestras de una misma campaña estaba asociado al aumento del contenido de feldespatos, feldespatoides y zeolitas. Este comportamiento coincidió con lo encontrado en el tercer artículo de esta tesis y en algunos casos de la literatura (Roviello et al.,

2020), poniendo de nuevo de manifiesto la influencia del contenido mineralógico de las muestras en sus concentraciones de actividad de ^{226}Ra, ^{228}Ra y ^{40}K .

Finalmente, en el caso del $^{210}Pb_{ex}$ el análisis de correlaciones encontró correlaciones directas entre la actividad del $^{210}Pb_{ex}$ y los porcentajes de tamaño de grano pequeño. Además, el análisis de diferencias significativas en las distintas fracciones identificó diferencias entre las fracciones de menor tamaño de grano (arenas muy finas y lodos) y las fracciones de tamaño de grano mayores. Estos resultados parecían estar relacionados con el origen y transporte del $^{210}Pb_{ex}$ adsorbido a los aerosoles atmosféricos.

Teniendo todo esto en cuenta, los resultados de este artículo corroboraron que las variaciones de las concentraciones de actividad de ^{226}Ra, ^{228}Ra y ^{40}K trazan los procesos de transporte de sedimentos en zonas costeras. Así mismo, se sugirió que las variaciones en las actividades de $^{210}Pb_{ex}$ son útiles para trazar áreas de poca erosión del fondo marino donde se produce acumulación por sedimentación.

Catena 235 (2024) 107672

Contents lists available at ScienceDirect

Catena

journal homepage: www.elsevier.com/locate/catena

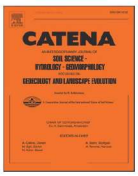

Natural radionuclides as tracers of coastal sediment dynamics in El Confital Bay (Spain): Spatial distribution and relationships with sediment characteristics

A.C. Arriola-Velásquez [a], A. Tejera [a,*], I. Alonso [b], F. Cámara [c], M. Cantaluppi [c], H. Alonso [a], N. Miquel-Armengol [a], J.G. Rubiano [a], P. Martel [a]

[a] Department of Physics, Instituto Universitario de Investigación en Estudios Ambientales y Recursos Naturales i-UNAT, Universidad de Las Palmas de Gran Canaria, Campus de Tafira, 35017 Las Palmas de Gran Canaria, Spain
[b] Instituto de Oceanografía y Cambio Global, IOCAG, Universidad de Las Palmas de Gran Canaria, Campus de Tafira, 35017 Las Palmas de Gran Canaria, Spain
[c] Dipartimento di Scienze della Terra, Università degli Studi di Milano, via Sandro Botticelli 23, 20133 Milano, Italy

ARTICLE INFO

Keywords:
Radionuclides
Tracer
Sediment dynamics
Coastal sediments
Grain size

ABSTRACT

Erosion and accumulation of coastal areas have become an increasing concern in recent years since they can result in important social and economic problems. In this framework, natural radionuclides have emerged as an alternative tool to study coastal sediment transport and help with the management of the littoral zone. However, there is still a lack of knowledge on how these radionuclides can be applied as tracers of coastal sediment dynamics and how the sediment characteristics can influence this use. Thus, a methodology is presented in this work to use natural radionuclides as tracers of coastal erosion, transport and accumulation of sediments. For this purpose, the spatial distributions of ^{226}Ra, ^{228}Ra, ^{40}K and unsupported ^{210}Pb (^{210}Pb$_{ex}$) in two periods of time were analysed and compared in a coastal area with diverse marine dynamics. The results showed that ^{226}Ra, ^{228}Ra and ^{40}K identified the different sediment erosion, transport and accumulation occurring in the study region. In addition, it was found that changes in the activity concentrations of the samples were mostly related to variations in their mineralogical composition. Finally, the activity concentration values of ^{210}Pb$_{ex}$ made it possible to trace the areas where accumulation due to the sedimentation of aerosol particles in the seabed is favoured. These results highlight the suitability of natural radionuclides to study coastal sediment transport.

1. Introduction

Uncontrolled sediment transport in the coastal environment can lead to considerable economic and social consequences. Some of these include long-term retreat of the shorelines that can result in beach losses and danger to coastal human settlements or the return to ports and harbours of material previously dredged from them affecting their navigation channels (International Atomic Energy Agency, 2014). In this framework, having tools to study the erosion, transport and accumulation of sediments in the environment is essential in order to obtain the necessary information for the building and maintenance of coastal and riverine infrastructures, as well as for the design of mechanisms for coastal protection such as barriers for beach and littoral protection.

In the past, artificial radionuclides were used to trace sediment erosion, transport and accumulation but, in recent years, natural radionuclides have emerged as better alternative tracers of coastal sediment dynamics since they do not require anthropogenic introduction in the system as they already belong to it (International Atomic Energy Agency, 2014). Most of these naturally occurring radionuclides are primordial radionuclides that can be found in the Earth's crust since its formation (like ^{40}K and those from the natural decay chains of ^{238}U, ^{232}Th and ^{235}U) and their activity concentrations in sediments are controlled by the natural geochemical characteristics of the original sediment sources (Froehlich, 2010). Therefore, changes in their activity concentrations in sediments from the same area are related to local physicochemical alterations including the transport of the sediment containing them.

In coastal areas, natural radionuclides, such as those from the ^{232}Th and ^{238}U series or ^{40}K have been used as tracers of different sedimentary processes. Some authors focused on the use of these radionuclides as

* Corresponding author.
E-mail address: alicia.tejera@ulpgc.es (A. Tejera).

https://doi.org/10.1016/j.catena.2023.107672
Received 16 February 2023; Received in revised form 30 October 2023; Accepted 3 November 2023

tracers of sedimentation rates (Cooper and Grebmeier, 2018; Eulie et al., 2018; Tsabaris et al., 2012). Other studies used, among others, ^{232}Th, ^{238}U, ^{210}Pb or ^{40}K to evaluate sediment transport and sources in coastal areas (Bezuidenhout, 2020; Feng et al., 2010; Thereska, 2009). Among the different methodologies applied in these types of studies, one of the most promising is the mapping of natural radioactivity using in situ gamma spectrometers, which have been applied in both beach sands and submerged coastal areas (Androulakaki et al., 2015; Kilel et al., 2022; Tsabaris et al., 2023b). These detectors with continuous acquisition gamma spectra capability enable a rapid mapping of natural radionuclides of the study region to identify high activity concentration areas as sediment accumulation zones (Mtshawu et al., 2023; Tsabaris et al., 2023a).

Despite the advantages that in situ measurements can present (e.g., the velocity at which results can be obtained), there are still some disadvantages that need to be addressed. For example, when using in situ gamma spectrometers, interferences of the surrounding elements of the study region can alter the resulting map and some sediment transport patterns can be misinterpreted. Considering this, lab-based measurements can ensure that the activity concentration values obtained come only from the sediment grains. This is because samples are taken from the study region and analysed in the laboratory so no interference from the surrounding objects such as rocks, construction materials or seawater can occur. In addition, since these measurements come directly from the samples, lab-based measurements can also be used to enhance the knowledge of the relationships between activity concentration values and different sediment characteristics. This can lead to a better understanding of the role and application of natural radionuclides as tracers of coastal erosion, transport and accumulation of sediments.

When assessing the use of natural radionuclides as tracers of sediment dynamics, one of the key steps is to identify their spatial distribution in the study region and to determine how they are related to different sediment characteristics. In this framework, some works have found that there is an existing relationship between the activity concentrations of both natural and artificial radionuclides in sediment samples and some sedimentological variables, such as the grain size or organic content (Alfonso et al., 2014; Charkin et al., 2022; Huang et al., 2013; Ligero et al., 2001; Lin et al., 2020; Madruga et al., 2014). According to these studies, an increase in the small-grain-size fraction in sediments is associated with an increase in the activity concentration values of different radionuclides, including, for example, ^{40}K, ^{137}Cs and various radium isotopes. These studies explain that this occurs because smaller particles of sediment present larger active surfaces, which favours the sorption of radionuclides. Nevertheless, some authors found that in some circumstances, such as when the clay and/or silt fractions in the samples are low, this relationship between small grain sizes and high activity concentrations of radionuclides does not necessarily occur (Charkin et al., 2022). Thus, it cannot be assumed that high activity concentration values of natural radionuclides are always associated with the accumulation of small grain-size sediments. Therefore, further studies on the subject are necessary to enhance the knowledge of how natural radionuclides relate to sediment characteristics so their role as tracers of the sediment erosion, transport and accumulation of these sediments can be better evaluated. Understanding this is especially important to properly apply and develop emerging methodologies used in the application of natural radionuclides as tracers of sediment dynamic processes such as the in situ mapping mentioned before.

In the case of El Confital Bay, in the northern part of Gran Canaria Island (Spain), previous baseline studies on natural radionuclides and their use as tracers of sediment dynamics have focused on Las Canteras Beach, which is located in the southern part of the bay (Arnedo et al., 2013; Arriola-Velásquez et al., 2019, 2021). This beach was chosen as a natural laboratory to assess the use of natural radionuclides as tracers of sediment dynamics due to its diverse sediment dynamics and heterogeneous sediment composition. According to the literature, this beach is divided into three arches, and its northern and central arches are protected from wave action by a natural offshore rocky bar. This bar has openings and fragmentations that present themselves more in the central arch. The beach exhibits more terrigenous materials and heavy minerals in the southern arch and more calcareous and organic content in the northern arch (Alonso, 1993; Alonso and Pérez Torrado, 1992). In addition, it presents seasonal variability in its sedimentary budget. During erosion periods, the sediments from the southern arch are eroded and longshore transport to the northern arch occurs. During accumulation periods, sediments arrive at the beach from the surrounding area, and in the northern arch, some longshore transport to the southern part of the beach can occur. Thus, the northern arch has a constant accumulation period, while the southern arch presents strong differences in its sediment budget between erosion and accumulation periods (Alonso, 2005, 1993; Alonso and Vilas, 1996).

The first studies carried out in this area addressed the spatial distribution of natural radionuclides in intertidal sand from Las Canteras Beach (Arnedo et al., 2013; Arriola-Velásquez et al., 2019). The results obtained showed that the samples with lower activity concentration values were from the southern part of the beach, which is the area that is completely exposed to wave action. The samples located in front of the openings of the bar, mostly in the central arch, presented intermediate activity concentration levels. The northern arch, the area fully protected from wave action, presented the highest activity concentration values. This distribution of natural radionuclides seemed to be identifying the distribution of sediments along the beach according to the different dynamics present in it. In addition, in the work of Arriola-Velásquez et al. (2019), a first approach for determining the relationships between the activity concentration values and the sedimentological variables of the samples was assessed. The results showed that the mean grain size of the samples had a direct correlation with the activity concentration values of ^{226}Ra, ^{232}Th and ^{40}K. This indicated that samples with a larger grain size corresponded to higher activity concentration values. Furthermore, the bulk density of the samples presented an inverse correlation with the activity concentration values of those same radionuclides. Therefore, it seemed that the spatial variability of natural radionuclides also indicated the different mineral compositions of the sediments.

The study of Arriola-Velásquez et al. (2021) focused on assessing the temporal variability of the activity concentration values of natural radionuclides in sand samples during a three-year period. In this case, the influence of meteorological and oceanographic variables on the activity concentrations of ^{226}Ra, ^{228}Ra and ^{40}K was studied. The results showed the presence of significant differences that depended on the significant wave height (H_S) in the activity concentration values of these radionuclides in the southern arch of the beach. Hence, campaigns that took place in periods with a low H_S presented higher activity concentration values of ^{226}Ra, ^{228}Ra and ^{40}K. In addition, a mineralogical analysis showed that the increases and decreases in the activity concentration values agreed with the presence or absence of feldspars in the sand samples during erosion and accumulation periods.

These earlier studies seem to validate the use of natural radionuclides as tracers of the erosion, transport and accumulation of sediments in the intertidal zone of beach areas. Therefore, this study aims to use the spatial distributions of the activity concentrations of ^{226}Ra, ^{228}Ra, ^{40}K and unsupported ^{210}Pb (^{210}Pb$_{ex}$) in two periods in time to trace different sediment dynamics in submerged areas from El Confital Bay and Las Canteras Beach. Moreover, the influence of the grain size and mineralogical composition of the samples on the activity concentration values found for these radionuclides will be assessed. This way, this study will provide a methodology that could be applied in other parts of the world to study coastal sediment dynamics using natural radionuclides as tracers and can help the development of emerging methodologies in the field.

2. Study region

El Confital Bay is a 10-km^2 bay located in the northern part of the island of Gran Canaria in the city of Las Palmas de Gran Canaria, Spain (Fig. 1). According to prior studies, the sediments that compose the sand on the bottom of El Confital Bay present different composition and granulometric characteristics. The grain size varies, with sizes that range from 0.13 to 3.66 mm (Medina et al., 2006). In addition, two main groups of materials can be found in the bay. On one hand, the sediments that are present in the north-eastern part of the bay have a high carbonate content; these sediments are mostly of organic origin. On the other hand, the south-western part of the bay presents more terrigenous sediments, including sediments that come from phonolitic lava flows and basic rocks and have a low organic material content (Balcells et al., 1990; Mangas and Julià-Miralles, 2015; Medina et al., 2006; Schmincke, 1993).

The sediments of Las Canteras Beach have similar grain sizes, which range between 0.2 and 0.5 mm; slightly larger sizes are present in the area between the central and northern arches (Alonso, 1993; Arriola-Velásquez et al., 2019; Medina et al., 2006). The origin of these sediments is the geological environment of the beach, including basic rocks from the islet in the north-eastern part of the bay, the natural offshore calcarenite rocky bar, magnetite and volcanic rocks from La Ballena Ravine in the southern part of the beach and the different sediments that can be found in the submerged sandbars of El Confital Bay (Balcells et al., 1990; Schmincke, 1993). Moreover, some calcimetry and petrological analyses that have been carried out over the years allow the differentiation of the various materials that can be found at Las Canteras Beach. In the northern arch, the sand is principally composed of bioclast and calcareous materials. Hence, some studies suggested that the sediments of the northern part of the beach come from the north-eastern part of El Confital Bay through the openings of the bar in that area (Medina et al., 2006). Nonetheless, the sand from the northern arch also presents calcarenites, with a significant feldspar content in its terrigenous part (Alonso, 1993; Alonso and Pérez Torrado, 1992). In the southern arch, sediments have lower carbonate and bioclast contents. The materials that accumulate mostly come from the outlet of the ravine that ends at this arch. These materials are mostly clinopyroxenes, amphiboles, Fe-Ti oxides and other heavy minerals, such as olivine. The lighter lithics that arrive at this part of the beach also include, among other things, feldspars, but these are redistributed along the beach (Alonso, 1993; Alonso and Pérez Torrado, 1992; Mangas and Julià-Miralles, 2015; Medina et al., 2006).

3. Materials and methods

3.1. Sand sample collection and preparation

An extensive campaign was designed to evaluate the spatial distributions of the activity concentration values of various natural radionuclides for the whole study region. A total of 39 submerged sand-sampling locations were selected to cover the whole area of El Confital Bay and the submerged part of the beach located between the natural offshore rocky bar and the beachline, as well as the northern and southern arches of Las Canteras Beach, during the first half of 2022 (Fig. 1B). To better specify their locations, the samples from outside the natural offshore rocky bar were considered deep sediment samples (D). The samples from the submerged part of the beach were identified as submerged sand samples (S). Finally, the samples from the intertidal beach were called intertidal sand samples (I). In total 16 deep samples were collected in the outer part of El Confital Bay. In addition, 15 samples were collected along the submerged part of Las Canteras Beach and its entrance in the southern arch. All submerged samples were collected aboard a vessel using a 2L Van Veen grab. The sediments collected correspond to seabed surface sediments. Pictures of the sampling device used for submarine sample collection can be checked in the supplementary material (Supplementary Fig. S1). Moreover, 8 sand samples were taken in the intertidal zone of the beach during low tide. For this, a 1-m^2 square was drawn in the sand and, after mixing in situ, superficial sand samples were taken from between depths of 0 and 5 cm. In addition to these samples, 37 samples from a campaign carried out between 2005 and 2006 as part of a prior sedimentary study of El Confital Bay (Medina et al., 2006) were also analysed in this work (Fig. 1A). These samples included 16 samples from the bay, 7 from the submerged part of the beach and 14 belonging to the intertidal zone.

All sand samples were taken to the laboratory, dried at 80 °C for 24 h and sieved through a 1-mm mesh to homogenise them. Finally, they were stored in PVC-trunk conical containers, which were filled to 40 cm^3 and sealed with aluminium strips for one month before measurements were taken. This month of storage allowed the secular equilibrium between ^{226}Ra, ^{222}Rn and its short-lived progenies to be reached since ^{214}Pb is used to determine ^{226}Ra (Bezuidenhout, 2013).

3.2. Gamma spectrometry analysis

The determination of radionuclides in sand samples using gamma spectrometry analysis was carried out using a Canberra Extended Range (XtRa) Germanium spectrometer, model GX3518, with a relative efficiency of 38 % with respect to a 3″ x 3″ active area NaI (Tl) detector and a nominal FWHM of 0.875 keV at 122 keV and 1.8 keV at 1.33 MeV. It was coupled to a Canberra DSA-1000 multichannel analyser with the software package Genie 2000. The efficiency calibration of the system was carried out using the Canberra LabSOCS package based on the Monte Carlo method (Arnedo et al., 2017; Arriola-Velásquez et al., 2019, 2021; Guerra et al., 2015, 2017). The reference standards IAEA RGK-1 (potassium sulphate), RGU-1 (uranium ore) and RGTh-1 (thorium ore) were used to verify the calibration. Energy calibration was performed using ^{155}Eu/^{22}Na (Canberra ISOXSRCE, 7F06-9/10138 series) and verified using the 1460.8 keV line of ^{40}K (IAEA RGK-1) (Arnedo et al., 2017).

Different photopeaks were analysed to determine the radionuclides of interest. The emission line 351.9 keV of ^{214}Pb was used to determine the activity concentration of ^{226}Ra. ^{210}Pb was directly measured using the emission line of 46.5 keV. The emission line of 911.2 keV, corresponding to ^{228}Ac, was used to obtain the activity concentration values of ^{228}Ra. The lines 1460.8 keV and 661.8 keV were used to directly measure the activity concentrations of ^{40}K and ^{137}Cs, respectively. The counting time for each sample was around 24 h. The activity concentration values have been expressed according to common standard of using only one significative figure for uncertainties, and a coverage factor k = 1 was assumed.

Moreover, the unsupported or excess ^{210}Pb (^{210}Pb$_{ex}$) was calculated from the activity concentrations of ^{210}Pb and ^{226}Ra. ^{222}Rn has a half-life of 3.8 days, and its decay produces ^{210}Pb. ^{222}Rn is a gas daughter of ^{226}Ra that partially diffuses into the atmosphere, where it rapidly decays into ^{210}Pb. After this, ^{210}Pb falls back to the Earth's surface through wet and dry deposition. This deposited ^{210}Pb that is not in equilibrium with the ^{226}Ra of the samples is what is known as unsupported or excess ^{210}Pb$_{ex}$ (Bobos et al., 2021; Dueñas et al., 2017; Gaspar et al., 2017; Gu et al., 2022; Hülse and Bentley, 2012). Therefore, the difference between the activity concentrations of ^{210}Pb and ^{226}Ra was used to determine the activity concentration of ^{210}Pb$_{ex}$.

3.3. Grain size and X-ray diffraction analysis

A dry-sieving grain size analysis (Alveirinho Dias, 2004) was performed on the samples from El Confital Bay and Las Canteras Beach. Aliquots of around 300 g of each sample were used. These aliquots were passed through nine sieves from 8 to 0.0625 mm with 1φ intervals, and each portion was weighed separately. After, the results of the granulometric analysis including the statistical parameters of mean grain size, sorting (standard deviation), skewness and kurtosis and the percentage of the different grain size fractions were obtained from the GRADISTAT

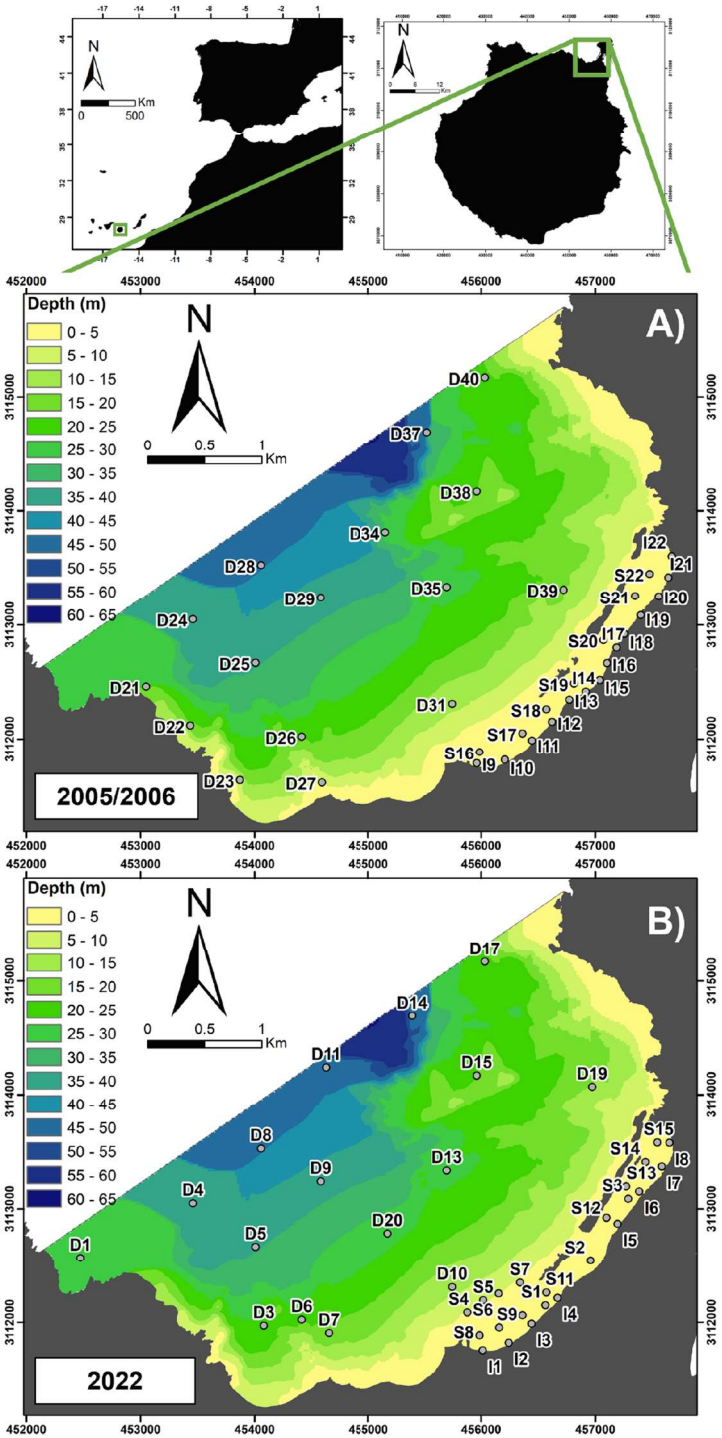

Fig. 1. Study region, bathymetry and sand sampling points in El Confital bay and Las Canteras beach for the 2005/2006 and the 2022 campaigns. Coordinates are in the UTM system.

software version 9.1 (Blott and Pye, 2001) using the Folk and Ward method (Folk and Ward, 1957). Then, each grain size fraction of the sand was stored in PVC-trunk conical containers, just like the original samples, for gamma spectrometry analysis.

Powder X-ray diffraction (XRPD) data acquisition was carried out with an X'Pert PRO Diffractometer (PANalytical), using the θ-2θ Bragg-Brentano geometry, that was equipped with an X'Celerator LPS detector. The 5°-80° 2θ range was investigated using CuKα radiation with a current tension of 40 kV, a current intensity of 40 mA and collection at 0.02° steps, and a fixed divergence-slits angle of 0.25°. Samples were ground on an agate mortar and then pressed in a back-load sample holder. The sample holder was spun during data acquisition. Diffraction patterns were analysed using X'Pert HighScore v. 2.1 (PANalytical©) and mineral phases were matched using PDF2 (ICDD). Quantitative analysis through Rietveld refinement was carried out using GSAS II (Toby and von Dreele, 2013) and crystallographic information files (CIFs) available in the literature and obtained from the Crystallographic Open Database – COD (Gražulis et al., 2009) for closely related matched phases. No clear evidence of amorphous material was observed on the pattern of diffraction ruling out a significant contribution of glassy material.

Selected grains of sample S8 were also checked using single crystal X-ray diffraction (SCXRD) using a Rigaku Oxford Diffraction XtaLAB Synergy diffractometer equipped with a PhotonJet (Mo) X-ray Source operating at 50 kV and 1 mA, and a Hybrid Pixel Array detector that was located 62 mm away from the sample position. Intensity data were extracted from images using CrysAlisPro 1.171.40.71a (Rigaku Oxford Diffraction, 2020). Crystal structures were refined using SHELX-2018 (Sheldrick, 2015), starting with atom coordinates from the literature. Crystallographic information files have been provided as supplementary material.

3.4. Map interpolation method

The maps of bathymetry, grain size and activity concentration values of ^{226}Ra, ^{228}Ra, ^{40}K and ^{210}Pb$_{ex}$ were drawn using the ArcGIS Desktop version 10.8.2. The interpolation algorithm used in all cases was the Inverse Distance Weighted (IDW). For IDW, it was used the formula that takes the inverse of the distance raised to the second power, which is the default in the ArcGIS and it is the most simple and widely used (Achilleos, 2011; Gong et al., 2014).

3.5. Statistical analysis

On the one hand, to establish the possible significant differences among the measurements of the activity concentration values from both campaigns, a u-test (IAEA, 2012) was performed using the following equation:

$$u_{test} = \frac{|A_A - A_B|}{\sqrt{u_A^2 + u_B^2}} \quad (1)$$

where A_A corresponds to the mean activity concentration value of one radionuclide in the campaign of 2005/2006, u_A is the uncertainty associated with that mean activity value, A_B is the mean activity concentration value of one radionuclide in the campaign of 2022 and u_B is the uncertainty of that activity concentration value. The u_{test} values obtained from Eq. (1) are compared with the threshold value 2.58 at level 99 %. Then, the null hypotheses of equality of activity concentration values are rejected for observed u_{test} values greater than 2.58. Therefore, when $u_{test} > 2.58$, the pair of values reported is significantly different.

On the other hand, a Shapiro-Wilk normality test (Shapiro and Wilk, 1965) was used to evaluate the distribution of all the results. Then, a correlation analysis was performed to establish the relationships between the activity concentration values of ^{226}Ra, ^{228}Ra, ^{40}K and ^{210}Pb$_{ex}$, the results of the granulometric analysis and the depth and bulk density values of the samples. In the case of the grain size fractions, if the activity concentrations of one radionuclide followed a normal distribution, a one-way ANOVA test was performed to determine if there were significant differences among the different grain size fractions. Then, Tukey's Honestly Significant Difference (HSD) test (Williams and Abdi, 2010) was used to establish the exact fractions within which significant differences were found. If the activity concentrations did not follow a normal distribution, a Kruskal-Wallis test (Theodorsson-Norheim, 1986) was used to determine if there were significant differences in the activity concentrations of samples with different grain sizes. In this case, a Wilcoxon rank-sum test (Rosner and Glynn, 2009) was applied to determine which grain size fractions presented such differences. These tests were carried out for a significance level of 0.05.

4. Results and discussion

4.1. Activity concentration distribution in sediment samples from El Confital Bay and Las Canteras Beach

The maps in Fig. 2 show the superficial sediment mean-grain-size distribution in El Confital Bay and Las Canteras Beach in both campaigns, 2005/2006 and 2022. Both maps show that most of the sediment with a higher mean grain size can be found in the south-western and north-eastern parts of the bay. In the case of the campaign of 2005/2006, the largest mean grain size was 2432 μm with sorting of 1.589, skewness of −0.140 and kurtosis of 1.188, while in the 2022 campaign, the maximum mean grain size was 1617 μm with sorting of 1.617, skewness of 0.087 and kurtosis of 1.354. However, the average grain size for all the samples of the bay in the 2005/2006 campaign was 473 μm (0.473 mm), while for 2022, it was 379 μm (0.379 mm). This means that, in both cases, the mean grain size of the whole bay classifies the sediments as medium sand according to the GRADISTAT software classification (Blott and Pye, 2001).

The activity concentration distributions of ^{226}Ra, ^{228}Ra and ^{40}K for the whole bay for both campaigns are represented in Fig. 3. The maximum, minimum and mean activity concentration values of these radionuclides are reported in Table 1. The mean activity concentration values of ^{226}Ra, ^{228}Ra and ^{40}K in both campaigns were compared using the u-test, and the results are also displayed in Table 1. The results of the test show that the mean values do not present significant differences between the campaigns. This suggests that in essence, the activity concentration values of ^{226}Ra, ^{228}Ra and ^{40}K correspond to the same sediments in both periods. From the maps in Fig. 3, it can be observed that the activity concentrations of ^{226}Ra, ^{228}Ra and ^{40}K have the same main spatial distribution in both campaigns, which can be used to delimit two areas: one with lower activity concentration values in the north-eastern part of the bay and one with higher activity concentration values in the south-western part of the bay.

Earlier studies of environmental radioactivity in volcanic islands showed that phonolitic rocks are among the volcanic rocks that present higher natural gamma radiation emissions and activity concentration values of ^{226}Ra, ^{232}Th (parent radionuclide of ^{228}Ra) and ^{40}K (Arnedo et al., 2017; Chiozzi et al., 2001; Fernández-Aldecoa et al., 1992). In fact, the work of Arnedo et al., (2017) reported that soils from the island of Gran Canaria in which phonolitic and trachytic rocks could be found presented the highest activity concentration values of ^{226}Ra (>50 Bq kg^{-1}), ^{232}Th (>90 Bq kg^{-1}) and ^{40}K (>1000 Bq kg^{-1}). As a matter of fact, the mean activity concentration values reported in the study of Arnedo et al., (2017) for this type of soil for ^{226}Ra and ^{40}K (75 Bq kg^{-1} and 869 Bq kg^{-1} respectively) clearly contrast with the mean activity concentration values reported for soils of basaltic rocks (30 Bq kg^{-1} for ^{226}Ra and 337 Bq kg^{-1} for ^{40}K). Therefore, the high activity concentration values obtained for the south-western part of the bay seem to be related to the presence of sediments from phonolitic rocks in the area (Balcells et al., 1990; Schmincke, 1993). On the other hand, in the case of the

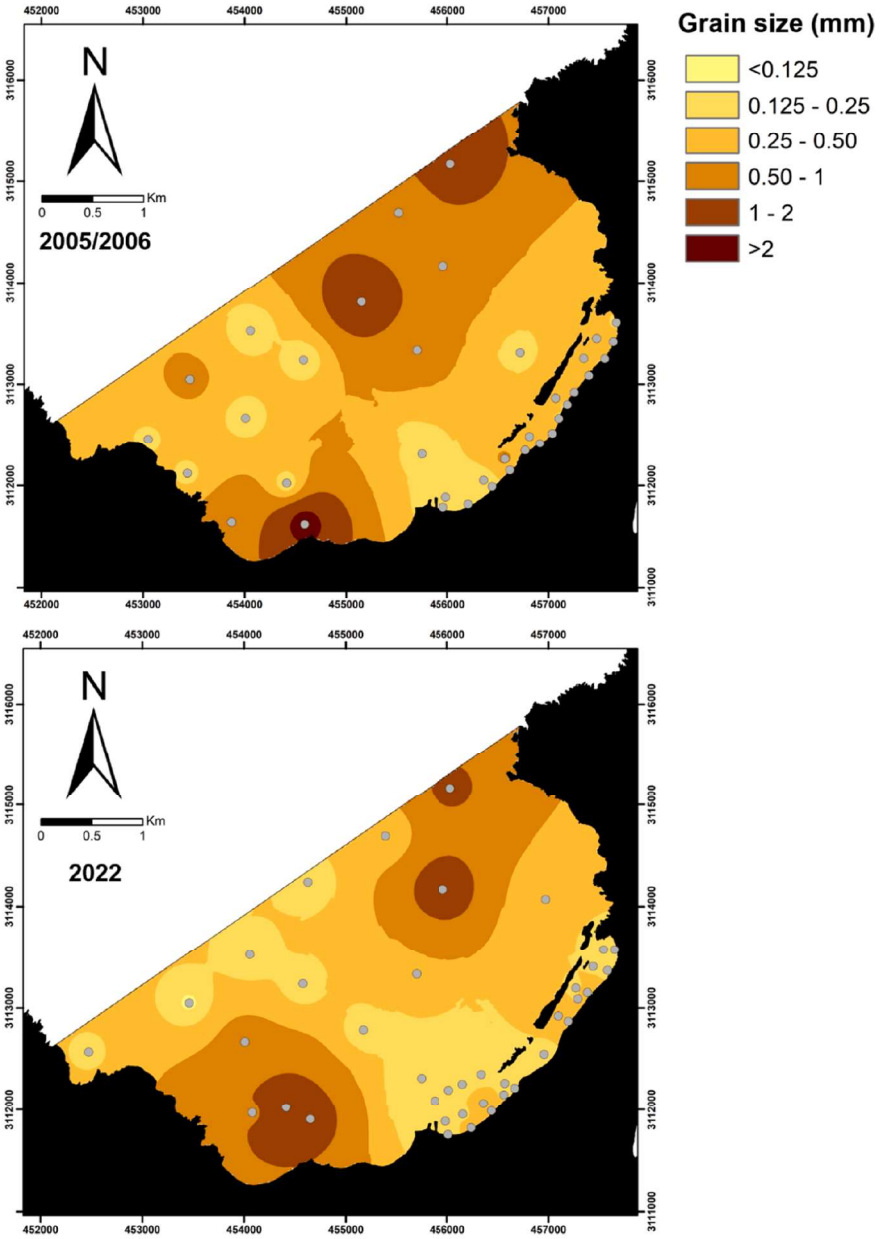

Fig. 2. Sediment grain size distribution of El Confital bay and Las Canteras beach for the 2005/2006 and the 2022 campaigns.

north-eastern part of the bay, preceding descriptions of El Confital Bay established a predominant content of CaCO3 in sediments from that area with values of more than 90 % of $CaCO_3$ content (Medina et al., 2006). This clearly indicates that the sediments from the north-eastern part of the bay have a predominant composition of bioclasts. Some studies in other parts of the world have found that increases and decreases in ^{226}Ra, ^{232}Th and ^{40}K in sediments are related to, among other factors, the amount of organic matter that can be found in such sediments (Alfonso et al., 2014; Ramadan and Diab, 2013). For those authors, a higher organic matter content was correlated with higher activity concentration values of different radionuclides. However, in the case of El Confital Bay, the area with the highest carbonate and organic content seems to be the one with lower activity concentration values of ^{226}Ra, ^{228}Ra and ^{40}K. This discrepancy could be explained by two characteristics of the sediments in the study region considered in this work.

First, in the studies mentioned earlier, the higher activity concentration values seemed to be related to the adsorption of radionuclides in the sediments with a small grain size and a high organic content. According to these studies, this occurs due to the larger active surface of the smaller grains of such sediments. However, the map in Fig. 2 shows that the north-eastern part of El Confital Bay has larger mean grain sizes, with all the samples being classified as medium to very coarse sand by the GRADISTAT software (Blott and Pye, 2001). Therefore, it could be possible that in areas like El Confital Bay, sediments with high carbonate

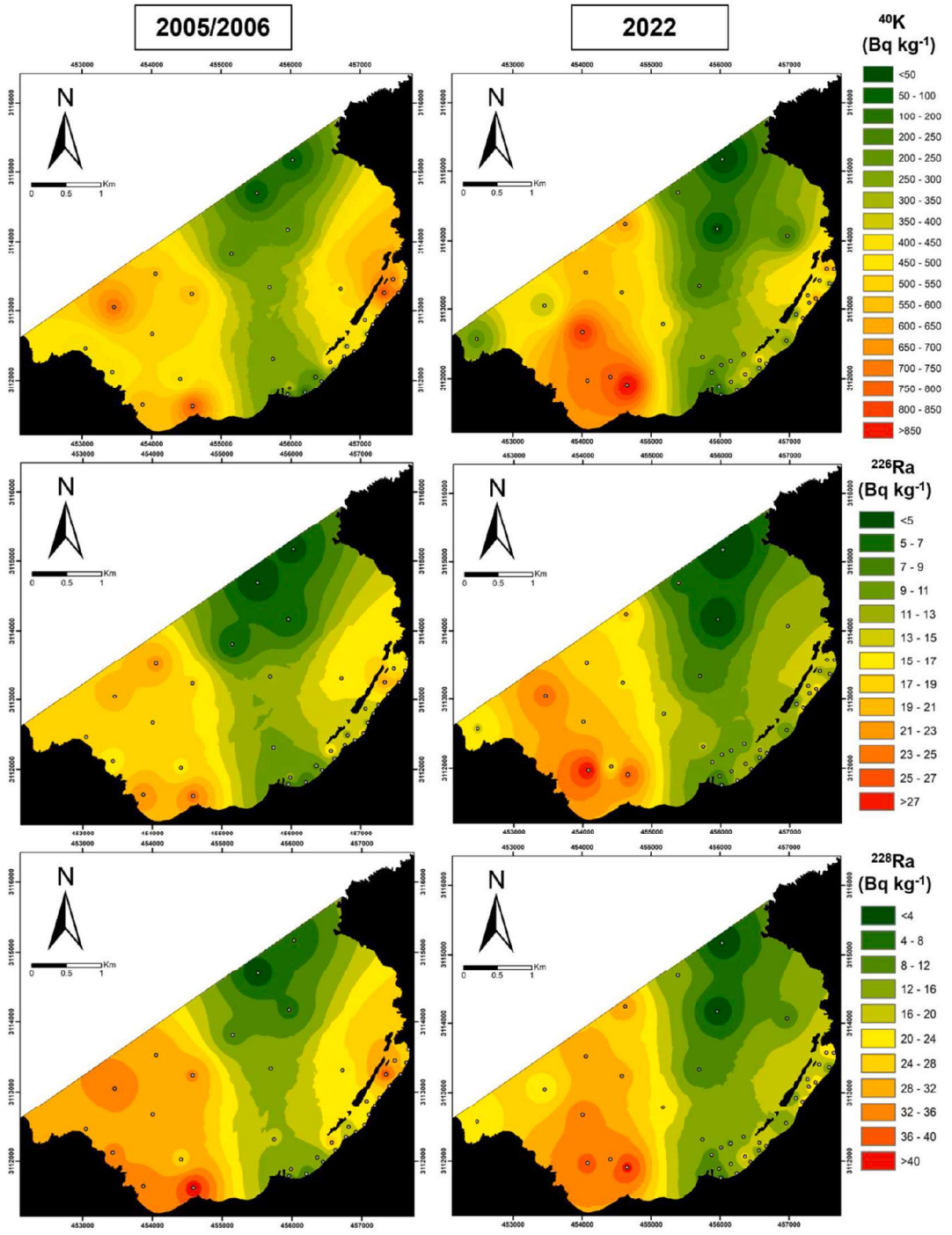

Fig. 3. Activity concentration distribution of ^{40}K, ^{226}Ra and ^{228}Ra in sediments from El Confital bay for the 2005/2006 and the 2022 campaigns.

and organic contents have larger grain sizes and correspondingly a smaller active surface. Thus, this adsorption of radionuclides might be less likely to occur.

Second, in prior studies of Las Canteras Beach, which is located in El Confital Bay and accordingly shares its geological characteristics, it was proven that the part of the beach with more carbonates presented higher activity concentration values of ^{226}Ra, ^{228}Ra and ^{40}K (Arriola-Velásquez et al., 2019, 2021). However, this increase in the activity concentration values of those three radionuclides, especially ^{40}K, seemed to be more related to the accumulation of K-feldspars (minerals typically found in

Table 1
Ranges of activity concentration values of ^{226}Ra, ^{228}Ra and ^{40}K in Bq kg^{-1} in the whole study region for both campaigns (2005/2006 and 2022). The mean activity concentration value for each radionuclide in each campaign is also reported in parenthesis below each range. In addition, the result of the u-test described in IAEA, (2012) is given.

Campaign	^{226}Ra	^{228}Ra	^{40}K
2005/ 2006	2.9 ± 0.7 – 24 ± 1 (13.8 ± 0.9)	< MDA (2) – 42 ± 3 (22 ± 2)	68 ± 8 – 820 ± 40 (420 ± 20)
2022	< MDA (1) – 29 ± 1 (13.1 ± 1.0)	< MDA (2) – 41 ± 3 (18 ± 2)	< MDA (3) – 940 ± 40 (380 ± 20)
u_{test}	0.54	1.27	1.37

(1) Minimum detectable activity (MDA) for ^{226}Ra = 2.9 Bq kg^{-1}

(2) MDA for ^{228}Ra = 2.8 Bq kg^{-1}

(3) MDA for ^{40}K = 29 Bq kg^{-1}

phonolitic rocks) in the areas with high carbonate and organic matter contents. Furthermore, earlier studies also indicated that feldspars could be found in the part of the beach with a higher carbonate content due to the presence of calcarenites, which contain feldspar in their terrigenous component (Alonso, 1993; Alonso and Pérez Torrado, 1992). Hence, the higher activity concentration values of ^{226}Ra, ^{228}Ra and ^{40}K found in sediments in the studies of 2019 and 2021 were apparently more related to the terrigenous content of the sediments than to the physico-chemical interactions of the carbonates and organic matter with the natural radionuclides of the environment. As mentioned earlier, a prior study showed that the north-eastern part of the beach possessed higher carbonate and foraminifera contents and less terrigenous content in its sediments (Medina et al., 2006). This, therefore, suggests another reason that the activity concentration values found for ^{226}Ra, ^{228}Ra and ^{40}K in that area are lower. Considering all of this, and since the north-eastern part of the bay has a lower terrigenous content and a larger grain size, the low activity concentration values found for this area in this work are to be expected. Nevertheless, the results of a mineralogical analysis of samples from different parts of the bay will be discussed later in this work to further understand the influence of these factors on the activity concentration values of the samples.

When comparing the spatial distributions of the activity concentration values of ^{226}Ra, ^{228}Ra and ^{40}K for both campaigns (Fig. 3), some differences can be observed. The lack of significant differences between the mean activity concentration values of the campaigns suggests that these distinctions could be associated with sediment transport within the study region. Focusing on the south-western part of the bay, the area with the highest activity concentration values seems to have moved from the edge of the bay to its interior. Furthermore, by comparing the two maps of the grain size distribution shown in Fig. 2, it can also be observed that in that same part of the bay, the larger-grain-size sediments also seem to have shifted in the same direction as the area with the highest activity concentration values of ^{226}Ra, ^{228}Ra and particularly ^{40}K. Given that high activity concentration values identify the accumulation of sediments and considering that the same shift patterns appear for the grain size distribution and activity concentration maps, this may suggest that there is some transport and accumulation of sediments from the coastline into the interior of the bay. To find possible agents controlling this sediment transport, the depth of closure (d1) was calculated for every year from 2005 to 2021. The depth of closure can be described as the limiting water depth at which there is no cross-shore sediment transport (Hallermeier, 1981). It was calculated using the following equation:

$$d_1 = 2.28H_{12h/y} - 68.5\left(\frac{H^2_{\frac{12h}{y}}}{gT^2_{\frac{12y}{y}}}\right) \quad (2)$$

where $H_{12h/y}$ corresponds to the highest significant wave height that is exceeded 12 h a year, $T_{12h/y}$ corresponds to the period associated with this height and g is the gravitational acceleration. The data of the significant wave height and the period associated to it were obtained from a buoy of the Puertos del Estado surveillance network, belonging to the government of Spain. The results obtained are shown in Table 2 and indicate that for almost every year, the depth of closure is located at less than 10 m, with a mean value of 8.6 m with a standard deviation of 1.3 m. However, in 2014, the significant wave height was higher than in other years, allowing the closure depth to descend to 12 m. Hence, it seems that in El Confital Bay, sand located at greater depths than 10 m could also be transported by the wave action during strong storm events. This could explain the sediment transport that Fig. 3 suggests for the south-western part of the bay. Nevertheless, further analysis on the coastline evolution of the area should be necessary to confirm the sediment transport that the changes in the activity concentration of ^{226}Ra, ^{228}Ra and ^{40}K suggest and the causes behind it.

Since the depth of closure established that the area where the net exchange of sediment can occur is at less than 10 m depth, the activity concentration distributions of ^{226}Ra, ^{228}Ra and ^{40}K for both campaigns are represented in more detail for the submerged and intertidal parts of Las Canteras Beach in Fig. 4. In both cases, the three radionuclides show higher activity concentration values in the submerged and intertidal parts of the northern arch of the beach and lower activity concentration values in the southern arch. The results agree with what was found in previous studies of the intertidal zone of this beach (Arriola-Velásquez et al., 2019, 2021). Those works ascertained that for the intertidal zone of Las Canteras Beach, the protected part of the beach experienced a constant accumulation of sediments, and thus, this was the part that presented higher activity concentration values of ^{226}Ra, ^{228}Ra and ^{40}K. On the other hand, the southern arch of the beach (the area that was totally exposed to wave action) was identified as an erosion area, and the activity concentration values of the radionuclides in this area were lower. Taking this into consideration, the results displayed in Fig. 4 also identify the accumulation area in the submerged northern arch, where activity concentration values are higher. However, the lower activity concentration values of ^{226}Ra, ^{228}Ra and ^{40}K in the submerged southern arch establish it as an erosion area. In addition, Fig. 4 displays a

Table 2
Significant wave height that is exceeded 12 h a year ($H_{12h/y}$), associated period ($T_{12h/y}$) and depth of closure (d1) for every year since 2005 to 2021.

Year	$H_{12h/y}$ m	$T_{12h/y}$ s	d1 m
2005	3.6	16.4	7.9
2006	3.7	12.7	7.8
2007	3.6	18.1	8.0
2008	4.4	17.9	9.6
2009	4.2	15.6	9.1
2010	3.9	17.3	8.6
2011	3.7	17.9	8.0
2012	3.1	16.6	6.7
2013	3.5	17.5	7.7
2014	5.9	13.6	12.1
2015	4.0	11.2	8.1
2016	4.0	16.2	8.6
2017	3.5	13.6	7.6
2018	4.4	19.5	9.6
2019	4.8	16.1	10.4
2020	4.3	16.1	9.2
2021	3.8	10.0	7.6

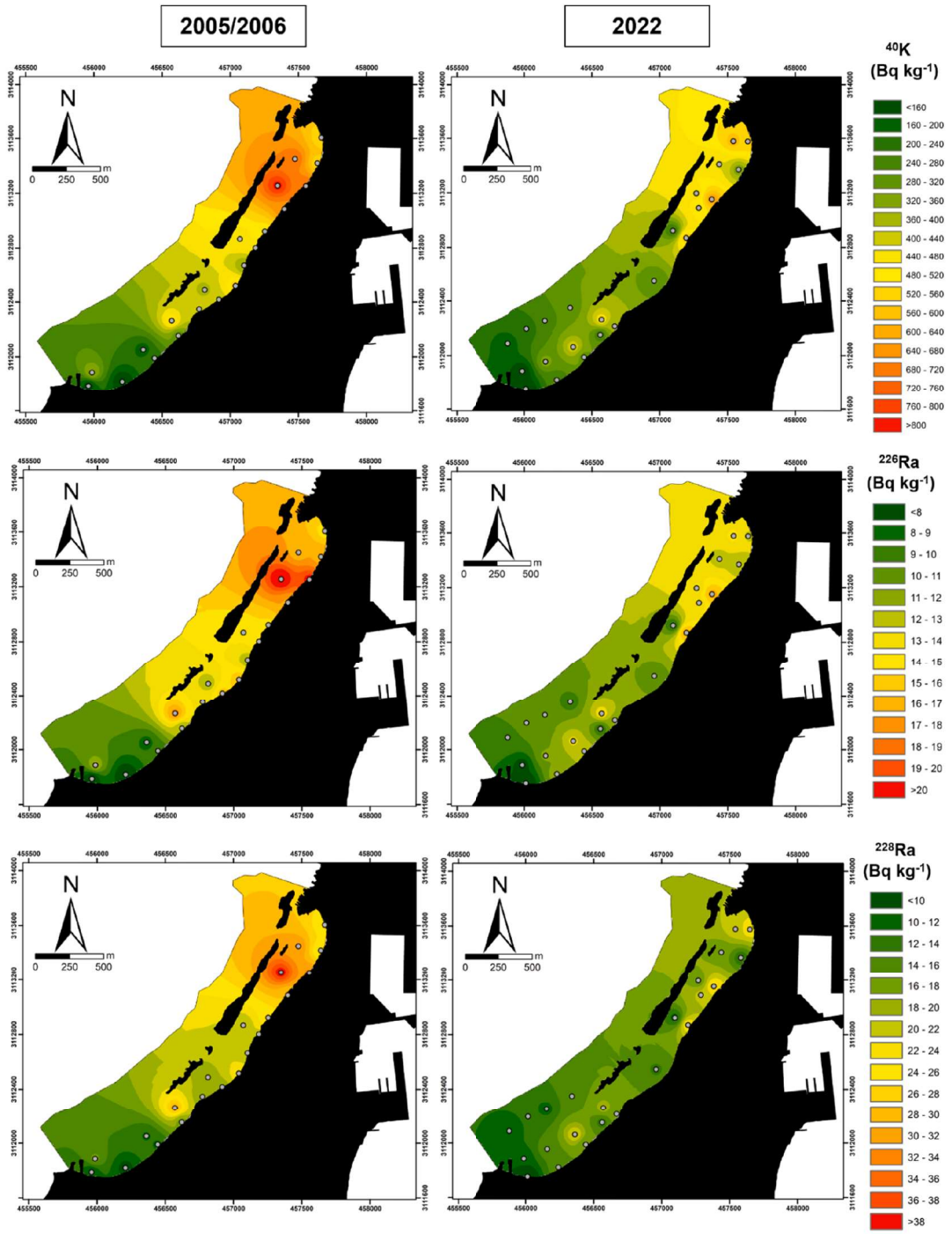

Fig. 4. Activity concentration distribution for ^{40}K, ^{226}Ra, and ^{228}Ra in sediments from Las Canteras beach for the 2005/2006 and the 2022 campaigns.

progressive increase in the activity concentration values of these three radionuclides from the southern arch to the northern arch. This also agrees with what was found in earlier works on the area (Arriola-Velásquez et al., 2019, 2021) and depicts, in both cases, for the intertidal and submarine parts of the beach, the longshore marine transport of sediments, which, according to the literature, occurs from the southern arch to the northern arch (Alonso, 1993; Alonso and Vilas, 1996).

Focusing on the accumulation area of the beach (the submerged and intertidal northern arch), the mean activity concentration value of ^{226}Ra in the 2005/2006 campaign was 17 ± 1 Bq kg^{-1}, and in the 2022

campaign, it was 13.4 ± 1.0 Bq kg^{-1}. For ^{228}Ra, the mean activity concentration values of the 2005/2006 and 2022 campaigns were 29 ± 2 and 19 ± 2 Bq kg^{-1}, respectively. Finally, ^{40}K presented a mean activity concentration value of 640 ± 30 Bq kg^{-1} for the 2005/2006 campaign and 470 ± 20 Bq kg^{-1} for the 2022 campaign. When comparing both campaigns, it can be seen that the mean activity concentration values of ^{226}Ra, ^{228}Ra and ^{40}K are higher in the 2005/2006 campaign, with differences of 4 ± 1 Bq kg^{-1} for ^{226}Ra, 10 ± 3 Bq kg^{-1} for ^{228}Ra and 170 ± 40 Bq kg^{-1} for ^{40}K. In the work of Arriola-Velásquez et al., (2019, 2021), it was suggested that even though the protected part of the intertidal beach is experiencing the constant accumulation of sediments, the intensity of the accumulation varied between months. Such changes in the intensity of accumulation were identified by monthly variations in the activity concentration values of ^{226}Ra, ^{228}Ra and ^{40}K during the three-year period of that study (Arriola-Velásquez et al., 2021). In that work, the mean activity concentration values for the samples belonging to the intertidal accumulation area (described as zone III) were calculated for each month. The results showed that the minimum and maximum activity concentration values of ^{226}Ra for that area were 13.6 ± 0.9 and 20 ± 1 Bq kg^{-1}, respectively. In the case of ^{228}Ra, the minimum activity concentration value was 16 ± 2 Bq kg^{-1} and the maximum activity concentration value was 29 ± 2 Bq kg^{-1}. In the case of ^{40}K, the minimum activity concentration value was 500 ± 20 Bq kg^{-1} and the maximum activity concentration value was 740 ± 30 Bq kg^{-1} (Arriola-Velásquez et al., 2021). This means that according to this previous study, the differences between the minimum and maximum activity concentration values in the accumulation area were 6 ± 1 Bq kg^{-1} for ^{226}Ra, 13 ± 3 Bq kg^{-1} for ^{228}Ra and 240 ± 40 Bq kg^{-1} for ^{40}K. Considering all of this, the differences in the mean activity concentration values of ^{226}Ra, ^{228}Ra and ^{40}K found in this study are within the maximum differences that were found in the 2021 study. Therefore, it seems that the differences that can be found in this work between the activity concentration values of ^{226}Ra, ^{228}Ra and ^{40}K for both campaigns in the submerged and intertidal zones of Las Canteras Beach could be related to the monthly oscillations found in 2021. Hence, the samples from the campaign of 2005/2006 were most likely collected during a period with a more intense accumulation of sediments compared to the 2022 samples.

In Fig. 5, the activity concentration distribution of ^{210}Pb$_{ex}$ for all of El Confital Bay (Fig. 5A) during the 2022 campaign is shown, and a more detailed image of its activity concentration distribution for the intertidal and submerged parts of Las Canteras Beach (Fig. 5B) during the 2022 campaign is also given. The samples from the 2005/2006 campaign were measured approximately 12 years after collection, and a radioactive decay correction was applied to them due to the half-life of ^{210}Pb (22 years). However, due to the amount of time that had passed between sampling and measurement, the results after the decay correction were unreliable. Thus, it was decided to only analyse the 2022 data since they did not require such a radioactive decay correction. In addition, the colour scale of Fig. 5B was modified to avoid confusion with the colour scale of Fig. 5A when both images are being interpreted.

Unsupported ^{210}Pb (^{210}Pb$_{ex}$) has a mainly atmospheric origin; it travels in the lower atmosphere adsorbed to small particles that reach the planet surface through wet or dry deposition (Dueñas et al., 2017; Gaspar et al., 2017). For the Canary Islands, it has been reported that one of the main inputs of natural radionuclides is the African aeolian dust depositions (López-Pérez et al., 2020), which are also known to be carriers of ^{210}Pb (Gordo et al., 2015). Once these aeolian dust particles arrive at the sea surface, they enter the water column and slowly sink, experiencing more scavenging of ^{210}Pb on their way to the seafloor (Hülse and Bentley, 2012). Depending on whether the erosion of the seabed is weaker or stronger, accumulation due to the sedimentation of these aerosols will be more or less favoured. Therefore, it would be expected that high ^{210}Pb$_{ex}$ activity concentration values would trace the less-eroded seabed areas where accumulation occurs.

For all of El Confital Bay, the activity concentration values of ^{210}Pb$_{ex}$ ranged from 15 ± 7 Bq kg^{-1} to 270 ± 20 Bq Kg^{-1} and had a mean value of 69 ± 9 Bq kg^{-1}. This indicates that there were large variations between different parts of the bay, which can be observed in Fig. 5A. The map shows a distribution that seems to agree with the bathymetry of the study region from Fig. 1. The higher activity concentration values of ^{210}Pb$_{ex}$ appear in the deeper areas of the bay, and lower activity concentration values appear in the shallower areas. This is because at higher depths in the water column, the reduced erosion of the seabed favours the sedimentation of the aerosol particles that carry ^{210}Pb$_{ex}$. Conversely, at shallower depths, there is more erosion of the seafloor, and thus, the sedimentation of these particles is less likely to happen. Hence, this explains why the activity concentration distribution of unsupported ^{210}Pb in El Confital Bay agrees with its bathymetry.

Fig. 5B shows the activity concentration distribution of ^{210}Pb$_{ex}$ in the submerged and intertidal zones of Las Canteras Beach. The activity concentration values ranged from 15 ± 7 Bq kg^{-1} to 86 ± 9 Bq kg^{-1} and had a mean value of 38 ± 8 Bq kg^{-1}. In Fig. 5B, the spatial distribution of ^{210}Pb$_{ex}$ delimits two areas. On the one hand, there is an area of low activity concentration values located in the open part of the beach. This area is totally exposed to wave action, and thus, there is constant erosion of the seabed, which prevents the sedimentation of the aerosol particles from occurring. Therefore, the activity concentration values of ^{210}Pb$_{ex}$ are lower in this part of the beach. On the other hand, the area of the beach that is protected from wave action by the natural offshore rocky bar presented higher activity concentration values. This is because, as mentioned before, the natural offshore rocky bar, and even the

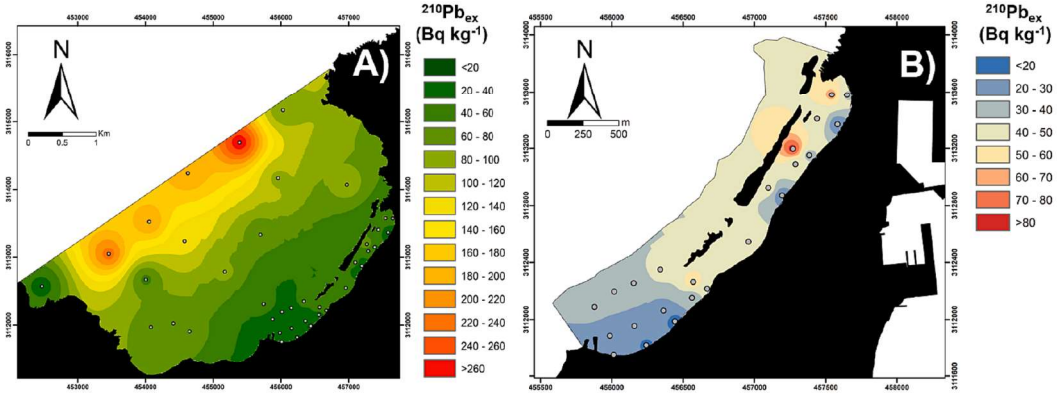

Fig. 5. Activity concentration distribution of ^{210}Pb$_{ex}$ in the 2022 campaign for A) El Confital bay and B) Las Canteras beach.

morphology of the bay, act as barriers against wave action (Alonso, 1993; Alonso and Vilas, 1996; Medina et al., 2006), generating an area with low erosion of the seafloor. Hence, the sedimentation of the particles of aeolian dust bearing $^{210}Pb_{ex}$ on the seafloor is enabled, and activity concentration values are higher in this part of the beach.

Focusing on the protected part of Las Canteras Beach, some differences can also be found in the submerged part of this beach. In the areas located near the structures of the natural offshore rocky bar, the activity concentration values of $^{210}Pb_{ex}$ are higher. This can occur because near the openings of the bar, its own structure, as well as the beach morphology, create some sheltered zones. These are calmer areas where the sedimentation of the aeolian dust carrying unsupported ^{210}Pb on the seafloor is even more favoured. Hence, higher activity concentration values of $^{210}Pb_{ex}$ appear in these areas. Considering the results obtained for both the entirety of El Confital Bay and Las Canteras Beach, it could be said that $^{210}Pb_{ex}$ can be used to identify sedimentation areas for aerosol particles on the seafloor.

4.2. *Influence of the grain size on the activity concentration values of sand samples*

In order to evaluate the influence of grain size in the activity concentration values of ^{226}Ra, ^{228}Ra, ^{40}K and $^{210}Pb_{ex}$ a correlation and a significant differences analysis were carried out. On one hand, a Shapiro-Wilk normality test (Shapiro and Wilk, 1965) was applied to the activity concentration values of ^{226}Ra, ^{228}Ra, ^{40}K and $^{210}Pb_{ex}$, the depth of collection, the bulk density, the mean grain size, sorting and the percentages of coarse sand, medium sand, fine sand, very fine sand and mud (clay + silt) of the samples. The percentages of larger-grain-size fractions, such as gravel and very coarse sand, were not considered because most of the samples presented a mean grain size below 1 mm and thus, the activity concentration values of the samples were only measured in sediments with a grain size below 1 mm. At a 0.05 significance level, most parameters followed a non-normal distribution. Therefore, the Spearman correlation coefficient was used to evaluate the correlations existing between the different activity concentration values and the remaining parameters. Since the mean depth of closure was established at 8.6 m, the correlation analysis was carried out for two different areas; the deeper part from El Confital Bay located below the depth of closure and the area above the depth of closure (including the submerged and intertidal zones of Las Canteras Beach).

On the other hand, 21 samples were selected from the 2022 campaign and separated into different grain size fractions that were analysed individually using gamma spectrometry to identify their activity concentrations of ^{226}Ra, ^{228}Ra, ^{40}K and $^{210}Pb_{ex}$. These samples included 6 from the high activity area of the deeper part of the bay (D3, D5, D7, D8, D9 and D11), 7 samples from the low activity area (D4, D10, D13, D14, D15, D17 and D19), 4 samples from the submerged part of Las Canteras Beach (S12, S13, S14 and S15) and 4 samples from the intertidal zone of the beach (I5, I6, I7 and I8). For a better analysis of the significant differences among grain sizes, the samples were divided into 4 categories (Table 3) following the GRADISTAT software sediment classification (Blott and Pye, 2001). The results of a Shapiro-Wilks normality test showed that at a significance level of 0.05, the activity concentration values of ^{226}Ra, ^{228}Ra and ^{40}K in the different grain size fractions followed a normal distribution, while $^{210}Pb_{ex}$ presented a non-normal distribution. Thus, a one-way ANOVA was applied to evaluate the significant differences in the activity concentrations of ^{226}Ra, ^{228}Ra and ^{40}K and a Kruskal-Wallis test was applied to $^{210}Pb_{ex}$.

Table 3
Grain size category classification. The grain size is given in mm. The number of samples obtained for each category is also indicated.

Category	Number of samples	Sediment grain size	Classification
A	13	0.5 – 2	Very coarse and coarse sand
B	16	0.25 – 0.5	Medium sand
C	16	0.125 – 0.25	Fine sand
D	9	<0.125	Very fine sands and mud

Tables 4A and 4B show the results obtained for the correlation analysis of the deeper samples from El Confital Bay and the submerged and intertidal parts of Las Canteras Beach respectively. In both analyses, ^{226}Ra, ^{228}Ra and ^{40}K were highly correlated between them. This suggests that their activity concentration values are related to the geochemical composition of the samples. Regarding the grain size fraction and the rest of the parameters, in the samples of the deeper parts of El Confital Bay, no correlation was found between them and the activity concentration values of ^{226}Ra, ^{228}Ra and ^{40}K. However, in the case of Las Canteras Beach, a direct correlation was found between the activity concentration values of these radionuclides, the grain size and the percentage of coarse sand. Moreover, in the case of the beach, an inverse correlation also appeared between the activity concentration values of these radionuclides and the percentage of very small sand and the bulk density. Thus, the results of the correlation analysis show that for the deeper parts of El Confital Bay, the activity concentration values of ^{226}Ra, ^{228}Ra and ^{40}K did not seem to be influenced by the grain size while in Las Canteras Beach higher activity concentration values of these radionuclides were found in lighter sediments with a larger grain size.

Moreover, Table 5A shows the results for significant differences of ^{226}Ra, ^{228}Ra and ^{40}K in the different grain size categories. While no significant differences were found, the boxplots from Fig. 6 show that 75 % of the samples in category A presented the highest activity concentration values of these radionuclides. This also agrees with the results of the correlation analysis indicating that, if something, higher activity concentration values of these radionuclides seem to appear in the larger grain size samples.

All these results were contrary to what other studies have found in other parts of the world, where the sediments that had higher clay and silt fractions presented higher activity concentration values due to the physico-chemical interactions of the radionuclides with the small-grain-size sediments (Alfonso et al., 2014; Ligero et al., 2001; Lin et al., 2020; Patiris et al., 2016). However, some authors have also suggested that in the absence or reduced presence of clay and silt fractions, the activity concentration values of sediments were not associated with the grain size of the sample or that the direct correlation between small grain size and high activity concentration might only be applicable in parts of the world with certain geological characteristics (Charkin et al., 2022; Ligero et al., 2001). Moreover, there are cases in which the activity concentration values of different radionuclides have been used to identify the sediment sources in areas with different lithologies, independent of the sediment grain size (Zebracki et al., 2015).

Furthermore, previous works carried out in the intertidal zone of Las Canteras Beach indicated that the higher activity concentration values of ^{226}Ra, ^{228}Ra and ^{40}K were found in samples with low density and high grain size (Arriola-Velásquez et al., 2019) and that they were also associated with an increase in K-feldspars during accumulation periods (Arriola-Velásquez et al., 2021). Considering the literature and the results from this study, it seems that the changes in activity concentration values of ^{226}Ra, ^{228}Ra and ^{40}K in the whole of El Confital Bay might be more directly related to the changes in their mineralogical composition than to grain size variations.

Regarding $^{210}Pb_{ex}$, no correlation was found with the activity concentration values of ^{226}Ra, ^{228}Ra and ^{40}K neither in the deeper part of El Confital Bay nor in Las Canteras Beach. In addition, for the deeper samples, direct correlations with the percentages of very fine sand, mud, and depth and an inverse correlation with the bulk density were reported. In the case of Las Canteras Beach, a direct correlation between the activity concentration of $^{210}Pb_{ex}$ and the percentage of fine sand and mud appeared, while an inverse correlation with the bulk density of the samples was also found.

In addition, the Kruskal-Wallis test result (Table 5B) shows that

Table 4A
Spearman correlation coefficients matrix of activity concentration in Bq kg^{-1} of ^{226}Ra, ^{228}Ra, ^{40}K, ^{210}Pb$_{xc}$, mean grain size in mm, sorting, percentage of coarse sand (CS), medium sand (MS), fine sand (FS), very fine sand (VFS), mud (M), depth in m and bulk density (ρ) in g cm^{-3} of samples from A) El Confital bay and B) Las Canteras beach. The p-value is set at 0.05.

A)	^{226}Ra	^{228}Ra	^{40}K	^{210}Pb$_{ex}$	Grain size	Sorting	CS	MS	FS	VFS	M	Depth	ρ
^{226}Ra	1	***0.000***	***0.000***	*0.649*	*0.572*	*0.579*	*0.594*	*0.617*	*0.770*	*0.200*	*0.770*	*0.173*	*0.333*
^{228}Ra	**0.915**	1	***0.000***	*0.471*	*0.931*	*0.778*	*0.633*	*0.339*	*0.721*	*0.362*	*0.983*	*0.191*	*0.294*
^{40}K	**0.879**	**0.979**	1	*0.405*	*0.983*	*0.854*	*0.617*	*0.269*	*0.778*	*0.387*	*1.000*	*0.150*	*0.347*
^{210}Pb$_{ex}$	−0.124	−0.194	−0.224	1	*0.068*	*0.196*	*0.060*	*0.311*	*0.610*	***0.039***	***0.012***	***0.015***	***0.000***
Grain size	−0.153	−0.024	−0.006	−0.468	1	*0.024*	*0.026*	*0.068*	*0.721*	*0.880*	*0.664*	*0.495*	*0.054*
Sorting	0.150	0.076	0.050	0.341	0.288	1	*0.176*	*0.026*	*0.068*	*0.721*	*0.880*	*0.664*	*0.495*
CS	−0.144	−0.129	−0.135	−0.479	0.768	0.356	1	*0.002*	*0.002*	*0.000*	*0.009*	*0.096*	*0.129*
MS	−0.135	−0.256	−0.294	−0.271	0.397	0.553	0.715	1	*0.105*	*0.064*	*0.274*	*0.157*	*0.276*
FS	−0.079	−0.097	−0.076	0.138	−0.818	−0.468	−0.715	−0.421	1	*0.001*	*0.001*	*0.398*	*0.461*
VFS	0.338	0.244	0.232	**0.521**	−0.918	−0.097	−0.829	−0.474	0.765	1	*0.000*	*0.020*	*0.065*
M	0.079	0.006	0.000	**0.612**	−0.868	0.041	−0.629	−0.291	0.729	0.882	1	*0.009*	*0.008*
Depth	0.358	0.345	0.377	**0.595**	−0.551	0.118	−0.430	−0.371	0.227	0.575	0.632	1	*0.008*
ρ	0.259	0.280	0.252	**−0.855**	0.490	−0.184	0.396	0.290	−0.199	−0.472	−0.640	−0.636	1

p-value 0.05.

Table 4B

B)	^{226}Ra	^{228}Ra	^{40}K	^{210}Pb$_{ex}$	Grain size	Sorting	CS	MS	FS	VFS	M	Depth	ρ
^{226}Ra	1	***0.000***	***0.000***	*0.460*	***0.004***	*0.326*	***0.012***	*0.254*	*0.761*	***0.005***	*0.450*	*0.387*	***0.017***
^{228}Ra	**0.899**	1	***0.000***	*0.340*	***0.003***	*0.383*	***0.013***	*0.270*	*0.690*	***0.004***	*0.500*	*0.220*	***0.008***
^{40}K	**0.912**	**0.942**	1	*0.100*	***0.018***	*0.975*	*0.069*	*0.446*	*0.177*	***0.001***	*0.391*	*0.297*	***0.000***
^{210}Pb$_{ex}$	0.162	0.209	0.352	1	*0.252*	***0.004***	*0.177*	*0.050*	***0.001***	*0.581*	***0.022***	*0.081*	***0.000***
Grain size	**0.573**	**0.586**	**0.489**	−0.249	1	*0.073*	*0.000*	*0.000*	*0.078*	*0.000*	*0.871*	*0.015*	*0.623*
Sorting	0.214	0.191	0.007	−0.572	0.380	1	*0.004*	*0.067*	*0.000*	*0.587*	*0.068*	*0.884*	*0.054*
CS	**0.515**	**0.509**	0.386	−0.292	0.917	0.571	1	*0.000*	*0.006*	*0.005*	*0.857*	*0.246*	*0.881*
MS	0.248	0.240	0.167	−0.413	0.828	0.388	0.840	1	*0.019*	*0.004*	*0.475*	*0.070*	*0.959*
FS	0.067	0.088	0.292	**0.639**	−0.375	−0.786	−0.551	−0.485	1	*0.565*	*0.071*	*0.936*	*0.028*
VFS	**−0.567**	**−0.582**	**−0.658**	−0.122	−0.744	0.120	−0.560	−0.581	−0.126	1	*0.719*	*0.004*	*0.009*
M	0.166	0.148	0.188	**0.474**	−0.036	−0.387	−0.040	−0.157	0.383	−0.079	1	*0.047*	*0.139*
Depth	−0.189	−0.266	−0.227	0.371	−0.501	0.032	−0.252	−0.384	0.018	0.576	0.419	1	*0.792*
ρ	**−0.492**	**−0.538**	**−0.690**	**−0.680**	−0.108	0.406	−0.033	0.011	−0.458	0.535	−0.318	0.058	1

p-value 0.05.

Table 5A
Statistical results for the identification of the presence of significant differences in the activity concentration values of the different grain size categories. The results displayed correspond to A) the One-way ANOVA test applied to the activity concentrations values of ^{226}Ra, ^{228}Ra and ^{40}K which followed a normal distribution and B) to the Kruskal-Wallis test applied to ^{210}Pb$_{ex}$ since this did not follow a normal distribution. In addition, the results of the Wilcoxon rank sum test are displayed to identify the groups within which significant differences were found.

A	field	F	Prob-F
^{226}Ra	Grain size categories	0.1925	0.9010
^{228}Ra	Grain size categories	0.0749	0.9732
^{40}K	Grain size categories	0.5255	0.6668

ANOVA prob-F 0.05.

Table 5B

B	field	p-value	Wilcoxon rank sum test
^{210}Pb$_{ex}$	Grain size categories	0.0026	D - A (0.00017) D - B (0.01401)

Kruskal-Wallis p-value 0.05.

Wilcoxon rank sum test p-value 0.05.

^{210}Pb$_{ex}$ presented significant differences among the different categories. Hence, a Wilcoxon rank-sum test was applied, and the results showed that the smallest-grain-size group (category D), displayed significant differences with the larger-grain-size groups (categories A and B). These higher activity concentration values of ^{210}Pb$_{ex}$ in the smallest grain size category can also be appreciated in the boxplot from Fig. 6.

All these results showed that in the whole study region, the samples that presented higher activity concentration values of ^{210}Pb$_{ex}$ were those lighter and with smaller grain sizes. This relationship is similar to that found by other authors (Huang et al., 2013; Lin et al., 2020; Pappa et al., 2016; Patiris et al., 2016) and can be explained by the origin of ^{210}Pb$_{ex}$. Unsupported ^{210}Pb is scavenged in small aerosol particles that reach the surface through, among other mechanisms, aeolian dust deposition. Since the particles that travel the longest distance generally present clay and silt sizes, these aerosol particles normally have small grain sizes (Lawrence and Neff, 2009; Papastefanou, 2008). Hence, what the correlation analysis is describing for the bay in the case of ^{210}Pb$_{ex}$ agrees with what could be expected for ^{210}Pb$_{ex}$ considering its origin.

4.3. Mineral composition of sand samples

The mineralogical content of 6 samples was analysed to try to identify the minerals that could be responsible for the activity concentration values of ^{226}Ra, ^{228}Ra and ^{40}K. The samples correspond to two samples from the high-activity part of the bay (D7 and D8) and two from the low-activity part of the bay (D15 and D19). Furthermore, one sample from the high-activity area (S3) and one sample from the low-activity area (S8) of the submerged part of the beach were also analysed. The intertidal zone of Las Canteras Beach was studied and described in an earlier work (Arriola-Velásquez et al., 2021) and thus, the results of this study could be compared to previous results.

The results of the XRPD analysis and the activity concentration values of ^{226}Ra, ^{228}Ra and ^{40}K for each sample are shown in Table 6. The SCXRD analysis determined that the feldspar is anorthoclase ($Ab_{0.83}Or_{0.16}An_{0.01}$), the clinopyroxene is Fe-rich diopside and the amphibole is potassic-pargasite (cell parameters are a = 9.8449(3), b = 18.0554(4), c = 5.3090(2) Å, α = 90°, β = 105.509(3)°, γ = 90°, V =

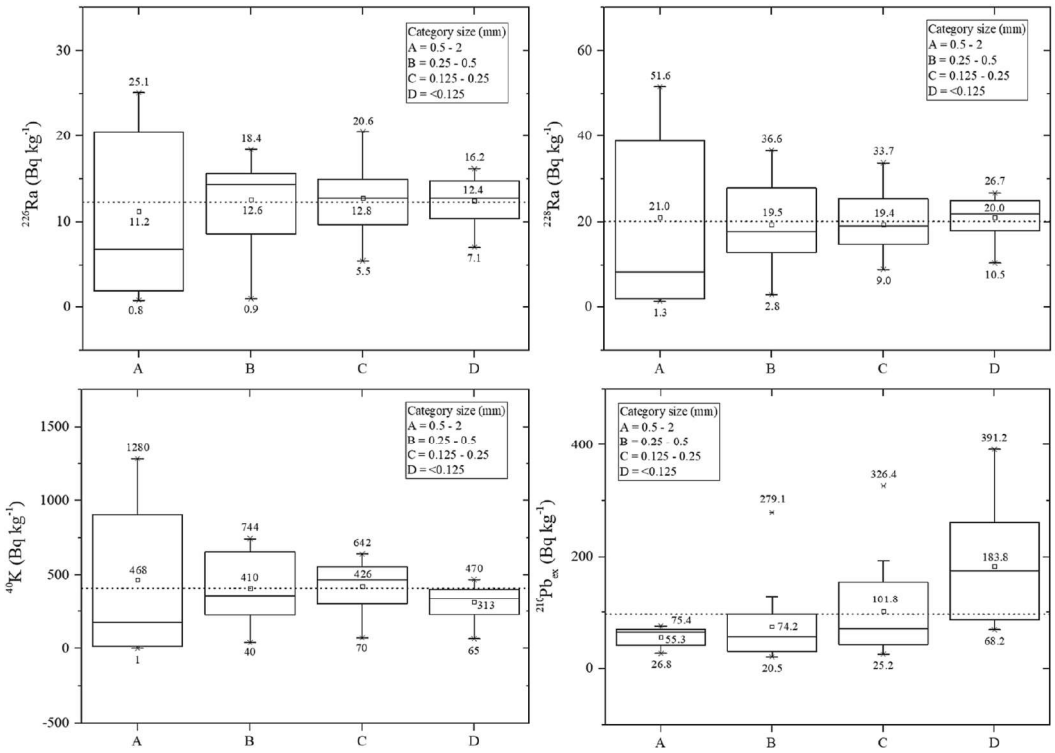

Fig. 6. Boxplots of the activity concentration values of ^{226}Ra, ^{228}Ra, ^{40}K and ^{210}Pb$_{ex}$ found for the different grain size fractions in El Confital bay and Las Canteras beach. The dot line indicates the mean activity concentration value of each radionuclide. The numbers that appear in each whisker correspond to the maximum and minimum activity concentration values. The number in the middle indicates the mean activity concentration value for each grain size category.

909.33(5) Å^3). Table 6 also includes the sum of biogenic carbonate, which was obtained by adding the percentages of calcite and aragonite. In addition, the sum of feldspars, feldspathoids and zeolites is also displayed. This last sum includes the percentages of labradorite, anorthoclase, sanidine, analcime, nepheline, phillipsite and fluorapatite.

The sample that presented the lowest amount of feldspars, feldspathoids and zeolites was sample D15, which was also the sample with the lowest activity concentration values of ^{40}K. In contrast, the sample with the highest activity concentration values of these radionuclides was sample D7, which presented the highest amount of feldspars, feldspathoids and zeolites. Considering that the main source of potassium identified in the samples is the group of feldspars, feldspathoids and zeolites, it seems that the increase in the activity concentration of ^{40}K is related to an increase in the content of these minerals in the samples. This idea was also suggested in an earlier study that was carried out on Las Canteras Beach (Arriola-Velásquez et al., 2021). According to these authors, the samples from the intertidal part of the beach that was completely exposed to wave action showed a decrease in the potassium feldspar content during erosion periods and an increase in the amount of these minerals during accumulation periods. In the protected area of the beach, these minerals were always present. Therefore, in this previous work, the increase in the activity concentration of ^{40}K was associated with the transport and accumulation of these K-feldspars. Moreover, in other parts of the world with sediments of volcanic origin, other authors also found that an increase in the activity concentration values of ^{40}K was associated with an increase in the feldspar content in the samples (Roviello et al., 2020). All of this seems to agree with what was found in this work, although in some of the results obtained here, other minerals like amphibole also contribute to the amount of potassium present in the samples. Nevertheless, the results seem to confirm that higher activity concentration values of ^{40}K are associated with a larger amount of potassium-bearing minerals in the samples.

Regarding the organic materials, at first, it seemed that the lower activity concentration values appeared in the samples with a higher biogenic carbonate content, as in the case of sample D15, which was 97.4 % biogenic carbonate. However, there are other samples, such as S3 and D19, in which the organic carbonate contents are similar, but one sample presents more than double the activity concentration value of ^{40}K of the other. Therefore, the biogenic content of the samples does not seem to influence the activity concentration value of ^{40}K in the samples. In fact, considering what was mentioned before, in the case of sample S3, the content of K-bearing minerals is 25.7 %, while for D19, it is 12.9 %. This again reinforces the idea that the activity concentration values found for ^{40}K in the samples are more associated with its terrigenous content, and there is no influence of the organic material.

The results of the mineralogical analysis showed that ^{40}K acts as a good tracer of the transport and accumulation of sediments due to its K-bearing minerals. Nevertheless, even though no Ra-bearing minerals were found in the study region, ^{226}Ra and ^{228}Ra follow a pattern similar to that followed by ^{40}K in all samples. These similarities between radium and potassium were also found in the work of Arriola-Velásquez et al. (2021). In different coordination environments, both potassium and radium present similar ionic radii (Shannon, 1976), which could favour the entrance of Ra in the K-feldspars. However, no data on this are available in this study region, and further studies would be necessary to better understand the reasons that ^{226}Ra and ^{228}Ra behave in the same way as ^{40}K.

Table 6
Results of quantitative analysis of mineralogical composition on the studied sand samples in percentage. The results include the sum of the percentage of feldspars, feldspathoids and zeolites of the samples (Σ Fdp + zeolites) and the sum of the percentage of biogenic carbonates (Σ Biogenic carbonates). The activity concentration values of ^{226}Ra, ^{228}Ra and ^{40}K for each sample is given in Bq kg^{-1}.

	S3	S8	D7	D8	D15	D19
Calcite ($CaCO_3$)	40.9 ± 0.5	12.5 ± 0.3	1.9 ± 0.2	13.7 ± 0.4	80.1 ± 0.2	44.6 ± 0.4
Aragonite ($CaCO_3$)	11.0 ± 0.3	6.7 ± 0.2	1.6 ± 0.3	–	17.3 ± 0.2	15.9 ± 0.3
Augite (Ca(Mg,Fe,Al)Si_2O_6)	18.0 ± 0.5	61.3 ± 0.6	17.8 ± 0.5	20.1 ± 0.5	–	16.2 ± 0.5
Amphibole (potassic-pargasite, $KCa_2(Mg_4Al)(Si_6Al_2)O_{22}(OH)_2$)	–	5.1 ± 0.2	–	–	–	–
Forsteritic olivine	–	6.6 ± 0.4	–	–	–	–
Cristobalite (SiO_2)	1.1 ⊥ 0.1	0.8 ⊥ 0.1	0.9 ⊥ 0.1	1.2 ⊥ 0.1	–	–
α-quartz (SiO_2)	–	–	–	1.2 ± 0.2	–	–
Haematite (Fe_2O_3)	–	–	1.4 ± 0.1	1.5 ± 0.2	–	–
Labradorite ($(Na_x,Ca_{1-x})(Al_{1+x}Si_{3-x})O_8$)	3.2 ± 0.2	0.9 ± 0.1	19.7 ± 0.6	15.0 ± 0.7	–	8.6 ± 0.4
Anorthoclase ($(Na_x,K_{1-x})(AlSi_3)O_8$)	15.9 ± 0.6	6.1 ± 0.4	32.1 ± 0.7	20.0 ± 0.6	–	4.1 ± 0.4
Sanidine ($KAlSi_3O_8$)*	9.8 ± 0.5	–	18.2 ± 0.6	13.2 ± 0.5	2.6 ± 0.2	3.1 ± 0.3
Analcime ($NaAlSi_2O_6{\cdot}H_2O$)	–	–	2.8 ± 0.2	2.2 ± 0.2	–	1.8 ± 0.2
Nepheline ($Na_3KAl_4Si_4O_{16}$)	–	–	3.5 ± 0.4	–	–	–
Phillipsite ($(CaNa_2K_2)Al_6Si_{10}O_{32}{\cdot}12H_2O$)	–	–	–	10.4 ± 0.6	–	5.7 ± 0.4
Fluorapatite ($Ca_4(PO_4)_3(F_2)$)	–	–	–	1.5 ± 0.3	–	–
Σ Biogenic carbonates	51.9 %	19.2 %	3.5 %	13.7 %	97.4 %	60.5 %
Σ Fdp + zeolites	28.9 %	7.0 %	76.3 %	62.3 %	2.6 %	23.3 %
^{40}K	490 ± 20	119 ± 8	940 ± 40	580 ± 30	37 ± 7	150 ± 10
^{226}Ra	14 ± 1	7.4 ± 0.7	25 ± 1	18 ± 1	<MDA (2.9)	12.7 ± 0.9
^{228}Ra	20 ± 2	10 ± 1	41 ± 3	30 ± 2	<MDA (2.8)	10 ± 2

* Or polymorph (orthoclase, microcline).

5. Conclusions

For both campaigns, 2005/2006 and 2022, higher and lower ^{226}Ra, ^{228}Ra and ^{40}K activity concentrations were found respectively in the western and eastern sediments of El Confital Bay. These values were mainly related to sediment mineralogy. Additionally, a transport of sediments from the west coastline to the deeper parts of the bay was seemingly traced by ^{226}Ra, ^{228}Ra and ^{40}K highest activity concentration values when the two campaigns were compared.

The spatial distribution of the ^{226}Ra, ^{228}Ra and ^{40}K activity concentration values also seemed to be tracing the sediment dynamics that occur in the submerged part of Las Canteras Beach. Lower values were found where erosion processes are more frequent, in the open part of the submerged beach, while the accumulation zone in the protected area of the submerged beach presented higher values. Furthermore, the progressive increase of activity concentrations from the erosion to the accumulation areas appears to trace the longshore sediment transport that occurs on the beach.

The spatial distribution of the activity concentration of $^{210}Pb_{ex}$ can be used to identify areas where accumulation due to particle sedimentation is favoured. Sediments from the deeper areas of El Confital Bay and sheltered parts of the submerged zone of Las Canteras Beach presented higher $^{210}Pb_{ex}$ activity concentrations. Conversely, lower activity concentration values were found in the shallower parts of the bay and open part of the beach, where more seabed erosion occurs. In addition, higher ^{210}Pb activity concentration values were related to smaller grain size sediment fractions, which agrees with the origin of unsupported ^{210}Pb adsorbed to atmospheric aerosols. Further studies including analysis of vertical profiles of $^{210}Pb_{ex}$ in the sediment column would be necessary to better comprehend its role as a tracer of these sedimentation areas.

Overall, this work identifies as tracers of sediment dynamics some natural radionuclides that are part of the coastal system under study, considering a variability analysis of their activity concentrations with local sediment characteristics (such as grain size or mineralogical composition), as well as with sediment transport. Therefore, the present paper establishes a basis for studies of sediment erosion and accumulation processes in coastal systems using natural radiotracers, including those studies based on emerging methodologies of mapping using in situ gamma spectroscopy. In addition, because the coastal system studied includes the opposing dynamic of a beach open to the wave action and a beach protected against it, the results and methods developed can be extrapolated to different parts of the world.

Declaration of Competing Interest

The authors declare that they have no known competing financial interests or personal relationships that could have appeared to influence the work reported in this paper.

Data availability

Data will be made available on request.

Acknowledgements

This work was partially supported by the Consejería de Economía, Industria, Comercio y Conocimiento del Gobierno de Canarias. F.C. and M.C. acknowledge financial support from the Italian Ministry of Education (MUR) through the project "Dipartimenti di Eccellenza 2023–2027". The authors are grateful to the anonymous reviewers and editor for their professional and meticulous evaluation and the International Atomic Energy Agency for all the discussions and suggestions made through the Coordinated Research Project F22074, "Development of Radiometric Methods and modelling for measurement of sediment transport in coastal systems and rivers".

Appendix A. Supplementary data

Supplementary data to this article can be found online at https://doi.org/10.1016/j.catena.2023.107672.

References

Achilleos, G.A., 2011. The Inverse Distance Weighted interpolation method and error propagation mechanism – creating a DEM from an analogue topographical map. J. Spat. Sci. 56, 283–304. https://doi.org/10.1080/14498596.2011.623348.

Alfonso, J.A., Pérez, K., Palacios, D., Handt, H., LaBrecque, J.J., Mora, A., Vásquez, Y., 2014. Distribution and environmental impact of radionuclides in marine sediments along the Venezuelan coast. J. Radioanal. Nucl. Chem. 300, 219–224. https://doi.org/10.1007/s10967-014-2999-z.

Alonso, I., 1993. Procesos sedimentarios en la playa de Las Canteras (Gran Canaria). Universidad de Las Palmas de Gran Canaria, Las Palmas de Gran Canaria.

Alonso, I., 2005. Costa Norte: Playa De Las Canteras. In: Hernández, L., Alonso, I., Mangas, J., Yanes, A. (Eds.), Tendencias Actuales En Geomorfología Litoral. Universidad de Las Palmas de Gran Canaria, La Palmas de Gran Canaria, pp. 219–238.

Alonso, I., Pérez Torrado, F.J., 1992. Estudio sedimentológico de la playa de Las Canteras (Gran Canaria). Datos preliminares. III Congreso Geológico De España y Tomo 2, 131–135.

Alonso, I., Vilas, F., 1996. Variabilidad sedimentaria en la playa de Las Canteras (Gran Canaria). Geogaceta 20, 428–430.
Alveirinho Dias, J., 2004. A análise sedimentar e o conhecimento dos sistemas marinhos: uma introdução à oceanografia geológica, First. ed. Universidade do Algarve, Faro.
Androulakaki, E.G., Tsabaris, C., Eleftheriou, G., Kokkoris, M., Patiris, D.L., Vlastou, R., 2015. Seabed radioactivity based on in situ measurements and Monte Carlo simulations. Appl. Radiat. Isot. 101, 83–92. https://doi.org/10.1016/j.apradiso.2015.03.013.
Arnedo, M.A., Tejera, A., Rubiano, J.G., Alonso, H., Gil, J.M., Rodríguez, R., Martel, P., 2013. Natural radioactivity measurements of beach sands in gran Canaria, Canary Islands (Spain). Radiat. Prot. Dosim. 156, 75–86. https://doi.org/10.1093/rpd/nct044.
Arnedo, M.A., Rubiano, J.G., Alonso, H., Tejera, A., González, A., González, J., Gil, J.M., Rodríguez, R., Martel, P., Bolivar, J.P., 2017. Mapping natural radioactivity of soils in the eastern Canary Islands. J. Environ. Radioact. 166, 242–258. https://doi.org/10.1016/j.jenvrad.2016.07.010.
Arriola-Velásquez, A., Tejera, A., Guerra, J.G., Alonso, I., Alonso, H., Arnedo, M.A., Rubiano, J.G., Martel, P., 2019. Spatio-temporal variability of natural radioactivity as tracer of beach sedimentary dynamics. Estuar. Coast. Shelf Sci. 231 https://doi.org/10.1016/j.ecss.2019.106476.
Arriola-Velásquez, A.C., Tejera, A., Guerra, J.G., Geibert, W., Stimac, I., Cámara, F., Alonso, H., Rubiano, J.G., Martel, P., 2021. ^{226}Ra, ^{228}Ra and ^{40}K as tracers of erosion and accumulation processes: A 3-year study on a beach with different sediment dynamics. Catena (amst) 207, 105705. https://doi.org/10.1016/j.catena.2021.105705.
Balcells, R., Barrera, J.L., Ruiz García, M.T., (Cartographers), 1990. Geological Map 1101-I-II Las Palmas de Gran Canaria, 1:25000 IGME.
Bezuidenhout, J., 2013. Measuring naturally occurring uranium in soil and minerals by analysing the 352keV gamma-ray peak of 214Pb using a NaI(Tl)-detector. Appl. Radiat. Isot. 80, 1–6. https://doi.org/10.1016/j.apradiso.2013.05.008.
Bezuidenhout, J., 2020. The investigation of natural radionuclides as tracers for monitoring sediment processes. J Appl Geophy 181, 104135. https://doi.org/10.1016/j.jappgeo.2020.104135.
Blott, S.J., Pye, K., 2001. Gradistat : a grain size distribution and statistics package for the analysis of unconsolidated sediments. Earth Surf. Proc. Land. 26, 1237–1248. https://doi.org/10.1002/esp.261.
Bobos, I., Madruga, M.J., Reis, M., Esteves, J., Guimarães, V., 2021. Clay mineralogy insights and assessment of the natural (228Ra, 226Ra, 210Pb, 40K) and anthropogenic (137Cs) radionuclides dispersion in the estuarine and lagoon systems along the Atlantic coast of Portugal. Catena (amst) 206, 105532. https://doi.org/10.1016/j.catena.2021.105532.
Charkin, A.N., Yaroshchuk, E.I., Dudarev, O., v., Leusov, A.E., Goriachev, V.A., Sobolev, I.S., Gulenko, T.A., Pipko, I.I., Startsev, A.M., Semiletov, I.P., 2022. The influence of sedimentation regime on natural radionuclide activity concentration in marine sediments of the East Siberian Arctic Shelf. J. Environ. Radioact. 253–254 https://doi.org/10.1016/j.jenvrad.2022.106988.
Chiozzi, P., Pasquale, V., Verdoya, M., Minato, S., 2001. Natural gamma-radiation in the Aeolian volcanic arc. Appl. Radiat. Isot. 55, 737–744.
Cooper, L.W., Grebmeier, J.M., 2018. Deposition patterns on the Chukchi shelf using radionuclide inventories in relation to surface sediment characteristics. Deep Sea Res 2 Top Stud Oceanogr 152, 48–66. https://doi.org/10.1016/j.dsr2.2018.01.009.
Dueñas, C., Gordo, E., Liger, E., Cabello, M., Cañete, S., Pérez, M., de la Torre-Luque, P., 2017. ^{7}Be, ^{210}Pb and ^{40}K depositions over 11 years in Málaga. J. Environ. Radioact. 178–179, 325–334. https://doi.org/10.1016/j.jenvrad.2017.09.010.
Eulie, D.O., Corbett, D.R., Walsh, J.P., 2018. Shoreline erosion and decadal sediment accumulation in the Tar-Pamlico estuary, North Carolina, USA: A source-to-sink analysis. Estuar. Coast. Shelf Sci. 202, 246–258. https://doi.org/10.1016/j.ecss.2017.10.011.
Feng, H., Zhang, W., Jia, L., Weinstein, M.P., Zhang, Q., Yuan, D., Tao, J., Yu, L., 2010. Short- and long-term sediment transport in western Bohai Bay and coastal areas. Chin. J. Oceanol. Limnol. 28, 583–592. https://doi.org/10.1007/s00343-010-9099-x.
Fernández-Aldecoa, J.C., Robayna, B., Allende, A., Poffijn, A., Hernández-Armas, J., 1992. Natural radiation in Tenerife (Canary Islands). Radiat. Prot. Dosim. 45, 545–548.
Folk, R.L., Ward, W.C., 1957. Brazos River Bar: A study in the significance of grain size parameters. J. Sediment. Petrol. 27, 3–26.
Froehlich, K., 2010. Environmental radionuclides: Tracers and Timers of Terrestrial Processes, First. ed. Elsevier B.V., Amsterdam. https://doi.org/10.1016/S1569-4860(09)01613-1.
Gaspar, L., Webster, R., Navas, A., 2017. Fate of ^{210}Pb$_{ex}$ fallout in soil under forest and scrub of the central Spanish Pre-Pyrenees. Eur. J. Soil Sci. 68, 259–269. https://doi.org/10.1111/ejss.12427.
Gong, G., Mattevada, S., O'Bryant, S.E., 2014. Comparison of the accuracy of kriging and IDW interpolations in estimating groundwater arsenic concentrations in Texas. Environ. Res. 130, 59–69. https://doi.org/10.1016/j.envres.2013.12.005.
Gordo, E., Liger, E., Dueñas, C., Fernández, M.C., Cañete, S., Pérez, M., 2015. Study of 7Be and 210Pb as radiotracers of African intrusions in Malaga (Spain). J. Environ. Radioact. 148, 141–153. https://doi.org/10.1016/j.jenvrad.2015.06.028.
Gražulis, S., Chateigner, D., Downs, R.T., Yokochi, A.F.T., Quirós, M., Lutterotti, L., Manakova, E., Butkus, J., Moeck, P., le Bail, A., 2009. Crystallography Open Database - An open-access collection of crystal structures. J. Appl. Cryst. 42, 726–729. https://doi.org/10.1107/S0021889809016690.
Gu, F., Zhang, X., Ren, B., Zhou, M., 2022. A new approach for dating recent silting soils of debris flow deposits from the changes of ^{210}Pb$_{ex}$ concentration in surface layers. Catena (amst) 214. https://doi.org/10.1016/j.catena.2022.106254.
Guerra, J.G., Rubiano, J.G., Winter, G., Guerra, A.G., Alonso, H., Arnedo, M.A., Tejera, A., Gil, J.M., Rodríguez, R., Martel, P., Bolivar, J.P., 2015. A simple methodology for characterization of germanium coaxial detectors by using Monte Carlo simulation and evolutionary algorithms. J. Environ. Radioact. 149, 8–18. https://doi.org/10.1016/j.jenvrad.2015.06.017.
Guerra, J.G., Rubiano, J.G., Winter, G., Guerra, G., A., Alonso, H., Arnedo, M.A., Tejera, A., Martel, P., Bolivar, J.P., 2017. Computational characterization of HPGe detectors usable for a wide variety of source geometries by using Monte Carlo simulation and a multi-objective evolutionary algorithm. Nucl. Instrum. Methods Phys. Res. A 858, 113–122. https://doi.org/10.1016/j.nima.2017.02.087.
Hallermeier, R.J., 1981. A profile zonation for seasonal sand beaches from wave climate. Coast. Eng. 4, 253–277.
Huang, D., Du, J., Deng, B., Zhang, J., 2013. Distribution patterns of particle-reactive radionuclides in sediments off eastern Hainan Island, China: Implications for source and transport pathways. Cont. Shelf Res. 57, 10–17. https://doi.org/10.1016/j.csr.2012.04.019.
Hülse, P., Bentley, S.J., 2012. A 210Pb sediment budget and granulometric record of sediment fluxes in a subarctic deltaic system: The Great Whale River, Canada. Estuar. Coast. Shelf Sci. 109, 41–52. https://doi.org/10.1016/j.ecss.2012.05.019.
Iaea, 2012. Worldwide Open Proficiency Test: Determination of Natural and Artificial Radionuclides in Moss-Soil and Water. IAEA Analytical Quality in Nuclear Applications Series, IAEA, Vienna.
International Atomic Energy Agency, 2014. Radiotracer and Sealed Source Applications in Sediment Transport Studies, Training Course Series No. 59. IAEA, Vienna.
Kilel, K.K., Bezuidenhout, J., Gatari, M.J., le Roux, R.R., Kaniu, M.I., 2022. A low-cost delta underwater gamma system (DUGS) for in-situ measurement of natural radionuclides in aquatic sediments. J. Radioanal. Nucl. Chem. https://doi.org/10.1007/s10967-022-08701-7.
Lawrence, C.R., Neff, J.C., 2009. The contemporary physical and chemical flux of aeolian dust: A synthesis of direct measurements of dust deposition. Chem. Geol. 267, 46–63. https://doi.org/10.1016/j.chemgeo.2009.02.005.
Ligero, R.A., Ramos-Lerate, I., Barrera, M., Casas-Ruiz, M., 2001. Relationships between sea-bed radionuclide activities and some sedimentological variables. J. Environ. Radioact. 57, 7–19.
Lin, W., Feng, Y., Yu, K., Lan, W., Wang, Y., Mo, Z., Ning, Q., Feng, L., He, X., Huang, Y., 2020. Long-lived radionuclides in marine sediments from the Beibu Gulf, South China Sea: Spatial distribution, controlling factors, and proxy for transport pathway. Mar. Geol. 424, 106157 https://doi.org/10.1016/j.margeo.2020.106157.
López-Pérez, M., Lorenzo-Salazar, J.M., Expósito, F.J., Díaz, J.P., Salazar, P., 2020. Impact of a massive dust storm on the gross alpha, gross beta, ^{40}K, ^{137}Cs, ^{210}Pb, ^{7}Be activities measured in atmospheric aerosols collected in Tenerife, Canary Islands. Atmos. Environ. 239, 117806 https://doi.org/10.1016/j.atmosenv.2020.117806.
Madruga, M.J., Silva, L., Gomes, A.R., Libânio, A., Reis, M., 2014. The influence of particle size on radionuclide activity concentrations in Tejo River sediments. J. Environ. Radioact. 132, 65–72. https://doi.org/10.1016/j.jenvrad.2014.01.019.
Mangas, J., Julià-Miralles, M., 2015. Geomorfología y naturaleza de las bajas submareales de Bajo Fernando, Los Roquerillos y La Zabala (NE de Gran Canaria). Geo-Temas 15, 37–40.
Medina, R., Bastón, S., Cánovas, V., Torres, A., Luque, Á., Alonso, I., Sánchez, I., Ortega, A., Rodríguez, S., Martín, J.A., 2006. Estudio integral de la playa de Las Canteras, Technical Report Dirección General de Costas.
Mtshawu, B., Bezuidenhout, J., Kilel, K.K., 2023. Spatial autocorrelation and hotspot analysis of natural radionuclides to study sediment transport. J. Environ. Radioact. 264 https://doi.org/10.1016/j.jenvrad.2023.107207.
Papastefanou, C., 2008. Radioactive aerosols, First. ed. Radioactivity in the Environment. Elsevier B. V, Amsterdam.
Pappa, F.K., Tsabaris, C., Ioannidou, A., Patiris, D.L., Kaberi, H., Pashalidis, I., Eleftheriou, G., Androulakaki, E.G., Vlastou, R., 2016. Radioactivity and metal concentrations in marine sediments associated with mining activities in Ierissos Gulf, North Aegean Sea, Greece. Appl. Radiat. Isot. 116, 22–33. https://doi.org/10.1016/j.apradiso.2016.07.006.
Patiris, D.L., Tsabaris, C., Anagnostou, C.L., Androulakaki, E.G., Pappa, F.K., Eleftheriou, G., Sgouros, G., 2016. Activity concentration and spatial distribution of radionuclides in marine sediments close to the estuary of Shatt al-Arab/Arvand Rud River, the Gulf. J. Environ. Radioact. 157, 1–15. https://doi.org/10.1016/j.jenvrad.2016.02.025.
Ramadan, A.A., Diab, H.M., 2013. Radiological characterization and environmental impact in northwestern coast of Egypt. J. Radioanal. Nucl. Chem. 89–95. https://doi.org/10.1007/s10967-012-2091-5.
Rosner, B., Glynn, R.J., 2009. Power and sample size estimation for the wilcoxon rank sum test with application to comparisons of C statistics from alternative prediction models. Biometrics 65, 188–197. https://doi.org/10.1111/j.1541-0420.2008.01062.x.
Roviello, V., De Cesare, M., D'Onofrio, A., Gialanella, L., Guan, Y.J., Roos, P., Ruberti, D., Sabbarese, C., Terrasi, F., 2020. New analytical methods for the assessment of natural (238U, 232Th, 226Ra, 40K) and anthropogenic (137Cs) radionuclides as actinides (239Pu, 240Pu): The case study of the Garigliano NPP releases along the Domitia sandy beaches (Southern Italy). Catena (amst) 193, 104612. https://doi.org/10.1016/j.catena.2020.104612.
Schmincke, H.U., 1993. Geological field guide of Gran Canaria, 6th ed. Pluto-Press, Kiel (Germany).
Shannon, R.D., 1976. Revised Effective Ionic Radii and Systematic Studies of Interatomic Distances in Halides and Chaleogenides. Acta Crystallographica Section A 32, 751–767.
Shapiro, S.S., Wilk, M.B., 1965. An Analysis of Variance Test for Normality (Complete Samples). Biometrika 52, 591–611. https://doi.org/10.2307/2333709.

Sheldrick, G.M., 2015. Crystal structure refinement with SHELXL. Acta Crystallogr C Struct Chem 71, 3–8. https://doi.org/10.1107/S2053229614024218.

Theodorsson-Norheim, E., 1986. Kruskal-Wallis test: BASIC computer program to perform nonparametric one-way analysis of variance and multiple comparisons on ranks of several independent samples. Comput. Methods Programs Biomed. 23, 57–62. https://doi.org/10.1016/0169-2607(86)90081-7.

Thereska, J., 2009. Natural radioactivity of coastal sediments as tracer in dynamic sedimentology. Nukleonika 54, 45–50.

Toby, B.H., von Dreele, R.B., 2013. GSAS-II: The genesis of a modern open-source all purpose crystallography software package. J. Appl. Cryst. 46, 544–549. https://doi.org/10.1107/S0021889813003531.

Tsabaris, C., Evangeliou, N., Fillis-Tsirakis, E., Sotiropoulou, M., Patiris, D.L., Florou, H., 2012. Distribution of natural radioactivity in sediment cores from Amvrakikos Gulf (western Greece) as a part of IAEA's campaign in the Adriatic and Ionian seas. Radiat. Prot. Dosim. 150, 474–487. https://doi.org/10.1093/rpd/ncr436.

Tsabaris, C., Patiris, D., Maramathas, C., Androulakaki, E., Eleftheriou, G., Pappa, F., Alexakis, S., 2023a. Surveillance of the seashore using the KATERINA II geo-referenced detection system. HNPS Advances in Nuclear Physics 29, 137–143. https://doi.org/10.12681/hnpsanp.2473.

Tsabaris, C., Patiris, D.L., Adams, R., Castillo, J., Henriquez, M.F., Hurtado, C., Munoz, L., Kalpaxis, L., Verri, M., Alexakis, S., Pappa, F.K., Lampousis, A., 2023b. In situ radioactivity maps and trace metal concentrations in beach sands of a mining coastal area at North Aegean, Greece. J. Mar. Sci. Eng. 11, 1207. https://doi.org/10.3390/jmse11061207.

Williams, L.J., Abdi, H., 2010. Tukey 's honestly signiflcant difference test (HSD). Encyclopedia of Research Design 2–7.

Zebracki, M., Eyrolle-Boyer, F., Evrard, O., Claval, D., Mourier, B., Gairoard, S., Cagnat, X., Antonelli, C., 2015. Tracing the origin of suspended sediment in a large Mediterranean river by combining continuous river monitoring and measurement of artificial and natural radionuclides. Sci. Total Environ. 502, 122–132. https://doi.org/10.1016/j.scitotenv.2014.08.082.

CAPÍTULO 4. Conclusiones de la tesis y líneas futuras

4.1. Conclusiones

Los resultados de esta tesis proporcionan un conjunto de varios radiotrazadores naturales que se podrían utilizar para el estudio de distintos fenómenos de erosión, transporte y acumulación de sedimentos costeros. Así mismo, como este trabajo se desarrolla en una región de estudio con dinámicas marinas muy diversas, los resultados obtenidos se podrían aplicar en otras partes del mundo. A continuación, se detallan las principales conclusiones que se pueden extraer de esta tesis:

1. La distribución espacial de las concentraciones de actividad del ^{226}Ra, ^{232}Th y ^{40}K dividen la playa de Las Canteras en 3 zonas acorde a las distintas dinámicas marinas que afectan a la playa. La zona I corresponde a una zona totalmente expuesta a la acción del oleaje, la zona II a una zona semiprotegida localizada enfrente de las aberturas de la barra y la zona III que es la zona totalmente protegida frente a la acción del oleaje.

2. Las concentraciones de actividad de ^{226}Ra, ^{228}Ra (descendiente del ^{232}Th) y ^{40}K en las zonas intermareal de la playa de Las Canteras y las distintas zonas sumergidas de la Bahía del Confital trazan los procesos de erosión, transporte y acumulación de sedimentos debido a dinámicas marinas. Esto se debe a que la variación temporal de las concentraciones de actividad de estos radionucleidos está condicionada por agentes de erosión y transporte marinos como puede ser el oleaje.

3. Las distintas concentraciones de actividad del ^{226}Ra, ^{228}Ra y ^{40}K que se encuentran en muestras de la Bahía del Confital y la playa de Las Canteras están fuertemente relacionadas con los cambios en su contenido mineralógico. Por tanto, los radionucleidos

primordiales de los sedimentos propios de la zona de estudio son trazadores óptimos de la erosión, transporte y acumulación de dichos sedimentos costeros.

4. El $^{210}Pb_{ex}$ se podría usar para trazar zonas submarinas donde se produce la acumulación por sedimentación de partículas de la columna de agua. Esto se debería a que las altas actividades de $^{210}Pb_{ex}$ parecían identificar zonas de abrigo de la parte sumergida de la playa y las zonas profundas de la bahía.

5. El uso de la ratio $^{226}Ra/^{228}Ra$ como indicador de periodos de acumulación parece estar limitado a regiones donde existan minerales arcillosos como la zona III de la playa de Las Canteras. Sin embargo, los resultados de esta tesis no fueron concluyentes para el uso de esta ratio como indicador de procesos de erosión.

4.2. Líneas futuras

Durante el desarrollo de esta tesis se han quedado abiertas diversas líneas futuras que se listan a continuación:

- Aplicar los métodos desarrollados en esta tesis para el estudio de las dinámicas sedimentarias de otras playas distintas a la playa de Las Canteras.
- Comparar las medidas y resultados obtenidos en esta tesis con los resultados que se puedan obtener mediante la realización de medidas por espectrometría in situ. Esto permitirá la validación de las medidas in situ, especialmente para su aplicación submarina.
- Analizar los equilibrios seculares de las series del ^{238}U y el ^{232}Th en las diferentes muestras de la playa. Esto permitirá buscar un

límite más adecuado de la ratio $^{226}Ra/^{228}Ra$ para cada parte de la playa, permitiendo así la realización de un estudio más detallado de su uso como indicador de procesos de erosión y acumulación de sedimentos.

- Analizar los sedimentos de las zonas submarinas con alto contenido en $^{210}Pb_{ex}$ para comprobar su uso como trazador de la acumulación por sedimentación de otras especies químicas que entren en la columna de agua a través de los aerosoles atmosféricos.
- Realizar un mapa de corrientes de la parte sumergida de la playa de Las Canteras y compararlo con un mapa más detallado del $^{210}Pb_{ex}$ para comprobar si sus máximas actividades localizan los puntos de remanso.

4.3. Conclusions

The results of this thesis provide a set of various natural radiotracers that could be applied to study different processes related to coastal sediment erosion, transport and accumulation. In addition, since the study is developed in an area with diverse marine dynamics, the results could be applied to other parts of the world. The main conclusions that can be extracted from this thesis are:

1. The spatial distribution of the activity concentrations of ^{226}Ra, ^{228}Ra and ^{40}K divides Las Canteras beach in 3 zones following the different marine dynamics that affect the beach. Zone I corresponds to the area totally expose to the wave action, zone II corresponds to the semi-protected area located in front of the openings of the natural offshore rocky bar and zone III is the area fully protected against the wave action.

2. The activity concentrations of ^{226}Ra, ^{228}Ra (daughter of ^{232}Th) and ^{40}K in the intertidal and submerged part of Las Canteras Beach and in the rest of El Confital Bay trace erosion, transport and accumulation of sediments due to marine dynamics. This is because the temporal variations of the activity concentration values of these radionuclides depend on marine erosion and transport agents such as waves.

3. The activity concentration values of ^{226}Ra, ^{228}Ra and ^{40}K in the different samples from El Confital Bay and Las Canteras Beach are strongly influenced by their mineralogical content. Therefore, primordial radionuclides belonging to the study region sediments are suitable tracers of coastal erosion, transport and accumulation.

4. $^{210}Pb_{ex}$ can be used to trace submerged areas where accumulation by sedimentation of particles from the water column occurs. This is because high activity concentration values of $^{210}Pb_{ex}$ seemed to identify sheltered areas of the submerged part of the beach and the deep parts of the bay.

5. The use of the ratio $^{226}Ra/^{228}Ra$ as an indicator of accumulation periods seems to be limited to regions with clay mineral content like zone III of Las Canteras Beach. However, the results of this thesis concerning the use of this ratio to identify erosion periods were not conclusive.

4.4. Future lines

During the development of this thesis, the following future research lines were open:

- To apply the methods developed in this thesis to study de sediment dynamics of other beaches different from Las Canteras Beach.
- To compare the results obtained in this thesis with results obtained by in situ gamma spectrometry measurements. This will enable validating in situ measurements, especially for submarine areas.
- To analyse the secular equilibriums of the ^{238}U and ^{232}Th decay series in the samples from Las Canteras Beach. This will allow a more appropriate limit of the $^{226}Ra/^{228}Ra$ ratio to be found for each part of the beach, so a more detailed study of its use as an indicator of erosion and accumulation processes can be carried out.

- To analyse the sediments with high content of $^{210}Pb_{ex}$ to verify its use as a tracer of the accumulation by sedimentation of other chemical species that enter the water column through atmospheric aerosols.
- To create a current map of the submerged part of Las Canteras Beach and compare it with a more detailed $^{210}Pb_{ex}$ map to verify that its maximum activity concentrations identify sheltered areas where the velocity of the current is zero.

BIBLIOGRAFÍA

Abbasi, A., Zakaly, H.M.H., Mirekhtiary, F., 2020. Baseline levels of natural radionuclides concentration in sediments East coastline of North Cyprus. Mar Pollut Bull 161, 111793. https://doi.org/10.1016/j.marpolbul.2020.111793

Akpan, A.E., Ebong, E.D., Ekwok, S.E., Eyo, J.O., 2020. Assessment of radionuclide distribution and associated radiological hazards for soils and beach sediments of Akwa Ibom Coastline, southern Nigeria. Arabian Journal of Geosciences 13, 753. https://doi.org/10.1007/s12517-020-05727-7/Published

Alfonso, J.A., Pérez, K., Palacios, D., Handt, H., LaBrecque, J.J., Mora, A., Vásquez, Y., 2014. Distribution and environmental impact of radionuclides in marine sediments along the Venezuelan coast. J Radioanal Nucl Chem 300, 219–224. https://doi.org/10.1007/s10967-014-2999-z

Alonso, I., 2005. Costa Norte: Playa De Las Canteras, in: Hernández, L., Alonso, I., Mangas, J., Yanes, A. (Eds.), Tendencias Actuales En Geomorfología Litoral. Universidad de Las Palmas de Gran Canaria, La Palmas de Gran Canaria, pp. 219–238.

Alonso, I., 1994. Spatial beach morphodynamics. An example from Canary Islands, Spain. Litoral 94, 169–183.

Alonso, I., 1993. Procesos sedimentarios en la playa de Las Canteras (Gran Canaria). Universidad de Las Palmas de Gran Canaria, Las Palmas de Gran Canaria.

Alonso, I., Pérez Torrado, F.J., 1992. Estudio sedimentológico de la playa de Las Canteras (Gran Canaria). Datos preliminares. III Congreso geológico de España y tomo 2, 131–135.

Alonso, I., Vilas, F., 1996. Variabilidad sedimentaria en la playa de Las Canteras (Gran Canaria). Geogaceta 20, 428–430.

Alveirinho Dias, J., 2004. A análise sedimentar e o conhecimento dos sistemas marinhos: uma introdução à oceanografia geológica, First. ed. Universidade do Algarve, Faro.

Androulakaki, E.G., Tsabaris, C., Eleftheriou, G., Kokkoris, M., Patiris, D.L., Vlastou, R., 2015. Seabed radioactivity based on in situ measurements and Monte Carlo simulations. Applied Radiation and Isotopes 101, 83–92. https://doi.org/10.1016/j.apradiso.2015.03.013

Arnedo, M.A., Rubiano, J.G., Alonso, H., Tejera, A., González, A., González, J., Gil, J.M., Rodríguez, R., Martel, P., Bolivar, J.P., 2017. Mapping natural radioactivity of soils in the eastern Canary Islands. J Environ Radioact 166, 242–258. https://doi.org/10.1016/j.jenvrad.2016.07.010

Arnedo, M.A., Tejera, A., Rubiano, J.G., Alonso, H., Gil, J.M., Rodríguez, R., Martel, P., 2013. Natural radioactivity measurements of beach sands in gran Canaria, Canary Islands (Spain). Radiat Prot Dosimetry 156, 75–86. https://doi.org/10.1093/rpd/nct044

Arriola-Velásquez, A., Tejera, A., Guerra, J.G., Alonso, I., Alonso, H., Arnedo, M.A., Rubiano, J.G., Martel, P., 2019. Spatio-temporal variability of natural radioactivity as tracer of beach sedimentary dynamics. Estuar Coast Shelf Sci 231. https://doi.org/10.1016/j.ecss.2019.106476

Arriola-Velásquez, A.C., Tejera, A., Guerra, J.G., Geibert, W., Stimac, I., Cámara, F., Alonso, H., Rubiano, J.G., Martel, P., 2021. ^{226}Ra, ^{228}Ra and ^{40}K as tracers of erosion and accumulation processes: A 3-year study on a beach with different sediment dynamics. Catena (Amst) 207, 105705. https://doi.org/10.1016/j.catena.2021.105705

Balcells, R., Barrera, J.L., Ruiz García, M.T., (Cartographers), 1990. Geological Map 1101-I-II Las Palmas de Gran Canaria, 1:25000 IGME.

Bam, W., Maiti, K., Baskaran, M., 2021. ^{210}Po and ^{210}Pb as Tracers of Particle Cycling and Export in the Western Arctic Ocean. Front Mar Sci 8, 697444. https://doi.org/10.3389/fmars.2021.697444

Bandeira, J. V., Salim, L.H., 2017. Technetium-99m: From nuclear medicine applications to fine sediment transport studies. Nukleonika 62, 295–302. https://doi.org/10.1515/nuka-2017-0043

Baskaran, M., Swarzenski, P.W., 2007. Seasonal variations on the residence times and partitioning of short-lived radionuclides (^{234}Th, ^{7}Be and ^{210}Pb) and depositional fluxes of ^{7}Be and ^{210}Pb in Tampa Bay, Florida. Mar Chem 104, 27–42. https://doi.org/10.1016/j.marchem.2006.06.012

Bejannin, S., van Beek, P., Stieglitz, T., Souhaut, M., Tamborski, J., 2017. Combining airborne thermal infrared images and radium isotopes to study submarine groundwater discharge along the French Mediterranean coastline. J Hydrol Reg Stud 13, 72–90. https://doi.org/10.1016/j.ejrh.2017.08.001

Bezuidenhout, J., 2020. The investigation of natural radionuclides as tracers for monitoring sediment processes. J Appl Geophy 181, 104135. https://doi.org/10.1016/j.jappgeo.2020.104135

Blott, S.J., Pye, K., 2001. Gradistat : a Grain Size Distribution and Statistics Package for the Analysis of Unconsolidated Sediments. Earth Surf Process Landf 26, 1237–1248. https://doi.org/10.1002/esp.261

Bradtmiller, L.I., McManus, J.F., Robinson, L.F., 2014. $^{231}Pa/^{230}Th$ evidence for a weakened but persistent Atlantic meridional overturning circulation during Heinrich Stadial 1. Nat Commun 5. https://doi.org/10.1038/ncomms6817

Buesseler, K.O., Benitez-Nelson, C.R., Roca-Martí, M., Wyatt, A.M., Resplandy, L., Clevenger, S.J., Drysdale, J.A., Estapa, M.L., Pike, S., Umhau, B.P., 2020. High-resolution spatial and temporal measurements of particulate organic carbon flux using thorium-234 in the northeast Pacific Ocean during the EXport Processes in the Ocean from RemoTe Sensing field campaign. Elementa: Science of the Anthropocene 8. https://doi.org/10.1525/elementa.2020.030

Castrillejo, M., Casacuberta, N., Vockenhuber, C., Lherminier, P., 2022. Rapidly Increasing Artificial Iodine Highlights Pathways of Iceland-Scotland Overflow Water and Labrador Sea Water. Front Mar Sci 9. https://doi.org/10.3389/fmars.2022.897729

Charkin, A.N., Yaroshchuk, E.I., Dudarev, O. v., Leusov, A.E., Goriachev, V.A., Sobolev, I.S., Gulenko, T.A., Pipko, I.I., Startsev, A.M., Semiletov, I.P., 2022. The influence of sedimentation regime on natural radionuclide activity concentration in marine sediments of the East Siberian Arctic Shelf. J Environ Radioact 253–254. https://doi.org/10.1016/j.jenvrad.2022.106988

Cooper, L.W., Grebmeier, J.M., 2018. Deposition patterns on the Chukchi shelf using radionuclide inventories in relation to surface sediment characteristics. Deep Sea Res 2 Top Stud Oceanogr 152, 48–66. https://doi.org/10.1016/j.dsr2.2018.01.009

Dai, Z.J., Du, J.Z., Chu, A., Zhang, X.L., 2011. Sediment characteristics in the North Branch of the Yangtze Estuary based on radioisotope tracers. Environ Earth Sci 62, 1629–1634. https://doi.org/10.1007/s12665-010-0647-7

Dias, T.H., de Oliveira, J., Sanders, C.J., Carvalho, F., Sanders, L.M., Machado, E.C., Sá, F., 2016. Radium isotope (^{223}Ra, ^{224}Ra, ^{226}Ra and ^{228}Ra) distribution near Brazil's largest port, Paranaguá Bay, Brazil. Mar Pollut Bull 111, 443–448. https://doi.org/10.1016/j.marpolbul.2016.07.004

Dione, D., Mbaye, M., Sane, M.L., Ahmadou, C., Dath, B., Dao, A.S.N., 2018. Survey of Activity Concentration and Dose Estimation of Naturally

Occurring Radionuclides (^{232}Th, ^{238}U and ^{40}K) in the Coastal area of Dakar, Senegal. Indian J Sci Technol 11, 1–7. https://doi.org/10.17485/ijst/2018/v11i40/131537

Du, J., Wu, Y., Huang, D., Zhang, J., 2010. Use of ^{7}Be, ^{210}Pb and ^{137}Cs tracers to the transport of surface sediments of the Changjiang Estuary, China. Journal of Marine Systems 82, 286–294. https://doi.org/10.1016/j.jmarsys.2010.06.003

El Zrelli, R., Rabaoui, L., van Beek, P., Castet, S., Souhaut, M., Grégoire, M., Courjault-Radé, P., 2019. Natural radioactivity and radiation hazard assessment of industrial wastes from the coastal phosphate treatment plants of Gabes (Tunisia, Southern Mediterranean Sea). Mar Pollut Bull 146, 454–461. https://doi.org/10.1016/j.marpolbul.2019.06.075

Faivre, S., Bakran-Petricioli, T., Barešić, J., Horvatinčić, N., 2015. New Data on Marine Radiocarbon Reservoir Effect in the Eastern Adriatic Based on Pre-Bomb Marine Organisms from the Intertidal Zone and Shallow Sea. Radiocarbon 57, 527–538. https://doi.org/10.2458/azu_rc.57.18452

Fallah, M., Jahangiri, S., Janadeleh, H., Kameli, M.A., 2019. Distribution and risk assessment of radionuclides in river sediments along the Arvand River, Iran. Microchemical Journal 146, 1090–1094. https://doi.org/10.1016/j.microc.2019.02.028

Feng, H., Zhang, W., Jia, L., Weinstein, M.P., Zhang, Q., Yuan, D., Tao, J., Yu, L., 2010. Short- and long-term sediment transport in western Bohai Bay and coastal areas. Chinese Journal of Oceanology and Limnology 28, 583–592. https://doi.org/10.1007/s00343-010-9099-x

Froehlich, K., 2010. Environmental radionuclides: Tracers and Timers of Terrestrial Processes, First. ed. Elsevier B.V., Amsterdam. https://doi.org/10.1016/S1569-4860(09)01613-1

Garcia-Orellana, J., Rodellas, V., Tamborski, J., Diego-Feliu, M., van Beek, P., Weinstein, Y., Charette, M., Alorda-Kleinglass, A., Michael, H.A., Stieglitz, T., Scholten, J., 2021. Radium isotopes as submarine groundwater discharge (SGD) tracers: Review and recommendations. Earth Sci Rev. https://doi.org/10.1016/j.earscirev.2021.103681

Ghosal, S., Agrahari, S., Guin, R., Sengupta, D., 2017. Implications of modelled radioactivity measurements along coastal Odisha, Eastern India for heavy mineral resources. Estuar Coast Shelf Sci 184, 83–89. https://doi.org/10.1016/j.ecss.2016.11.006

González-Fernández, D., Garrido-Pérez, M.C., Casas-Ruiz, M., Barbero, L., Nebot-Sanz, E., 2012. Radiological risk assessment of naturally occurring radioactive materials in marine sediments and its application in industrialized coastal areas: Bay of Algeciras, Spain. Environ Earth Sci 66, 1175–1181. https://doi.org/10.1007/s12665-011-1325-0

Gulin, S.B., Gulina, L. V., Sidorov, I.G., Proskurnin, V.Y., Duka, M.S., Moseichenko, I.N., Rodina, E.A., 2014. ^{40}K in the Black Sea: A proxy to estimate biogenic sedimentation. J Environ Radioact 134, 21–26. https://doi.org/10.1016/j.jenvrad.2014.02.011

Hajdas, I., Ascough, P., Garnett, M.H., Fallon, S.J., Pearson, C.L., Quarta, G., Spalding, K.L., Yamaguchi, H., Yoneda, M., 2021. Radiocarbon dating. Nature Reviews Methods Primers 1, 62. https://doi.org/10.1038/s43586-021-00058-7

Hallermeier, R.J., 1981. A profile zonation for seasonal sand beaches from wave climate. Coastal Engineering 4, 253–277.

Hemalatha, P., Madhuparna, D., Jha, S.K., Tripathi, R.M., 2015. An investigation of ^{210}Po distribution in marine organisms in the Mumbai Harbour Bay. J Radioanal Nucl Chem 303, 271–276. https://doi.org/10.1007/s10967-014-3350-4

Hewamanna, R., Sumithrarachchi, C.S., Mahawatte, P., Nanayakkara, H.L.C., Ratnayake, H.C., 2001. Natural radioactivity and gamma dose from Sri Lankan clay bricks used in building construction. Applied Radiation and Isotopes 54, 365–369.

Hougham, A.L., Moran, S.B., 2007. Water mass ages of coastal ponds estimated using ^{223}Ra and ^{224}Ra as tracers. Mar Chem 105, 194–207. https://doi.org/10.1016/j.marchem.2007.01.013

Huang, D., Du, J., Deng, B., Zhang, J., 2013. Distribution patterns of particle-reactive radionuclides in sediments off eastern Hainan Island, China: Implications for source and transport pathways. Cont Shelf Res 57, 10–17. https://doi.org/10.1016/j.csr.2012.04.019

Hülse, P., Bentley, S.J., 2012. A 210Pb sediment budget and granulometric record of sediment fluxes in a subarctic deltaic system: The Great Whale River, Canada. Estuar Coast Shelf Sci 109, 41–52. https://doi.org/10.1016/j.ecss.2012.05.019

International Atomic Energy Agency, 2014. Radiotracer and Sealed Source Applications in Sediment Transport Studies, Training Course Series No. 59. IAEA, Vienna.

Jones, D.G., 2001. Development and application of marine gamma-ray measurements: a review. J Environ Radioact 53, 313–333.

Kadko, D., Johns, W., 2011. Inferring upwelling rates in the equatorial Atlantic using 7Be measurements in the upper ocean. Deep Sea Res 1 Oceanogr Res Pap 58, 647–657. https://doi.org/10.1016/j.dsr.2011.03.004

Kilel, K.K., Bezuidenhout, J., Gatari, M.J., le Roux, R.R., Kaniu, M.I., 2022. A low-cost delta underwater gamma system (DUGS) for in-situ measurement of natural radionuclides in aquatic sediments. J Radioanal Nucl Chem. https://doi.org/10.1007/s10967-022-08701-7

Kim, J.-S., Kim, J.-B., Jung, S.-H., Lee, J.-S., 2005. Sediment Transport Study in Haeundae Beach using Radioisotope Labelled Compound, in: Proceedings of the Korean Nuclear Society Conferences. Korean Nuclear Society, Busan, pp. 749–750.

Léon, M., van Beek, P., Scholten, J., Moore, W.S., Souhaut, M., De Oliveira, J., Jeandel, C., Seyler, P., Jouanno, J., 2022. Use of ^{223}Ra and ^{224}Ra as chronometers to estimate the residence time of Amazon waters on the Brazilian continental shelf. Limnol Oceanogr 67, 753–767. https://doi.org/10.1002/lno.12010

Li, W., Li, X., Mei, X., Zhang, F., Xu, J., Liu, C., Wei, C., Liu, Q., 2021. A review of current and emerging approaches for Quaternary marine sediment dating. Science of the Total Environment 780, 146522. https://doi.org/10.1016/j.scitotenv.2021.146522

Ligero, R.A., Ramos-Lerate, I., Barrera, M., Casas-Ruiz, M., 2001. Relationships between sea-bed radionuclide activities and some sedimentological variables. J Environ Radioact 57, 7–19.

Ligero, R.A., Vidal, J., Meléndez, M.J., Hamani, M., Casas-Ruiz, M., 2009. Sedimentology models from activity concentration measurements: application to the “Bay of Cadiz” Natural Park (SW Spain). J Environ Radioact 100, 203–208. https://doi.org/10.1016/j.jenvrad.2008.11.011

Lin, W., Feng, Y., Yu, K., Lan, W., Wang, Y., Mo, Z., Ning, Q., Feng, L., He, X., Huang, Y., 2020. Long-lived radionuclides in marine sediments from the Beibu Gulf, South China Sea: Spatial distribution, controlling factors, and proxy for transport pathway. Mar Geol 424, 106157. https://doi.org/10.1016/j.margeo.2020.106157

Lippold, J., Luo, Y., Francois, R., Allen, S.E., Gherardi, J., Pichat, S., Hickey, B., Schulz, H., 2012. Strength and geometry of the glacial Atlantic

Meridional Overturning Circulation. Nat Geosci 5, 813–816. https://doi.org/10.1038/ngeo1608

Livingston, H.D., 2004. Radioactivity in the environment: Marine Radioactivity, First. ed. Elsevier Ltd, Oxford.

Madruga, M.J., Silva, L., Gomes, A.R., Libânio, A., Reis, M., 2014. The influence of particle size on radionuclide activity concentrations in Tejo River sediments. J Environ Radioact 132, 65–72. https://doi.org/10.1016/j.jenvrad.2014.01.019

Mahu, E., Nyarko, E., Hulme, S., Swarzenski, P., Asiedu, D.K., Coale, K.H., 2016. Geochronology and historical deposition of trace metals in three tropical estuaries in the Gulf of Guinea. Estuar Coast Shelf Sci 177, 31–40. https://doi.org/10.1016/j.ecss.2016.05.007

Mangas, J., Julià-Miralles, M., 2015. Geomorfología y naturaleza de las bajas submareales de Bajo Fernando, Los Roquerillos y La Zabala (NE de Gran Canaria). Geo-Temas 15, 37–40.

Medina, R., Bastón, S., Cánovas, V., Torres, A., Luque, Á., Alonso, I., Sánchez, I., Ortega, A., Rodríguez, S., Martín, J.A., 2006. Estudio integral de la playa de Las Canteras, Technical Report Dirección General de Costas.

Mikelić, I.L., Oreščanin, V., Škaro, K., 2017. Variation of sedimentation rate in the semi-enclosed bay determined by ^{137}Cs distribution in sediment (Kaštela Bay, Croatia). J Environ Radioact 166, 112–125. https://doi.org/10.1016/j.jenvrad.2016.03.027

Moore, W.S., 2006. Radium isotopes as tracers of submarine groundwater discharge in Sicily. Cont Shelf Res 26, 852–861. https://doi.org/10.1016/j.csr.2005.12.004

Moore, W.S., 2000. Ages of continental shelf waters determined from ^{223}Ra and ^{224}Ra. J Geophys Res Oceans 105, 22117–22122. https://doi.org/10.1029/1999jc000289

Mtshawu, B., Bezuidenhout, J., Kilel, K.K., 2023. Spatial autocorrelation and hotspot analysis of natural radionuclides to study sediment transport. J Environ Radioact 264. https://doi.org/10.1016/j.jenvrad.2023.107207

Not, C., Hillaire-Marcel, C.C., 2010. Time constraints from ^{230}Th and ^{231}Pa data in late Quaternary, low sedimentation rate sequences from the Arctic Ocean: An example from the northern Mendeleev Ridge. Quat Sci Rev 29, 3665–3675. https://doi.org/10.1016/j.quascirev.2010.06.042

Pappa, F.K., Tsabaris, C., Ioannidou, A., Patiris, D.L., Kaberi, H., Pashalidis, I., Eleftheriou, G., Androulakaki, E.G., Vlastou, R., 2016. Radioactivity and metal concentrations in marine sediments associated with mining activities in Ierissos Gulf, North Aegean Sea, Greece. Applied Radiation and Isotopes 116, 22–33. https://doi.org/10.1016/j.apradiso.2016.07.006

Patiris, D.L., Tsabaris, C., Anagnostou, C.L., Androulakaki, E.G., Pappa, F.K., Eleftheriou, G., Sgouros, G., 2016. Activity concentration and spatial distribution of radionuclides in marine sediments close to the estuary of Shatt al-Arab/Arvand Rud River, the Gulf. J Environ Radioact 157, 1–15. https://doi.org/10.1016/j.jenvrad.2016.02.025

Pope, J.A., 1989. Options in Physics: Medical physics. Heinemann Educational books Ltd, Oxford.

Raghu, Y., Chandrasekaran, A., Ravisankar, R., 2020. Acta Ecologica Sinica Statistical analysis of natural radioactivity data of clay samples in Tiruvannamalai , Tamilnadu , India. Acta Ecologica Sinica 40, 254–261. https://doi.org/10.1016/j.chnaes.2019.12.006

Ravisankar, R., Sivakumar, S., Chandrasekaran, A., Prince Prakash Jebakumar, J., Vijayalakshmi, I., Vijayagopal, P., Venkatraman, B., 2014. Spatial distribution of gamma radioactivity levels and radiological hazard indices in the East Coastal sediments of Tamilnadu, India with statistical approach. Radiation Physics and Chemistry 103, 89–98. https://doi.org/10.1016/j.radphyschem.2014.05.037

Renfro, A.A., Cochran, J.K., Hirschberg, D.J., Bokuniewicz, H.J., Goodbred, S.L., 2016. The sediment budget of an urban coastal lagoon (Jamaica Bay, NY) determined using ^{234}Th and ^{210}Pb. Estuar Coast Shelf Sci 180, 136–149. https://doi.org/10.1016/j.ecss.2016.06.008

Rodellas, V., Garcia-Orellana, J., Trezzi, G., Masqué, P., Stieglitz, T.C., Bokuniewicz, H., Cochran, J.K., Berdalet, E., 2017. Using the radium quartet to quantify submarine groundwater discharge and porewater exchange. Geochim Cosmochim Acta 196, 58–73. https://doi.org/10.1016/j.gca.2016.09.016

Rodellas, V., Roca-Martí, M., Puigcorbé, V., Castrillejo, M., Casacuberta, N., 2023. Radionuclides as Ocean Tracers, in: Marine Analytical Chemistry. Springer International Publishing, pp. 199–273. https://doi.org/10.1007/978-3-031-14486-8_4

Roviello, V., De Cesare, M., D'Onofrio, A., Gialanella, L., Guan, Y.J., Roos, P., Ruberti, D., Sabbarese, C., Terrasi, F., 2020. New analytical methods for the assessment of natural (^{238}U, ^{232}Th, ^{226}Ra, ^{40}K) and anthropogenic

(^{137}Cs) radionuclides as actinides (^{239}Pu, ^{240}Pu): The case study of the Garigliano NPP releases along the Domitia sandy beaches (Southern Italy). Catena (Amst) 193, 104612. https://doi.org/10.1016/j.catena.2020.104612

Sanial, V., Van Beek, P., Lansard, B., Souhaut, M., Kestenare, E., D'Ovidio, F., Zhou, M., Blain, S., 2015. Use of Ra isotopes to deduce rapid transfer of sediment-derived inputs off Kerguelen. Biogeosciences 12, 1415–1430. https://doi.org/10.5194/bg-12-1415-2015

Schmincke, H.U., 1993. Geological field guide of Gran Canaria, 6th ed. Pluto-Press, Kiel (Germany).

Shah, C., Banerji, U.S., Chandana, K.R., Bhushan, R., 2020. ^{210}Pb dating of recent sediments from the continental shelf of western India: factors influencing sedimentation rates. Environ Monit Assess 192, 468. https://doi.org/10.1007/s10661-020-08415-x

Shaw, P.J.A., 2003. Multivariate Statistics for the Environmental Science, First. ed. Hodder Headline Group, London.

Smith, J.N., Ellis, K.M., 1982. Transport mechanism for Pb-210, Cs-137 and Pu fallout radionuclides through fluvial-marine systems. Geochim Cosmochim Acta 46, 941–954.

Subha Anand, S., Rengarajan, R., Sarma, V.V.S.S., 2018. ^{234}Th-Based Carbon Export Flux Along the Indian GEOTRACES GI02 Section in the Arabian Sea and the Indian Ocean. Global Biogeochem Cycles 32, 417–436. https://doi.org/10.1002/2017GB005847

Sun, X., Fan, D., Liao, H., Liu, M., Tian, Y., Zhang, X., Yang, Z., 2020. Variation in sedimentary ^{210}Pb over the last 60 years in the Yangtze River Estuary: New insight to the sedimentary processes. Mar Geol 427, 106240. https://doi.org/10.1016/j.margeo.2020.106240

Szmytkiewicz, A., Zalewska, T., 2014. Sediment deposition and accumulation rates determined by sediment trap and ^{210}Pb isotope methods in the outer puck bay (Baltic Sea). Oceanologia 56, 85–106. https://doi.org/10.5697/oc.56-1.085

Tamborski, J., Bejannin, S., Garcia-Orellana, J., Souhaut, M., Charbonnier, C., Anschutz, P., Pujo-pay, M., Conan, P., Crispi, O., Monnin, C., Stieglitz, T., Rodellas, V., Andrisoa, A., Claude, C., van Beek, P., 2018. A comparison between water circulation and terrestrially-driven dissolved silica fluxes to the Mediterranean Sea traced using radium isotopes.

Geochim Cosmochim Acta 238, 496–515. https://doi.org/10.1016/j.gca.2018.07.022

Tamborski, J.J., Cai, P., Eagle, M., Henderson, P., Charette, M.A., 2022. Revisiting 228Th as a tool for determining sedimentation and mass accumulation rates. Chem Geol 607, 121006. https://doi.org/10.1016/j.chemgeo.2022.121006

Tejera, A., Pérez-Sánchez, L., Guerra, G., Arriola-Velásquez, A.C., Alonso, H., Arnedo, M.A., Rubiano, G., Martel, P., 2019. Natural radioactivity in algae arrivals on the Canary coast and dosimetry assessment. Science of the Total Environment 658, 122–131. https://doi.org/10.1016/j.scitotenv.2018.12.140

Thereska, J., 2009. Natural radioactivity of coastal sediments as tracer in dynamic sedimentology. Nukleonika 54, 45–50.

Thomson, R.E., Emery, W.J., 2014. The spatial analyses of data fields, in: Thomson, R.E., Emery, W.J. (Eds.), Data Analysis Methods in Physical Oceanography. Elsevier Science, Amsterdam, pp. 335–340. https://doi.org/10.1017/CBO9781107415324.004

Tsabaris, C., Patiris, D., Maramathas, C., Androulakaki, E., Eleftheriou, G., Pappa, F., Alexakis, S., 2023a. Surveillance of the seashore using the KATERINA II geo-referenced detection system. HNPS Advances in Nuclear Physics 29, 137–143. https://doi.org/10.12681/hnpsanp.2473

Tsabaris, C., Patiris, D.L., Adams, R., Castillo, J., Henriquez, M.F., Hurtado, C., Munoz, L., Kalpaxis, L., Verri, M., Alexakis, S., Pappa, F.K., Lampousis, A., 2023b. In Situ Radioactivity Maps and Trace Metal Concentrations in Beach Sands of a Mining Coastal Area at North Aegean, Greece. J Mar Sci Eng 11, 1207. https://doi.org/10.3390/jmse11061207

UNSCEAR, 2000. Sources and Effects of Ionizing Radiation. Report of the United Nations Scientific Committee on the Effects of Atomic Radiation to the General Assembly, with Scientific Annexes. United Nations, New York.

Vasconcelos, D.C., Pereira, C., Oliveira, A.H., Santos, T.O., Rocha, Z., de B.C. Menezes, M.Â., 2011. Determination of Natural Radioactivity in Beach Sand in the Extreme South of Bahia , Brazil , Using Gamma Spectrometry. Radiation Protection and Environment 34, 178–184.

Vineethkumar, V., Akhil, R., Shimod, K.P., Prakash, V., 2020. Geospatial analysis of the source of monazite deposits and the dynamics of natural

radionuclides in the selected coastal environs of Kerala, south west coast of India. J Radioanal Nucl Chem 326, 983–996. https://doi.org/10.1007/s10967-020-07418-9

Wefing, A.M., Casacuberta, N., Christl, M., Gruber, N., Smith, J.N., 2021. Circulation timescales of Atlantic Water in the Arctic Ocean determined from anthropogenic radionuclides. Ocean Science 17, 111–129. https://doi.org/10.5194/os-17-111-2021

Williams, L.J., Abdi, H., 2010. Tukey 's Honestly Signiflcant Difference test (HSD). Encyclopedia of Research Design 2–7.

Yamashiki, Y., Onda, Y., Smith, H.G., Blake, W.H., Wakahara, T., Igarashi, Y., Matsuura, Y., Yoshimura, K., 2014. Initial flux of sediment-associated radiocesium to the ocean from the largest river impacted by Fukushima Daiichi Nuclear Power Plant. Sci Rep 4. https://doi.org/10.1038/srep03714

Yu, A.I., 2002. Radioactive Fallout After Nuclear Explosions and Accidents, First. ed. Elsevier Ltd, Oxford.

Zebracki, M., Eyrolle-Boyer, F., Evrard, O., Claval, D., Mourier, B., Gairoard, S., Cagnat, X., Antonelli, C., 2015. Tracing the origin of suspended sediment in a large Mediterranean river by combining continuous river monitoring and measurement of artificial and natural radionuclides. Science of the Total Environment 502, 122–132. https://doi.org/10.1016/j.scitotenv.2014.08.082

ANEXO I. Material suplementario de los artículos

Radiological risk assessment of beaches from volcanic oceanic islands: A case study of the Eastern Canary Islands (Spain)

El material suplementario este artículo incluye las dos tablas y la figura incluidas a continuación en este anexo. Además, se puede descargar de la versión web del artículo.

https://doi.org/10.1016/j.envpol.2023.122809

The supplementary material of this paper that is included in this annexe consists of two tables and a figure. In addition, they can be downloaded from the online version of the paper.

https://doi.org/10.1016/j.envpol.2023.122809

Table S1.

Complete list of samples, island and coordinates where they were collected. Coordinates are given in the UTM system at 28R.

Sample	Island	Beach	X-UTM	Y-UTM
LG1	LA GRACIOSA	Pedro Barbas	647607	3237902
LG2	LA GRACIOSA	Playa del Ambar	646036	3240021
LG3	LA GRACIOSA	Las Conchas	644143	3239355
LG4	LA GRACIOSA	Las Conchas	644226	3239608
LG5	LA GRACIOSA	Francesa	642804	3233291
LG6	LA GRACIOSA	Francesa	643072	3233330
LG7	LA GRACIOSA	Francesa	643274	3233278
LG8	LA GRACIOSA	Caleta Sebo	645422	3234445
LG9	LA GRACIOSA	Caleta Sebo	645381	3234408
LZ1	LANZAROTE	Orzola	651405	3233068
LZ2	LANZAROTE	Teguise	647440	3208885
LZ3	LANZAROTE	Teguise	647278	3208744
LZ4	LANZAROTE	Teguise	646570	3208149
LZ5	LANZAROTE	Arrecife	640746	3204158
LZ6	LANZAROTE	Arrecife	640568	3204218
LZ7	LANZAROTE	Arrecife	640325	3204167
LZ8	LANZAROTE	Honda	637431	3203365
LZ9	LANZAROTE	Honda	637017	3203156
LZ10	LANZAROTE	Honda	636807	3203112
LZ11	LANZAROTE	Pto. Carmen	634489	3201150
LZ12	LANZAROTE	Pto. Carmen	634124	3200940
LZ13	LANZAROTE	Pto. Carmen	633950	3200774
LZ14	LANZAROTE	Pto. Carmen	633525	3200800
LZ15	LANZAROTE	Pto. Carmen	633225	3200698
LZ16	LANZAROTE	Pto. Carmen	632790	3200224
LZ17	LANZAROTE	Pto. Carmen	631021	3199842
LZ18	LANZAROTE	Pto. Carmen	630628	3199828
LZ19	LANZAROTE	Pto. Carmen	630110	3199784
LZ20	LANZAROTE	Quemada	623282	3198341
LZ21	LANZAROTE	Papagayo	618873	3191296
LZ22	LANZAROTE	Papagayo	618209	3191167
LZ23	LANZAROTE	Papagayo	618132	3191368
LZ24	LANZAROTE	Papagayo	618057	3191653
LZ25	LANZAROTE	Papagayo	617672	3192352
LZ26	LANZAROTE	P.BlancaLZ	614879	3193224
LZ27	LANZAROTE	P.BlancaLZ	614718	3193286
LZ28	LANZAROTE	P.BlancaLZ	614154	3193325

LZ29	LANZAROTE	Janubio	614011	3201290
LZ30	LANZAROTE	Hervideros	613983	3204142
LZ31	LANZAROTE	Famara	639818	3221853
LZ32	LANZAROTE	Famara	640277	3221708
LZ33	LANZAROTE	Famara	640760	3221829
LZ34	LANZAROTE	Famara	641416	3222130
FV1	FUERTEVENTURA	Corralejo	610568	3179559
FV2	FUERTEVENTURA	Corralejo	612888	3178319
FV3	FUERTEVENTURA	Corralejo	613494	3176357
FV4	FUERTEVENTURA	Corralejo	613728	3175624
FV5	FUERTEVENTURA	Corralejo	613770	3175557
FV6	FUERTEVENTURA	Corralejo	614095	3174282
FV7	FUERTEVENTURA	Corralejo	613982	3172333
FV8	FUERTEVENTURA	P. BlancaFV	610931	3150675
FV9	FUERTEVENTURA	P. BlancaFV	611016	3150351
FV10	FUERTEVENTURA	Caleta de Fuste	611835	3141442
FV11	FUERTEVENTURA	Salinas del Carmen	610609	3138226
FV12	FUERTEVENTURA	Pozo Negro	608326	3133619
FV13	FUERTEVENTURA	Las Playitas	599537	3122902
FV14	FUERTEVENTURA	Gran Tarajal	596071	3120934
FV15	FUERTEVENTURA	Gran Tarajal	586729	3118737
FV16	FUERTEVENTURA	Gran Tarajal	585957	3118648
FV17	FUERTEVENTURA	Costa Calma	576791	3115805
FV18	FUERTEVENTURA	Costa Calma	575841	3114588
FV19	FUERTEVENTURA	Jandia	574584	3112442
FV20	FUERTEVENTURA	Jandia	572394	3109595
FV21	FUERTEVENTURA	Jandia	571212	3108155
FV22	FUERTEVENTURA	Jandia	568294	3105094
FV23	FUERTEVENTURA	Jandia	564687	3102523
FV24	FUERTEVENTURA	La Punta	549179	3105366
FV25	FUERTEVENTURA	Cofete	560069	3109768
FV26	FUERTEVENTURA	Ajuy	582629	3141697
FV27	FUERTEVENTURA	Los Molinos	591592	3157855
FV28	FUERTEVENTURA	El Cotillo	596517	3171452
FV29	FUERTEVENTURA	El Cotillo	596509	3173994
FV30	FUERTEVENTURA	El Cotillo	596765	3176380
FV31	FUERTEVENTURA	El Cotillo	603745	3179544
GC1	GRAN CANARIA	El Puertito de Bañaderos	447498	3114091
GC2	GRAN CANARIA	Sardina del Norte	431632	3114211
GC3	GRAN CANARIA	La Laja	458715	3104014
GC4	GRAN CANARIA	La Laja	458769	3104159

GC5	GRAN CANARIA	La Laja	458893	3103655
GC6	GRAN CANARIA	La Laja	459099	3103325
GC7	GRAN CANARIA	Arinaga	460683	3081119
GC8	GRAN CANARIA	Arinaga	460788	3081375
GC9	GRAN CANARIA	Arinaga	461051	3081412
GC10	GRAN CANARIA	El Inglés	444374	3070639
GC11	GRAN CANARIA	El Inglés	444198	3070296
GC12	GRAN CANARIA	El Inglés	444043	3069650
GC13	GRAN CANARIA	El Inglés	443990	3068871
GC14	GRAN CANARIA	El Inglés	443839	3068244
GC15	GRAN CANARIA	El Inglés	444277	3070526
GC16	GRAN CANARIA	Las Alcaravaneras	457881	3111858
GC17	GRAN CANARIA	Las Alcaravaneras	457921	3111617
GC18	GRAN CANARIA	Maspalomas	441068	3067983
GC19	GRAN CANARIA	Maspalomas	441771	3068114
GC20	GRAN CANARIA	Maspalomas	442362	3068080
GC21	GRAN CANARIA	Maspalomas	443140	3068117
GC22	GRAN CANARIA	San Agustín	446474	3071504
GC23	GRAN CANARIA	San Agustín	446594	3071648
GC24	GRAN CANARIA	San Agustín	446929	3071845
GC25	GRAN CANARIA	Las Canteras	456006	3111757
GC26	GRAN CANARIA	Las Canteras	456311	3111854
GC27	GRAN CANARIA	Las Canteras	456455	3111979
GC28	GRAN CANARIA	Las Canteras	456655	3112177
GC29	GRAN CANARIA	Las Canteras	456950	3112461
GC30	GRAN CANARIA	Las Canteras	457166	3112820
GC31	GRAN CANARIA	Las Canteras	457237	3112916
GC32	GRAN CANARIA	Las Canteras	457373	3113108
GC33	GRAN CANARIA	Las Canteras	457583	3113351
GC34	GRAN CANARIA	Las Canteras	457635	3113668

Table S2.

Activity concentration values of ^{226}Ra, ^{232}Th, and ^{40}K in Bq kg^{-1} in all samples analysed. In the cases where activity was below the minimum detectable activity (MDA) this value is given in brackets.

Sample	Island	Beach	^{226}Ra	^{232}Th	^{40}K
LG1	LA GRACIOSA	Pedro Barbas	10.6±0.8	3.5±0.3	<MDA (21)
LG2	LA GRACIOSA	Playa del Ambar	9.9±0.8	2.1±0.3	<MDA (21)
LG3	LA GRACIOSA	Las Conchas	7.6±0.6	1.7±0.3	<MDA (24)
LG4	LA GRACIOSA	Las Conchas	6.4±0.7	2.3±0.3	20±5
LG5	LA GRACIOSA	Francesa	13.3±1.0	4.8±0.4	74±7
LG6	LA GRACIOSA	Francesa	11.9±0.9	4.0±0.4	60±7
LG7	LA GRACIOSA	Francesa	9±1	4.7±0.5	68±9
LG8	LA GRACIOSA	Caleta Sebo	14.9±1.0	4.3±0.4	86±7
LG9	LA GRACIOSA	Caleta Sebo	14±1	4.5±0.4	100±8
LZ1	LANZAROTE	Orzola	<MDA (3.4)	<MDA (4.1)	<MDA (45)
LZ2	LANZAROTE	Teguise	11.9±1	5.8±0.5	<MDA (28)
LZ3	LANZAROTE	Teguise	13.7±0.8	6.4±0.5	41±7
LZ4	LANZAROTE	Teguise	9.5±0.8	12.2±0.6	97±8
LZ5	LANZAROTE	Arrecife	12.4±1.0	5.8±0.5	34±7
LZ6	LANZAROTE	Arrecife	9.6±0.8	5.2±0.4	35±6
LZ7	LANZAROTE	Arrecife	9.7±0.9	5.0±0.5	42±7
LZ8	LANZAROTE	Honda	19±1	12.2±0.7	130±9
LZ9	LANZAROTE	Honda	18±1	12.4±0.7	150±10
LZ10	LANZAROTE	Honda	29±1	10.7±0.6	99±8
LZ11	LANZAROTE	Pto. Carmen	17±1	12.8±0.7	87±8
LZ12	LANZAROTE	Pto. Carmen	12.4±0.9	12.2±0.6	64±7
LZ13	LANZAROTE	Pto. Carmen	16±1	17.0±0.8	121±9
LZ14	LANZAROTE	Pto. Carmen	21±1	12.3±0.6	113±8
LZ15	LANZAROTE	Pto. Carmen	13.7±1.0	11.9±0.6	87±8
LZ16	LANZAROTE	Pto. Carmen	10.4±0.9	10.4±0.6	84±8
LZ17	LANZAROTE	Pto. Carmen	16±1	13.0±0.7	146±9
LZ18	LANZAROTE	Pto. Carmen	20±1	14.7±0.8	160±10
LZ19	LANZAROTE	Pto. Carmen	13.6±1.0	13.9±0.7	160±10
LZ20	LANZAROTE	Quemada	15±1	20.7±1.0	190±10
LZ21	LANZAROTE	Papagayo	12.6±0.9	3.7±0.4	<MDA (22)
LZ22	LANZAROTE	Papagayo	9.7±0.8	3.5±0.3	<MDA (21)
LZ23	LANZAROTE	Papagayo	9.9±0.8	2.3±0.3	<MDA (23)
LZ24	LANZAROTE	Papagayo	10.2±0.9	3.1±0.4	<MDA (27)

LZ25	LANZAROTE	Papagayo	9.7±0.8	3.2±0.3	<MDA (22)
LZ26	LANZAROTE	P.BlancaLZ	12.6±0.9	2.8±0.4	29±6
LZ27	LANZAROTE	P.BlancaLZ	12.2±0.9	3.8±0.4	46±7
LZ28	LANZAROTE	P.BlancaLZ	6.4±0.9	5.7±0.5	92±9
LZ29	LANZAROTE	Janubio	17±1	17.0±0.8	170±10
LZ30	LANZAROTE	Hervideros	14.2±1.0	15.2±0.7	170±10
LZ31	LANZAROTE	Famara	12±1	6.3±0.5	<MDA (30)
LZ32	LANZAROTE	Famara	14±1	7.4±0.5	<MDA (30)
LZ33	LANZAROTE	Famara	12.2±1.0	12.2±0.7	90±8
LZ34	LANZAROTE	Famara	10.2±0.8	9.3±0.5	47±7
FV1	FUERTEVENTURA	Corralejo	9.3±0.7	3.4±0.4	<MDA (22)
FV2	FUERTEVENTURA	Corralejo	4.5±0.9	<MDA (3.0)	<MDA (32)
FV3	FUERTEVENTURA	Corralejo	7±1	<MDA (2.7)	38±9
FV4	FUERTEVENTURA	Corralejo	6.5±0.9	<MDA (2.5)	<MDA (30)
FV5	FUERTEVENTURA	Corralejo	6.3±0.8	<MDA (1.9)	<MDA (30)
FV6	FUERTEVENTURA	Corralejo	8.9±0.6	2.4±0.4	<MDA (23)
FV7	FUERTEVENTURA	Corralejo	8.3±0.9	<MDA (2.1)	<MDA (26)
FV8	FUERTEVENTURA	P. BlancaFV	8.1±0.9	8.6±0.6	130±10
FV9	FUERTEVENTURA	P. BlancaFV	7.1±0.9	7.0±0.8	120±10
FV10	FUERTEVENTURA	Caleta de Fuste	9.7±0.9	5.5±0.5	64±8
FV11	FUERTEVENTURA	Salinas del Carmen	11.6±1.0	7.2±0.5	69±8
FV12	FUERTEVENTURA	Pozo Negro	8.4±0.9	8.8±0.6	150±10
FV13	FUERTEVENTURA	Las Playitas	4.1±0.7	6.5±0.7	132±8
FV14	FUERTEVENTURA	Gran Tarajal	10.5±0.8	13.9±0.7	275±14
FV15	FUERTEVENTURA	Gran Tarajal	7.2±0.7	9.5±0.5	190±10
FV16	FUERTEVENTURA	Gran Tarajal	13.2±0.9	17.5±0.8	300±10
FV17	FUERTEVENTURA	Costa Calma	11±0.8	6.2±0.5	76±7
FV18	FUERTEVENTURA	Costa Calma	6.0±0.7	3.8±0.4	<MDA (22)
FV19	FUERTEVENTURA	Jandia	7.1±0.8	3.9±0.4	<MDA (23)
FV20	FUERTEVENTURA	Jandia	8.0±0.9	3.8±0.4	<MDA (28)
FV21	FUERTEVENTURA	Jandia	8.0±0.7	6.7±0.4	63±6
FV22	FUERTEVENTURA	Jandia	7.2±0.8	4.5±0.4	<MDA (25)
FV23	FUERTEVENTURA	Jandia	7.4±0.7	2.9±0.3	<MDA (22)
FV24	FUERTEVENTURA	La Punta	5.2±0.8	6.9±0.5	28±6

FV25	FUERTEVENTURA	Cofete	7.5±0.9	3.5±0.4	45±7
FV26	FUERTEVENTURA	Ajuy	6.8±0.7	10.2±0.5	137±8
FV27	FUERTEVENTURA	Los Molinos	9.4±0.8	14.9±0.7	320±20
FV28	FUERTEVENTURA	El Cotillo	4.7±0.6	3.2±0.4	<MDA (21)
FV29	FUERTEVENTURA	El Cotillo	3.8±0.8	1.7±0.4	<MDA (30)
FV30	FUERTEVENTURA	El Cotillo	<MDA (4.1)	2.3±0.5	<MDA (34)
FV31	FUERTEVENTURA	El Cotillo	8.0±0.9	3.7±0.4	<MDA (27)
GC1	GRAN CANARIA	El Puertito de Bañaderos	20±1	29±1	420±20
GC2	GRAN CANARIA	Sardina del Norte	24.8±0.8	26±1	210±10
GC3	GRAN CANARIA	La Laja	15.2±1.0	22±1	170±10
GC4	GRAN CANARIA	La Laja	24±1	34±1	480±20
GC5	GRAN CANARIA	La Laja	14.2±0.9	19.9±0.9	117±7.51
GC6	GRAN CANARIA	La Laja	20±1	31±1	300±10
GC7	GRAN CANARIA	Arinaga	15.0±0.9	21.6±1	240±10
GC8	GRAN CANARIA	Arinaga	15.7±1	17.2±0.8	260±10
GC9	GRAN CANARIA	Arinaga	37±2	20.3±1.0	330±20
GC10	GRAN CANARIA	El Inglés	32±2	64±3	1070±50
GC11	GRAN CANARIA	El Inglés	26±1	52±2	1020±40
GC12	GRAN CANARIA	El Inglés	22±1	44±2	910±40
GC13	GRAN CANARIA	El Inglés	21±1	32±1	780±30
GC14	GRAN CANARIA	El Inglés	15.7±0.9	18.8±0.8	340±20
GC15	GRAN CANARIA	El Inglés	28±1	46±2	980±40
GC16	GRAN CANARIA	Las Alcaravaneras	17±1	28±1	590±30
GC17	GRAN CANARIA	Las Alcaravaneras	16±1	21.9±1.0	510±20
GC18	GRAN CANARIA	Maspalomas	23±1	35±1	670±30
GC19	GRAN CANARIA	Maspalomas	23±1	38±2	900±40
GC20	GRAN CANARIA	Maspalomas	27±1	47±2	1090±50
GC21	GRAN CANARIA	Maspalomas	19±1	28±1	660±30
GC22	GRAN CANARIA	San Agustín	19±1	35±2	710±30
GC23	GRAN CANARIA	San Agustín	24±1	34±1	680±30
GC24	GRAN CANARIA	San Agustín	22±1	32±1	610±30
GC25	GRAN CANARIA	Las Canteras	8.8±0.7	10±1	160±9
GC26	GRAN CANARIA	Las Canteras	9.8±0.8	11±1	180±10
GC27	GRAN CANARIA	Las Canteras	11.4±0.8	13±1	260±10
GC28	GRAN CANARIA	Las Canteras	13±1	15±2	340±20
GC29	GRAN CANARIA	Las Canteras	13.3±0.9	16±2	409±20
GC30	GRAN CANARIA	Las Canteras	13.6±0.9	16±2	400±20
GC31	GRAN CANARIA	Las Canteras	18.2±1.1	26±2	660±30
GC32	GRAN CANARIA	Las Canteras	15.8±1	22±2	610±30
GC33	GRAN CANARIA	Las Canteras	13±0.9	15±2	390±20
GC34	GRAN CANARIA	Las Canteras	17±1	24±2	630±30

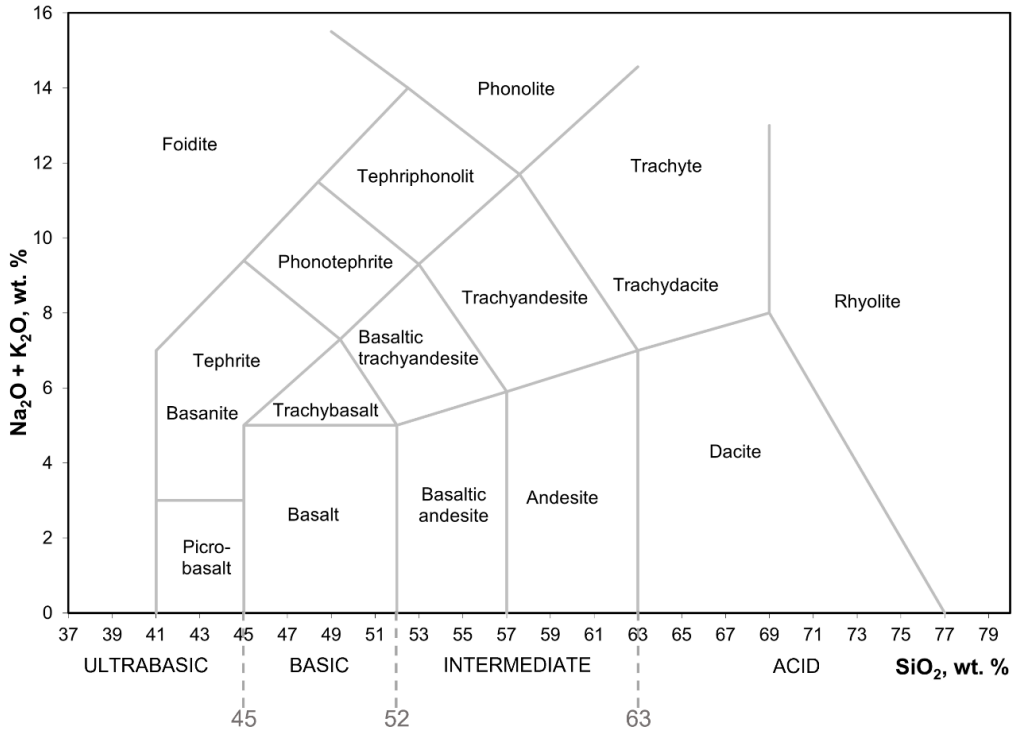

Fig. S1. Total Alkalinity Silica (TAS) diagram for volcanic rocks classification. Modified from (Le Bas et al., 1986)

^{226}Ra, ^{228}Ra and ^{40}K as tracers of erosion and accumulation processes: A 3-year study on a beach with different sediment dynamics

El material suplementario de este artículo consiste en tres archivos .CIF que contienen la información cristalográfica de los análisis mineralógicos. Se pueden descargar en la versión web del artículo.

https://doi.org/10.1016/j.catena.2021.105705

The supplementary material of this paper consists of three .CIF files with the crystallographic information of the mineralogical analysis. They can be downloaded from the online version of the paper.

https://doi.org/10.1016/j.catena.2021.105705

Natural radionuclides as tracers of coastal sediment dynamics in El Confital Bay (Spain): spatial distribution and relationships with sediment characteristics

El material suplementario de este artículo consiste en tres archivos .CIF que contienen la información cristalográfica de los análisis mineralógicos y una figura. Los tres archivos cristalográficos y la figura (la cual se incluye en este anexo) se pueden descargar en la versión web del artículo.

https://doi.org/10.1016/j.catena.2023.107672

The supplementary material of this paper consists of three .CIF files with the crystallographic information of the mineralogical analysis and one figure. The three crystallographic files and the figure (which is included in this annexe) can be downloaded from the online version of the paper.

https://doi.org/10.1016/j.catena.2023.107672

Fig S1. Pictures of the Van Veen dredge that was used for submerged sampling collection.

ANEXO II. Publicación relacionada con la tesis

Beach sediment dynamics from natural radionuclides point of view

Autores: ***Ana del Carmen Arriola Velásquez,*** *Alicia Tejera Cruz, Ignacio Alonso Bilbao, Walter Geibert, Ingrid Stimac, Fernando Cámara Artigas, Neus Miquel Armengol, Héctor Eulogio Alonso Hernández, Jesús García Rubiano, Pablo Martel Escobar*

Tipo de publicación: *Capítulo de libro*

DOI: *https://doi.org/10.36253/979-12-215-0030-1.02*

Libro: *Ninth International Symposium "Monitoring of Mediterranean Coastal Areas: Problems and Measurement Techniques"*

Editores: *Laura Bonora, Donatella Carboni, Matteo De Vincenzi, Giorgio Matteucci*

Editorial: *Firenze University Press*

ISBN: *979-12-215-0030-1*

Año: 2022

BEACH SEDIMENT DYNAMICS FROM NATURAL RADIONUCLIDES POINT OF VIEW

Ana del Carmen Arriola Velásquez[1], Alicia Tejera[1], Ignacio Alonso[1], Walter Geibert[2], Ingrid Stimac[2], Fernándo Cámara[3], Neus Miquel-Armengol[1], Héctor Alonso[1], Jesús G. Rubiano[1], Pablo Martel[1]

[1]Departmen of Physiscs, Instituto Universitario de Investigación en Estudios Ambientales y Recursos Naturales I-UNAT, Universidad de Las Palmas de Gran Canaria, Campus de Tafira, 35017, Las Palmas de Gran Canaria (Spain),
phone +34 928454502, e-mail: ana.arriola101@alu.ulpgc.es

[2]Alfred Wegener Institute, Helmholtz Centre for Polar and Marine Research, Bremerhaven (Germany)

[3]Dipartimento di Scienze della Terra, Università degli Studi di Milano, Via Sandro Botticelli 23, 20133, Milano (Italy)

Abstract – This study is focused on assess the use of radionuclides ^{226}Ra, ^{228}Ra, ^{40}K and $^{210}Pb_{ex,}$ as well as the ratio $^{226}Ra/^{228}Ra$, as tracers of marine sediment dynamic. For this the spatio-temporal variability of the activity concentration of these radionuclides was analysed in Las Canteras beach (Spain). This beach was selected due to its heterogenic composition and marine dynamics. A Cluster analysis and a Principal Component analysis (PCA) were performed to evaluate the spatial variability. The results grouped the samples in three zones related to the sediment distribution under the effects of the marine dynamics that are created by the different geomorphologies of the beach. In the temporal variability analysis, an ANOVA test and Tukey's Honestly Significant Difference (HSD) Test pointed out that the wave action influences the activity concentration found for the different radionuclides during erosion and accumulation periods. In addition, the results of a geochemical analysis of samples from maximum and minimum activity concentration campaigns suggested that the radionuclides studied could be used as tracers of marine sediment dynamic in beach areas.

Introduction

Natural radionuclides in the Earth's crust have different origins. Some of them come from the elements that compose it and others are generated by the interaction of the cosmogenic radiation with the elements in the atmosphere. These last ones are then deposited on the planet surface by different processes. Since all of these elements can be found in the soils of the planet that generate sediments, natural radionuclides could be used to evaluate different sediment dynamics. In the case of beaches, the morphology and sedimentary budget is mainly controlled by sand erosion and accumulation periods. Therefore, monitoring these processes closely is a key factor to a sustainable management of this high-value areas, as well as can be useful to better understand how beaches morphology can evolve with time. Different techniques can be used to evaluate sediment dynamics in beach areas, and among them, natural radionuclides have proven to be an interesting tool in coastal areas [7], [15].

Referee List (DOI 10.36253/fup_referee_list)
FUP Best Practice in Scholarly Publishing (DOI 10.36253/fup_best_practice)

Ana del Carmen Arriola Velásquez, Alicia Tejera Cruz, Ignacio Alonso, Walter Geibert, Ingrid Stimac, Fernándo Cámara Artigas, Neus Miquel-Armengol, Héctor Alonso Hernández, Jesús Garcia Rubiano, Pablo Martel Escobar, *Beach sediment dynamics from natural radionuclides point of view,* pp. 16-26 © 2022 Author(s), CC BY-NC-SA 4.0, 10.36253/979-12-215-0030-1.02

In this study the use of natural radionuclides has been assessed in Las Canteras beach, in Las Palmas de Gran Canaria, Spain. This beach is very heterogenous in sand composition and marine dynamics that affect it. In addition, the sediment dynamic as well as its sedimentary budget have been very well studied during the years. According to these studies, Las Canteras beach is divided in three arches, and it presents a natural offshore rocky bar that covers the northern and central arch (figure 1). This bar is not a complete block, but it presents fragmentations and openings that are more present in front of the central arch. The southern arch, on the contrary, does not present any bar and it is totally open to the wave action. Due to these different morphological characteristics, Las Canteras beach combines the characteristic dynamic of a closed beach protected against the wave action and that associated with a beach open to it, presenting seasonal variability in its sedimentary budget [1]. During erosion periods, sand is eroded from the southern arch and a lengthwise transport of these sediments can occur to the northern arch. During accumulation periods the sand from submerged sandbars arrive to the beach and, since the northern arch is under a constant accumulation period, some berms can appear and a lengthwise transport of sediments from the northern arch to the southern arch can occur [1].

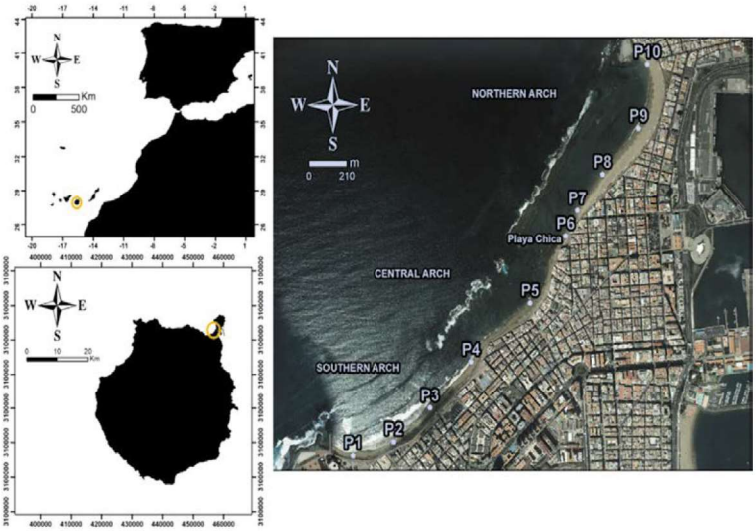

Figure 1 – Location of the study region and the sampling points in Las Canteras beach. Coordinates are in the UTM system [4].

Regarding the sand composition of Las Canteras beach, different sources can be identified: basic volcanic rocks from La Isleta, in the northeast of El Confital bay, phonolitic lava flow from the southwestern side of the bay, basic rocks and magnetite from the mouth of La Ballena ravine in the south part of the beach, submerged sandbars located between the bathymetric curve of 50 m and the beachfront and the natural offshore calcarenite rocky bar

[6], [14]. Furthermore, there are some calcimetry and petrological analyses of the beach sand and the geological composition of El Confital Bay (where Las Canteras beach is located) that identify different materials that can be found along Las Canteras beach. The sand from the northern arch has a higher content of bioclast and calcareous materials, as well as it presents a higher content in calcarenite. This calcarenite displays a higher content of feldspars in its terrigenous part and thus, feldpars seem to accumulate in the northern part of the beach. The southern part of the beach, on the contrary, tends to accumulate clinopyroxenes and other heavy minerals, such as olivine, amphiboles and Fe-Ti oxides that come from the ravine that ends in this part. The lighter lithics that can be found in this part are redistributed along the beach due to erosion and accumulation phenomena [1], [2], [12].

All these differences along Las Canteras beach enabled to evaluate the changes of natural radionuclides associated to the sediments that are transported under different marine dynamics and geological environments. On the one hand the southern arch resembles a beach open to the wave action and with sand composed mostly by heavy minerals. On the other hand, the northern arch presents the characteristics of a beach protected against the wave action and with sediments mainly composed by organic materials and calcarenite. Therefore, the results could resemble to those obtained after assessing the role of natural radionuclides in two different beaches with very different dynamic and geological characteristics. Hence, the results obtained could be expected to be applied in other parts of the world. In this framework, a spatio-temporal analysis of the activity concentrations of natural radionuclides was performed in Las Canteras beach during 2016 and 2019 [4], [5] and it is described in this work. These studies evaluated the role of gamma emitting radionuclides ^{226}Ra, ^{228}Ra, ^{40}K, $^{210}Pb_{ex}$ and the ratio ^{226}Ra/^{228}Ra as tracers of erosion and accumulation periods in beach areas.

Material and Methods

Samples collection took part monthly from September 2016 to April 2019, with a total of 360 samples collected. For each campaign ten samples were collected in the intertidal zone of the beach during low tide time (Figure 1). At each sampling point, a square of 1 m^2 was drawn in the sand and, after mixing in situ, samples were taken from the superficial sand (between 0 and 5 cm depth). After this, samples were taken to the laboratory, they were dried at 80 ◦C for 24 h. They were then sieved through a 1 mm mesh size to homogenise them and kept inside PVC-trunk conical containers, filled to 40 cm^3. They were sealed with aluminium strips, because they are impermeable to radon gas [4]. Finally, the samples were stored for a duration of approximately one month before measurement to allow secular equilibrium between ^{226}Ra and ^{222}Rn and its short-lived progenies (as ^{214}Pb is used for determining ^{226}Ra).

The determination of radionuclides in sand samples by gamma spectrometry analysis was carried out using a Canberra Extended Range (XtRa) Germanium spectrometer, model GX3518, with 38 % relative efficiency with respect to a 3” x 3” active area NaI (Tl) detector and nominal FWHM of 0.875 keV at 122 keV and 1.8 keV at 1.33 MeV. It works coupled to a Canberra DSA-1000 multichannel analyser with the software package Genie 2000. Efficiency calibration of the system was performed using the Canberra LabSOCS package based on the Monte Carlo method [3], [5], [10], [11]. Calibration was verified using reference standards for IAEA RGK-1 (potassium sulfate), RGU-1 (uranium ore) and RGTh-1 (thorium ore). Energy

calibration was carried out using a $^{155}Eu/^{22}Na$ (Canberra ISOXSRCE, 7F06-9/10138 series) and confirmed using the 1460.8 keV line of ^{40}K (IAEA RGK-1) [3].

The radionuclides of interest were determined from different photopeaks. ^{226}Ra was determined from the ^{214}Pb using the 351.9 keV emission line. ^{210}Pb was directly measured using the emission line of 46.5 keV. The activity concentration of ^{228}Ra was calculated from ^{228}Ac by the emission line of 911.2 keV. Activity concentrations of ^{40}K and ^{137}Cs were directly measured using emission lines 1460.8 keV and 661.8 keV, respectively. The counting time for each sample was around 24 hours. With the values of ^{210}Pb and ^{226}Ra unsupported or excess ^{210}Pb ($^{210}Pb_{ex}$) [9] was calculated.

In order to better understand the role of natural radionuclides as tracers of sediment transport during erosion and accumulation periods, the variations in the chemical and mineralogy composition of 4 sand samples were evaluated. The first 2 samples selected belong to the maximum gamma activity campaign and the other 2 to the minimum one. For this, a multielement analysis using a coupled plasma optical emission spectrometry (ICP-OES), a Powder X-ray diffraction (XRPD) and a single crystal X-ray diffraction (SCXRD) analysis were performed. The X-ray diffraction analysis was selected as a technique to search the minerals that are transported during erosion and accumulations periods and could contain the radionuclides studied. With these techniques, it was expected to identify and better characterize the different sediments and minerals that mix in the sand and are responsible for the activity concentrations found [5].

A cluster analysis (CA) [13] and a principal component analysis (PCA) [16] were carried out in order to evaluate the spatial distribution of the activity concentrations of the radionuclides studied [4]. For the temporal analysis a one-way ANOVA test was performed to evaluate the presence of significant difference among the difference groups. Finally, a Tukey's Honestly Significant Difference (HSD) Test [17] was used to stablish the exact groups among which significant differences were found [5].

Results and Discussion

Figure 2 shows the dendrogram of the hierarchical cluster and the biplot corresponding to the PCA results. The same three groups were observed in both analyses. The first group that will be referred as zone I grouped samples from sampling points P1, P2, and P3, which are located in the open part of the beach in the southern arch. The second group that can be observed, and will be referred as zone III, includes samples from sampling points P7, P8 and P10. This sampling stations are located in the northern arch, in the part of the beach that is completed protected against the wave action by the natural offshore rocky bar. The last group that can be observed combines samples from sampling stations located in both the central arch and the northern arch. It includes samples from sampling stations P4, P5, P6 and P9, that are located in front of the openings of the natural offshore rocky bar. In addition, the biplot points out that the variance of ^{226}Ra, ^{228}Ra, and ^{40}K is mostly explained by PC1. Moreover, these radionuclides appear very close togeher in the biplot, meaning that they activity concentration variance is very well correlated. In the case of $^{210}Pb_{ex}$ it is load far from the other radionuclides, indicating that its variance is more explained by PC2 and it is badly correlated to them. These seems to suggest that the agent controling the distribution along the beach of $^{210}Pb_{ex}$ is different from that controlling the spatial distribution of ^{226}Ra, ^{228}Ra,

and ^{40}K. Moreover, the presence of the distinct parts of the offshore rocky bar seems to be one of the main influences in the distribution of sediment transport and accumulation of radionuclides along the beach. Therefore, ^{226}Ra, ^{228}Ra, and ^{40}K seem to be tracing marine sediment dynamics [4].

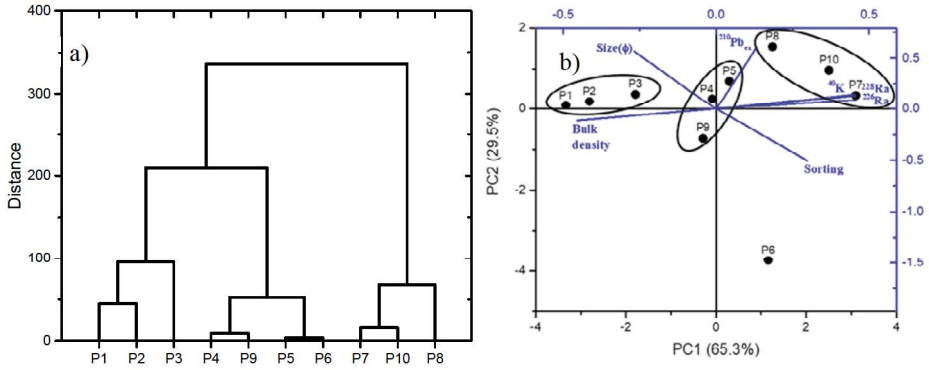

Figure 2 – a) Dendrogram showing clustering for the different sampling points based on their activity concentrations of ^{226}Ra, ^{228}Ra, and ^{40}K. b) Biplot of loading plot with the eigenvectors obtained for the grain size in the phi scale (Size φ), sorting, bulk density of the sample and activity concentrations of ^{226}Ra, ^{228}Ra, ^{40}K and ^{210}Pb$_{ex}$ (blue axes) and scores of observations (black axes) Modified from [4].

Considering the zones described in the spatial analysis, the temporal series of the mean values of ^{226}Ra, ^{228}Ra, ^{40}K, ^{210}Pb$_{ex}$ and the ratio ^{226}Ra/^{228}Ra during the whole study in each zone appear in figure 4. The ratio was also analysed since it had been proposed before as a tracer of erosion/accumulation periods [8]. This is because in the crystal framework of clay minerals both ^{226}Ra and ^{228}Ra can be found, but the carbonate and exchangeable phases contain more ^{228}Ra. Hence accretion or erosion periods could be measured by a change in the ratio between ^{226}Ra and ^{228}Ra. During accumulation periods the ratio would be below 1 due to the higher input of ^{228}Ra in this periods. On the contrary, during erosion events there would be a loss of ^{228}Ra and the ratio would increase above 1. Hence, this ratio was also analysed as tracer of erosion and accumulation periods. In the temporal series of the three zones, it can be appreciated that ^{226}Ra, ^{228}Ra and ^{40}K follow a similar pattern while ^{210}Pb$_{ex}$ behaves diferently. This again suggest that the agents controlling the distribution of the first three radionuclides are different to the ones controlling the distribution of ^{210}Pb$_{ex}$. Regarding the ratio ^{226}Ra/^{228}Ra, it can be observed that for zones I and II it presents values that are above and below 1, while in zone III is always under 1. The zone III is the area protected against the wave action and thus, in this part the ratio would always be below 1 which seems to be what can be observerd in the temporal series. In addition, in zones I and, a bit lesser, in zone II, the maximum values of ^{226}Ra, ^{228}Ra and ^{40}K seem to agree with values of the ratio below 1. All of these seem to agree with what would happen during erosion periods and thus, the temporal series seem to indicate that the three radionuclides, as well as the ratio, are tracing erosion/accumulation periods in the beach.

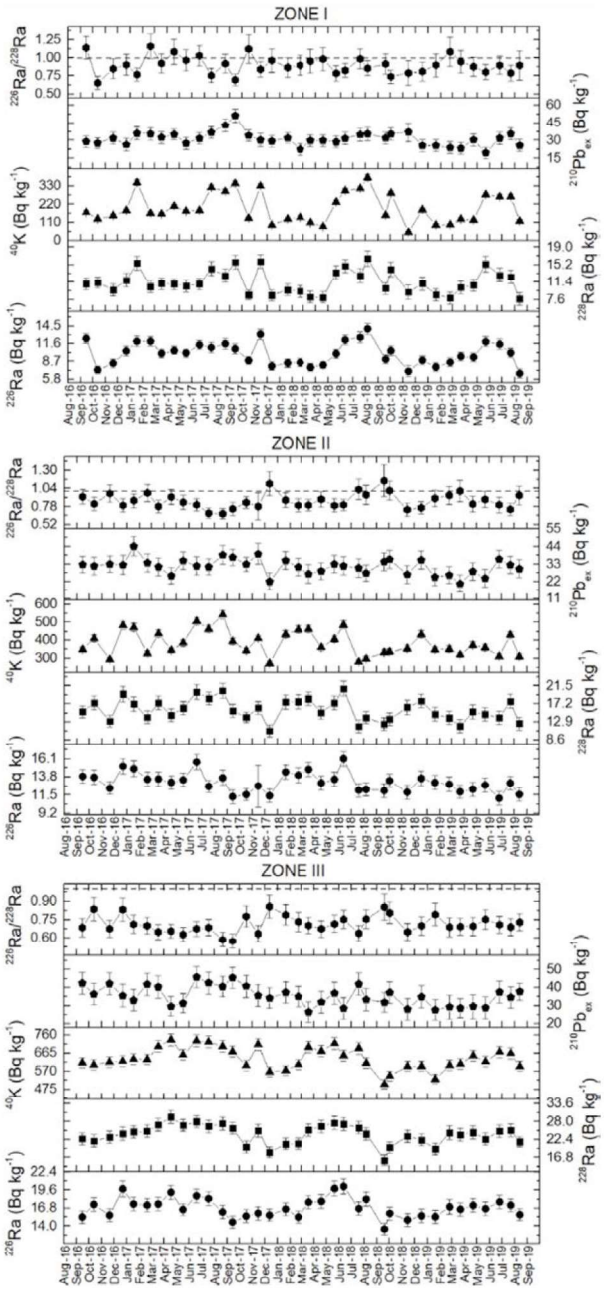

Figure 4 – Temporal series of the activity concentration of ^{226}Ra, ^{228}Ra, ^{40}K, $^{210}Pb_{ex}$ and the ratio $^{226}Ra/^{228}Ra$ during the study period for the different zones established in [4] for Las Canteras beach [5].

In order to further analyse the role of the three radionuclides and the ratio as tracers of marine sediment dynamics, the effect of different erosion and accumulation agents such as wave approach direction and significant wave height. In table 1 the results obtained for the One-way ANOVA and the Tukey's Honestly Significant Difference (HSD) Test are shown. The One-way ANOVA identified the presence of significant differences in the temporal series of ^{226}Ra, ^{228}Ra, ^{40}K and the ratio $^{226}Ra/^{228}Ra$. The HSD identified the exact groups that present significant differences in relation to the different erosion/accumulation agents studied.

Table 1 – Results of zone I for the one-way ANOVA test and Tukey's Honestly Significant Difference (HSD) Test. Modified from [5].

Area	Field	F	Prob-F	Tuckey's test
^{226}Ra	Significant wave height	9.61900	0.0005110	Low-high (0.0009) Low-medium (0.0114)
	Wave direction	6.02300	0.0194000	NW-NE (0.0194)
^{228}Ra	Significant wave height	19.14000	0.0000030	Low-High (0.0000065) Low- Medium (0.0004618)
	Wave direction	6.67200	0.0143000	NW-NE (0.0142665)
^{40}K	Significant wave height	25.34000	0.0000002	Low-High (0.0000008) Low- Medium (0.0000358)
	Wave direction	9.12100	0.0047700	NW-NE (0.0047708)
$^{226}Ra/^{228}Ra$	Significant wave height	1.98000	0.1540000	-
	Wave direction	0.21400	0.6470000	-
ANOVA prob-F 0.05 Tuckey's test p-value 0.05				

In the case of the ratio, no significant differences were found for any of the zones. According to the literature [1] the area fully protected by the natural offshore rocky bar (zone III) is in a constant accumulation period. Moreover, zone II is also protected by the bar, so the lack of significant differences can be expected in these two parts of the beach. In addition, some clay minerals have been found in the northern part of the bay where the beach is located [12] so the ratio seems to work in this part of the beach. However, this could not justify the lack of significant differences in zone I and since other minerals could also contain ^{228}Ra, this ratio might not be suitable to use as marine sediment dynamic tracer worldwide, but it could be used in areas with similar characteristics to the northern part of Las Canteras beach [5].

In the case of ^{226}Ra, ^{228}Ra and ^{40}K the results relating to the significant wave height showed significant differences for zone I between the low wave height and the medium and high wave height. According to the polar plots of figure 5, the campaigns with lower values of significant wave height for zone I would present higher activity concentrations values of these three radionuclides. For zones II and III no significant differences were found [5].

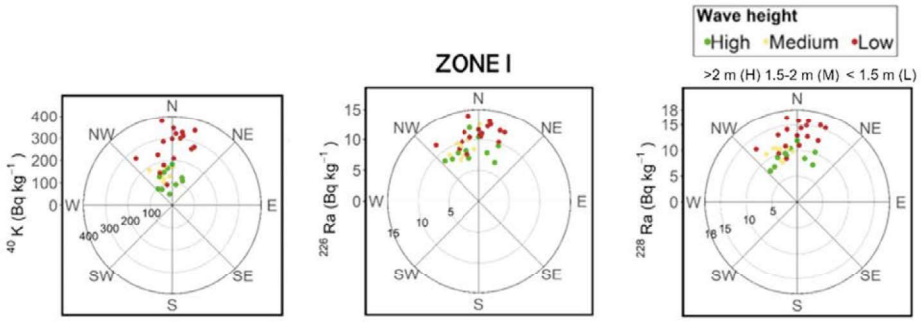

Figure 5 – Azimuth plot of wave height and direction and activity concentration of ^{226}Ra, ^{228}Ra and ^{40}K for the different zones in Las Canteras beach. Modified from [5].

The results relating to wave approach direction also reported significant differences for zone I between the campaign when the wave approach direction was NE or NW. The boxplots of figure 6 represents the activity concentration values of ^{226}Ra (figure 6a), ^{228}Ra (figure 6b) and ^{40}K (figure 6c) for the campaigns with NE and NW wave approach directions. They shows that, in campaigns with a NE wave approach direction, the activity concentration values of these elements were higher. The NE part of the bay and the north part of the beach is where the clay minerals and feldspars were found [2], [12]. Therefore, the results point to the possible influence of the minerals located in the northern part of the beach, in the changes of activity concentration values found in zone I during the whole study period [5]. In this case, zones II and III did not show any significant differences either.

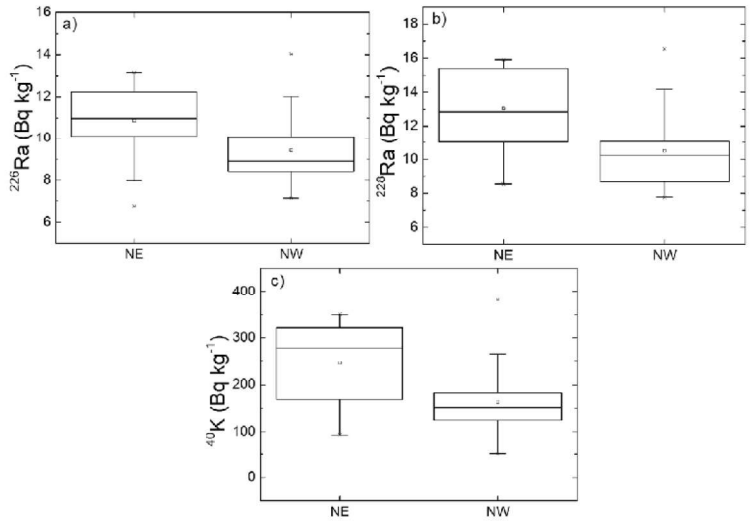

Figure 6 – Boxplot of the activity concentrations obtained for zone I in each campaign for each of the wave approach directions. a) ^{226}Ra, b) ^{228}Ra and c) ^{40}K [5].

In order to comprehend what mineral could be transporting ^{226}Ra, ^{228}Ra and ^{40}K a total of 4 samples were analysed by Powder X-ray diffraction (XRPD). The samples were chosen from two sampling stations (figure 1), one located in the open part of the beach (P2) and another located in the closed part of the beach (P8). From each sampling station a sample from a minimum activity concentration campaign (November 2018) and a sample from a maximum activity concentration value (August 2018) where analyzed. Hence, the samples from November 2018 would correspond to an erosion periods and samples from August 2018 would belong to an accumulation period. In addition, the sample from zone I was analysed by single crystal X-ray diffraction (SCXRD). The results of the X-ray diffraction analysis pointed out the increase of feldspar with potassium content in the samples from the open part of the beach during the accumulation periods. In the case of the samples from the closed part of the beach, this K-feldspar is present in both samples from erosion and accumulation campaigns. It has been described for Las Canteras beach that feldspars arrive to the southern part of the beach and are redistributed along the beach, as well as they are constantly present and accumulated in the northern part of the beach [1], [2]. Therefore, the results of the X-ray diffraction analysis seem to suggest that K-feldspar is the main K-bearing mineral. Hence, ^{40}K seems to be tracing the movement of this feldspar contained in the light fraction of the sand, making it a good tracer of the beach sedimentary dynamics [5]. The results of the multielement analysis showed that total K increases its concentration during accumulation periods and a decrease during erosion periods. In addition, Ba and Ca followed the same pattern as total K. Since it was no possible to measure Ra concentration by this method and, considering Ba has similar chemical properties to Ra, we could be assumed that total Ra follows the same pattern as total K too. Therefore, that would be why ^{226}Ra and ^{228}Ra follow a similar pattern to ^{40}K and could also trace marine sediment dynamics.

Table 2 – Multielement analysis of the total rock composition of each sand sample. Concentrations given in g kg-1 of Ba, Ca and K were analyzed. Modified from [5].

Sample	Ba	Ca	K
LOD of detector	0.0002	0.0552	0.0203
LOB	0.0113	3.1764	0.109
LOD of the method	0.0226	6.3529	0.2181
LOQ	0.0435	11.9209	0.4227
PLC18_8.2	0.3611±0.0047	172±2	16.03±0.10
PLC18_11.2	0.0519±0.0005	25±0	0.65±0.01
PLC18_8.8	0.3805±0.0023	167±1	15.48±0.09
PLC18_11.8	0.3484±0.0021	163±1	22.27±0.08

Conclusions

The assessment of the spatial and temporal variability of activity concentration of ^{226}Ra, ^{228}Ra, ^{40}K and the ratio $^{226}Ra/^{228}Ra$ in Las Canteras beach suggest that these could be used as tracers of beach sediment. Since this beach encapsulates both the dynamics of a beach

protected against the wave action and that open to it, the results could be apply to areas all over the world. Therefore, the main conclusions are:

- The CA and PCA analysis used for the spatial analysis pointed out that samples are grouped in three zones related to the marine dynamics created by the natural offshore rocky bar. The biplot of the PCA also showed that ^{226}Ra, ^{228}Ra and ^{40}K are very well correlated while $^{210}Pb_{ex}$ is less correlated. Due to the atmospheric origin of $^{210}Pb_{ex}$, the results of the spatial analysis also suggest that ^{226}Ra, ^{228}Ra and ^{40}K might be tracing marine sediment dynamics.
- The statistical analysis of the temporal variability of activity concentration of ^{226}Ra, ^{228}Ra and ^{40}K suggested that these radionuclides follow a marine sediment dynamic with higher activity concentrations values found for zone I during accumulation periods, when significant wave height was lower. In addition, activity concentrations values would increase with NE wave approach direction, which suggests these radionuclides are also tracing the origin of the sediments that arrive to the beach.
- In the case of the ratio $^{226}Ra/^{228}Ra$, no significant differences were found for any of the zones. However, zone III is the area protected by the natural offshore rocky bar and the ratio was below 1 during the whole study period, as it would be expected for a constant accumulation period. Hence, the lack of significant difference could be pointing out the lack of differences between erosion and accumulation periods. Therefore, the ratio could be applied as tracer of sediment dynamics in areas with similar characteristics to the northern arch of Las Canteras beach.
- Moreover, the mineralogical analysis suggested that the activity concentration values found for ^{40}K correspond to the movement of potassium feldspar that are transport in the light fraction of the sand into and along the beach during erosion/accumulation periods. Hence, ^{40}K seems to be the most fitting tracer for sediment dynamics in all the parts of Las Canteras beach. Nevertheless, the multi-element analysis of the composition of the total rock of the sand that can be found in the different parts of the beach in erosion and accumulation periods, indicates that Ba and Ca behave similarly to K. Since Ba has similar chemical properties to Ra, this could explain why ^{226}Ra and ^{228}Ra follow the same pattern as ^{40}K. Thus, these two elements could also be used as tracers of beach sediment dynamics.

References

[1] Alonso, I. (1993) - *Procesos sedimentarios en la playa de Las Canteras (Gran Canaria)*, Universidad de Las Palmas de Gran Canaria, Las Palmas de Gran Canaria.

[2] Alonso, I. and Pérez Torrado, F. J. (1992) - *Estudio sedimentológico de la playa de Las Canteras (Gran Canaria). Datos preliminares*, Proceeding of the III Congreso geológico de España y VII Congreso Latinoamericano de Geología, Salamanca, España, volume 2, pp. 131–135.

[3] Arnedo, M.A., Rubiano, J.G., Alonso, H., Tejera, A., González, A., González, J., Gil, J.M., Rodríguez, R., Martel, P., Bolivar, J.P. (2017) - *Mapping natural radioactivity of soils in the eastern Canary Islands*, J. Environ. Radioact. 166, 242–258.

[4] Arriola-Velásquez, A., Tejera, A., Guerra, J.G., Alonso, I., Alonso, H., Arnedo, M.A., Rubiano, J.G., Martel, P. (2019) - *Spatio-temporal variability of natural radioactivity as tracer of beach sedimentary dynamics*, Estuar. Coast. Shelf Sci. 231,106476.

[5] Arriola-Velásquez, A. C., Tejera, A., G. Guerra, J., Geibert, W., Stimac, I., Cámara, F., Alonso, H., Rubiano, J.G., Martel, P. (2021) - *^{226}Ra, ^{228}Ra and ^{40}K as tracers of erosion and accumulation processes: A 3-year study on a beach with different sediment dynamics*, Catena, 207, 105705.

[6] Balcells, R., Barrera, J. L., Ruiz García, M. T. and (Cartographers) (1990) - *Geological Map 1101-I-II Las Palmas de Gran Canaria*, 1:25000, vol. 207, IGME.

[7] Bezuidenhout, J. (2020) - *The investigation of natural radionuclides as tracers for monitoring sediment processes*, J. Appl. Geophys. 181, 104135.

[8] Dai, Z.J., Du, J.Z., Chu, A., Zhang, X.L. (2011) - *Sediment characteristics in the North Branch of the Yangtze Estuary based on radioisotope tracers*, Environ. Earth Sci. 62, 1629–1634.

[9] Gaspar, L., Webster, R., Navas, A. (2017) - *Fate of $^{210}Pb_{ex}$ fallout in soil under forest and scrub of the central Spanish Pre-Pyrenees*, Eur. J. Soil Sci. 68, 259–269.

[10] Guerra, J.G., Rubiano, J.G., Winter, G., Guerra, A.G., Alonso, H., Arnedo, M.A., Tejera, A., Gil, J.M., Rodríguez, R., Martel, P., Bolivar, J.P. (2015) - *A simple methodology for characterization of germanium coaxial detectors by using Monte Carlo simulation and evolutionary algorithms*, J. Environ. Radioact. 149, 8–18.

[11] Guerra, J.G., Rubiano, J.G., Winter, G., G. Guerra, A., Alonso, H., Arnedo, M.A., Tejera, A., Martel, P., Bolivar, J.P. (2017) - *Computational characterization of HPGe detectors usable for a wide variety of source geometries by using Monte Carlo simulation and a multi-objective evolutionary algorithm*, Nucl. Instruments Methods Phys. Res. Sect. A Accel. Spectrometers, Detect. Assoc. Equip. 858, 113–122.

[12] Mangas, J. and Julià-Miralles, M. (2015) - *Geomorfología y naturaleza de las bajas submareales de Bajo Fernando, Los Roquerillos y La Zabala (NE de Gran Canaria)*, Geo-Temas, 15, 37–40.

[13] Ravisankar, R., Sivakumar, S., Chandrasekaran, A., Prince Prakash Jebakumar, J., Vijayalakshmi, I., Vijayagopal, P., Venkatraman, B. (2014) - *Spatial distribution of gamma radioactivity levels and radiological hazard indices in the East Coastal sediments of Tamilnadu, India with statistical approach*, Rad. Phy. and Chem. 103, 89–98.

[14] Schmincke, H. U. (1993) - *Geological field guide of Gran Canaria*, 6th ed. Pluto-Press, Kiel.

[15] Thereska, J. (2009) - *Natural radioactivity of coastal sediments as tracer in dynamic sedimentology*, Nukleonika. 54 (1), 45–50.

[16] Thomson, R.E., Emery, W.J. (2014) - *The spatial analyses of darta fields, in Data Analysis Methods in Physical Oceanography,*3rd ed, ELSEVIER Science, Amsterdam

[17] Williams, L.J., Abdi, H. (2010) - *Tukey 's Honestly Signiflcant Difference test (HSD)*, Encyclopedia of Research Design, June, 2–7.

ANEXO III. Contribuciones a congresos

El Comité Organizador certifica que:

ANA DEL CARMEN ARRIOLA

Ha presentado la ponencia titulada

Variabilidad espacio-temporal de la radiactividad ambiental en una playa urbana: Las Canteras (Gran Canaria)

en la Sesión VI de Jóvenes Investigadores de las X Jornadas Sobre Calidad en el Control de la Radiactividad Ambiental, celebradas en Bilbao, durante los días 19 al 22 de Junio de 2018.

El Presidente

D. Fernando Legarda Ibáñez

Variabilidad espaciotemporal de la radiactividad ambiental en una playa urbana: Las Canteras (Gran Canaria).

Ana del Carmen Arriola Velásquez

E-mail: ana.arriola101@alu.ulpgc.es

Departamento de Física, Universidad de Las Palmas de Gran Canaria, 35017 Las Palmas de Gran Canaria, España

En esta presentación se expondrán los resultados más relevantes obtenidos tras una monitorización a lo largo de un año de la radiactividad ambiental de La Playa de Las Canteras, una de las playas urbanas más importante de España. Dicha playa se sitúa al norte de la isla de Gran Canaria en la ciudad de Las Palmas de Gran Canaria. Esta zona se encuentra sometida a diversas actividades antropogénicas que pueden alterar el entorno radiológico como, por ejemplo, el tráfico marítimo de buques cargueros de petróleo crudo que transcurre por el norte de la isla.

Se seleccionaron 10 estaciones de muestreo a lo largo de la zona intermareal de la playa (figura 1). El muestreo se llevó a cabo con periodicidad mensual, desde septiembre de 2016 a agosto de 2017. Una vez en el laboratorio se analizaron los distintos emisores gamma de cada muestra a través de un detector coaxial de HPGe (Camberra) y de rango extendido (XtRa) con un 40% de eficiencia y una FWHM de 1.1 keV a 88 keV.

Figura 1. Localización del área de estudio (playa de Las Canteras) y estaciones de muestreo. Coordenadas en UTM.

Los resultados se dividieron en tres partes. Primero se realizó un análisis de los riesgos radiológicos en la playa de las canteras donde se muestra que, a pesar de estar localizada en una zona de alto transito marítimo, no existe riesgo radiológico en la zona de estudio, con una dosis media de 35.1 nGy h^{-1}, valor que se sitúa por debajo de la dosis media obtenida en otras partes del mundo (figura 2). Segundo, se realizó un análisis de la distribución espacial de la actividad del ^{226}Ra, ^{232}Th, ^{40}K y $^{210}Pb_{xc}$, donde un análisis de clusters y un análisis de componentes principales mostraron una nueva división de la playa definida por la presencia de las distintas partes de la barra sedimentaria que se puede encontrar enfrente de la playa (figura 1). Por último, se llevó a cabo un análisis temporal de la variación del coeficiente $^{226}Ra/^{228}Ra$ en las distintas partes de la playa, a fin de poder

relacionar las variaciones en actividad con la dinámica sedimentaria de la playa de Las Canteras.

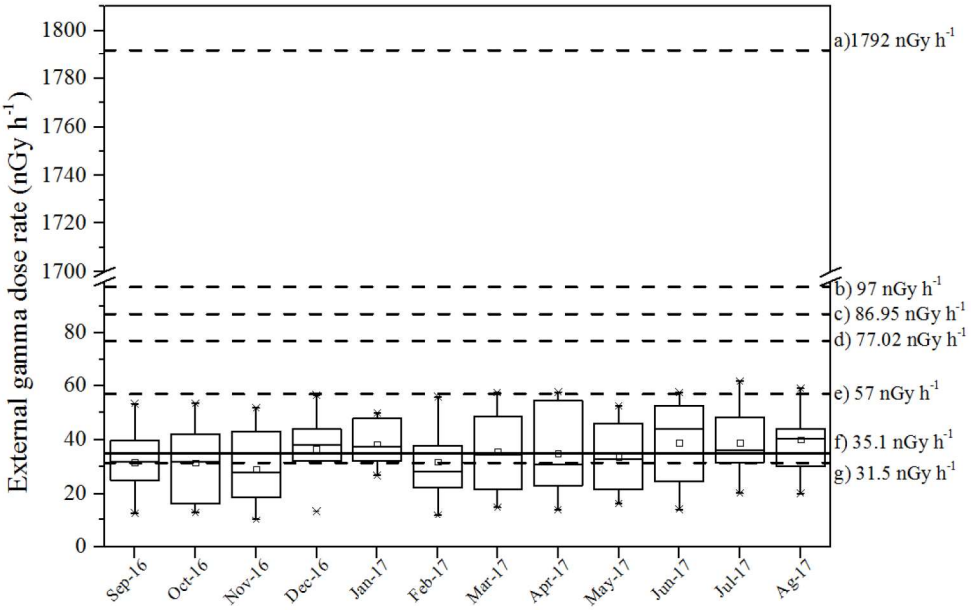

Figura 2. Diagrama de cajas y bigotes de la dosis obtenidas a lo largo del estudio y su comparación con otras partes del mundo. a) Dosis externa media en Bahía, Brasil (Vasconcelos et al., 2011). b) Dosis externa media en Malasia (Shuaibu et al., 2017). c) Dosis externa media en Tamilnadu, India (Ravisankar et al., 2015). d) Dosis externa media en Ghana (Amekudzie et al., 2011). e) Dosis externa media mundial (UNSCEAR, 2000). f) Dosis externa media en la playa de Las Canteras obtenida en este trabajo. g) Dosis externa media en la playa de Las Canteras (Arnedo et al., 2013).

CONFIRMATION OF PRESENTATION

We herewith confirm that

Ana del Carmen ARRIOLA VELÁSQUEZ

presented the following contribution

184

Variations of natural radionuclides as tracers of beach sedimentary dynamics

at the „5th International Conference on Environmental Radioactivity"
held in the Czech Republic – Prague, 8 – 13 September 2019.

Ivo Světlík
on behalf of the Organising Committee

ENVIRA 2019

EUROPEAN UNION
European Structural and Investment Funds
Operational Programme Research,
Development and Education

MINISTRY OF EDUCATION, YOUTH AND SPORTS

Variations of natural radionuclides as tracers of beach sedimentary dynamics

A.C. Arriola-Velásquez, A. Tejera, J.G. Guerra, I. Alonso, H. Alonso, M.A. Arnedo, J.G. Rubiano, P. Martel

Department of Physics, Instituto Universitario de Investigación en Estudios Ambientales y Recursos Naturales i-UNAT, Universidad de Las Palmas de Gran Canaria, Campus de Tafira, Las Palmas de Gran Canaria, 35017, Spain
Keywords: natural radionuclides, tracer, sedimentary processes, variability
Ana del Carmen Arriola Velásquez, ana.arriola101@alu.ulpgc.es

Natural and artificial radionuclides have been used as tracers of different marine sedimentary processes (Renfro, et al., 2016; Woszczyk, et al., 2017). The knowledge of coastal sedimentary dynamics is key to the sustainable management of high-value natural places for humans, such as beaches. Following this aim, the results from a three years study (from 2016 to 2019) of the spatial and temporal variability of natural radionuclides ^{226}Ra, ^{232}Th, ^{40}K, ^{210}Pb in Las Canteras beach, Spain, will be shown. This beach was selected due to its diverse sedimentary dynamic, combining the characteristic dynamic of a closed beach with that associated with a beach open to wave action (Alonso, 1994). Thus, this study could easily be extended to the management of other beaches of similar sedimentary dynamics.

For the spatial analysis a cluster and principal component analyses were performed by using stationary averages of the studied radionuclides activity concentrations and other quantities, such as grain size and or bulk density. The results show three zones of sediment distribution related to one of the main geomorphological characteristics of the beach (Figure 1).

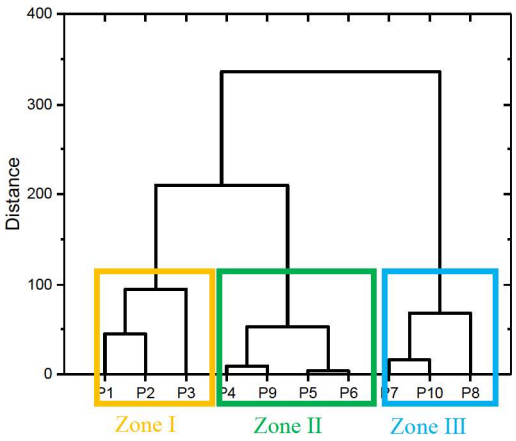

Figure 1. Dendrogram showing clustering for the different sampling points based on their activity concentrations of ^{226}Ra, ^{232}Th and ^{40}K.

The temporal analysis of the ratio ^{226}Ra/^{228}Ra (Dai et al., 2011) was used to stablish patterns of erosion and accumulation periods. The results agree with previous erosion/acucmulation studies at Las Canteras beach. Along with this ratio, ^{40}K is also analyzed as a tracer of the aforementioned sedimentary processes. Finally, relation of these potential tracers with some erosion and accumulation agents such as wave direction or the wave height, is studied (Figure 2).

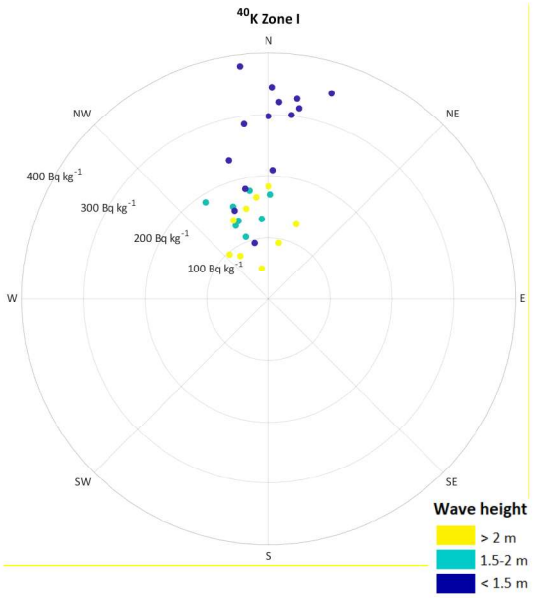

Figure 2. Azimuth plot of wave height and direction and activity concentration of ^{40}K for one of the established zones.

Alonso, I., 1994. Spatial beach morphodynamics. An example from Canary Islands, Spain. *Litoral* 94, 169–183.

Dai, Z.J., Du, J.Z., Chu, A., Zhang, X.L., 2011. Sediment characteristics in the North Branch of the Yangtze Estuary based on radioisotope tracers. *Environ. Earth Sci.* 62, 1629–1634.

Renfro, A.A., Cochran, J.K., Hirschberg, D.J., Bokuniewicz, H. J., Goodbred Jr, S.L., 2016. The sediment budget of an urban coastal lagoon (Jamaica Bay, NY) determined using ^{234}Th and ^{210}Pb. *Estuarine, Coast. Shelf Sci.* 180, 136–149.

Woszczy, M., Poreba, G., Malinowski, Ł., 2017. ^{210}Pb, ^{137}Cs and ^{7}Be in the sediments of coastal lakes on the Polish coast: Implications for sedimentary processes. *J. Environ. Radioact.* 169–170, 174–185.

9th International Symposium
MONITORING OF MEDITERRANEAN COASTAL AREAS:
PROBLEMS AND MEASUREMENT TECHNIQUES
Livorno 14th- 16th June 2022

Firenze, 27th June 2022

We declare that the **ANA DEL CARMEN ARRIOLA VELÁSQUEZ** has contributed to the Symposium by the work:

BEACH SEDIMENT DYNAMICS FROM NATURAL RADIONUCLIDES POINT OF VIEW

Authors: *Ana del Carmen Arriola Velásquez, Alicia Tejera, Ignacio Alonso, Walter Geibert, Ingrid Stimac, Fernándo Cámara, Neus Miquel-Armengol, Héctor Alonso, Jesús G. Rubiano, Pablo Martel*

that was selected as oral presentation in the Session "Morphology and evolution of coastlines and seabeds" of Ninth International Symposium *Monitoring of Mediterranean coastal areas: problems and measurement techniques*, held in Livorno (Italy) 14-15-16 June 2022.

The paper is being published, in full, in the Symposium Proceedings.

Dr. Matteo De Vincenzi
Coordinator of Scientific Board
9th International Symposium
MONITORING OF
MEDITERRANEAN COASTAL AREAS
Livorno June 14 -16, 2022

Nineth International Symposium

MONITORING OF MEDITERRANEAN COASTAL AREAS: PROBLEMS AND MEASUREMENT TECHNIQUES

Livorno (Italy), June 2022

FORM FOR ABSTRACTS PRESENTATION

TITLE: BEACH SEDIMENT DYNAMICS FROM NATURAL RADIONUCLIDES POINT OF VIEW

SESSION: MORPHOLOGY AND EVOLUTION OF COASTLINES AND SEABEDS

Authors: A.C. ARRIOLA-VELÁSQUEZ[A], A. TEJERA[A], I. ALONSO[A], W. GEIBERT[B], I. STIMAC[B], F. CÁMARA[C], H. ALONSO[A], J.G. RUBIANO[A], P. MARTEL[A]

AFFILIATIONS:

[A] DEPARTMENT OF PHYSICS, INSTITUTO UNIVERSITARIO DE INVESTIGACIÓN EN ESTUDIOS AMBIENTALES Y RECURSOS NATURALES I-UNAT, UNIVERSIDAD DE LAS PALMAS DE GRAN CANARIA, CAMPUS DE TAFIRA, 35017, LAS PALMAS DE GRAN CANARIA, SPAIN

[B] ALFRED WEGENER INSTITUTE, HELMHOLTZ CENTRE FOR POLAR AND MARINE RESEARCH, BREMERHAVEN, GERMANY

[C] DIPARTIMENTO DI SCIENZE DELLA TERRA, UNIVERSITÀ DEGLI STUDI DI MILANO, VIA SANDRO BOTTICELLI 23, 20133 MILANO, ITALY

E-MAIL ADDRESS:
ANA.ARRIOLA101@ALU.ULPGC.ES

ABSTRACT (MIN 3000 MAX 5000 CHARACTERS):

The morphology and sedimentary budget of beaches is mainly controlled by sand erosion and accumulation periods. Therefore, monitoring these processes closely is a key factor to a sustainable management of this high-value areas and better understand how beaches morphology can evolve with time. Thus, different techniques can be used to evaluate sediment dynamics and among them, natural radionuclides have proven to be an interesting tool in coastal areas (Thereska, 2009). Following this, a spatio-temporal analysis of the activity concentrations of natural radionuclides was performed in Las Canteras beach, Spain, during 2016 and 2019 (Arriola-Velásquez et al., 2021). This study evaluated the role of gamma emitting radionuclides ^{226}Ra, ^{228}Ra, ^{40}K, as well as the ratio proposed in the work of Dai et al., (2011) ^{226}Ra/^{228}Ra, as tracers of erosion and accumulation periods in beach areas. The sediment dynamics of this beach has been well studied in past years and it combines the characteristic dynamic of a closed beach protected against the wave action and that associated with a beach open to it (Alonso, 2005). These differences make this beach an ideal natural laboratory to evaluate the changes of natural radionuclides associated to the sediments that are transported under different dynamics, allowing to obtain results that could be applied in other parts of the world.

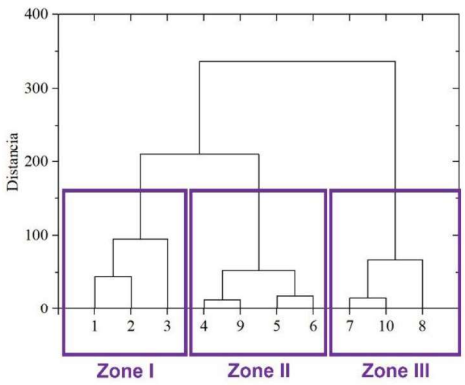

Fig. 1. Dendrogram showing clustering for the different sampling points based on their activity concentrations of ^{226}Ra, ^{228}Ra and ^{40}K.

For studying the spatial variability, a cluster and a principal component analysis were performed to the samples corresponding to the first year of study (a total 120 samples). The stationary averages activity concentrations of the studied radionuclides and other quantities, such as grain size or bulk density, were used to performs these tests. The results (Fig. 1) show that the activity concentration of ^{226}Ra, ^{228}Ra, ^{40}K group the samples in three clusters that agreed with three different zones related to the sediment distributions occurring due to the different sediment dynamics present in the beach.

The temporal variability analysis showed that the activity of the natural radionuclides studied was influenced by marine erosion and accumulation agents, such as significant wave height. As it is shown in Fig. 2, in zone I (the area totally exposed to the wave action) the activity concentration values found were lower when the significant wave height was higher (expected to occur during erosion periods). This pattern is clearer for ^{40}K and this could be related to the appearance and loss of some potassium rich minerals during erosion and accumulation periods. Therefore, ^{40}K seems to be a suitable tracer of beach sedimentary dynamics.

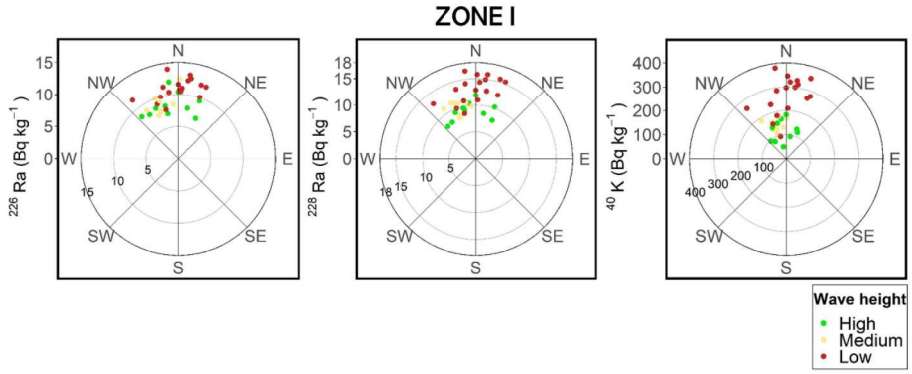

Fig. 2. Azimuth plot of wave height and direction and activity concentration of ^{226}Ra, ^{228}Ra and ^{40}K for zone I.

REFERENCES: (MAX 4)

1. Alonso, I., 2005. Costa Norte: Playa De Las Canteras, in: Hernández, L., Alonso, I., Mangas, J., Yanes, A. (Eds.), Tendencias Actuales En Geomorfología Litoral. Universidad de Las Palmas de Gran Canaria, La Palmas de Gran Canaria, pp. 219–238.

2. Arriola-Velásquez, A.C., Tejera, A., Guerra, J.G., Geibert, W., Stimac, I., Cámara, F., Alonso, H., Rubiano, J.G., Martel, P., 2021. ^{226}Ra, ^{228}Ra and ^{40}K as tracers of erosion and accumulation processes: A 3-year study on a beach with different sediment dynamics. Catena 207, 105705. https://doi.org/10.1016/j.catena.2021.105705

3. Dai, Z.J., Du, J.Z., Chu, A., Zhang, X.L., 2011. Sediment characteristics in the North Branch of the Yangtze Estuary based on radioisotope tracers. Environmental Earth Sciences 62, 1629–1634. https://doi.org/10.1007/s12665-010-0647-7

4. Thereska, J., 2009. Natural radioactivity of coastal sediments as tracer in dynamic sedimentology. Nukleonika 54, 45–50.

VIII INTERNATIONAL SYMPOSIUM ON MARINE SCIENCES
LAS PALMAS DE GRAN CANARIA

THE ORGANIZING COMMITTEE OF THE VIII INTERNATIONAL SYMPOSIUM ON MARINE SCIENCES (ISMS 2022) CERTIFIES THAT THE ORAL COMMUNICATION ENTITLED:

"NATURAL RADIONUCLIDES AS TRACERS OF BEACH SEDIMENT DYNAMICS: A STUDY IN A HETEROGENEOUS ENVIRONMENT"

190

HAS BEEN PRESENTED BY:

ANA DEL CARMEN ARRIOLA VELASQUEZ

COAUTHORS: Ana del Carmen Arriola Velásquez, Alicia María Tejera Cruz, Neus, Miquel Armengol, Héctor Alonso Hernández, Jesús García Rubiano and Pablo Martel Escobar

HELD IN LAS PALMAS DE GRAN CANARIA, FROM JULY 6TH TO JULY 8TH, 2022

María Esther Torres Padrón,
Director of ISMS 2022

ORGANIZERS

COLLABORATES

NATURAL RADIONUCLIDES AS TRACERS OF BEACH SEDIMENT DYNAMICS: A STUDY IN A HETEROGENEOUS ENVIRONMENT

A.C. Arriola-Velásquez*[1], A. Tejera[1], N. Miquel-Armengol[1], H. Alonso[1], J.G. Rubiano[1], and P. Martel[1]

[1] Department of Physics, Instituto Universitario de Investigación en Estudios Ambientales y Recursos Naturales i-UNAT, Universidad de Las Palmas de Gran Canaria, SPAIN.
ana.arriola101@alu.ulpgc.es, alicia.tejera@ulpgc.es, neus.miquel101@alu.ulpgc.es, hector.alonso@ulpgc.es, jesus.garciarubiano@ulpgc.es, pablo.martel@ulpgc.es

Abstract: Natural radionuclides have been used as tracers of sediment dynamics in coastal areas before (Thereska 2009, Dai et al, 2011) and therefore they present an interesting tool to evaluate sedimentary processes in coastal areas. To enhance the knowledge of natural radionuclides as tracers of erosion and accumulation periods in beach and coastal areas, a spato-temporal analysis of the activity concentrations of natural radionuclides in sand samples was performed in Las Canteras beach (LC), Spain, during 2016 and 2019. This beach was selected because it combines two different dynamics; one of a closed beach, and thus protected against the wave action, and that associated with a beach open to it. Moreover, the sediment dynamics of this beach has been well studied before (Alonso, 1992). Therefore, Las Canteras beach is a suitable natural laboratory to evaluate the use of natural radionuclides as tracers of beach sediment dynamics under different marine dynamics. The results of the spatial analysis showed that the activity concentration of ^{226}Ra, ^{228}Ra, ^{40}K group the samples in three clusters that agreed with three different zones related to the sediment distributions occurring due to the different sediment dynamics present in the beach. The temporal analysis seemed to prove that the activity concentrations of the radionuclides studied were influenced by erosion and accumulation agents such as significant wave height. Moreover, submarine sand samples from El Confital Bay, where LC is located, were also analysed in order to evaluate if the origin of the sediments that arrive and move along the beach are also traced by natural radionuclides.

Key words: Natural radionuclides, beach, tracers, erosion and accumulation

References:

Alonso, I. 1993. Procesos sedimentarios en la playa de Las Canteras (Gran Canaria). PhD tesis, Universidad de Las Palmas de Gran Canaria, Spain.

Dai, Z.J., Du, J.Z., Chu, A., Zhang, X.L. (2011). Sediment characteristics in the North Branch of the Yangtze Estuary based on radioisotope tracers. Environmental Earth Sciences 62, 1629–1634.

Thereska, J. (2009). Natural radioactivity of coastal sediments as tracer in dynamic sedimentology. Nukleonika 54, 45–50.

ENVIRA 2023

02 October 2023

CONTRIBUTION CERTIFICATE

ANA DEL CARMEN ARRIOLA VELASQUEZ

has presented the Oral contribution titled:

"Tracing sediment dynamics in El Confital bay (Spain):

natural radionuclides distribution and their relationships

with sediment characteristics"

in the 7th International Conference on Environmental Radioactivity – ENVIRA 2023, held in Seville, Spain, during 17th-22nd September 2023.

Manuel García-León

Chair of the Local Organizing Committee

Tracing sediment dynamics in El Confital bay (Spain): natural radionuclides distribution and their relationships with sediment characteristics

A. C. Arriola-Velásquez[1], A. Tejera[1], I. Alonso[2], F. Cámara[3], M. Cantaluppi[3], H. Alonso[1], N. Miquel-Armengol[1], J.G. Rubiano[1], P. Martel[1]

[1] Department of Physics, Instituto Universitario de Investigación en Estudios Ambientales y Recursos Naturales i-UNAT, Universidad de Las Palmas de Gran Canaria, Campus de Tafira, 35017, Las Palmas de Gran Canaria , Spain. e-mail: ana.arriola101@alu.ulpgc.es
[2] Instituto de Oceanografía y Cambio Global, IOCAG, Universidad de Las Palmas de Gran Canaria, Campus de Tafira, 35017 Las Palmas de Gran Canaria, Spain
[3] Dipartimento di Scienze della Terra, Università degli Studi di Milano, via Sandro Botticelli 23, 20133 Milano, Italy

Keywords: Natural radionuclides, Tracers, Coastal sediments, Sediment dynamics

In this study, the spatial distribution of different natural radionuclides was compared for two periods of time in El Confital Bay (Spain). For this, the activity concentration values of ^{226}Ra, ^{228}Ra and ^{40}K were determined by gamma spectrometry for 37 submarine samples collected in 2005/2006 and 39 samples that were gathered in 2022. This comparison showed that ^{226}Ra, ^{228}Ra and ^{40}K trace the sediment erosion, transport and accumulation that can be found in diverse parts of the bay. Additionally, the spatial distribution of unsupported ^{210}Pb ($^{210}Pb_{ex}$) was analysed for the 2022 samples. This showed that $^{210}Pb_{ex}$ is a useful tracer of areas of the bay that present lower erosion of the seabed and thus, where accumulation by sedimentation is favoured. Besides this, an assessment of the influences of the grain size and mineral composition of the samples in their activity concentration values of ^{226}Ra, ^{228}Ra and ^{40}K and $^{210}Pb_{ex}$ was also carried out. The result showed that the variations in activity concentration values of these radionuclides in the different samples are more related to their mineral composition than to their grain size.

ENVIRA 2023

02 October 2023

CONTRIBUTION CERTIFICATE

ANA DEL CARMEN ARRIOLA VELASQUEZ

has presented the Poster contribution titled:

"Gamma emitter radionuclides as tracers of sediment dynamics in beach areas: a comparison between in situ and lab-based gamma spectrometry measurements"

in the 7th International Conference on Environmental Radioactivity – ENVIRA 2023, held in Seville, Spain, during 17th-22nd September 2023.

Manuel García-León

Chair of the Local Organizing Committee

ENVIRA 2023
7th International Conference on Environmental Radioactivity
Seville, Spain
September 17th - 22nd, 2023

Gamma emitter radionuclides as tracers of sediment dynamics in beach areas: a comparison between in situ and lab-based gamma spectrometry measurements

A. C. Arriola-Velásquez[1], A. Tejera[1], H. Alonso[1], N. Miquel-Armengol[1], J.G. Rubiano[1], S. Alexakis[2], D.L. Patiris[2], C. Tsabaris[2], P. Martel[1]

[1] Department of Physics, Instituto Universitario de Investigación en Estudios Ambientales y Recursos Naturales i-UNAT, Universidad de Las Palmas de Gran Canaria, Las Palmas de Gran Canaria, Spain

[2] Hellenic Centre for Marine Research, Institute of Oceanography, 46.7 Km Avenue Athens-Sounio, 19013, Anavyssos, Greece

Motivation and study region

In recent years the use of natural radionuclides as tracers of beach sediment dynamics has gained popularity since, contrary to artificial radionuclides, their use does not require anthropogenic introduction in the system as they already belong to it. In this framework, in situ and lab-based gamma spectrometry have been applied to measure these natural radionuclides in beach sands [1, 2, 3, 4]. However, the weaknesses and strengths of each methodology need to be further comprehended in order to provide more reliable results when studying radionuclides as tracers of beach sediment dynamics. In this work, the results obtained in the same beach location with both methodologies are shown and compared.

Las Canteras beach is one of the main urban beaches in the Canary Islands (Spain). It is 3 km long and is divided into three main areas; the northern arch, central arch and southern arch (Fig. 1). One of the main characteristics of his beach is that it is partially protected by a natural offshore rocky bar located in front of the northern and central arches, presenting at the same time dynamics of a beach fully protected against wave action (northern arch) and that of a beach open to it (southern arch). Hence, the northern arch is under a constant accumulation period while the southern arch presents seasonal variability with periods of erosion and accumulation of sediments well differentiated [5, 6]. This well-known sediment dynamics has prompted the development of some studies that have assessed the viability of natural radionuclides as tracers of sediment dynamics in beach areas using Las Canteras beach as a natural laboratory [3, 4]. These studies found that the accumulation of sediments in the northern arch is identified by high activity concentration values of ^{40}K, ^{226}Ra and ^{228}Ra. Additionally, the erosion and accumulation periods that occur in the southern arch were traced by decreases and increases in activity concentrations of these same radionuclides. All this already existing information about Las Canteras beach makes it an ideal site to compare the results obtained by in situ and lab-based gamma spectrometry and thus, it was chosen as the study region of this work.

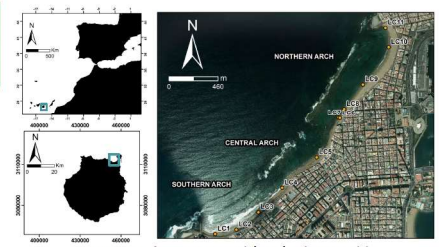

Fig 1. Location of Las Canteras Beach (Spain) and 11 intertidal sampling points used for lab-based measurements.

Material & Methods

In situ gamma spectrometry- KATERINA II gamma spectrometer

This is a compact and autonomous underwater gamma-ray spectrometer capable of monitoring ^{222}Rn and ^{220}Rn progenies. All parts of the system are tightly assembled inside a cylindrical housing made of acetal, with a maximum operation depth of 600 m. Acetal is a light and durable material which ensures minimum gamma ray attenuation during operation. In this application, it was integrated into a backpack along with a battery and communication module. The user carried the backpack steadily walking into transects on the beach at a height of 1m (Fig. 2). The **spectrometer characteristics** are:

- NaI (Tl) detector with 3'' x 3'' active area with no need for cooling or extremely high voltage input (5-18V DC).
- Energy range from 50 keV to 2800 keV.
- FWHM of 6.5% for ^{137}Cs detection at 661 keV.

The radionuclides **activity concentrations** were obtained as follows:

- 1 spectra was acquired each 20 seconds (1156 total spectra)
- ^{214}Bi (daughter of ^{226}Ra) was measured at 1720 keV.
- ^{208}Tl (daughter of ^{228}Ra) was measured at 2600 keV.
- ^{40}K was measured at 1460 keV.

Fig 2. In situ gamma spectrometry measurement process with KATERINA II detector.

Lab-based gamma spectrometry – Germanium gamma spectrometer

For lab-based measurements in the Universidad de Las Palmas de Gran Canaria (ULPGC), 11 samples (Fig. 1) from the intertidal zone of the beach were collected and measured as shown in Fig. 3. The detector used was a Canberra Extended Range (XtRa) Germanium spectrometer (model GX3518). This detector is shielded with a 15 cm thick Fe-box and located in a room with concrete walls and ceiling in the garage of a 3-floor building. The **spectrometer characteristics** are:

- Energy range from 7 keV to 10 MeV.
- Nominal FWHM of 0.875 keV at 122 keV and 1.8 keV at 1.33 MeV.
- Relatively Efficiency of 38%.

The radionuclides **activity concentrations** were obtained as follows:

- 24 hours for 1 spectra acquisition.
- ^{226}Ra was obtained from the emission line of ^{214}Pb (359.2 keV).
- ^{228}Ra was obtained from the emission line of ^{228}Ac (911.6 keV).
- ^{40}K was measured at 1460.81 keV.

Fig 3. Lab-based gamma spectrometry measurement process using a Canberra XtRa coaxial Germanium spectrometer.

Results and discussion

Fig 4. Interpolation maps of the activity concentration values in Bq kg^{-1} of a) ^{40}K, b) ^{226}Ra and c) ^{228}Ra obtained from the lab-based measurements.

Fig 5. Interpolation maps of the activity concentration values in Bq kg^{-1} of a) ^{40}K, b) ^{214}Bi and c) ^{208}Tl obtained from the in situ measurements.

ULPGC lab-based measurement results

- Activity concentration values of ^{40}K range from 72 to 631 Bq kg^{-1}.
- Activity concentration values of ^{226}Ra ranges from 4 to 16 Bq kg^{-1}.
- Activity concentration values of ^{228}Ra ranges from 8 to 27 Bq kg^{-1}.

The activity concentration distributions of the three radionuclides identify the three different sediment distribution zones that agree with prior results from the literature [3, 4]:

- High activity concentration values are found in the northern arch, identifying the area of the beach fully protected by the bar as an accumulation area.
- Intermediate activity concentration values are given in front of the openings of the bar in the central arch and in the northern arch. Hence, these areas present lower accumulation probably due to the influence of the openings of the bar.
- Low activity concentration values are located in the part of the southern arch that is fully exposed to the wave action. Thus, this is the area where erosion of sediments occurs.

KATERINA II in situ measurements results

- Activity concentration values of ^{40}K range from 99 to 317 Bq kg^{-1}.
- Activity concentration values of ^{214}Bi ranges from 22 to 39 Bq kg^{-1}.
- Activity concentration values of ^{208}Tl ranges from 11 to 21 Bq kg^{-1}.

The activity concentration distributions of the three radionuclides show a similar sediment distribution pattern to what was found with the lab-based measurements. However, some differences appear that might be related to the interference of the surrounding elements like the water or the ocean drive construction materials:

- The central arch presents a low activity area in front of the opening of the bar indicating erosion of sediments in that part of the beach.
- At the end of the southern arch, in the area fully exposed to the wave action, there is an increase in activity concentration values near the wall of the ocean drive, indicating a small accumulation of sediments there.

Conclusions

1. **In less time of measurement (2 days of in situ measurements vs 11 days of sample lab-based measurements) the in situ spectrometer allows to map not only the intertidal part of a beach but also the dry part of it.**
2. **Results of both methods describe a similar sediment distribution pattern. However, since the in situ measurements can be influenced by the interference of the surrounding elements of the beach (e.g., seawater, rocks or construction materials) some parts of the map can hide some behaviours like the accumulation occurring in the central arch of Las Canteras Beach.**
3. **The results of the activity concentration obtained by lab-based measurements ensure that the activity concentration values obtained come from the sediment grains and not from the elements surrounding the study region like rocks, construction material or seawater.**
4. **The results obtained from the lab-based measurements are sufficiently reliable to describe the sediment distribution in beach areas associated with the marine dynamics.**

References

[1] Bezuidenhout, J., 2020. The investigation of natural radionuclides as tracers for monitoring sediment processes. J Appl Geophy 181, 104135. https://doi.org/10.1016/j.jappgeo.2020.104135

[2] Tsabaris, C., Patiris, D.L., Adams, R., Castillo, J., Henriquez, M.F., Hurtado, C., Munoz, L., Kalpaxis, L., Verri, M., Alexakis, S., Pappa, F.K., Lampousis, A., 2023. In Situ Radioactivity Maps and Trace Metal Concentrations in Beach Sands of a Mining Coastal Area at North Aegean, Greece. J Mar Sci Eng 11, 1207. https://doi.org/10.3390/jmse11061207

[3] Arriola-Velásquez, A., Tejera, A., Guerra, J.G., Alonso, I., Alonso, H., Arnedo, M.A., Rubiano, J.G., Martel, P., 2019. Spatio-temporal variability of natural radioactivity as tracer of beach sedimentary dynamics. Estuar Coast Shelf Sci 231. https://doi.org/10.1016/j.ecss.2019.106476

[4] Arriola-Velásquez, A.C., Tejera, A., Guerra, J.G., Geibert, W., Stimac, I., Cámara, F., Alonso, H., Rubiano, J.G., Martel, P., 2021. ^{226}Ra, ^{228}Ra and ^{40}K as tracers of erosion and accumulation processes: A 3-year study on a beach with different sediment dynamics. Catena (Amst) 207, 105705. https://doi.org/10.1016/j.catena.2021.105705

[5] Alonso, I., 1993. Procesos sedimentarios en la playa de Las Canteras (Gran Canaria). Universidad de Las Palmas de Gran Canaria.

[6] Alonso, I., 1994. Spatial beach morphpdynamics. An example from Canary Islands, Spain. Litoral 94, 169–183.

Acknowledgement: This work was developed in the framework of the international project IAEA CPR F22074

ULPGC
Universidad de
Las Palmas de
Gran Canaria